
Imaging spectroscopy for characterisation of grass swards

Promotor: prof.dr.ir. J. Goudriaan, persoonlijk hoogleraar bij de
leerstoelgroep Plantaardige Productiesystemen

Co-promotor: dr.ir. J.J.M.H. Ketelaars, Plant Research International

Promotiecommissie:

prof.dr. A. Stein	(Wageningen Universiteit)
dr.ir. J.G.P.W. Clevers	(Wageningen Universiteit)
dr.ir. E.A. Lantinga	(Wageningen Universiteit)
prof.dr. J. de Baerdemaeker	(Katholieke Universiteit Leuven)

Imaging spectroscopy for characterisation of grass swards

A.G.T. Schut

Proefschrift
ter verkrijging van de graad van doctor
op gezag van de rector magnificus van Wageningen Universiteit
prof.dr.ir. L. Speelman
in het openbaar te verdedigen
op woensdag 11 juni 2003
des namiddags te 16.00 uur in de Aula

A.G.T. Schut, 2003

Imaging spectroscopy for characterisation of grass swards

Ph. D. Thesis, Wageningen University, -With references-, With summaries in English and Dutch

ISBN 90-5808-837-5

Keywords: Imaging spectroscopy, imaging spectrometry, remote sensing, reflection, reflectance, grass sward, white clover, recognition, characterisation, ground cover, growth monitoring, stress detection, heterogeneity quantification.

Abstract

Schut, A.G.T., 2003. Imaging spectroscopy for characterisation of grass swards. PhD thesis. Wageningen University, The Netherlands, English and Dutch summaries.

The potential of imaging spectroscopy as a tool for characterisation of grass swards was explored with respect to growth monitoring, detection of nitrogen and drought stress, and assessment of dry matter yield, clover content, nutrient content, feeding value, sward heterogeneity and production capacity. To this end, an experimental imaging spectroscopy system was developed. The system detects reflection in image lines in the wavelength range from 405-1659 nm with three different sensors at 1.3 m above the soil surface. Spectral resolution varies between 5-13 nm, and spatial resolution between 0.28-1.45 mm² per pixel at the soil. As a result of system design, reflection intensity is a function of leaf height and leaf angle. The system was tested on mini swards grown in containers. For each mini sward, 42 image lines were recorded in a regular sampling pattern per recording event.

Five experiments were conducted with *Lolium perenne* L. and/or *Trifolium repens* L. mini swards. In these experiments degree of sward damage, level of nitrogen (N) application (two experiments), water supply and white clover content were varied. In the sward damage experiment and in one N experiment light interception was recorded regularly; at harvest, also crop height and canopy reflectance (with a CropScan) was measured. Mini swards were harvested at a fixed level and in one of the N experiments in three strata. During the experiments, hyperspectral reflectance was recorded 2-4 times per week.

Image lines were classified to separate pixels containing soil, dead material and green leaves. These classes were subdivided into reflection intensity classes. Ground cover (GC), reflection intensity, image line texture, spatial heterogeneity and patterns, and spectral characteristics of green leaves were quantified. An index of reflection intensity (IRI) measured the distribution of green pixels over intensity classes and quantified vertical canopy geometry. Horizontal sward heterogeneity was quantified with the spatial standard deviation of GC (GC-SSD) and logarithmically transformed GC (TGC-SSD), and image line texture and spatial patterns with wavelet entropy (WE). Spectral characteristics were quantified with shifts of various spectral edges. Partial least squares (PLS) models combining spectral and spatial information were calibrated and validated on two separate data-sets from the sward damage and one N experiment, in order to predict dry matter (DM) yield, feeding quality

and nutrient content. Effects of replicate observations on reduction of prediction error were studied for different fractions of model bias.

GC was differently related to light interception under a cloudy sky and under a clear sky ($R^2_{\text{adj}} = 0.87-0.94$) and also for dense and open swards. Growth was accurately monitored with evolution of GC and IRI, and GC and IRI at harvest were strongly related to DM yield ($R^2_{\text{adj}} = 0.75-0.82$). Seasonal means of GC and IRI were strongly ($R^2_{\text{adj}} = 0.77-0.93$) related to annual DM matter yield and light interception capacity. There was a clear ($R^2_{\text{adj}} = 0.69$) relation between seasonal mean GC-SSD and tiller density. Seasonal means of GC-SSD differentiated dense from damaged swards. The WE of image line texture robustly differentiated clover from grass swards, while mixtures had intermediate values. Position of spectral edges was strongly related to reflection intensity. This relation differed for grass and clover swards, varied with N supply level and changed after harvesting canopy strata. Leaf angle was identified as the most important factor affecting this relationship. Drought stress was detected in an early stage, when DM content of leaves was still below 20%, from shifts of edges near water absorption features. A combination of shifts of the green and red edge was strongly related ($R^2=0.95$) to DM yield reduction due to N shortage. The prediction errors relative to the mean (of validation sets) of the PLS models were 6.2-11.7 % for N content, 5.5-9.1 % for DM content, 13.6-18.7 % for sugar content, 6.0-7.5 % for ash content, and 3.5-4.8 % for crude fibre content. Predictions of P, K, S, Mg, Na and Fe were robust in both experiments. Combining GC and IRI with mean sward spectra resulted in a prediction error of 235-268 kg DM ha⁻¹ for yields of less than 1000 up to 4000 kg DM ha⁻¹. Multiple observations may reduce the mean prediction error for DM yield with 27 to 54%, depending on model bias and number of observations. The accuracy of DM yield assessment with imaging spectroscopy was better than with the disk plate meter or Cropscan. It is concluded that imaging spectroscopy is a powerful tool in grassland research and may provide valuable information for fine-tuning of grassland management. In this study it provided fast, automatic and non-destructive means for monitoring and quantification of growth, and estimating dry matter yield, spatial heterogeneity and sward damage, nitrogen and water deficiency, clover content, feeding quality and nutrient content of swards. Finally, system requirements for application of imaging spectroscopy in the field are discussed.

Keywords: Imaging spectroscopy, imaging spectrometry, remote sensing, reflection, reflectance, grass sward, white clover, recognition, characterisation, ground cover, growth monitoring, stress detection, heterogeneity quantification

Voorwoord

Dit proefschrift is het resultaat van samenwerking met velen; ik wil een ieder bedanken voor zijn of haar bijdrage. Een speciaal dankwoord is voor Jan Ketelaars; als bedenker van het onderzoeksvoorstel is hij vanaf het begin intensief betrokken geweest bij het project. Jan, bedankt voor al je kritische en enthousiaste denkwerk, maar vooral voor de inbreng van het nodige gezond verstand. In 1998 is een intensieve samenwerking gestart met Kees Lokhorst, Jan Meuleman en Jan Kornet van het IMAG. Dankzij ideeën van met name Jan Meuleman is beeldvormende spectroscopie als onderzoeksmethodiek in beeld gekomen. Jan Kornet heeft veel kennis ingebracht over optiek. De kennis en kunde van Jan en Jan hebben de bouw van een innovatieve experimentele opstelling mogelijk gemaakt. Kees, je hebt je door al mijn verhalen geworsteld en ze van constructief commentaar voorzien, waarvoor hulde. De samenwerking heeft in 2002 een vervolg gekregen bij het ontwerpen en bouwen van een nieuw, mobiel systeem voor het opnemen van spectroscopische beelden in het veld.

Ook wil ik graag Jan Goudriaan bedanken voor zijn bijdrage aan het proefschrift. Jan, ik heb je snelle reactie op de hoofdstukken en je heldere kijk op het werk altijd zeer gewaardeerd. Daarnaast wil ik graag Hans van den Berg, Hans Helsper, Magriet Hendriks en Gerrit Kasper bedanken voor hun bijdrage aan enkele hoofdstukken. Tevens hebben velen, o.a. Riet de Kock, Willem de Visser, Arie Hoogerbrugge en medewerkers van de proeftechnische dienst gewild en ongewild een bijdrage geleverd bij het tellen van spruiten, schatten van de bedekking, verzorgen van de minizoden etc. Ook wil ik Gon van Laar danken voor haar adviezen. Rina Kleinjan-Meijerink en Tina de Kleijn hebben gezorgd voor een mooie opmaak van het proefschrift, waarvoor dank. Graag wil ik de BU AGRO danken voor de bijdrage aan de drukkosten en voor het in mij gestelde vertrouwen. Tenslotte wil ik allen die mij af en toe geprikkeld hebben of een schouderklop hebben gegeven bedanken, met name mijn oud kamergenoten Jules Bos en Ries de Visser. De collegae waarmee ik bijna elke woensdagmiddag heb mogen voetballen hebben geen noemenswaardige bijdrage geleverd aan dit proefschrift, maar leuk was het wel! De bijdrage van mijn familie kan moeilijk onderschat worden. Kasper en Matteo hebben gezorgd voor de nodige afleiding, ontspanning en relativering. Esther, ik waardeer je begrip en geduld voor de lange werkdagen, het werken in de weekenden en de weinige vakanties zeer.

Table of contents

Chapter 1.	General introduction	1
Chapter 2.	Novel imaging spectroscopy for grass sward characterisation	9
Chapter 3.	Monitoring growth of grass swards using imaging spectroscopy	31
Chapter 4.	Imaging spectroscopy for early detection of nitrogen deficiency in grass swards	57
Chapter 5.	Effects of angle, height, and pigment content of leaves on reflection characteristics of grass swards	81
Chapter 6.	Early detection of drought stress in grass swards with imaging spectroscopy	107
Chapter 7.	Detection of clover cover in grass swards with imaging spectroscopy	127
Chapter 8.	Assessment of seasonal dry matter yield and grass sward quality with imaging spectroscopy	153
Chapter 9.	Potential of imaging spectroscopy as tool for pasture management	179
Chapter 10.	General discussion	205
	References	225
	Summary	249
	Samenvatting	257
Appendix 1.	Accuracy of imaging spectroscopy and effects of spatial resolution	14 pp.
Appendix 2.	Comparison of imaging spectroscopy with disk plate meter and Cropscan for dry matter yield assessment	14 pp.

Abbreviations

ADS	Artificially Damaged Swards
APAR	Apparent Photosynthetically Active Radiation
BE	Blue edge (nm)
C / Co / CS	Control Swards
CAW	Chlorophyll absorption width (nm)
CCD	Charge Coupled Device
Chl	Chlorophyll
CV	Coefficient of Variation (-/-)
DM	Dry Matter yield (kg ha ⁻¹)
FM	Fresh Matter yield (ton ha ⁻¹)
GE	Green Edge (nm)
GC / GC _i	Ground Cover (%)
GC-SSD	Spatial Standard Deviation of GC (%)
GC _v	Visually scored ground cover (%)
GCD	Ground Cover of Dead material (%)
GCS	Ground Cover of leaves with Specular reflection (%)
IC	Intensity Class
IRI	Index of Reflection Intensity (%)
LI	Light Interception (%)
LAI	Leaf Area Index (-/-)
MSS	Mean Sward Spectra
MICS	Mean Intensity Class Spectra
NDS	Naturally Damaged Swards
NIR	Near Infrared wavelength range
PLS	Partial Least Squares
RE	Red Edge (nm)
SDM	Seasonal Dry Matter yield (kg ha ⁻¹ yr ⁻¹)
SE	Standard Error
SM	Seasonal Mean
TGC	Logistically Transformed Ground Cover (-/-)
TGC-SSD	Spatial standard deviation of TGC (-/-)
TCV	Tiller Coefficient of Variation (-/-)
VIS	Visible wavelength range
WE	Wavelet Entropy

1

General introduction

1. General introduction

In this thesis, the potential of imaging spectroscopy for characterisation of grass swards is studied. This chapter reviews the concept of imaging spectroscopy, information requirements for grass sward management and applications of imaging spectroscopy in agriculture. Finally, the potential of close range or proximate imaging spectroscopy is discussed and the objectives and the structure of this thesis are listed.

1.1 Imaging spectroscopy

Images can reflect various parts, called ‘bands’, of the electromagnetic spectrum *e.g.* grey value (black and white) images represent one (broad) band and colour images can combine up to three bands. Imaging spectrometry is defined as the acquisition of image data in many contiguous spectral bands (Goetz, 1992). The images are called multispectral when 10-15 bands are included and hyperspectral when (far) beyond this number. Imaging spectroscopy encompasses the complete process of data acquisition and image processing and interpretation. Imaging spectroscopy is used on a wide range of scales and has various applications, from earth observation in remote sensing to magnetic resonance imaging in medicine.

Just before the project started, new technology was developed combining dispersing elements with charge coupled devices (CCD) (Herrala & Okkonen, 1996). Light from a line entering the dispersing element is split up and projected on the CCD of a digital camera. With this new technology, hyperspectral images can be recorded instantaneously, providing means to combine high spatial resolution (small field of view per picture element) with a large number of spectral bands. A number of agricultural research groups have incorporated this technique into their research with focus on nitrogen in wheat and crop-weed differentiation (Borregaard *et al.*, 2000; Feyaerts & Van Gool, 2001; Jørgensen, 2002).

1.2 Grass sward characterisation

The term ‘grass sward’ normally refers to all material within the upper soil layer and above the soil in grasslands or lawns (Van Dale). In this thesis, only

above-ground parts of the sward are considered. Dairy husbandry systems under temperate climatic conditions mostly use grass as a major feed source. Grassland management and grassland productivity have a large impact on dairy farm profits (Rougoor *et al.*, 1999; Van Dijk, 1999). Vellinga & Van Loo (1994) calculated that (genetic) improvement of nitrogen (N) efficiency with 10% for *Lolium perenne* L. could increase annual farm profits with 54 – 179 € ha⁻¹, and an improvement of digestibility (5%) was expected to raise farm profits with 100-111 € ha⁻¹. Grass sward management also affects digestibility and N efficiency: digestibility is affected by N application and growth stage (Groot, 1999; Lazenby, 1988); N efficiency is strongly related to N application level and grass sward quality (Deenen, 1994; Mooij & Vellinga, 1993; Ten Berge *et al.*, 2000). N efficiency, nutritive value and dry matter (DM) yield of grass swards also strongly affect the farm nutrient balance and, thereby, emissions from farming systems to the environment (Smit *et al.*, 2003). Currently, grass sward management on farms largely depends on qualitative expert knowledge. Information for management decisions (grass sward renewal or renovation, optimal harvest time, fertiliser application and irrigation) is derived from guidelines and rules of thumb.

Fertiliser application

The fertiliser application guidelines recommend fertiliser supply based on an expected nutrient demand within the next growing period, corrected for the amount of nutrients available from the soil pool, *e.g.* residual nutrients from previous growth periods or mineralisation (Vellinga, 1998). These guidelines are based on relations found in field experiments. These relations are only valid for swards with characteristics similar to swards in these field experiments, and different relations may be required for other swards. Deenen (1994, p38) found that ‘sward quality strongly affects the absolute and marginal response of herbage and implicitly animal production to fertiliser N applied’. Therefore, N supply requires fine-tuning for differences in sward quality for a maximum N efficiency (Mooij & Vellinga, 1993). The correction for residual nutrients of previous growth periods requires an accurate estimate of the amount of nutrient removed with the harvested material. Currently, no fast and accurate methods are available to quantify DM- or nutrient yield. Another approach would be to monitor the degree of depletion of N in the soil pool available for plant uptake. Plants respond quickly to depletion of the soil N pool by adjusting leaf chlorophyll content, the fraction of assimilates allocated to the shoot, tillering

dynamics, leaf morphology and, consequently, growth rate (Van Loo, 1993). Therefore, growing plants themselves might be used as indicator of soil nutrient availability.

Grassland renovation and reseeded

Annually about 7-15 % of permanent grassland is reseeded in order to improve sward quality, mainly on sandy soils (Keuning & Vellinga, 1986; Anonymous, 2001; Aarts *et al.*, 2002). Sward quality is defined as the production capacity of a sward as determined by botanical composition and sward density (Lantinga, 1986), i.e. spatial distribution of plants and tillers. Sward quality deteriorates in case of local tiller or plant death as a result of *e.g.* frost or drought damage, urine scorch, treading, poaching or heavy cuts (*e.g.* Deenen, 1990; Keuning & Vellinga, 1986). Local tiller or plant death creates gaps, which may be filled with weeds (Keuning & Vellinga, 1986; Marriott *et al.*, 1997).

Grassland renewal or renovation is expensive, and may only be economically justified when swards are heavily deteriorated (Elsässer, 1991; Keuning & Vellinga, 1986; MacCarthy, 1982; Smith & Allcock, 1985; Spatz *et al.*, 1981). Sward renewal is economically attractive when the production increase compensates the cost of reseeded or renovation. Aarts *et al.* (2002) found that reseeded is economically justified at a yield increase of 18-23% at 5 year reseeded intervals and 10-15% at 10 year reseeded intervals. They concluded that there were no good judgement criteria for economically justified grassland renovation or reseeded.

Dry matter yield assessment

Accurate assessment of DM yield could provide valuable information for evaluation of management practices, fine-tuning of nutrient supply, harvest planning and comparison of fields and farms. The required accuracy of DM yield predictions for fertilization and planning practices on the farm is at least 10% (Harmony *et al.*, 1997; Sanderson *et al.*, 2001; Virkajärvi, 1999). Several methods have been developed to measure herbage mass (Hutchings *et al.*, 1990; Stockdale, 1984a; b; Vickery *et al.*, 1980). These methods depend directly or indirectly on a regression of sward height or sward density and herbage mass. Trampling or sward structure differences are major sources of error in this relation (Gabriels & Van den Berg, 1993; Gonzalez *et al.*, 1990; Hutchings, 1991; 1992; King *et al.*, 1986; Stockdale & Kelly, 1984). Accuracy of DM yield

estimates based on crop reflectance is comparable to plate meter estimates (King *et al.*, 1986; Lokhorst & Kasper, 1998). Gabriels & Van den Berg, (1993) & Lokhorst & Kasper (2001) concluded that the disk plate meter and crop reflection are not accurate enough for practical use.

1.3 Imaging spectroscopy in agriculture

Imaging spectroscopy may be used to study the spectral, spatial and textural characteristics from the object under study.

Identification of plant stress from leaf reflectance

The interaction of electromagnetic radiation with plant leaves is determined by their chemical and physical properties. In the visible region (VIS) from 400 to 700 nm, various pigments such as chlorophyll, xanthophyll, and carotene dominate leaf reflectance. In the absence of pigments in the near-infrared (NIR) from 700 to 1300 nm, leaf reflectance is mainly dominated by water absorption, cellular arrangement and leaf constituents (Büker & Clevers, 1992). Species, growth stage and environmental conditions determine the composition and concentration of plant pigments. Nitrogen deficiency can be identified through its effects on chlorophyll content (Bausch *et al.*, 1998; Blackburn, 1998; Blackmer *et al.*, 1994; Schepers *et al.*, 1996). Dehydration of leaves decreases light absorption by water, affects pigment light-absorption and changes internal leaf structure (Carter, 1991). Therefore, reflectance of dehydrated leaves increases in both visible and infrared wavelengths. These changes can be used to quantify water loss from leaf reflectance (Bowman, 1989; Danson *et al.*, 1992; Inoue *et al.*, 1993; Penuelas & Inoue, 1999; Ripple, 1986).

Concentrations of Mg, Zn, Fe and Mn are also closely related to chlorophyll content and leaf reflectance (Adams *et al.*, 2000a; b; Mariotti *et al.*, 1996; Milton *et al.*, 1991; Gáborčík *et al.*, 2000). Gausman *et al.* (1973) and Graeff *et al.* (2001) concluded that with specific wavelength ranges deficiencies of N, Mg, Fe, P and S could be identified from leaf reflectance.

Plant constituents (*e.g.* starch, lignin, cellulose and sugar) also affect leaf reflectance (Curran, 1989; Curran *et al.*, 1992; Jacquemoud *et al.*, 1996; Jacquemoud *et al.*, 1995). However, practical applications are severely limited by the strong confounding with water content (Fourty & Baret, 1998).

Discrimination of plant species

Various information sources from images were used to recognise plant species, such as recognition of leaf shape (Franz *et al.*, 1991a; Gerhards *et al.*, 1993; Guyer *et al.*, 1986; Manh *et al.*, 2001; Petry & Kuhbauch, 1989; Woebbecke *et al.*, 1995). Differences in spectral properties of leaves have also been used to discriminate between species (Franz *et al.*, 1991b; Shearer & Holmes, 1990). Crop reflectance may also be used to separate species (Borregaard *et al.*, 2000; Feyaerts & Van Gool, 2001). Critten (1997) used procedures to quantify image texture for species identification.

Remote sensing and imaging spectroscopy for agricultural applications

Until recently, crop reflectance was measured at spatial resolutions far beyond the size of individual leaves. Therefore, remotely sensed reflectance is a mixture of reflectance of leaves and background. Under low vegetation cover, litter and dead stubble material alter the measured reflectance signal (Asner, 1998; McCloy *et al.*, 1993). This mixed nature allows that intensity of canopy reflectance strongly responds to fraction of ground cover and leaf stacking (Birnie *et al.*, 1987; Bouman *et al.*, 1992; Gausman *et al.*, 1976). Relations between canopy reflectance and canopy characteristics typically have an asymptotic nature (Ripple, 1985). This asymptotic nature may explain the limited predictability of dry matter yield in grasslands from crop reflectance, as observed by Lokhorst & Kasper (1998).

Spectra of moist soils with normal organic matter and water contents lack strong absorption features, and reflectance of soils steadily increases with wavelength up to 1300 nm (Stoner & Baumgardner, 1981). Horler *et al.* (1983) found that derivative spectra are insensitive to soil properties, but sensitive to leaf area index (LAI). The red edge, defined as the position of maximum slope on the transition from red to infrared wavelengths, strongly correlates with chlorophyll content in various species, but is also sensitive to LAI and standing litter (Blackburn, 1998; Boochs *et al.*, 1990; Horler *et al.*, 1983). Therefore, the red edge informs on chlorophyll amount rather than concentration (Pinar & Curran, 1996). Interpretation of canopy reflectance is further complicated by the effects of leaf angle distribution on reflectance and red edge position (Asner, 1998; Guyot *et al.*, 1992; B ker & Clevers, 1992). Identification of environmental stress (e.g. drought stress) is complicated by simultaneous changes in LAI and ground cover, canopy geometry, fraction of dead leaf

material and background soil reflectance (Fernandéz *et al.*, 1994; Hunt *et al.*, 1987; Jackson & Ezra, 1985; Penuelas *et al.*, 1993; Ripple, 1986).

1.4 Potential of proximate imaging spectroscopy

Proximate imaging spectroscopy may combine the potential of leaf reflectance measurements, imaging and remote sensing. Grass canopies are characterised by a relatively long period of incomplete foliage cover, due to frequent defoliation (Alberda, 1968; Van Loo, 1993). Therefore, the background effects of dead material in the stubble and soil are expected to be considerable, especially shortly after cutting and in deteriorated swards with an open or heterogeneous canopy.

With proximate sensing, spatial resolution can be increased to sub-leaf level. With classification procedures, leaf pixels can be differentiated from pixels containing dead material and soil, prior to spectral analysis. This may strongly reduce the effects of background on measured spectra of leaves. The relative fractions of pixels in the different classes may inform about ground cover fraction. Recently, the fraction of ground cover was successfully estimated from (digital) images with high spatial resolutions (Lukina *et al.*, 1999; Tomasel *et al.*, 2001; White *et al.*, 2000; Zhou & Robson, 2001). In regular remote sensing, the use of spectral regions with strong water absorption features is limited due to water absorption in the atmosphere. Proximate sensing in combination with an artificial light source does not have this limitation.

1.5 Problem definition and objectives

Ground cover, the spatial distribution of leaf pixels and reflectance of leaves can be measured with proximate imaging spectrometry. Ground cover and the spatial distribution of leaf pixels may inform about growth and status of the grass-sward and accumulated dry matter above the ground. Leaf reflectance may inform about the occurrence of nitrogen- and water stress and leaf constituents.

It is yet unclear whether leaf reflectance can be measured in standing grass swards or can accurately quantify and diagnose stress. It is also unclear how and to what extent reflection of individual leaves is affected by the canopy. Shadow, overlapping leaves, leaf angle, canopy density and spatial variability may be factors influencing the measured reflectance of leaves. It is also unclear

whether sward biomass and heterogeneity can be quantified accurately from images. The sensitivity and temporal aspects of leaf reflectance for stress detection in systems with a short defoliation interval is unknown.

There were three major objectives in the study reported by this thesis. The first objective was to develop and build an experimental imaging spectrometry system, capable of recording reflection of leaves within a standing grass sward in the visible and near infrared wavelength range. The second objective was to derive and select parameters from the images that characterise growth and heterogeneity and identify nutrient- and drought stress. The third objective was to study and quantify the relation of image parameters with growth, DM yield, sward heterogeneity and growth capacity, degree of N and drought stress and nutritive value of grass swards. During the study, the requirements of a field application of imaging spectroscopy were always kept in mind.

1.6 Structure of this thesis

In Chapter 2, the experimental imaging spectroscopy system is described. During the project, five experiments were conducted (four in 2000 and one in 2001), with mini swards in containers. The degree of sward damage, clover content, N (2000 and 2001) and water supply varied. The sward damage experiment was used to study the relation between ground cover and reflection intensity and light interception, leaf area index and DM yield (Chapter 3). The relation between changes in sward characteristics in relation to N supply and image parameters are discussed in Chapter 4. Chapter 5 gives more detail about the underlying factors affecting the relations found and presented in Chapter 4. In Chapter 6, the response of image parameters was studied in relation to swards under (severe) drought stress. Chapter 7 describes the relation between image texture from one image dimension and presence of clover within a sward. Data from the sward damage experiment were also used to study the relation between image parameters with sward density, spatial heterogeneity of swards and seasonal DM yield (Chapter 8). In Chapter 9, data from the 2000 N- and sward damage experiments were used to study the accuracy and robustness of predictions of yield, nutritional value and mineral content, combining information from spectra, ground cover and reflection intensity. Chapter 10 presents an overview and a general discussion in relation to the objectives of this thesis and to practical implications from a technical and agronomic point of view.

2

Novel Imaging Spectroscopy for Grass Sward Characterisation

A.G.T. Schut, J.J.M.H. Ketelaars, J. Meuleman, J.G. Kornet & C. Lokhorst

Based on Biosystems Engineering 82, 2002 pp.131-141

2. Abstract

Attempts to improve grassland management may benefit from the use of new sensing techniques, such as imaging spectroscopy. In order to explore the potential of hyperspectral imaging spectroscopy for rapid and objective characterisation of grass swards an experimental prototype has been developed. From a height of 1.3 meter, the system detects reflections at high spatial (0.28-1.45 mm²) and high spectral resolutions (5-13 nm) at wavelengths between 405 and 1659 nm. Detailed information is provided on design, characteristics and test results. Results show that reflection intensity is related to height position in the sward and leaf angle. Grass leaves were recognised accurately. Images of a sports-field and a production sward with similar ground cover fractions could be easily distinguished. With the described system, canopy structure can be characterised by ground cover, the distribution of reflection intensity, image texture. Spectral characteristics can be obtained at leaf level.

2.1 Introduction

Grass swards are known for their high spatial and temporal variability, due to disturbing events such as cutting and grazing, urine scorching, trampling, frost and drought damage. As a result, ground cover pattern becomes irregular and gaps in the canopy occur. In the past several (laborious) methods have been developed to describe this irregular cover pattern, such as expert estimates, absence frequencies in rings (Neuteboom *et al.*, 1992) and light sensitive cells using red/infrared ratio (Silvertown *et al.*, 1988). Digital imaging techniques provide objective and automatic means for canopy characterisation, and have been used to estimate coverage in wheat (Ewing & Horton, 1999; Lukina *et al.*, 1999). Hyperspectral reflection measurements on leaves correlate *e.g.* with chlorophyll, nitrogen (Blackburn, 1998; Blackmer *et al.*, 1994; Schepers *et al.*, 1996) and water content (Bowman, 1989; Curran *et al.*, 1992; Danson *et al.*, 1992) and can, therefore, be used as water and nitrogen stress indicators. Imaging spectroscopy combines the potential of digital images and hyperspectral measurements. In remote sensing, imaging spectroscopy has been used to estimate nitrogen and lignin content of forest canopies (Martin & Aber, 1997; Zagolski *et al.*, 1996) and recognition of weed species (Vrindts & de Baerdemaeker, 1997; Vrindts *et al.*, 1999). Reflection patterns (Asner, 1998)

and red edge position (Blackburn, 1998) are strongly influenced by standing litter. To explore the full potential of imaging spectroscopy in heterogeneous canopies, pure and unmixed spectra of leaves are required. In this paper, a novel hyperspectral imaging spectroscopy assembly for grass sward characterisation is described, with detailed information about requirements, construction, the equipment used and tests results.

2.2 Design of the experimental system

2.2.1 Design criteria

The assembly is developed to produce images of mini grass swards, grown in containers of 0.7 m wide, 0.9 long and 0.4 m high. Hence a number of criteria are formulated. The assembly has to make images from the zenith, since the range in which ground cover changes during growth is largest at this angle. To obtain a high fraction of pure leaf area pixels, pixel diameter has to be smaller than 0.2 mm (one tenth of minimum leaf width of *Lolium perenne* L., about 2 mm). The spectral range should include regions where soil, dead material and grass can be discriminated, and where minor changes in chlorophyll and water content can be detected. For detecting changes in chlorophyll content, mostly the red and green edge (Blackburn, 1998; Blackmer *et al.*, 1994; Schepers *et al.*, 1996) are used. Water is mostly detected in the regions around 970, 1200 and 1450 nm. Water absorption features overlap with those of starch, lignin, cellulose and sugar (Curran, 1989). At least four spectral bands are required, to detect the inflection point of an edge (Guyot & Baret, 1988). Detection of small changes in the edge regions requires resolutions smaller than 10 nm. For an accurate estimate of ground cover and a representative spectral curve for one sward, it is not needed to make a two-dimensional (2D) image covering the complete container. With a good sampling routine, recording time is limited and amount of data is reduced. The system should be able to sample in a regular pattern.

The combination of high spatial and high spectral resolution requires high irradiances throughout the sward profile. Direct light, contrary to diffuse light, can be focused on a small area minimising energy inputs. When light is projected on a surface under an angle, shadows will be produced. To minimise this effect, the angle between light beam and measured reflection is minimised.

Table 2.1 Sensor characteristics and charge coupled device (CCD) camera type.

Sensor	Spectral range, <i>nm</i>		Spectral resolution, <i>nm</i>	Spectral bands, #	CCD type	CCD	
	<i>from</i>	<i>up to</i>				<i>rows</i>	<i>columns</i>
V7	405	710	5	565	Silicium	768	565
N10	675	970	5	565	Silicium	768	565
N17	906	1659	13	128	InGaAs	128	128

2.2.2 Choice of sensors

The imaging spectrometer technology combines high spatial and high spectral resolution. The reflectance spectrum of points on a narrow line is measured (Herrala & Okkonen, 1996). An image of one line will be referred to as image line. With a 768 by 565 pixel charge coupled device (CCD) camera, 768 spectral curves are made per image line, where each spectral curve is built up by 565 elements, or 'spectral bands'. Three imaging spectrometers, the V7 (405-710 nm), N10 (675-970 nm), and N17 (906-1659 nm) with an 80 μm slit are used. Each sensor consists of four parts, an objective lens, spectrometer, camera (see Table 2.1) and light source, and will be referred to as the V7, N10, and N17. The V7 sensor uses a 768 by 565 pixel CCD camera, with a high sensitivity in the blue region of the spectrum. This camera is modified to control exposure time. A xenon (flash) light source is used, in combination with fibreglass, for a high and constant light yield in the blue region of the spectrum. As a result of the relatively strong emission of xenon around 530 and 542 nm, the number of flashes per image is limited by the surface with the highest reflection value (the reflection standard). The N10 sensor uses a 768 by 565 pixel CCD camera with a high-pass filter, transmitting only wavelengths above 590 nm. The camera has a high sensitivity above 900 nm. A normal 300 W halogen light source is used, with a reflector at the back of the light bar. The N17 sensor uses an InGaAs camera, equipped with a high-pass filter, through which wavelengths above 960 nm can pass. For all sensors lenses with 75 mm focal length are used, which are focused on the soil surface, yielding an instantaneous field of view (FOV) of 60.66° . This corresponds with a FOV per image line point of 7.9×10^{-2} degree for the V7 and N10 and 47.4×10^{-2} degree

for the N17 sensor. The sensors are calibrated according to the manufacturer's manual.

The distance to the container is the same for each camera, ranging from approximately 1.05 m (sward top) to 1.3 m (for the soil surface). Due to the combination of CCD and lens characteristics, pixel area increases with distance to the sensor, as shown in Table 2.2. Reflection is measured relative to a reflection standard. Reflection of this standard increases from 49.5 to 54.7% from 400 up to 1660 nm, as shown in Table 2.3.

Table 2.2 Pixel resolution as a function of distance from the sensor.

Sensor	Pixels per image line	Distance from sensor, m	Length of image line, mm	Width of image line, mm	Pixel area, mm ²
N17	128	1.0	102.4	1.07	0.856
		1.1	112.6	1.17	1.029
		1.2	122.9	1.28	1.229
		1.3	133.1	1.39	1.445
V7, N10	768	1.0	117.3	1.07	0.163
		1.1	129.1	1.17	0.197
		1.2	140.8	1.28	0.235
		1.3	152.5	1.39	0.276

Table 2.3 Reflection of standard reflection surface as a function of wavelength.

Sensor	Wavelength, nm	Reflection, %
V7	400	49.5
	700	50.8
N10	670	50.7
	970	52.3
N17	900	52.2
	1660	54.7

2.2.3 General construction

In Figure 2.1, the schematic configuration of the assembly is given. With a horizontal sensor orientation in combination with mirrors, instrument height can be limited. The lower sensors are shifted horizontally preserving an equal distance to the soil for each sensor. A bar lens is placed in front of the light sources to concentrate light on a narrow line. Light sources are located near the sward, to maximise light intensity. Extra cooling elements are placed above the halogen lamp to prevent the cameras from heating. The light beams are redirected by mirrors (aluminium coated, first-surface), which are moved by air pressure to select the right light source and camera combination. With these mirrors, each sensor can record identical objects. The angle between incoming light and measured reflection is 2 degrees. The sensors and mirrors are connected to a XY step-table. This assembly (sensors, mirrors and XY table) is placed on a portal cart, which can ride over the grass containers. The reflection standard is placed in a small box to prevent contamination, 18.5 cm above soil surface. The portal is completely covered eliminating sunlight influences. At

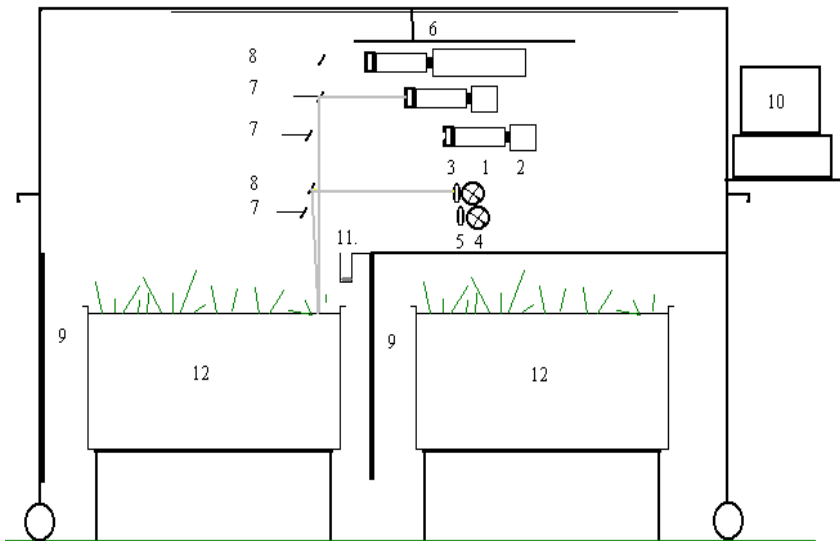


Figure 2.1 Schematic configuration (1) spectrograph; (2) camera; (3) objective lens; (4) light source; (5) bar lens; (6) translation table; (7) displaceable mirror; (8) fixed mirror; (9) light blocking curtain; (10) personal computer controller; (11) reflection standard; and (12) grass sward container.

the sides of the table, two black curtains are placed which can be moved for transport. The positioning of XY translation table, the mirrors and the sensors are controlled by a personal computer (PC). A frame-grabber is used to load the images in the PC, equipped with a compact-disk writer, for easy data storage and transport. A software program is written to operate the cameras, light sources, step-table, and mirrors. Images are stored as bitmap files and have standard names. These names are supplied with experimental code, container number, treatment, sensor, date and x - and y - position in the container, available from an input file. The names of the recorded images are stored in a log file. The step-table operation scheme is stored and operated in a separate driver, and the image taking process in the PC software is tuned with this driver scheme.

2.3 Operation of equipment

2.3.1 Procedure for taking images

The portal can be placed above a container, with a horizontal accuracy of 2.5 cm. When the portal is fixed on its position, curtains are lowered and the sampling procedure starts. First, the step-table is moved to the position of the reflection standard. Background images (images recorded with light sources off) and five image lines at distance of 1 mm are taken at the reflection standard to eliminate minor texture effects. At every stop of the step-table the sensors take their images one by one, after moving mirrors and switching on the accompanying light source. Image lines are taken in a regular scheme within a net area of 50 cm by 70 cm (Figure 2.2). After taking the images of the standard, the XY table moves along the three tracks, in the direction as indicated in Figure 2.2. In total, 126 image lines per container are made (42 images per sensor). The images are stored on the PC hard disc. After a day of scanning, images are written to a CD in a zipped format. Sampling one container takes 5 minutes. Including the time needed for moving the portal, a total of 8-10 containers per hour can be sampled. The software can also be instructed to scan adjacent image lines, for construction of a 2D image. The XY step-table is then moved one mm (perpendicular to the image line) for each image line and 10 minutes for 100 adjacent image lines are required (a surface of 10 long and 15 cm wide).

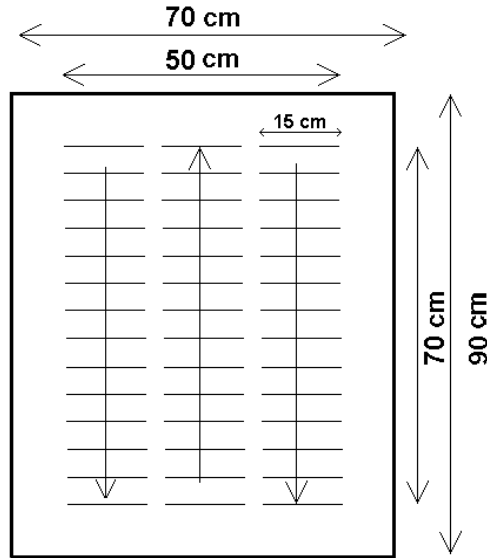


Figure 2.2 Position of image lines in container mini sward.

2.3.2 Processing of images

To handle the large amount of data, a software program is written. The procedures in this program are optimised for images in imaging spectrometry format. When an image is opened, from the image names, container and sensors are recognised and the appropriate reference and background image(s) are opened. The spectral range divided by the number of bands is larger than the spectral resolution. Thus, individual bands overlap and adjacent bands are highly correlated. To minimise calculation time, values are integrated over 4 pixels in the spectral direction. Then, the relative reflection R is calculated for each pixel on the image line and for each spectral band according to:

$$R_{ij} = R_s \frac{I_{ij} - B_{ij}}{S_{ij} - B_{ij}} \quad (1)$$

Where: R_s is the reflection percentage of standard surface; I is the input image line; B is the image line of background (dark); S is the average image line of the

reflection standard; i is the spectral band; and j is the pixel number on the image line.

The image of the reflection standard S is an average of five images, to minimise texture effects. The standard reflection R_s is a function of wavelength and is linearly interpolated between the minimum and maximum wavelength for each sensor (see Table 2.3). After this, images were filtered with a 5 by 5 median filter.

The software is developed to handle image lines and can construct 2D images based on image lines. For classification of the images, the software uses the log file produced by the image taking process. Classification procedures are developed to classify images of one sensor at the time. With one command, all images taken on the same day can be classified. Output of the classification procedures consists of three text files. In the first file an average classification result of coverage per image, grouped per container is given.

In the second file, for every classifier defined, an average reflection curve per container is given, based on pixels assigned to that class. When classifying a grass sward in different grass classes, one might be interested in an average reflection curve for the complete sward. For this, a third output file is generated with, for each container, an overall average spectral curve for a group of classifiers (*e.g.* all grass pixels). Reflection intensity was found to be a function of canopy height (see Section 4). Before averaging over classes, spectral curves are corrected for this effect according to the following function:

$$R_{n,ijk} = \frac{R_{ijk}}{R_{r,jk}} \quad (2)$$

where: R_n is the normalised reflection; R is the reflection value; R_r is the reference reflection; and k is the sensor.

The reference reflection R_r is the average reflection over a range of bands that are (1) always above zero, and (2) relatively insensitive for changes in water and pigment content. The chosen ranges are 550-555 nm, 800-850 nm and 1070-1100 nm for the sensors V7, N10, N17, respectively. The range 550-555 nm does show some absorption features. Under the assumption that both the collection of objects from which reflectance is measured and sensor sensitivity in the overlapping spectral range (from 675 nm up to 709 nm) from the V7 and N10 sensor is comparable, the V7 spectral curve can be normalised to 800 - 850 nm. These assumptions can be made for the V7 and N10 sensors if the spectral curve is an average of a large number of pixels, which is the case for the

average spectral curve per container for a group of classes. The normalised reflection of the V7 sensor can be transformed to reflection normalised at 800-850 nm ($R_{n, V7-N10}$), according to:

$$R_{n, V7-N10} = A \times R_{n, V7} \quad (3)$$

The value of A can be calculated from reflection in the overlapping spectral region.

In this region the average reflection value should be equal for both the V7 and N10 sensor. Accordingly, the ratio between the V7 and N10 sensor response can be attributed to the ratio between 550-555 nm and 800-850 nm:

$$A = \frac{R_{n, avN10}}{R_{n, avV7}} \quad (4)$$

where $R_{n, av}$ is the average R_n over the overlapping spectral region (675 to 709 nm).

For supervised classification, there are two methods: applying a predefined description of the spectral curve using thresholds for reflection values and ratios; applying a set of spectra on which a classifier can be trained (*e.g.* with maximum likelihood or nearest neighbours). The first procedure is simple and relative insensitive for changes in chlorophyll and water content but uses only a limited number of spectral bands. The second method is mostly used in remote sensing, since a large number of bands can be used for classification. The quality of the trained classifier depends strongly on the quality of the training set.

For using the first procedure, spectral curves of various sward elements were measured individually with the equipment. These spectral curves were characterised, for each sensor, by simple thresholds and ratios, where boundaries of classes cannot overlap. Boundaries between grass, soil and dead material were optimised by calibration with visual ground cover scores. With these sharply defined class boundaries, spectra can be selected from a collection of images. These selected spectra can be used to construct a spectral library, on which classifiers can be trained. With a normal PC with a Pentium III

processor, the full sequential process of opening images and classification takes 20 s per container for the V7 and N10 images, and 10 s for the N17 images.

2.4 Influence of leaf position in the sward and leaf angle

2.4.1 Experimental testing

Although a bar lens is placed in front of the light source, light beams still diverge a little. The effects of this phenomenon on light intensity per pixel and relative reflection of a standard surface as function of position in the sward were tested. The light intensity was measured on different heights in the grass sward. For the halogen light source, the voltage of the electric signal of a 1 cm² light sensitive cell is measured. For the xenon flashlight the maximum amplitude of the electric signal produced by that cell is measured. Also image lines were made of a 10 cm by 15 cm standard reflecting (50%) surface at different positions in the canopy. For each image line, reflection was averaged over all spectral bands and over all pixels on the image line. Also the effect of leaf angle on leaf reflection was measured. For this, three leaves were fixed on a plate covered with a black cloth with the upper cuticle up, and connected on a plate that could rotate around its axis. This axis was perpendicular to the image line, with its centre exactly under the image line. The leaves were at a similar height position as the reflection standard, and oriented perpendicular to the image line. While images were taken, the plate was rotated around its axis. The maximum reflection value was recorded for each leaf, and averages were taken from the three leaves.

2.4.2 Reflection measurements

Figure 2.3 shows that irradiance decreases with distance by a third order polygon for xenon, and linearly for Halogen. This difference can partly be attributed to the positioning of the bar lenses. For xenon the distance between fibreglass and bar lens is fixed, and there is only one focal point. The reflector behind the halogen lamp produces multiple focal points, and the light beam is built up by several overlays, causing the linear decline in light intensity. In Figure 2.4 the reflection of a 50% reflecting surface is given as function of the position in the sward. Positions higher in the canopy yield higher reflection

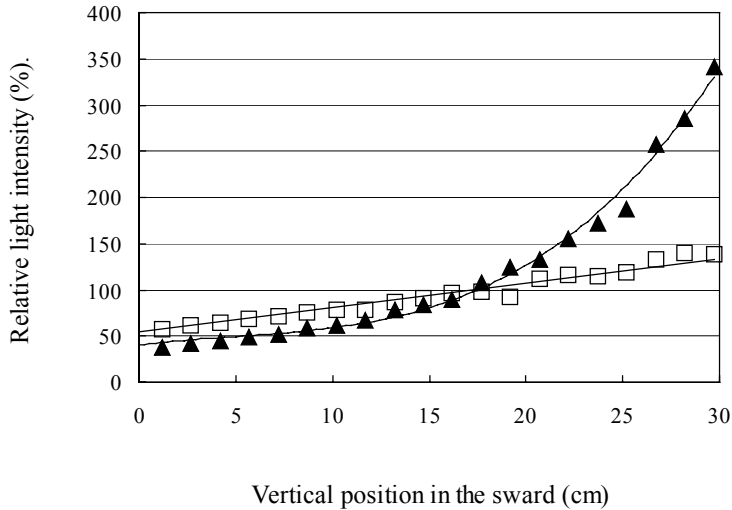


Figure 2.3 Light intensity relative to the reflection standard (at 18.5 cm) of the xenon (▲) and halogen (□) light source as function of vertical position (in cm above soil surface) in the sward; for halogen a linear function and for xenon a third order polynomial was fitted.

values. The character of this increase is quadratic. Above 20 cm sward height the V7 camera is saturated. Although the N10 and the N17 use the same light source, the N10 shows a stronger effect of sward height, as a result of camera characteristics. The decline in reflection with positions deeper in the sward is caused by a combination of two effects, (1) changes in irradiance level and (2) the fraction of the reflecting sphere intercepted by one pixel. This is shown in Figure 2.5 for the N10 and N17 sensor, where the effects are expressed as fraction compared to the position of the 50% reflecting standard. The fraction of the reflecting sphere intercepted by one pixel is calculated as a $1/r^2$, where r is equal to the distance from the sensor. The combined effect of irradiance and fraction of the reflecting sphere intercepted yields a similar curve as in Figure 2.4. Thus with this configuration of lenses and light source close to the reflecting surface, the amount of reflection can be used as measure of distance to the sensor and thus the position of the reflecting surface in the sward.

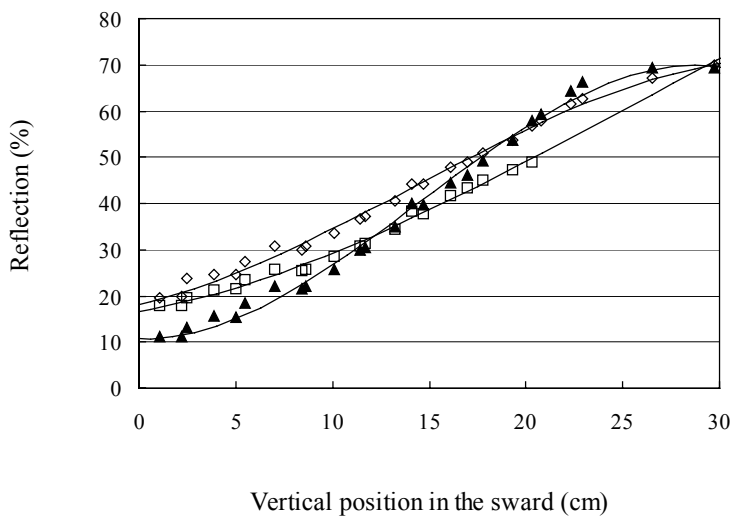


Figure 2.4 Reflection of a 50% reflecting surface as function of vertical position in the sward for the three sensors V7 (□), N10 (▲) and N17 (◇).

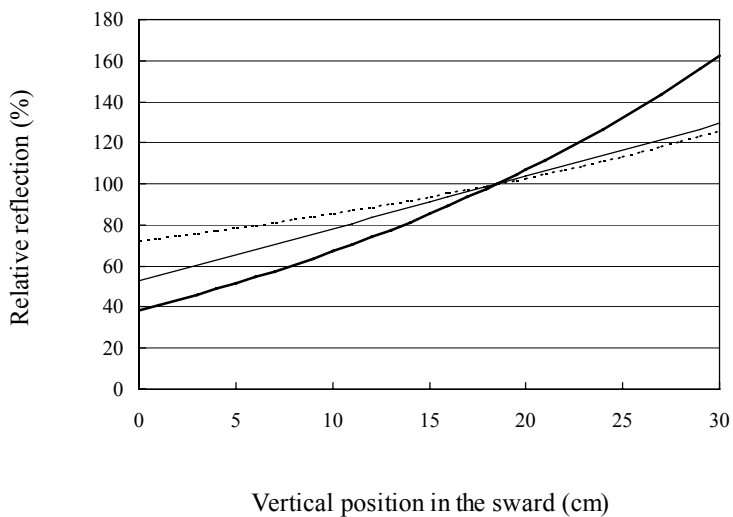


Figure 2.5 The decreasing reflection decomposed into the effects of distance (---), irradiance (-·-) and combined effect (—) for the N10 and N17 sensor.

Leaf angles also play an important role. Reflection values increase when leaf angle with the horizontal plane decreases, as shown in Figure 2.6. In horizontal position, reflection is extra strong due to specular reflections. These specular reflections are additive to the normal body reflection, at all wavelengths. The effects of leaf angle on reflection of individual leaves, is comparable to the effects of leaf angle distribution on reflection at the canopy scale (Asner, 1998; Clevers & Verhoef, 1993). In grass swards, leaves are oriented more horizontal at higher canopy positions. As a result, the effect of increasing reflection at higher canopy positions, as described above, will be even more pronounced.

In Table 2.4, class boundaries are defined for soil, a class with both pixels of dead material and soil (DSoil), a class with both pixels of green material and soil (GrSoil), and classes of dead and green material and grass leaves with specular reflections. These latter classes are subdivided into a number of intensity classes (IC). The number of IC's and the boundaries are arbitrarily chosen. For the separation of these IC's, the 550, 746 and 1100 nm wavelengths are used. These wavelengths are selected since they have a relatively neutral response to changes in pigment and water concentration. The boundaries

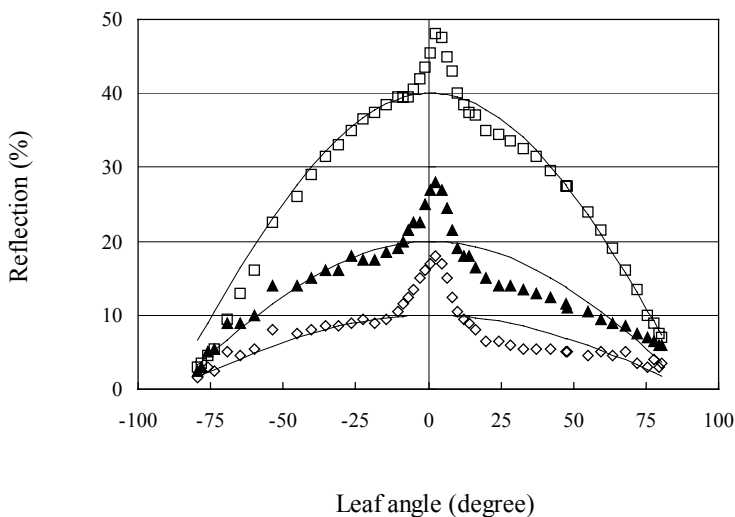


Figure 2.6 Reflection of a grass leaf (at a sward height of 18.5 cm), as function of leaf angle (defined relative to the horizontal plane) for 550 nm (▲), for 600 nm (◇) and for 800 nm (□).

Table 2.4 Classification boundaries for library spectra.

Main class Intensity class		Discriminating wavelengths (wvl), and minimum (min) and maximum (max) reflection thresholds per class for each sensor								
		V7			N10			N17		
		wvl*	min,%	max,%	wvl*	min,%	max,%	wvl*	min,%	max,%
Soil		680	0.00	3.00	683	0.00	4.99	985	0.00	6.99
		680/550	1.00	100.00	746	0.00	4.99	1100	0.00	7.99
GrSoil					683	0.00	4.99	985	0.00	6.99
					746	5.00	7.99	1100	8.00	100.00
					683/746	0.00	0.49			
DSoil		680	3.01	4.00	746	5.00	7.99			
		680/550	1.00	100.00	683/746	0.50	100.00			
Grass	All**	680/550	0.00	0.99	683	0.00	6.50	985	7.00	100.00
	All**	450/550	0.00	0.50	683/746	0.00	0.49	1450/1100	0.00	0.70
	0	550	1.00	2.00	746	8.00	9.99	1100	8.00	14.99
	1	550	2.01	3.00	746	10.00	12.99	1100	15.00	17.99
	2	550	3.01	5.00	746	13.00	18.99	1100	18.00	21.99
	3	550	5.01	7.00	746	19.00	24.99	1100	22.00	26.99
	4	550	7.01	9.00	746	25.00	30.99	1100	27.00	29.99
	5	550	9.01	12.00	746	31.00	36.99	1100	30.00	33.99
	6	550	12.01	100.00	746	37.00	100.00	1100	34.00	39.99
	7				746	43.00	49.99	1100	40.00	45.99
	8				746	49.00	54.99	1100	46.00	51.99
9				746	55.00	60.99	1100	52.00	60.99	
10				746	61.00	100.00	1100	61.00	100.00	
Dead	All**	680/550	1.00	100.00	683/746	0.50	100.00	1450/1100	0.7001	100.0
Material	0	680	4.01	6.00	746	8.00	17.99	1100	8.00	12.99
	1	680	6.01	9.00	746	18.00	28.99	1100	13.00	23.99
	2	680	9.01	12.00	746	29.00	60.00			
	3	680	12.01	20.00						
Grass with	All**	450/550	0.501	1.00	683	6.51	100.00			
Specular	All**	680/550	0.00	0.99	683/746	0.00	0.49			
Reflection	0	550	2.01	6.00						
	1	550	6.01	12.00						
	2	550	12.01	100.00						

* Absolute values or ratios (e.g 680/550, reflectance at 680 nm divided by reflectance at 550 nm)

** These boundaries and discriminating wavelengths apply to all intensity classes within a main class

consist of threshold values or ratios of specific wavelengths. Soils containing normal levels of iron and organic matter typically have reflection values below 30% throughout the spectral region of 400-1650 nm, with a maximum around 1300 nm (Stoner & Baumgardner, 1981). Soil reflection is further reduced by its low position in the sward. As a result, reflection of soil is only a fraction of leaf reflection. Consequently, only a few wavelengths are needed with a high contrast between soil and green material for classification. For the V7 sensor the following wavelengths are needed: the ratio between reflection in the green (550 nm) and red (680 nm) for recognition of green material. When reflection at 550 nm is higher than the reflection at 680 nm, the pixel is classified as green material. The ratio between blue (450 nm) and green (550 nm) is needed for recognition of leaves with clear specular reflection. For the N10 sensor, the occurrence of a red edge, defined as a maximum reflectance ratio of 0.5 between red (683 nm) and infrared (746 nm), is sufficient for recognition of green leaves. For the N17 sensor, green material can be recognised by the 1450 nm and 1100 nm reflectance ratio. Boundaries were optimised for detecting grass leaves, based on visual judgement of example images and comparison with visual cover estimates. With an average leaf angle of 45°, the boundaries of the IC's, combined with the reflection characteristics from Figure 2.3, can be used to derive a distance estimate. Horizontal grass leaves, positioned at a similar height as the reflection standard, have typical reflections of 15, 43, and 41% at 550, 746 and 1100 nm. Combining these reflection values with the equations in Figure 2.4 and Figure 2.6, the boundaries of the IC's can be used to calculate a sward height estimate. For a large number of pixels, IC's can be related to an average sward height (for the V7 sensor: grass IC 1 < 3.5 cm, grass IC 2 < 9.5 cm, grass IC 3 < 14.5 cm, grass IC 4 < 18 cm, grass IC 5 < 21.5 cm, grass IC 6 > 21.5 cm). These distance estimates have to be used with caution. The assumption of an average leaf angle of 45° is only valid when large numbers of pixels are measured, including all leaf angles. The fraction of mixed pixels and overlapping leaves also influence the sward height estimate.

2.5 Images of grass swards

In Figure 2.7 clockwise a normal photo, a false colour image of the V7 sensor, a classified V7 sensor image and a N10 sensor image of a small grass sward (15 cm by 10 cm) are depicted. Due to the non-square pixels (0.2 mm by 1.4 mm),

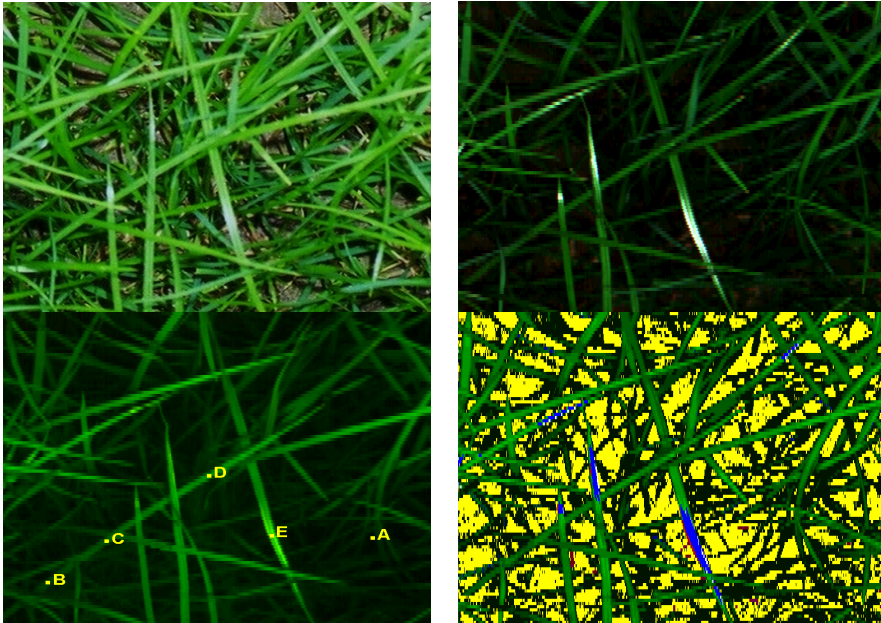


Figure 2.7 Photo of a 18 cm high grass sward (left top), false colour image (red=680 nm, green=550 nm, blue=450 nm) from the V7 sensor (right top), false colour image (red=680 nm, green=800 nm, blue is not used) from the N10 sensor (left bottom), and the V7 sensor image classified (right bottom); for explanation of the letters A, B, C, D and E see Figure 2.8.

leaves perpendicular to the image line appear sharper than parallel oriented leaves. In the images a clear distinction between soil and grass can be made. Due to the effect of canopy height on reflection, intensity can be used as depth estimate. In general, brightness increases from the origin of the grass plant to the leaf top. This can be seen in Figure 2.8, where spectra of points indicated by marks B, C, and D in Figure 2.7 are given. With this characteristic, an image of a sports field (Figure 2.9) looks very different from a production sward image (Figure 2.7). Leaf angles have a major impact on reflection intensity (Figure 2.5). On horizontal leaves, specular reflections are visible. In the V7 image they appear stronger than in the N10 image, since reflection values show a relatively large increase at low reflection values. The occurrence of these specular reflections can be used as indicator of leaf angle distribution.

2.5.1 *Discrimination and classification*

The spectral curves of points indicated in Figure 2.7 are shown in Figure 2.8. Soil (A) has low reflections at all wavelengths, as result of its reflection characteristic and low canopy position. Reflection values of grass leaves close to the plant base (B) show lower reflection values than pixels at intermediate positions (C) and at higher canopy positions (D). Horizontal leaves with specular reflection (E) have normal grass spectra, where the reflection values are increased by an additive term, equal for all wavelengths. The sensors react differently on the effect of sward height, and therefore the additive term appears slightly different for each sensor. The V7 sensor images are classified according to the boundaries in Table 2.4 and depicted in Figure 2.7 and Figure 2.9 in the right bottom image. The colour green is assigned to grass classes, red to dead material, blue to specular and yellow to soil. A brighter colour corresponds to a higher intensity class. All unrecognised pixels appear white. With this simple classification, grass, leaves with specular reflections, soil and dead material in different intensity classes are recognised. Even better results could be obtained with sharper definitions of the classes, but then classification becomes sensitive for temporal changes in leaf water and pigment content. As can be seen in the classified images, mixed pixels (mixels) of soil and grass occur at the leaf edges. These mixed pixels are assigned to a lower IC, when compared to the centre of the leaf. Due to the very low reflection values for soil, mixels containing soil and grass will have the grass reflection characteristic, but reflection values will be diluted by the fraction of soil in the pixel. The resulting spectral curve will be similar to pure grass pixels lower in the canopy. The classification of the V7 image in Figure 2.7, with the boundaries in Table 2.4, yielded the following ground cover estimates: 30.2% soil, 0.4% dead material, 36.8% grass IC 0, 9% grass IC 1, 11% grass IC 2, 7% grass IC 3, 3.5% grass IC 4, 1.0% grass IC 5, 0.1% grass IC 6 and 1% specular. The V7 image in Figure 2.9 yielded: 27% soil, 7% dead material, 31% grass IC 0, 22% grass IC 1, 12% grass IC 2 and 1% grass IC 3. Although total ground cover, calculated as sum of all grass classes and the specular class, was similar for the sports field (66%) and the production sward (69%), the production sward can be easily distinguished by the occurrence of the higher intensity classes grass IC 4, grass IC 5, grass IC 6 and the specular classes.

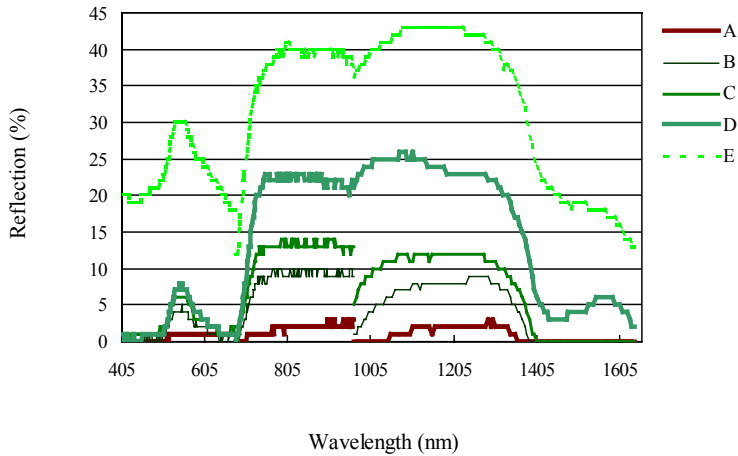


Figure 2.8 Spectral curves of soil (A), grass leaves (B, C and D) and a grass leaf with specular reflection (E) as indicated in Figure 2.7.

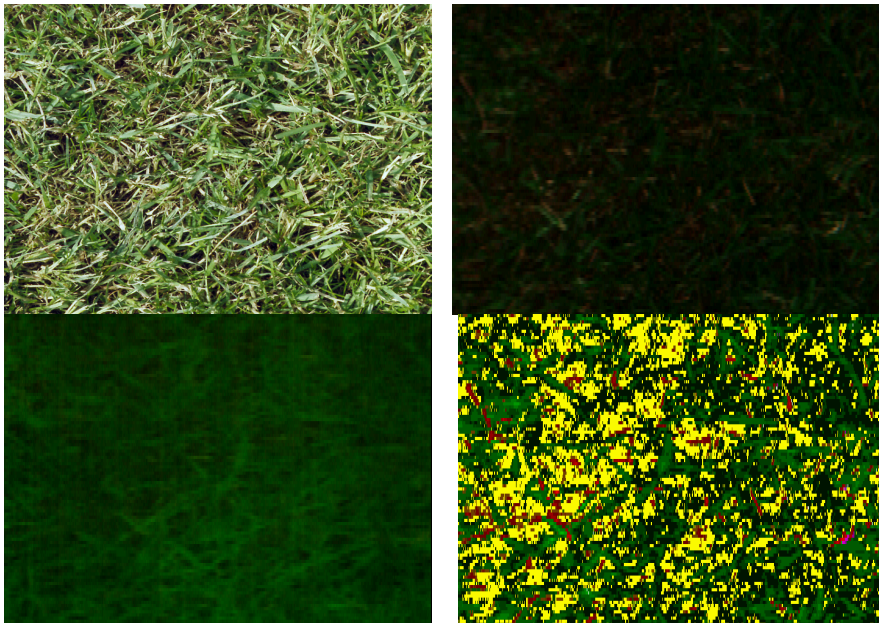


Figure 2.9 Photograph of 3 cm high sports-field grass sward (left top), a false colour image (red=680 nm, green=550 nm, blue=450 nm) from the V7 sensor (right top), a false colour image (red=680 nm, green=800 nm, blue is not used) from the N10 sensor (left bottom), and the V7 sensor image classified (right bottom).

2.5.2 *Prospective applications*

As shown in the previous section, ground cover can be easily estimated with the described imaging spectroscopy system. In most periods of the growing season, ground cover of grass swards is incomplete (Alberda, 1968). Therefore, pixels in most remote sensing applications are a mixture of soil, grass leaves and dead material. In the described assembly, spatial resolution is much higher than leaf dimension, yielding mostly unmixed pixels. As result, leaf reflectance is independent of soil and dead material in the background, and evolution of ground cover and spectral composition of leaf reflectance can be studied separately. In future papers, the temporal dynamics of ground cover, reflection intensity distribution, spectral composition of leaf reflectance and image texture, in relation to sward quality and nutrient and water supply, will be studied in container experiments. Also the relation between these parameters and other sward descriptors (*e.g.* visual ground cover estimates, biomass, leaf area index *etc.*) will be studied.

Although the described assembly is designed for container experiments, it can be used in field applications. In the field, a number of factors will vary stronger than in the mini sward containers. An important difference between the containers and the field are lighting conditions, as it is difficult to eliminate sunlight influence. It is not necessary to exclude sunlight completely, as long as it is only a minor fraction of the total irradiation. Another approach would be to accept some sunlight influence and eliminate it later when processing the signal. A different challenge is spatial variation in soil spectral characteristics. Discrimination between soil and green material is, however, not expected to give extra problems. Firstly, most soil spectra are quite similar in the 400-1650 nm domain, as iron oxide and organic matter absorption features dominated them. Secondly, reflection intensity from the soil surface is low, since soil is in a low canopy position. Small-scale soil level variations in the field might influence the recorded reflection intensity. This effect can be limited by adjusting the position of the light source to the soil level under measurement. An alternative is the correction of the reflection intensity according to the reflection intensity of soil pixels.

2.6 Conclusion

In most periods of the growing season, ground cover of grass swards is incomplete. Therefore, pixels in most remote sensing applications are a mixture of soil, grass leaves and dead material. In the described assembly, pixel width is much smaller than leaf width, yielding mostly unmixed pixels. The assembly was designed to obtain a spectral curve from 400-1650 nm for each pixel. Although image lines of the sensors overlap, they could not be positioned accurately enough to match on pixel level. Bar lenses were used for light focusing to reduce required energy inputs. Despite these lenses, irradiance levels and even more leaf reflectance decreased with positions deeper in the grass sward. This characteristic can be used to study the geometry of swards. To fully exploit this phenomenon, a balanced sensor design is required, in order to obtain reflection values above noise level at low canopy position, and still within the dynamic range of the camera at high canopy position.

Soils containing normal levels of iron and organic matter typically have reflection values below 30% throughout the spectral region of 400-1650 nm. Soil reflection is further reduced by its low position in the sward. As result, reflection of soil is only a fraction of leaf reflection, and grass-soil mixels are similar to pure grass pixels lower in the sward.

In this study a strong effect of leaf angle was found, comparable to the effects of leaf angle distribution on reflection at the canopy scale. Body reflection for nearly vertical leaves is a factor 4 lower when compared to horizontal leaves. For leaves with right angles to incident light a strong additive effect on reflection of nearly 10% was found for various wavelengths.

Images of a production sward and sports-field swards could be easily distinguished by differences in reflection intensity. Based on the spectral characteristic, grass could be easily distinguished from soil and dead material by simple thresholds and ratios. Pixels assigned to grass classes are further subdivided into intensity classes. These intensity classes were related to sward height and leaf angle, and could be used as indicators of canopy height and vertical sward structure. With the described assembly, canopy structure can be characterised by ground cover, the distribution of pixels over intensity classes and image texture. Spectral characteristics can be obtained at leaf level.

3

Monitoring growth of grass swards using imaging spectroscopy

A.G.T. Schut & J.J.M.H. Ketelaars

Provisionally accepted at Grass and Forage Science

3. Abstract

The potential of an experimental imaging spectroscopy system, with high spatial (0.16-1.45 mm²) and spectral resolution (5-13 nm), was explored for monitoring growth of grass swards. An experiment was conducted with 36 *Lolium perenne* L. mini swards, differing in sward quality. In total 11 consecutive growth periods were studied between September 1999 and October 2000. Hyperspectral images and light interception (LI) was recorded twice a week. On two dates ground cover was scored visually (GC_v). At harvest, leaf area index (LAI), fresh matter (FM) yield and dry matter (DM) yield were determined. Classification of images using maximum likelihood procedures yielded (several) estimates of image ground cover (GC_i) and index of reflection intensity (IRI). The GC_i was highly correlated with GC_v ($R^2_{\text{adj}}=0.94$), LAI ($R^2_{\text{adj}}=0.88$), and LI ($R^2_{\text{adj}}=0.94$, for dense swards under a cloudy sky). However, relations between GC_i and LI depended on sky conditions (clear vs. cloudy sky) and sward quality (open vs. dense). Under a cloudy sky, LI was linearly related to GC_i, whereas under a clear sky, this relation had a more logistic character. From the relation between LAI vs. LI, a light extinction coefficient of 0.7 was derived. Initial LAI after cutting was estimated at 0.3. Open swards had on average a lower GC_i and a lower IRI when compared to dense swards at similar growth stages. Regression analysis of GC_i and yields showed correlations with R^2_{adj} ranging between 0.75-0.82. The mean error of DM yield estimates was 340 kg DM ha⁻¹. Estimates of GC_i can be used to predict DM yields, even for high yield levels (up to 3500 kg). It is concluded that imaging spectrometry allows accurate, non-destructive monitoring of grass sward growth from increases in estimated GC_i and IRI.

3.1 Introduction

The currently available techniques for non-destructive herbage mass measurements have a limited accuracy (Gabriels & Van den Berg, 1993; Harmoney *et al.*, 1997; Lokhorst & Kasper, 1998; Murphy *et al.*, 1995; Sanderson *et al.*, 2001; Stockdale & Kelly, 1984; Virkajärvi, 1999). In the absence of fast and automatic means to monitor grass growth, the quality of grassland management strongly depends on visual judgements of the farmer. With the recently developed imaging spectroscopy system, novel methods for rapid, non-destructive grass sward characterisation can be explored (Schut *et al.*, Chapter 2).

This experimental system produces images with high spatial resolution (0.16-1.45 mm²) and high spectral resolution (5-13 nm). With these high-resolution images soil, dead material and green material are classified accurately. In addition, reflection intensity of leaves in this system was found to be dependent on vertical position in the canopy and leaf angle. With these features, ground cover can be differentiated into reflection intensity classes, which are related to height positions of leaves in the canopy. Monitoring of grass sward growth can thus be carried out by following the increase in cover of individual leaf classes (Schut *et al.*, Chapter 2). Due to the non-destructive nature of imaging spectrometry, growth curves of grass swards might be constructed based on the temporal and spatial development of image ground cover (GC_i). This opens up new means for visualising differences in grass growth dynamics between fields or between treatments in experiments.

The objective of this paper is to explore the potential of the imaging spectroscopy system for monitoring growth of grass swards accurately. To this end, images of mini swards were compared with visual scores of ground cover and measurements of light interception (LI), leaf area index (LAI), fresh matter (FM) yield and dry matter (DM) yield. Grass swards were created that differed in sward quality due to drought damage or artificial removal of tillers.

3.2 Materials and methods

3.2.1 Swards

In total 36 mini swards were available from experiments in which effects of drought damage on sward productivity was investigated in 1999 and 2000. Swards were established from seed in April 1999 using a mixture of *Lolium perenne* L. cultivars (BG3, Barenburg). Swards were grown in containers of 0.9 m long, 0.7 m wide and 0.4 m high, filled with a sandy soil containing 3% organic matter. Throughout the growing season, containers were kept under a rain shelter, covered with foil (1999: 70% transparent, new foil in 2000: 80% transparent) and wind breaking fences at the sides. Water was supplied through perforated drains at 10 cm depth. Soil moisture content was monitored by weighing containers twice a week. During winter, containers were placed outside the greenhouse.

Mini swards, 1999

In 1999 mini swards from a drought experiment were available (Grashoff *et al.*, 2001). In April, mini swards received $8.1 \text{ g m}^{-2} \text{ N}$, $13.8 \text{ g m}^{-2} \text{ P}_2\text{O}_5$ and $24 \text{ g m}^{-2} \text{ K}_2\text{O}$. The mini swards were hand cut to a stubble height of 4 cm. After every harvest $9.4 \text{ g m}^{-2} \text{ N}$ (dissolved in water) was supplied. After 15 September this dose was reduced to $5.1 \text{ g m}^{-2} \text{ N}$.

Drought stress was created at two periods, in June-July (T1) and August-September (T2), and differed in length (control, 10, 20, 30 and 40 days without extra water). Each treatment had 8 replicates, from which 4 were used to study tiller growth after the drought period. From this drought experiment, control (4 from T1 and 4 from T2) and 40 days drought mini swards (8 from T1 and 8 from T2) were used. For 12 of the T1 mini swards (the mini swards that were used to study tiller growth after the drought period from the treatments 10, 20 and 30 days without extra water), artificial sward damage was created. These swards were damaged in order to create a wide range of sward quality. This range in sward quality was required for the study of the potential of imaging spectroscopy for quantification of heterogeneity and sward deterioration (Schut & Ketelaars, Chapter 8).

First, any sward damage already present due to sampling for tiller analysis in the drought experiment was restored. Then an area of approximately 25%, 50% and 70% of the sward was removed in the first week of September with circular patches of 12.5 cm (S) and 22.5 cm (L) in diameter. The locations of patches in the sward were selected by picking random cross-points on a grid, restricted to non-overlapping patches.

The experimental period started on 15 September and ended on 9 November. The last harvest prior to the experiment was on 23 August (T1) and 14 September (T2). Within the experimental period, harvests were made on 29 September (T1 only) and on 9 November (T1 and T2).

Mini swards, 2000

In 2000 another drought experiment was conducted. From the 1999 experiment, mini swards without sward damage were selected and assigned randomly to 5 drought treatments. These treatments were control, 10, 20, 30 and 40 days without water in the period from 1 June to 10 July. From this experiment, the control and 20, 30 and 40 days without water were used, see Table 3.1.

Table 3.1 Treatments in the 2000 experiment, and seasonal mean values \pm standard error of the mean for image ground cover of green (SM-GC_i) and dead material (SM-GCD_i) and index of reflection intensity (SM-IRI).

Treatment description	Code	Mini swards (#)	Sward quality	SM-GC _i	SM-GCD _i	SM-IRI
Control	C	4	Dense	54.0 \pm 0.9	8.4 \pm 1.1	5.7 \pm 0.6
40 days drought from 1 June – 10 July 2000	T1-40	4	Dense	47.4 \pm 1.4	14.6 \pm 1.6	6.1 \pm 0.0
30 days drought from 11 June – 10 July 2000	T1-30	4	Dense	49.8 \pm 1.5	11.9 \pm 1.8	6.1 \pm 0.4
20 days drought from 21 June – 10 July 2000	T1-20	4	Dense	51.6 \pm 0.5	10.6 \pm 0.7	5.3 \pm 0.4
Drought damaged swards from 1999	NDS	8	Open	51.2 \pm 0.8	12.2 \pm 0.7	4.3 \pm 0.6
Small circular patches, 25% of sward removed	S25	2	Open	43.3	21.6	2.5
Small circular patches, 47% of sward removed	S50	2	Open	49.9	11.9	3.7
Small circular patches, 68% of sward removed	S75	2	Open	47.2	13.4	2.4
Large circular patches, 25% of sward removed	L25	2	Open	40.9	18.8	2.9
Large circular patches, 55% of sward removed	L50	2	Open	44.2	12.1	2.2
Large circular patches, 75% of sward removed	L75	2	Open	48.6	8.7	2.7

On 17 March 2000, above ground fertiliser was supplied at 8.1 g m⁻² N, 6.6 g m⁻² P₂O₅ and 12 g m⁻² K₂O. On the 11th of July 3 g m⁻² P₂O₅, 20 g m⁻² K₂O and 6 g m⁻² S was supplied. On 30 August an additional 6.3 g m⁻² K₂O was supplied. After every harvest 9.4 g m⁻² N (dissolved in water) was supplied. The mini swards were harvested on 25 April, 12 May, 30 May, 20 June, 11 July, 8 and 29 August, 27 September and 31 October. The intermediate harvests just before the drought period of the T1-30 (on 9 June) and just after the drought period (T1-30 and T1-40) were excluded from the data set.

Dense and open mini swards

Mini swards in Table 3.1 were divided into either dense or open swards. Mini swards of control and the drought treatments T2 (1999) and T1 (2000) were considered as dense swards as the 1999 T2 and the 2000 T1 drought period did not affect sward quality (Grashoff, personal communication). Mini swards of all other treatments were assigned to open swards. The C and T1-20 mini swards had a mean tiller density with standard errors of 5330 ± 250 tillers m^{-2} , artificially damaged swards (S25, S50, S75, L25, L50 and L75) 2610 ± 270 tillers m^{-2} and drought damaged swards (NDS) 3600 ± 340 tillers m^{-2} in the autumn of 1999. In spring 2000, mean tiller densities increased to 6250 ± 360 tillers m^{-2} for C and T1-20, 3860 ± 240 tillers m^{-2} for the artificially damaged swards and to 3660 ± 390 tillers m^{-2} for drought damaged swards. The spatial heterogeneity of tiller density also differed considerably. In 1999, the mean coefficients of variation with standard errors were 0.23 ± 0.02 (C and T1-20), 0.66 ± 0.05 (artificially damaged swards) and 0.83 ± 0.08 (drought damaged swards), and in 2000 0.19 ± 0.02 (C and T1-20), 0.52 ± 0.03 (artificially damaged swards) and 0.74 ± 0.08 (drought damaged swards) (Schut & Ketelaars, Chapter 8). Surprisingly, increasing the degree of artificial damage was not reflected in a proportional decrease in GC_i and DM yield.

3.2.2 *Light interception measurements*

Light interception (LI) was measured twice a week by hand, simultaneously with image line recording, with a DECAGON LI-meter. This LI-meter has 80 light sensitive cells of 1 cm^2 on a 1 m long, 1 cm wide and 1 cm high stick. The LI-stick was longer than the containers were wide. For below canopy measurements, the LI-stick was placed on the container sides, 0-2 cm above soil surface. Per mini swards 7-14 alternating measurements above and below canopy were made. Afterwards, absorbed photosynthetic active radiation (APAR) was calculated per cell by $100 - 100\% \times \text{below} / \text{above canopy readings}$. Only cells that fell within the three bands in the 50 cm wide and 70 cm long area, where also image lines were recorded were included (Figure 3.1). Results were then averaged per mini sward. Fast changes in cloud cover strongly disturbed measurements of LI. Therefore, only LI measurements on days with constant sky conditions (i.e. clear sky or uniform cloud cover) were used in the analysis.

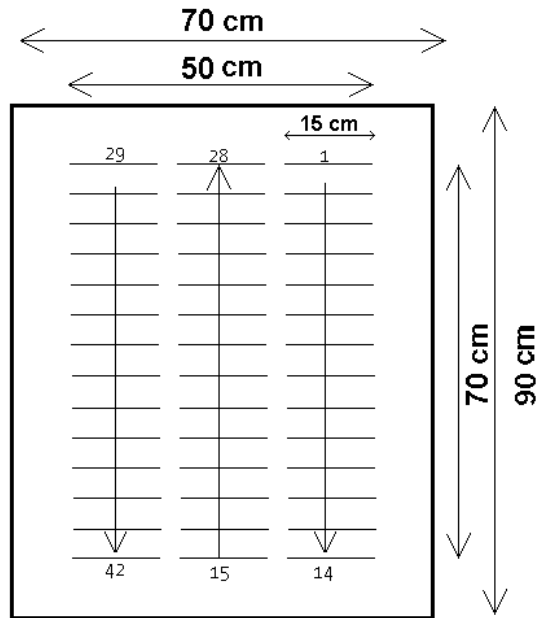


Figure 3.1 Position of image lines in the mini swards, numbers indicate image line number.

On two days (1 and 20 October 1999), visual scores of ground cover (GC_v) were made to check image estimates of ground cover (GC_i). For this, a fine wire raster with 2×3 cm cells were laid over the mini swards. On each crossing point of wires, presence of green grass leaves or soil was scored visually, by looking down vertically (Korva, 1996). For each container 300 points were scored. Results were averaged per mini sward.

At each harvest, FM yield was determined and samples were taken for DM content determination. From this yield, samples were taken for leaf area measurement (LICOR leaf area meter) and leaf area ratio (LAR, $m^2 g^{-1}$ DM) and LAI ($m^2 m^{-2}$) were calculated. Standing LAI is underestimated, since only material above cutting height is included. The underestimation is equal to the initial LAI at the beginning of a following growth period.

3.2.3 Image line recording

The experimental system used for imaging spectrometry is described in detail elsewhere (Schut *et al.*, Chapter 2). In short, this system records image lines,

from a distance of about 1.3 m from the soil using three different sensors. The sensors are placed in a darkened box, eliminating solar light. This paper presents only results of the V7 sensor. The V7 sensor detects reflection in the 404-709 nm wavelength range with a spectral resolution of 5 nm. At soil level, an image line recorded by the V7 is 1.39 mm wide and 152.5 mm long. Each image line has 768 pixels for the spatial dimension, resulting in a spatial resolution of 0.28 mm² per pixel at the soil surface. Per pixel, radiance is measured in 565 spectral bands. The system uses a xenon light source with lenses, illuminating only the area where an image line is recorded. Light was projected vertically to the soil, and reflection was measured under an angle of 2° from nadir, minimising shadow effects. As part of the sampling routine, the imaging spectroscopy system records image lines with the light sources switched off and 5 image lines from a 50% reflection standard. With these standard image lines, reflection was calculated from the radiance data. The reflection intensity of grass leaves measured with this imaging spectroscopy system depends on the height in the canopy and on leaf angle. Leaves high in the canopy and horizontally oriented leaves have a higher reflection than leaves low in the canopy and more vertically oriented leaves (Schut *et al.*, Chapter 2). The image lines are recorded in a regular pattern with 3 bands next to one another per mini sward. In each band 14 image lines were recorded, each 5 cm apart, resulting in 42 image lines per mini sward (Figure 3.1). Mini swards were scanned twice a week during the growing season from 15 September up to 8 November in 1999 and from 5 April up to 30 October in 2000. The harvests were always planned one day after image line recording. The recordings of one day before harvest were used to study the relation between image parameters and FM and DM yield.

3.2.4 *Image line classification*

Set-up of a library for training classifiers

Schut *et al.* (Chapter 2) defined threshold values for soil, grass leaves (G), leaves with specular reflection (S), and dead material (D) classes and an intermediate class between soil and dead material (MDSO). Separation between classes was based on ratios of reflectance (R) at 450, 550 and 680 nm. A pixel was classified as green when $R_{680} / R_{550} < 1$, and dead when $R_{680} / R_{550} > 1$ and R at 680 nm > 3%. These classes are subdivided into reflection intensity classes (IC), ranging from grass IC 0 (low reflection intensity, mostly vertical

leaves or leaves at the soil surface) to grass IC 6 (high reflection intensity, mostly horizontal leaves located in the top of the canopy). For leaves with specular reflection, IC ranged from 0 up to and including 2, and for dead material from IC 0 up to and including 3. Per class 40 - 2500 spectra which fulfil the boundary conditions were collected in a library. These spectra were selected from images of the 1999 experiment, taken on various dates and covering all stages within the growth period of grass.

Feature selection

Fast classification of hyperspectral images requires a selection of features from the total feature space. A set of spectral bands is selected according to the following function (Moshou *et al.*, 1999):

$$F_i = |X_i - Y_i| / \sqrt{V_{x,i} + V_{y,i}} \quad (1)$$

where X and Y are the mean reflection values for class X and Y, and where *i* is the spectral band. V_x and V_y are the variances for classes X and Y. For each class to class combination, at all spectral bands, the F value is calculated. Then, for each class to class combination, the wavelengths (10-17) with maximum F_i value are selected, where the selected bands must be at least some (5-10) nm apart, to prevent selection of highly correlating wavelengths. With these selected wavelengths a correlation matrix was made and pixels were classified using maximum likelihood procedures (Stein *et al.*, 1999).

For classification a 99.99% confidence interval is used to eliminate effects of extreme or noisy pixels on the average spectral curve. Pixels beyond this confidence interval are assigned to a class 'not classified'. For every date, images were classified and cover fractions of all classes were estimated. Images with a high fraction (>10%) of 'not classified' pixels were removed from the data set, as they resulted from errors in the recording process.

Total image line ground cover (GC_{il} , %) was calculated as the sum of grass (GCG) and specular classes (GCS):

$$GC_{il} = \sum_{ic=0}^6 GCG_{ic} + \sum_{ic=0}^2 GCS_{ic} \quad (2)$$

where *ic* is the index number of the intensity class.

Sward GC_i was calculated as mean over the 42 GC_{il} estimates. The index of reflection intensity (IRI) is then calculated as:

$$IRI = 100 \times \frac{\sum_{ic=3}^6 \frac{1}{42} \sum_{il=1}^{42} GCG_{il,ic}}{GC_i} \quad (3)$$

This IRI measures the presence of highly reflecting green pixels as a percentage of ground cover. The classes GCG_3 through GCG_6 are chosen since the fraction of pixels in these classes is limited just after cutting (typical <5%), and do not appear on short-cut sports-field images (Schut *et al.*, Chapter 2). The fraction of dead material (GCD) was calculated as sum of the classes dead material D_{0-3} and MDSO. Seasonal means (SM) of GC_i , IRI and GCD were calculated as mean over all measurements in 2000.

Bootstrap analysis was used to test the quality of the library. With this analysis, one spectral curve is selected from the data set, the classifier is trained on the complete data set minus one, and the selected curve is classified. This is repeated for the first 100 lines in the data set for each classifier.

Statistics

The relationship between LI and GC_i was examined to determine whether it was affected by sward structure under clear and cloudy skies. For this, linear models were fitted:

$$LI = a + b \times GC_i + c \times IRI + d \times GC_i \times IRI \quad (4)$$

As IRI gives information on canopy geometry, limited here to the angular and vertical distribution of above ground plant parts, IRI and the interaction between GC_i and IRI are included in the models.

The model of equation 4 was fitted for both dense and for open swards. The null hypothesis, estimates of parameters are equal for dense and open swards, was tested by comparing the parameter estimates $\pm z\text{-value} \times \text{standard error}$.

For the relations LI vs. LAI, GC_i vs. LAI and GC_i vs. DM yield the following formula was fitted:

$$y = a + b \times (1 - e^{-k \times x}) \quad (5)$$

Where a is the intercept with the y -axis, $a + b$ equals the maximum y value and k is the extinction coefficient.

This formula is widely used for the LI vs. LAI relation (Goudriaan & Van Laar, 1994), where the value of k ranges between 0.5-0.8 depending on canopy geometry (Van Keulen & Wolf, 1986). When leaves are randomly distributed, overlapping decreases the visible fraction of each extra leaf exponentially. When using formula 5 to describe the GC_i vs. DM yield relation, LAR and canopy geometry determine the extinction coefficient k , which has than the dimension $ha \text{ unit}^{-1} DM$.

Linear models were fitted for the relation between GC_i and FM and DM yields. The response for the first harvest of 2000 was different from the other harvests. The equations were fitted on all harvests without this first harvest. Estimates of GC_i include all green material, even below cutting height. Separating GC_i into contributions of individual leaf classes provides a new range of GC estimates; for instance GC_i , GC_i without GCG_0 ($GC_i - GCG_0$) and GC_i with only classes 'above' GCG_1 ($GC_i - GCG_0 - GCG_1$). For leaves under a 45° angle with the horizontal plane, $GC_i - GCG_0 - GCG_1$ is equivalent to all leaves above 3.5 cm (Schut *et al.*, Chapter 2). The relation between GC_i and DM yield had a curvilinear character but this relation became linear when excluding GCG_0 and GCG_1 from the GC_i estimate. Therefore, DM and FM yield values were converted with a natural logarithm before regression analysis when GCG_0 and GCG_1 were included. It is likely that canopy geometry has effect on the relation between GC_i and DM yield and between GC_i and FM yield. For this, the IRI was included as extra regression variable.

The standard error (SE) of observations was calculated as root of the residual mean square.

3.3 Results

3.3.1 Classification success rates of classes in the library

The overall results of bootstrap classification success rates are given in Table 3.2. Grass is classified correctly for 99.2%. Grass leaves with specular reflections are classified correctly for 92.1%, and are confused with the higher reflecting classes of grass in 5.3% of the cases. Soil is classified correctly as soil for 91.0%, and for 5.5% as an intermediate class (MDSO).

3.3.2 *Ground cover*

In Table 3.1, the seasonal mean GC of green (SM-GC_i), dead material (SM-GCD) and IRI (SM-IRI) in 2000 is given. Control swards had a SM-GC_i of 54%, a SM-GCD of 8.4% and a SM-IRI of 5.7%. The GC_i values at harvest varied within the season where relatively high GC_i values usually coincide with high DM yield values (Table 3.3). On average, open swards had a lower SM-GC_i, a higher SM-GCD and a lower SM-IRI than dense swards (Table 3.1). The SM-IRI of dense swards ranged from 5.3-5.7%, whereas SM-IRI for open swards ranged from 2.2-4.3%. The seasonal mean GCD ranged from 8.4-21.6%. Drought periods increased the fraction of dead material, although the SM-GCD of T1-40 and T1-30 also increased as result of the low GC_i values during the drought period. The S25 and L25 treatments had the lowest SM-GC_i and highest SM-GCD estimates.

In Figure 3.2, the image GC (GC_i) versus visually scored GC (GC_v) is given for 20 September and 1 October. GC_i underestimates GC_v, as indicated by the intercept (8.63) of the regression curve (Table 3.4). At harvest, some cut leaves fell on the soil. The colour of these leaves turned from green into red within a few days. With the high spatial resolution of the experimental system, pixels on these dying leaf parts were assigned to GCD classes (defined as: more reflection in red than in the green part of the spectrum). This is reflected in the value of the class GCD₁, which ranged from 0.9-8.7 for mini swards with GC_v scores <40%. Including this class into the GC_i estimate would then especially affect the lower regions of the GC_i. The intercept in the relation (between visual GC estimates and GC_i estimates) was no longer significant when class GCD₁ was included in the GC_i estimate (Table 3.4).

Table 3.2 Bootstrap classification results for main classes of the V7 sensor.

Class	soil	Dead	Grass	MDSO	Specular
Soil	91.0	0.0	3.5	5.5	0.0
Dead	0.0	94.0	1.4	3.3	1.3
Grass	0.3	0.3	99.2	0.0	0.2
MDSO	1.0	2.0	0.0	96.0	1.0
Specular	0.0	1.1	5.3	0.5	92.1

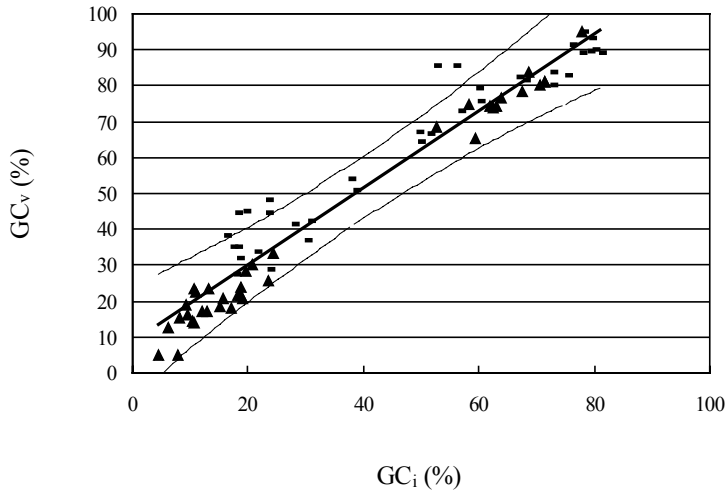


Figure 3.2 Visual GC estimates (GC_v) vs. image GC estimates (GC_i) for 20 September 2000 (–) and 1 October 2000 (▲). Thick line indicates fit ($GC_v = 8.63 + 1.08 \times GC_i$) thin lines indicate 95% confidence intervals of regression line.

Table 3.3 Average DM yield, LAR and GC_i at harvest for control treatments.

	DM yield (kg DM ha ⁻¹)	LAR (m ² g ⁻¹ DM)	GC_i (%)
-----1999-----			
29 September	1234	0.011	66.2
9 November	993	0.010	56.5
-----2000-----			
25 April	3308	-	67.0
12 May	1953	-	78.6
30 May	912	-	59.8
20 June	1643	0.016	60.9
11 July	1156	0.011	40.9
8 August	2941	0.019	86.8
29 August	2348	0.013	85.5
27 September	2358	0.014	86.6
31 October	1115	-	73.7

Table 3.4 Parameter values and standard errors of regression of GC_i and GC_v , $GC_i = a + b \times GC_v$.

Model	n	a	b	Standard error of observations	R^2_{adj}
$GC_v = a + b \times GC_i$	72	8.63 ± 1.45	1.076 ± 0.031	6.73	0.94
$GC_v = a + b \times (GC_i + GCD_i)$	72	0*	1.208 ± 0.016	6.49	0.95

* Not significant ($p > 0.05$), set to zero

3.3.4 Light interception (LI)

As GC_i increases, also LI will increase. On cloudy days (Figure 3.3) there was a strong linear relation between LI and GC_i (dense swards: $R^2_{adj} = 0.94$). Including IRI improved predictions slightly (Table 3.5). The negative intercept (-20.58) means that sward material near the soil surface had no effect on LI measurements, and can be interpreted as bias in LI meter readings. The confidence intervals (CI) for the intercept (-24.66 up to -16.50) and GC_i slope (1.23 up to 1.43) were different for dense swards when compared to intercept (-5.52 up to -0.04) and GC_i slope (0.97 up to 1.13) of open swards.

Table 3.5 Parameter estimates and standard errors for linear regression of light interception,

$$LI = a + b \times GC_i + c \times IRI + d \times GC_i \times IRI$$

Sward quality	N, #	A	B	C	D	Standard error of observations	R^2_{adj}
-----Cloudy sky-----							
All	326	-14.65 ± 1.62	1.22 ± 0.04	4.00 ± 0.72	-0.039 ± 0.009	7.08	0.93
Dense	167	-20.58 ± 2.08	1.33 ± 0.05	4.03 ± 1.01	-0.039 ± 0.014	6.82	0.95
Open	158	-2.78 ± 1.40	1.05 ± 0.04	0.82 ± 0.30	0*	6.42	0.92
-----Clear sky-----							
All	345	-9.03 ± 2.05	1.21 ± 0.04	1.52 ± 0.62	-0.016 ± 0.008	10.70	0.85
Dense	155	0*	1.18 ± 0.01	0*	0*	9.68	0.87
Open	190	-10.19 ± 1.74	1.14 ± 0.04	0.55 ± 0.14	0*	8.52	0.90

* not significant ($p > 0.05$), set to zero

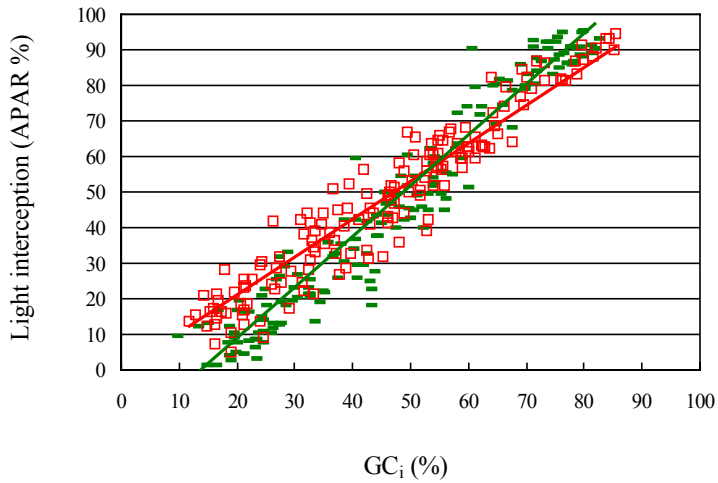


Figure 3.3 Influence of sward density on light interception (LI) as function of GC_i on days with a cloudy sky. Lines indicate linear fits, green line ($LI = -19.34 + 1.42 \times GC_i$, $R^2_{adj}=0.94$) for dense swards (—), red line ($LI = -3.98 + 1.14 \times GC_i$, $R^2_{adj}=0.92$) for open swards (□).

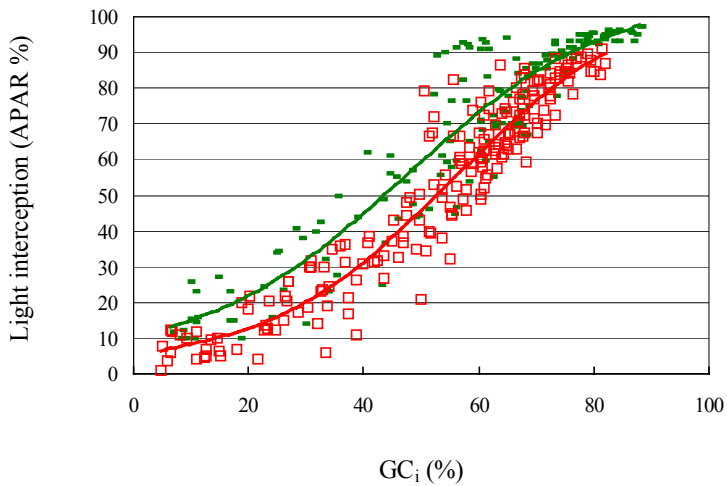


Figure 3.4 Influence of sward density on light interception as function of GC_i on days with a clear sky. Lines indicate logistic fits, green for dense swards (—), red for open swards (□).

At similar GC_i levels for the dense swards, LI was 8-10% higher in the lower GC_i regions under a clear sky than under a cloudy sky (compare Figure 3.3 with Figure 3.4). There was a significant effect of sward openness, as the intercepts were different for dense and open swards (Table 3.5). Estimates for GC_i slope were not different (CI dense swards: 1.16 up to 1.20, CI open swards: 1.06 up to 1.22). When including only GC_i , residuals deviated from normality, and a logistic fit was more appropriate (Figure 3.4 and Table 3.6).

3.3.5 Leaf area index (LAI)

At a LAI of 0, LI was equal to 20% (Figure 3.5). As stated above (see materials and methods) LAI was underestimated due to remaining leaf material in the stubble after harvest. This residual LAI can be recalculated with the formula in Figure 3.5 under the assumption that when LAI equals 0, LI also equals 0. This value of LAI in the stubble was 0.31. The light extinction coefficient k was 0.70. The LAI was also strongly related to the GC_i estimates ($R^2_{adj}=0.88$, Figure 3.6). In this curvilinear relation, the extinction coefficient (k) was 0.83. At high GC values, GC_i underestimated the ground cover of green material (Figure 3.2). Therefore, the maximum GC_i value in the LAI vs. GC_i relation was only 86%.

3.3.6 Monitoring ground cover

The GC_i changed during growth periods. In Figure 3.7 the GC_i development is given for three treatments: control (C), L25 (25% of the sward removed) and L75 (75% of the sward removed). Each point represents the mean of all mini swards in the treatment. Fluctuations in GC_i between consecutive measurements were limited, and thus GC_i was insensitive to disturbing factors

Table 3.6 Parameter values and standard errors of light interception under a clear sky with a logistic

$$\text{regression, } LI = \frac{A + C}{1 + e^{-B(GC_i - M)}}.$$

Sward quality	N	A	B	C	M	Standard error of observations	R^2_{adj}
All	345	6.92 ± 3.64	0.064 ± 0.009	99.93 ± 9.06	53.96 ± 1.76	10.40	0.86
Dense	155	4.06 ± 8.18	0.057 ± 0.012	102.6 ± 14.3	47.26 ± 2.57	9.47	0.87
Open	190	2.02 ± 4.28	0.060 ± 0.010	106.4 ± 14.0	56.13 ± 2.88	8.10	0.91

like *e.g.* heavy winds. Within the first days after harvest sometimes a small decline in GC_i was visible, representing deteriorating litter leaves. The C treatment had higher GC_i estimates than the L25 and L75 treatments throughout the season, with exception of the first growth period. The GC_i shortly after harvest varied throughout the season.

The cumulative GC_i illustrates how the importance of reflection intensity classes varied with changes in canopy geometry during growth (Figure 3.8). In this figure, the cumulative GC_i of class GCG_2 was equal to the GC_i of GCG_2 and total cover of all classes with lower reflection intensities. Just after a harvest, the classes GCG_0 , GCG_1 and GCG_2 were already present. In time, the cover of these classes increased, until leaves in more intense reflecting classes came up. Then, the ground cover fraction of these less intense reflecting classes decreased. The reflection intensity classes appeared in consecutive order, from low reflection intensity to high reflection intensity.

Except for the 24th of April harvest, IRI of heavy harvests was much higher than for lighter harvests (compare yields in Table 3.3 with IRI values for C in Figure 3.9). For example, in 2000 the September harvest (2.3 ton DM yield) and the October harvest (1.1 ton DM yield), clearly differed in IRI (22.1% in September and 5.5% in October) whereas GC_i was only 13% higher in the

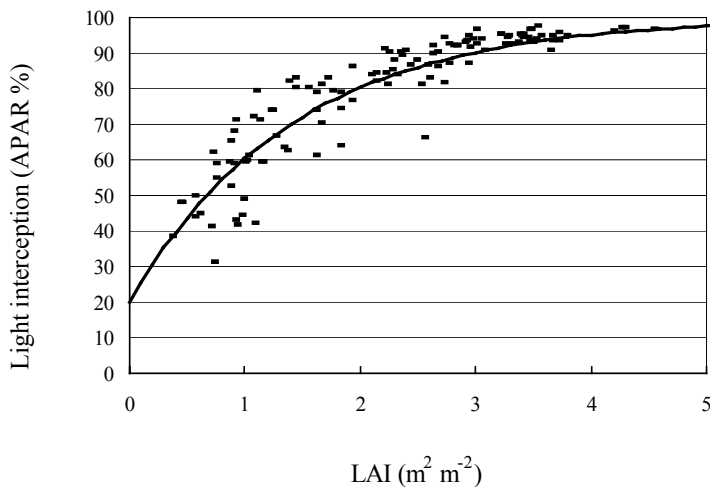


Figure 3.5 Fraction of APAR intercepted as function of LAI. Fitted line:

$$y = 20.12 + 81.9 \times (1 - e^{-k \times LAI}), \quad k=0.7 \text{ (SE=0.1)}, \quad R^2_{\text{adj}}=0.85 \text{ (SE observations=6.61)}.$$

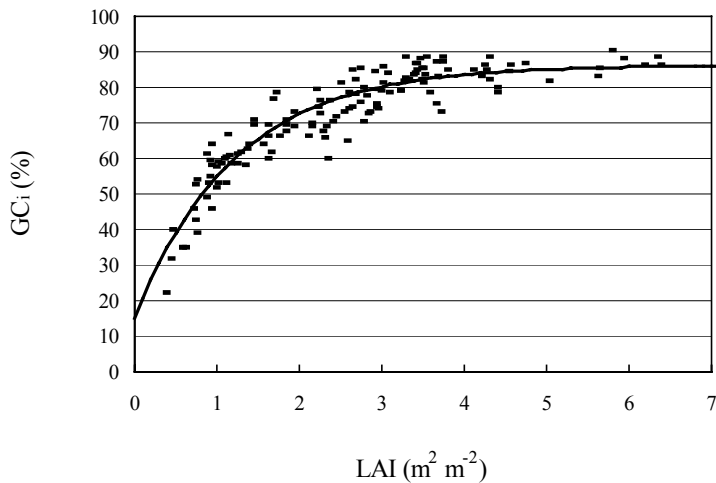


Figure 3.6 GC_i as function of LAI of harvested material. Fitted line:

$$y = 14.97 + 71.22 \times (1 - e^{-k \times LAI}), \quad k=0.83 \text{ (SE=0.07)}, \quad R^2_{\text{adj}}=0.88 \text{ (SE observations=4.96)}.$$

September harvest (86.6% in September and 73.3% in October). Hence, yield differences between these two harvests could be attributed to canopy geometry. There was a clear difference in IRI at harvests with a high DM yield (May, July, August and September), for the treatments C, L25 and L75 (Figure 3.9). The open swards (L25 and L75) had lower values for IRI than the dense sward (C). Open swards, when compared to dense swards, were thus characterised by a lower GC_i and IRI at similar growth stages.

3.3.7 *Estimating yields*

There was a strong relation between dry matter (DM) yield and GC_i (Figure 3.10), except for the first harvest from 2000. For the fitted curve ($R^2_{\text{adj}}=0.82$) the data of the first harvest in 2000 were excluded. This was a heavy harvest (Table 3.3), with tall material that might have had very different LAR values than the other harvests. The analysis below is based on all harvests without this first harvest of 2000. With higher leaf densities, leaves will only be partly visible in the GC_i estimate. At lower leaf densities, the probability of overlapping leaves approaches zero.

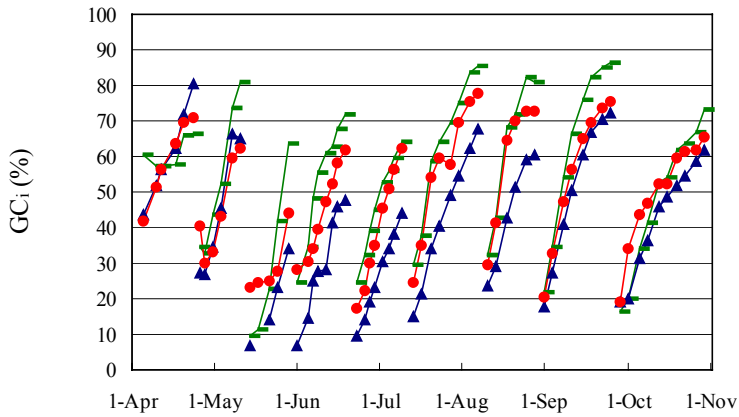


Figure 3.7 GC_i development in 2000 for dense (—) and open swards (25% (▲) and 75% (●) of the sward removed).

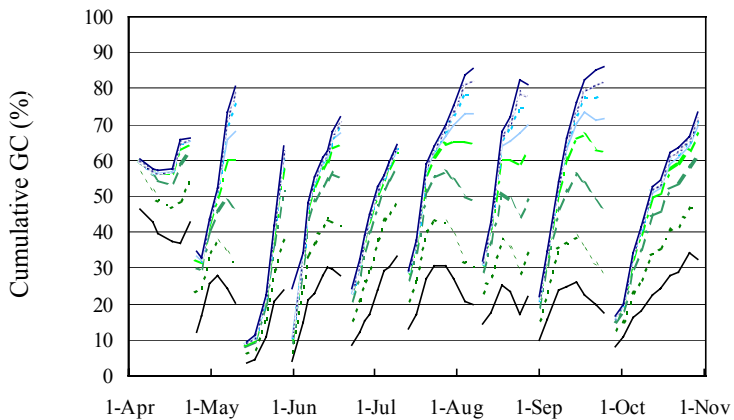


Figure 3.8 Development of cumulative ground cover, including subsequently GCG₀ (—), GCG₁ (.....), GCG₂ (---), GCG₃ (-.-), GCG₄ (—), GCG₅ (.....), GCG₆ (.....) and GCS_{0,2} (—), data refer to dense swards in the 2000 growing season

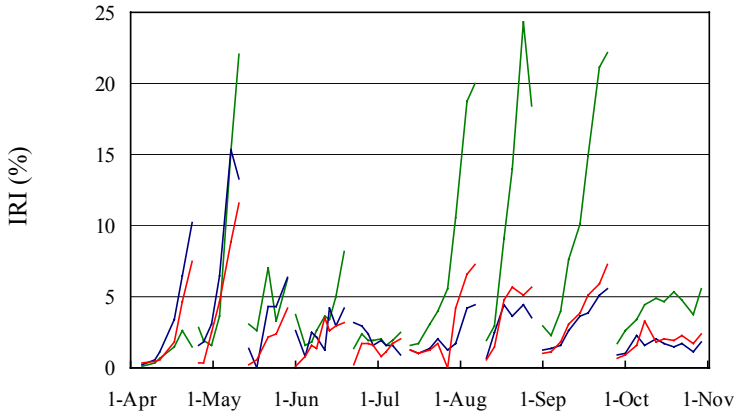


Figure 3.9 IRI development in 2000 for dense (—) and open swards (25% (—) and 75% (—) of the sward removed).

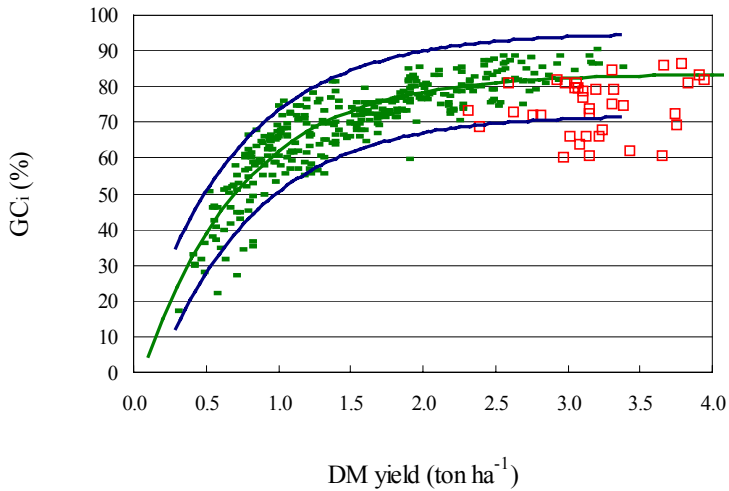


Figure 3.10 GC_i as function of DM yield (all harvests (—) except first harvest of 2000 (□)), blue lines indicate 95% confidence interval for one new observation. Fitted line: $y = -7.9 + 91.5 \times (1 - e^{-k \times DM})$, $k = 1.44$ (SE=0.1), $R^2_{adj} = 0.82$ (SE observations=5.86).

This was the case when only ground cover of higher IC's were included (higher in the canopy and a more horizontal leaf angle). When GC_i rose above 60%, IRI increased (Figure 3.11). This relation showed a higher variability for open swards than for dense swards. This relation came from the growth characteristics of grass, as an increase in biomass rose ground cover, the height of the canopy as well as the fraction of horizontally oriented leaves. The IRI was linearly related to DM yield ($IRI = -3.2 + 8.07 \times DM \text{ yield (t ha}^{-1}\text{)}$, $R^2_{\text{adj}} = 0.56$). With IRI included, DM yield could be described with an exponential equation ($R^2_{\text{adj}} = 0.82$, Table 3.7). A linear relation was found when only higher intensity classes were included in the GC_i estimate. Now, also higher DM yields could be estimated with good accuracy (Figure 3.12). With GC_i estimates below 60% (in the more linear phase), the confidence interval was smaller for the GC_i DM estimate (standard deviation <195 kg DM, estimated from Figure 10 at 60% GC_i) than for the linear estimates (SE of observation=340 kg DM ha⁻¹, Table 3.7). With GC_i estimates above 60%, confidence intervals of the curvilinear fit increased strongly.

Fresh matter yield showed a slightly stronger relation with GC_i than DM yields (compare Tables 3.7 and 3.8). The factor $GC_i \times IRI$ was only significant for the FM yield fit. FM included both water content and DM, and the $GC_i \times IRI$ interaction term might be linked with changes in canopy geometry with changing water content and LAR.

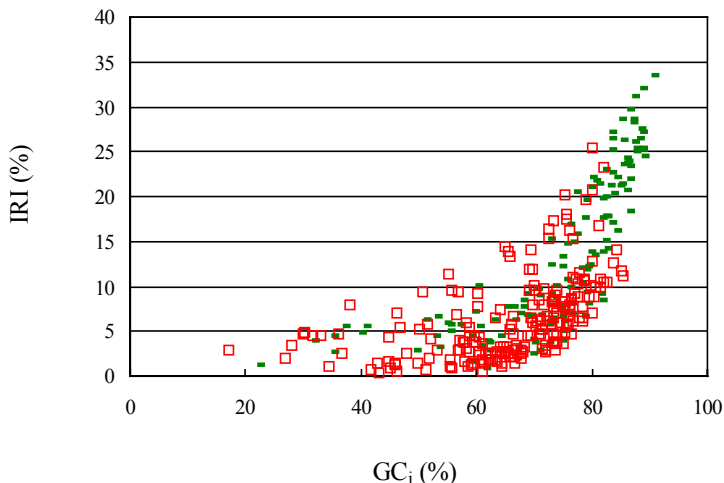


Figure 3.11 Index of reflection intensity (IRI) versus image ground cover (GC_i) for open (\square) and dense swards (\bullet).

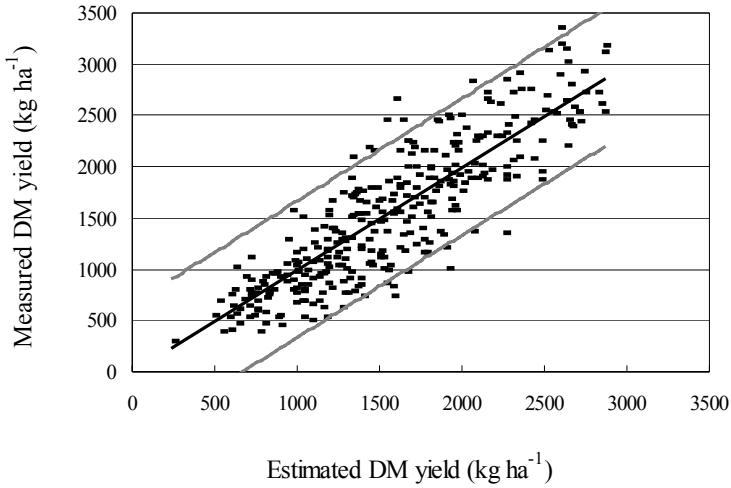


Figure 3.12 Estimated DM yield as function of ground cover of higher intensity classes (GC_i exclusive GCG_0 and GCG_1) and the index of reflection intensity (IRI) ($y = 63.41 \times (GC_i - GCG_0 - GCG_1) - 46.46 \times IRI$) versus measured DM yield for all harvests except first harvest of 2000. Solid line: $y=x$, grey lines indicate 95% confidence intervals for 1 new observation.

Table 3.7 Parameter values and standard errors for linear regression of kg dry matter (DM) yield per harvest, $DM\ yield = a + b \times GC + c \times IRI + d \times GC \times IRI$ (all harvests except first harvest in 2000, 333 observations), for different GC estimates.

GC estimate	A	B	C	D	Standard error of observations	R^2_{adj}
*GC= GC_i	5.19 ± 0.07	0.028 ± 0.001	0.010 ± 0.002	0**	0.21	0.82
GC= $GC_i - GCG_0$	-603.1 ± 94.8	51.81 ± 3.10	-15.70 ± 5.64	0**	337	0.76
GC= $GC_i - GCG_0 - GCG_1$	0**	63.41 ± 1.84	-46.46 ± 5.31	0**	340	0.75

* DM yield values converted with natural logarithm

** not significant ($p > 0.05$), set to zero

Table 3.8 Parameter values and standard errors for linear regression of tons fresh matter (FM) yield per harvest, $FM\ yield = a + b \times GC + c \times IRI + d \times GC \times IRI$ (all harvests except first harvest in 2000, 333 observations), for different GC estimates.

	A	B	C	D	Standard error of observations	R^2_{adj}
*GC=GC _i	-0.52 ± 0.06	0.035 ± 0.001	0.014 ± 0.002	0**	0.180	0.90
GC=GC _i -GCG ₀	-3.81 ± 0.63	0.299 ± 0.012	-0.212 ± 0.089	0.003 ± 0.001	2.01	0.80
GC=GC _i -GCG ₀ -GCG ₁	-1.19 ± 0.44	0.406 ± 0.024	-0.424 ± 0.080	0.003 ± 0.001	1.96	0.81

* FM yield values converted with natural logarithm

** not significant ($p > 0.05$), set to zero

3.4 Discussion and conclusion

With the imaging spectroscopy system, green and dead material can be separated by their chlorophyll and water absorption bands at a 0.28-1.45 mm² level, depending on sensor type (Schut *et al.*, Chapter 2). A library was constructed with 4 main groups of cover classes: soil, dead material, green material and green material with specular reflections. Within these groups, subdivisions were made in leaf height and leaf angle related intensity classes. Although large variations in spectral characteristics of leaves within a growth period existed, it was concluded that the between class variation in the spectral library is large enough for successful classification. The image ground cover (GC_i) estimates of green leaves were found comparable with visually scored ground cover ($R^2_{adj} = 0.96$), where GC_i underestimates the coverage of grass leaves slightly. In the lower range of GC_i, this could be explained by the fraction of dying material near the soil surface.

The GC_i could be used as accurate indicator of the amount of light intercepted (LI) under cloudy sky conditions (dense swards: $R^2_{adj} = 0.95$), and under clear sky conditions (dense swards: $R^2_{adj} = 0.87$). The LI vs. GC_i relation was a function of sky conditions (linear under a cloudy sky and more logistic under a clear sky), and sward openness. In the GC_i vs. LI relation, the index of reflection intensity (IRI) was a significant variable except for dense swards under clear sky conditions. The importance of IRI was larger under cloudy sky conditions than under clear sky conditions.

The canopy structure is defined as the distribution and arrangement of the above ground plant parts within a plant community (Davies *et al.*, 1993). The horizontal distribution of plant parts was described with GC. The relation between reflection intensity and leaf height in the canopy and leaf angle, specific for the measurement system used, allowed classification in intensity classes. The distribution of pixels over these intensity classes, as described with IRI, quantified changes in the vertical arrangement of plant parts.

The LI vs. LAI showed a curvilinear relation ($R^2_{\text{adj}}=0.85$). The average LAI remaining in the stubble after harvest was found to be 0.31. The estimated light extinction coefficient ($k=0.7$) is similar to values found in literature (Goudriaan and Van Laar, 1994).

For site-specific models of grass growth, automatic detection of the actual value of LAI is of great importance, as LAI is used to calculate the amount of intercepted radiation (Goudriaan and Van Laar, 1994). GC_i showed a strong relation with LAI (curvilinear, $R^2_{\text{adj}}=0.88$, extinction coefficient $k=0.83$). For initialisation of site-specific growth models and monitoring growth, GC_i is a better parameter than LAI as GC_i and IRI at harvest were slightly stronger correlated to LI ($R^2_{\text{adj}}=0.85-0.93$) than LAI ($R^2_{\text{adj}}=0.85$), and GC_i detection is non-destructive and easy to automate.

Just after a harvest, only classes with lower reflection intensities contributed to the GC_i estimate. In time, importance of classes with higher reflection intensity values increased. The intensity classes appeared in consecutive order after harvest. Ground cover provided information about the presence of leaves, whereas IRI provided information about the vertical distribution of leaves in combination with leaf angle distribution within a canopy.

Image ground cover was a sensitive parameter to identify differences between mini swards in initial condition, growth and growth rate. This opens up new means for in-situ comparison of grass swards, and other canopies. Open swards (L25, L75) had on average a lower GC_i and a lower IRI compared to dense swards at a similar growth stage. The lower values for IRI for open swards when compared to dense swards mean that leaf angle and leaf height distribution differed. These differences in canopy geometry were linked with the differences in light intercepting capacity for open and dense swards, at comparable GC_i levels.

The dry matter (DM) yield vs. GC_i relation had a curvilinear nature ($R^2_{\text{adj}}=0.82$) and vertical canopy geometry (in terms of IRI) had a significant effect on this relation. With this factor included, logarithmically transformed DM yield could be predicted with a linear equation ($R^2_{\text{adj}}=0.82$). Schut *et al.*

(Chapter 2) found that leaf pixels from leaves with an angle of 45° , assigned to the two lower reflection intensity classes (GCG_0 and GCG_1), were located below 3.5 cm in the sward. When including only IC with high reflection intensity, the intercept with the y-axis, in the DM yield vs. GC_i relation, was equal to zero. Thus, it is concluded that, indeed, the GC_i fraction of the two lowest IC's were not related to harvested material. When including only higher IC's, DM yield could be estimated with a linear equation ($R^2_{adj}=0.75$). This resulted in good accuracy for higher DM yields. Linear estimates of FM yield were slightly better than for DM yield ($R^2_{adj}=0.81$), indicating that individual harvests differed in leaf area ratio and canopy geometry.

In literature on remote sensing, various vegetation indices are defined that predict the amount of vegetation from mixed spectra of canopies (including green leaves, dead material and soil) (e.g. Baret *et al.*, 1995; King *et al.*, 1986). These vegetation indices are more or less linearly related to the fraction of ground cover (Baret *et al.*, 1995; Bouman *et al.*, 1992). Ground cover is asymptotically related to herbage mass and leaf area index. Therefore, vegetation indices are also asymptotically related to herbage mass and leaf area index (Bouman *et al.*, 1992; Ripple, 1985). This limits the applicability of vegetation indices from remote sensing for estimation of herbage mass in the higher yield range.

The accuracy found for DM yield estimates (<340 kg DM yield ha^{-1}) is already promising for development of an imaging system for on-farm application. Gabriels and Van den Berg (1993) reported a residual standard error of about 450 kg DM yield ha^{-1} at 1600 kg DM yield for the capacitance probe and rising plate meter in *Lolium perenne* L. swards. Standard errors further increased at higher DM yields. Even higher inaccuracies were found for various methods by Harmoney *et al.* (1997), Sanderson *et al.* (2001) and Virkajärvi (1999).

The spectra obtained with the imaging spectroscopy system are mainly unmixed, due to the detailed spatial resolution. This allows straightforward pixel classification into soil, green leaves, leaves with specular reflection and dead material. The specific illumination of the imaging spectroscopy measurement system minimises shadow, and reflection intensity of leaf pixels depends solely on leaf angle and leaf height in the canopy (Schut *et al.*, Chapter 2). The index of reflection intensity responded strongly at large amounts of biomass. Therefore, this index is extremely helpful to monitor biomass accumulation in the higher DM yield and LAI range.

The results in this study were based on ground cover and reflection intensity data. The reflection curve contains additional spectral information, for instance

related to water content. These spectral features may further improve predictions of DM yield. The relation between sward spectra and feeding value, nutrient contents and DM yield will be presented in a future paper.

For the experiments reported here imaging spectroscopy allowed accurate and non-destructive monitoring of grass sward growth from increases in estimated GC_i and IRI. With these parameters, the actual sward status in terms of LI, LAI and accumulated DM could be described. The data needed for this purpose were collected using a complicated and expensive system with three different sensors, two independent light sources and advanced software. To make the technique ready for more general use in the field it should be made mobile, the number of sensors should be preferably reduced and the software made user-friendlier. A mobile version of the imaging spectroscopy system is currently being built. This mobile equipment will allow quantification of differences in growth and sward quality between fields and farms. Experience with this new equipment will also allow a more careful selection of minimum requirements in terms of sensor type, spectral and spatial resolution, and sampling routines.

4

Imaging spectroscopy for early detection of nitrogen deficiency in grass swards

A.G.T. Schut & J.J.M.H. Ketelaars

Submitted to Netherlands Journal of Agricultural Science

4. Abstract

The potential of an experimental imaging spectroscopy system, with high spatial (0.28-1.45 mm²) and spectral resolution (5-13 nm) is explored for early detection of nitrogen (N) stress. A greenhouse study was conducted with 15 *Lolium perenne* L. mini swards and 5 N treatments from June through October 2000. Images were recorded two times a week. With the experimental system, spectra of grass leaves in the canopy can be obtained. Treatment effects on ground cover (GC) and changes in leaf spectral characteristics were studied separately. Leaf pixels with similar reflection intensity were grouped in intensity classes (IC). An index of reflection intensity (IRI) indicates the percentage of strongly reflecting grass pixels. Blue edge, green edge and red edge positions were calculated for each IC. Both GC and IRI increased until harvest, with largest increases for liberal N treatments. The width of the chlorophyll dominated absorption band around 680 nm (CAW) increased up to a maximum of 133 nm for both liberal and limited N in the first two weeks after harvesting. The CAW decreased for limited N in the second half of the growth period in contrast to liberal N. At harvest, CAW explained 95% of the variation in relative DM yield between treatments. Principal component analyses showed an intertwined response of the principal components to both DM yield and N concentration. Edge positions changed strongly with IC. Possible effects of sensor characteristics, canopy geometry, leaf angle and changes in leaf characteristics with canopy position on the observed relation between IC and edge position are discussed.

4.1 Introduction

In the absence of fast, reliable and accurate methods for yield and nitrogen (N) stress indicators, accuracy of grassland fertilisation planning strongly depends on farmer's judgement. In literature, many authors describe the effects of N stress on reflection characteristics of leaves and canopies. In dried material, N concentration can be detected directly from reflection at the 2.1 µm absorption feature (Kokaly *et al.*, 2001). For fresh material, N stress can be remotely sensed by its effect on chlorophyll (Chl) concentration. The concentration of Chl *a* and Chl *b* relates to reflection at various wavelengths and to various reflection indices (Everitt *et al.*, 1985; Chappelle *et al.*, 1992; Blackmer *et al.*, 1994; Blackburn, 1998a; b). Chl concentration is highly correlated with leaf N

concentration, especially when N is deficient (Schepers *et al.*, 1996; Bausch *et al.*, 1998). However, variations in background reflectance, LAI and leaf angle distribution confound the detection of subtle differences in canopy reflection due to changes in Chl concentration (Clevers & B ker, 1991; Daughtry *et al.*, 2000). Increasing amounts of biomass normally leads to higher Chl amount per unit surface. Therefore, relations between remotely sensed parameters and Chl are better for Chl amount per unit surface than for Chl amount per unit biomass (Pinar & Curran, 1996). Problems of background reflection and LAI (or biomass) can be reduced when using spatial resolutions smaller than single leaves.

With the recently developed imaging spectroscopy system, new and automatic means for grass sward characterisation become available (Schut *et al.*, Chapter 2). Reflection intensity measured with this system is related to leaf height in the canopy and leaf angle. With this feature, image ground cover (GC) can be differentiated into reflection intensity classes. For each intensity class, spectral parameters can be determined which allows construction of spectral profiles. The non-destructive nature of reflection measurements allows the study of the evolution of GC and leaf pixel spectra. With GC estimates light interception, leaf area index (LAI) and biomass can be determined (Schut & Ketelaars, Chapter 3). Spatial GC variability can be used to study sward deterioration (Schut & Ketelaars, Chapter 8).

In this paper, the potential of the experimental imaging spectroscopy system is explored for early detection of N stress. For this, two experiments were conducted with 5 N treatments (0, 30, 60, 90, 120 kg N ha⁻¹ per harvest). Evolution of GC, spatial variability of GC, index of reflection intensity (IRI) and spectral characteristics (blue edge (BE), green edge (GE), red edge (RE) and Chl absorption width (CAW)) in response to N supply were studied.

4.2 Materials and methods

4.2.1 Experiments

In 2000, two N experiments were conducted with grass mini swards in containers of 0.9 m long, 0.7 m wide and 0.4 m high, filled with a sandy soil (3% organic matter). There were 5 N treatments (0, 30, 60, 90 and 120 kg N ha⁻¹ per harvest) and 3 replicates per treatment. These treatments will be referred to as 0N, 30N, 60N, 90N and 120N. The mini swards were placed under a rain

shelter, covered with 80% light-transparent foil, with wind breaking fencing at the sides. After each harvest, N was applied by hand. Potassium, phosphorus and sulphur were kept at sufficient levels. Soil moisture content was maintained at field capacity (22 volume %) by weighing the containers twice a week. At harvest, mini swards were hand cut to a stubble height of 4 cm.

Mini-swards in the first experiment were measured from 1 through 19 June. Per mini sward, 8.1 g m⁻² N, 13.8 g m⁻² P₂O₅ and 24 g m⁻² K₂O was applied in April. Then, grass was sown with a commercially available mixture of four *Lolium perenne* L cultivars. Once a good sward was established, grass was cut (30 May) and N was supplied according to the treatments. After the first growth period, grass was harvested on a hot day (20 June) creating severe sward damage, and this ended the first experiment.

For the second experiment, 5-10 cm thick, autumn 1999 sown swards were transplanted into the containers on July 6. After an initial start-up period (with an intermediate harvest on 25th of July), swards were harvested on August 8 and then N was supplied according to the treatments. Swards were harvested on 29 August, 27 September, and 31 October. Because of the time in the season, N levels were reduced after the September harvest, to 0, 20, 40, 60 and 90 kg N per ha⁻¹. Soil samples for mineral N analysis were taken after the September harvest. Application of N was further reduced with 1 N level (e.g. 60 instead of 90 kg N per ha⁻¹) when N-min content was higher than 22.5 kg ha⁻¹.

4.2.2 Measurements

On 42 positions in each container, from a height of 1.3 m above the soil, hyperspectral image lines were recorded with the V7 and N10 sensor, for details see Schut *et al.* (Chapter 2). The V7 sensor measures reflection in wavelengths from 404-709 nm and the N10 sensor from 680-970 nm. At soil level, an image line was 1.39 mm wide with a length of 152.5 mm, resulting in a spatial resolution of 0.28 mm² at soil level. The spectral resolution was 5 nm. Light was focussed with a bar lens, and only a 2-4 cm wide strip was illuminated. Light was projected vertically onto the soil, and reflection was measured under an angle of 2 degree from nadir.

In general, containers were scanned twice a week. During the June growing period (6, 8, 10, 13, 15 and 17 June), 100 adjacent image lines were recorded from one container of each treatment, scanning an area of 100 mm long and 152.5 mm wide. These image lines were recorded on similar locations in the container, and were used to construct 2D images.

4.2.3 *Chemical analysis*

At harvesting, fresh matter yield was weighed and samples were taken for analyses of dry matter (DM), total N, nitrate and sugar concentration. Total N was determined with the Dumas method on a Vario EL (Elementar analyse systemen, GmbH Hanau), and nitrate on a Bran and Luebbe Traacs 800 continuous flow system (Maarsen, the Netherlands). Sugars were determined from dried material. The sugars were extracted by adding demineralised water to a ground sample. On a Bran and Luebbe AutoAnalyzerII (Maarsen, the Netherlands, Method NL213-89FT), the amount of reducing sugars (glucose and fructose) was measured by reaction with ferricyanide which is reduced to colourless ferrocyanide. The reduction in light absorbance at 420 nm was used to calculate the amount of sugars as glucose equivalents. Total sugars after hydrolysis were determined in the same extract but the autoanalyser was now equipped with a hydrolysis-step to convert di- and oligosaccharides to glucose and fructose.

4.2.4 *Calculation of image parameters*

Classification

Schut *et al.* (Chapter 2) defined threshold values for soil, grass leaves (G), leaves with specular reflection (S), and dead material (D) classes and an intermediate class between soil and dead material. Separation between classes was based on ratios of reflectance (R) at 450, 550 and 680 nm. These classes are subdivided into reflection intensity classes (IC), based on the reflection intensity at predefined wavelengths (550 nm for the V7 and 746 nm for the N10). The intensity classes ranged for grass from IC 0 up to and including IC 6 for the V7 sensor and from IC 0 up to and including IC 10 for the N10 sensor. For leaves with specular reflection, IC ranged from 0 up to and including 2, and for dead material from IC 0 up to and including 3. A large number of pixel reflection spectra in these intensity classes are stored in a spectral library. With this library, pixel spectra of the recorded image lines were classified with maximum likelihood procedures (Schut & Ketelaars, Chapter 3). The classification procedure was based on a limited number of wavelengths, selected according to a statistical function (Feyaerts & Van Gool, 2001) maximising class to class separation.

After classification, spectra of pixels were normalised, according to equations in Schut *et al.* (Chapter 2). Normalisation means that reflection was divided by the mean reflection in the 550-555 nm range for the V7 sensor, and the 800-850 nm range for the N10 sensor. Mean sward reflection spectra (MSS) were calculated from normalised spectra of all pixels in grass IC 1 trough 10. In addition, mean reflection spectra were calculated from normalised spectra for each IC (MICS). It is stressed that for this procedure only grass pixels were selected, eliminating pixels containing soil and dead material. Under the assumption that the data of the V7 sensor and the N10 sensor were from identical objects and that the sensitivity of the sensors in overlapping regions was comparable, the data of the V7 sensor were normalised to the 800-850 nm range (Schut *et al.*, Chapter 2). These assumptions seem valid for MSS.

Ground cover, index of reflection intensity and spatial heterogeneity of GC

Ground cover was calculated per mini sward for each IC. Total image line (IL) ground cover (GC_{IL} , %) was calculated as sum of ground cover of all grass IC (GCG) and IC of all specular classes (GCS) from the V7 sensor:

$$GC_{IL} = \sum_{ic=0}^6 GCG_{ic} + \sum_{ic=0}^2 GCS_{ic} \quad (1)$$

where ic is the index number of the intensity class. The mini sward GC was calculated as the average of the GC_{IL} over the 42 image lines. This mini sward GC estimate underestimates visually scored GC, visually scored GC equals $8.63 + 1.076 \times GC$ (Schut & Ketelaars, Chapter 3). The index of reflection intensity (IRI, %) was then calculated as:

$$IRI = 100 \times \frac{\sum_{ic=3}^6 \frac{1}{42} \sum_{IL=1}^{42} GCG_{IL,ic}}{GC} \quad (2)$$

This IRI measures the presence of highly reflecting green pixels as a percentage of GC. A high value represents a dense canopy with horizontally oriented leaves (Schut & Ketelaars, Chapter 3).

The spatial heterogeneity was quantified with the spatial standard deviation of GC (GC-SSD) and logistically transformed values of GC (TGC-SSD). These were calculated according to equations in Schut & Ketelaars (Chapter 8). The spatial standard deviation was calculated per mini sward as the standard deviation of the 42 GC_{IL} estimates.

Calculation of edges

Reflectance spectra of green material typically have a sharp transition from minimum reflection around 680 and maximum reflection around 750 nm, known as the red edge (RE) (Horler *et al.*, 1983). Green material reflects more radiation in the green part than in blue or red parts of the spectrum, and a blue edge (BE) and a green edge (GE) can be found around 520 and 600 nm respectively. In this study we used a simple method for determination of edge position. From the normalised spectra, minimum (R_{\min}) and maximum (R_{\max}) reflection values were determined for BE, GE and RE within the spectral range of 472-800 nm. Then, a threshold value (T) was calculated according to:

$$T = R_{\min} + (R_{\max} - R_{\min}) \times CV \quad (3)$$

where CV is the critical value. At the RE, the transition between the V7 and N10 sensor typically occurs between a normalised reflection value of 0.35 and 0.5. To minimise effects of this transition, the CV was set at 0.55. The reflection value of band i was calculated as the average of band i , band $i-1$ and band $i+1$. Then, the wavelength position with a reflection value equal to T was calculated. For this, two neighbouring bands were determined where reflection in one band was smaller, and in the other band was greater than T . The exact wavelength position of T was calculated by linear interpolation of reflection values and wavelength positions. Edges were calculated for MSS and for each MICS.

The chlorophyll dominated absorption width (CAW) around 680 nm was calculated as the difference between RE and GE.

Canopy reflection profiles

Reflection intensity, measured with the system, is affected by both leaf angle and leaf height (Schut *et al.*, Chapter 2). Each MICS was calculated as mean over a large number of pixels. Therefore, effects of angles of individual leaves and mixed pixels (for IC 0) on MICS were considered small. Therefore, the change in reflection characteristics of MICS may contain additional information about the canopy, or canopy strata. Plotting the edges on the x-axis and IC number on the y-axis created a canopy profile. For illustration purposes, only profiles of 30 October are shown.

Edges in 2D Images

First, the composed 2D images were classified. For each grass pixel BE and GE position was calculated. To this end, position of R_{\min} and R_{\max} was fixed at 472 and 555 nm for the BE and 670 and 555 nm for the GE. Then, edge position was averaged over 4 neighbouring grass pixels, minimising noise effects. For illustration purposes, the image of the 120N treatment from 13 June is used.

Principal component analysis

Principal component analysis on the sums of squares and products was performed. For this, spectral data recorded just before harvest were used. For regression on relative DM yield, MSS of replicates were averaged per spectral band. This resulted in 10 principal components (PC) per treatment per harvest. These PCs were related to relative DM yields, DM concentration, total N concentration, organic N concentration and sugar concentration. Organic N was calculated as the difference between the concentrations of total N and nitrate. Only significant ($p < 0.05$) terms were included in the linear regression models.

4.2.5 *Relative DM yield*

The relative DM (RDM, %) yield is calculated as

$$RDM_{yield} = 100 \times \frac{DM_{yield}}{DMR_{yield}}, \quad (4)$$

where DMR indicates the 120N treatment mean DM yield. Standard errors were calculated for treatment means of DM yield and RDM yield, exclusive the error in DMR yield.

4.3 Results

Effects of N treatments on DM yield and N, nitrate and sugar concentrations are shown in Table 4.1. Liberal N supply (90N and 120N) resulted in higher DM yields and nitrate concentrations and lower DM and total sugar concentrations than 30N. The 0N of the August, September and October harvests was lower in total sugars than 30N. The newly sown sward of the 20 June harvest had high sugar and low nitrate concentrations, suggesting N deficiency even at high

yields and high N application rates. The differences in the concentration of reducing sugars between treatments were small, while concentration decreased for harvests later in the season. The 30N treatment had highest concentration of total sugars in the August, September and October harvests.

Table 4.1 Treatment means and standard errors of dry matter (DM) yield, and foliar concentrations of DM, total nitrogen (N), nitrate, reducing sugars and total sugars.

Treatment	DM (kg ha ⁻¹)	DM (%)	Total N (%)	Nitrate (%)	Reducing sugars (%)	Total sugars (%)
-----20 June-----						
0N	2430 ± 124	18.90± 0.15	1.73±0.03	0.00±0.00	5.08±0.61	31.98±0.48
30N	3161 ± 23	18.07± 0.95	1.88±0.12	0.00±0.00	4.59±0.43	27.17±1.57
60N	3198 ± 49	17.37± 0.26	1.99±0.03	0.01±0.00	4.45±0.05	25.01±0.60
90N	3612 ± 165	16.43± 0.38	2.24±0.07	0.02±0.00	4.38±0.22	22.00±1.70
120N	3786 ± 146	16.63± 0.30	2.39±0.03	0.03±0.01	4.59±0.13	21.26±0.55
-----29 August-----						
0N	591 ± 68	23.33± 0.38	2.05± 0.09	0.01± 0.00	3.40± 0.32	14.76± 0.43
30N	1381 ± 87	19.73± 0.72	1.91± 0.06	0.01± 0.00	3.28± 0.15	23.61± 1.73
60N	1514 ± 232	19.07± 1.28	3.05± 0.07	0.17± 0.01	3.01± 0.19	12.35± 0.70
90N	2066 ± 15	16.00± 0.32	2.96± 0.10	0.13± 0.04	3.51± 0.09	12.06± 0.83
120N	2001 ± 281	18.47± 0.78	3.07± 0.43	0.21± 0.10	3.12± 0.07	13.66± 2.76
-----27 September-----						
0N	356 ± 62	19.50± 0.61	2.25± 0.11	0.01± 0.01	2.00± 0.18	11.47± 1.88
30N	1304 ± 144	19.27± 1.63	1.94± 0.08	0.02± 0.01	2.19± 0.05	20.27± 1.38
60N	1913 ± 179	16.33± 0.76	2.33± 0.43	0.12± 0.03	2.66± 0.20	14.36± 0.47
90N	2587 ± 116	14.57± 0.20	2.83± 0.23	0.30± 0.01	2.77± 0.10	11.41± 0.68
120N	2696 ± 151	14.30± 0.5	3.54± 0.10	0.49± 0.05	2.37± 0.07	10.12± 0.45
-----31 October-----						
0N	253 ± 32	17.33± 0.64	2.67± 0.18	0.02± 0.01	1.79± 0.09	6.28± 1.01
30N	836 ± 19	15.50± 0.26	2.88± 0.07	0.04± 0.02	2.38± 0.18	10.71± 0.60
60N	1109 ± 115	15.33± 0.86	3.34± 0.08	0.14± 0.01	2.39± 0.10	10.25± 0.69
90N	1298 ± 45	13.63± 0.69	3.87± 0.27	0.42± 0.11	2.28± 0.19	8.07± 1.11
120N	1403 ± 72	12.97± 0.92	4.54± 0.09	0.72± 0.06	1.89± 0.10	6.39± 0.20

4.3.1 *Ground cover, canopy structure and spatial GC standard deviation*

The June growth period differed from the other three growing periods in initial GC (Figure 4.1). This is presumably caused by a different sward history. The preceding harvest for the June growing period was the first harvest of the newly sown sward, without dead material in the stubble and with a high tiller density. This resulted in a high GC just after harvest. The second experiment (August through October) had a second year sward with a lower tiller density and with dead material in the stubble. In this experiment, there was a long period without N supply before the experiment started, creating poor starting conditions. This was not the case in the first experiment where starting conditions were relative rich.

Limiting N supply (0N and 30N) retarded GC development compared to liberal N supply in the last two growth periods (Figure 4.1). In this figure, the 60N curve is only a little lower when compared to 90N and 120N. GC showed a typical development within a growth period, with steep increases at low GC and smaller changes at high GC levels (Figure 4.1). In the September harvest maximum GC level was reached for the liberal N supply but not for the limited N supply, decreasing treatment differences in GC towards harvesting. Treatments of the June harvest were much better discriminated with IRI than GC (Figure 4.2), indicating that N affects both GC and canopy geometry. Differences in IRI were larger in the June and September growth periods than in the August and October growth periods. The low IRI values in the October growth period probably resulted from low DM yields (Table 4.1) and limited height development.

The values of GC-SSD were smaller than 10% at all intervals for all treatments (Table 4.2). The GC-SSD values of the 0N treatment increased up to harvesting, whereas GC-SSD values of the other treatments first increased and later decreased towards harvesting. At 5-8 days after- and just before harvesting, 0N significantly differed from the 90N and 120N. The TGC-SSD values were smaller than 0.65 at all intervals for all treatments (Table 4.2). The TGC-SSD values of the 0N and 30N were significantly smaller than 120N at 14-21 days after harvesting and just before harvesting. The maximum value of GC-SSD is reached at 50% GC and TGC-SSD peaks at low values of GC (Schut & Ketelaars, Chapter 8). GC values for 0N exceeded 50% in the interval 14-21 days after harvesting, whereas GC for all other treatments exceeded this value already in the 9-13 days interval. In the 1-4 and 5-8 days after harvesting

intervals, treatments were not different in TGC-SSD value (Table 4.2). Therefore, treatment differences arose from differences in GC dynamics.

4.3.2 Position of BE, GE and RE

As with GC, the June growing period differed from the other harvests in edge positions, especially just after harvesting (Figure 4.3, 4.4 and 4.5). The harvest prior to this growth period was the first harvest of the new sward and leaves just continued their growth after harvesting. After harvesting in the second experiment (existing sward) new leaves had to emerge from the tillers, and here the position of the BE, GE and RE changed considerably within one growth period (Figure 4.3, 4.4 and 4.5). The 0N differed markedly in BE, GE, and RE from the other N treatments. Differences between 30N and 120N were small one week after harvesting. Then, GE increased and RE decreased for 30N whereas 120N changed less (GE) or increased slightly (RE).

Therefore, the largest treatment differences were found just before harvesting. For the 120N, the BE maximum and GE minimum was reached within 10 days after harvesting for the August and September growth period, and within 19 days for the October growth period. The RE reached its maximum a few days later (Figure 4.5). The CAW parameter showed a similar behaviour, but with a larger range and larger treatment differences (Figure 4.6).

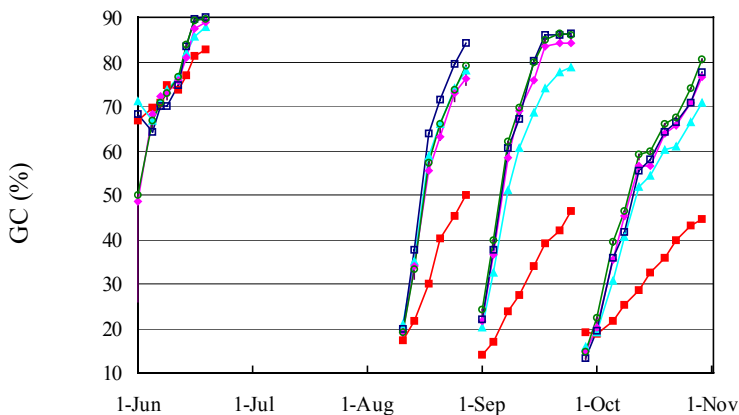


Figure 4.1 Development of image ground cover (GC) for 0N (■), 30N (▲), 60N (◆), 90N (□) and 120N (○).

Table 4.2 Mean values of spatial standard deviation of ground cover (GC-SSD) and logistically transformed ground cover (TGC-SSD) and standard error of treatment mean for intervals of days after harvesting (DAH). Different uppercase letters within rows indicate significant ($p < 0.05$) differences between treatment means.

DAH	0N	30N	60N	90N	120N
-----GC-SSD-----					
1-4	7.45 ± 0.52 ^a	8.09 ± 0.49 ^a	7.97 ± 0.54 ^a	7.69 ± 0.32 ^a	8.38 ± 0.24 ^a
5-8	7.63 ± 0.35 ^a	8.61 ± 0.07 ^b	8.50 ± 0.18 ^{ab}	8.95 ± 0.44 ^b	9.06 ± 0.18 ^b
9-13	8.68 ± 0.35 ^a	8.95 ± 0.23 ^a	9.05 ± 0.45 ^a	9.60 ± 0.26 ^a	9.47 ± 0.16 ^a
14-21	8.74 ± 0.24 ^a	8.05 ± 0.18 ^a	8.36 ± 0.51 ^a	8.35 ± 0.45 ^a	8.66 ± 0.15 ^a
Day before harvest	9.61 ± 0.10 ^a	8.08 ± 0.15 ^b	8.16 ± 0.53 ^b	8.12 ± 0.37 ^b	8.62 ± 0.20 ^b
-----TGC-SSD-----					
1-4	0.55 ± 0.02 ^a	0.58 ± 0.02 ^a	0.58 ± 0.05 ^a	0.58 ± 0.04 ^a	0.59 ± 0.03 ^a
5-8	0.47 ± 0.02 ^a	0.44 ± 0.00 ^a	0.43 ± 0.01 ^a	0.47 ± 0.03 ^a	0.45 ± 0.02 ^a
9-13	0.48 ± 0.02 ^a	0.44 ± 0.01 ^a	0.45 ± 0.03 ^a	0.47 ± 0.02 ^a	0.46 ± 0.01 ^a
14-21	0.47 ± 0.01 ^a	0.49 ± 0.02 ^a	0.54 ± 0.05 ^{ab}	0.57 ± 0.04 ^{ab}	0.62 ± 0.02 ^b
Day before harvest	0.48 ± 0.02 ^a	0.51 ± 0.01 ^{ab}	0.58 ± 0.05 ^{bc}	0.59 ± 0.04 ^{bc}	0.64 ± 0.02 ^c

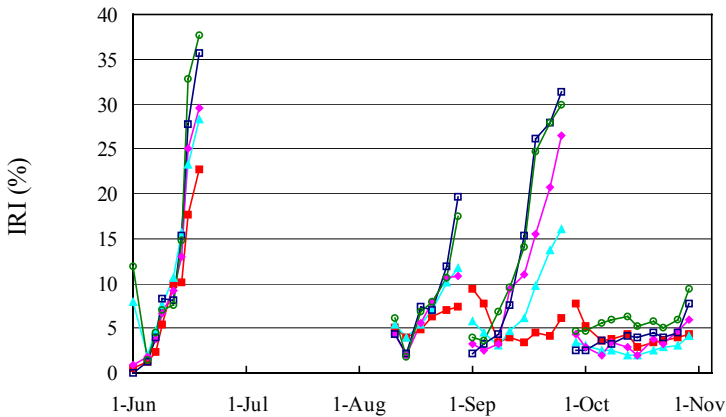


Figure 4.2 Development of index of reflection intensity (IRI) for 0N (■), 30N (▲), 60N (◆), 90N (□) and 120N (○).

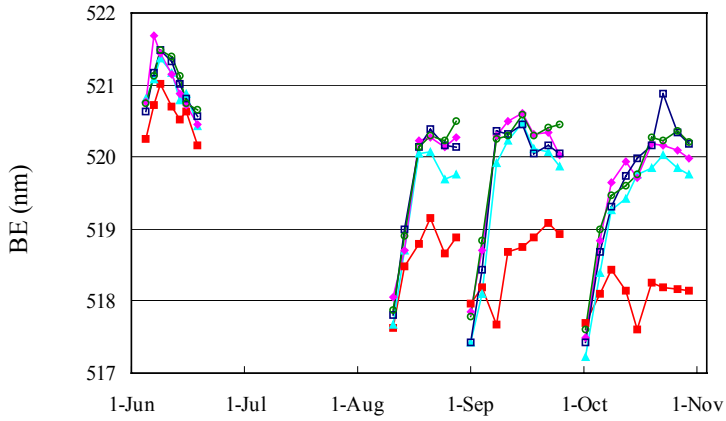


Figure 4.3 Development of blue edge (BE) position for averaged sward curves for 0N (■), 30N (▲), 60N (◆), 90N (□) and 120N (○).

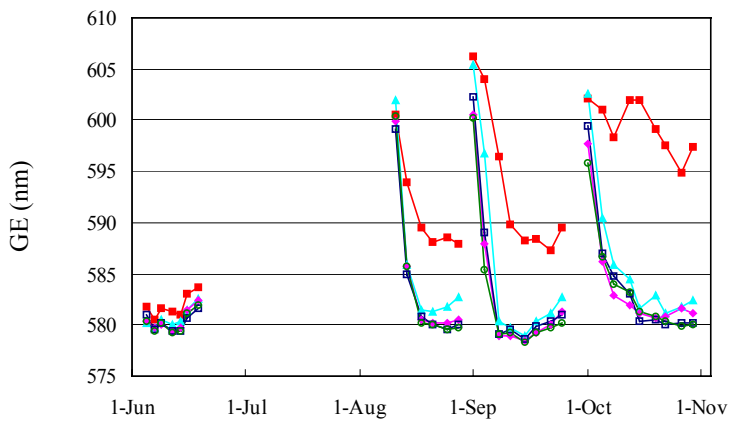


Figure 4.4 Development of green edge (GE) position for averaged sward curves for 0N (■), 30N (▲), 60N (◆), 90N (□) and 120N (○).

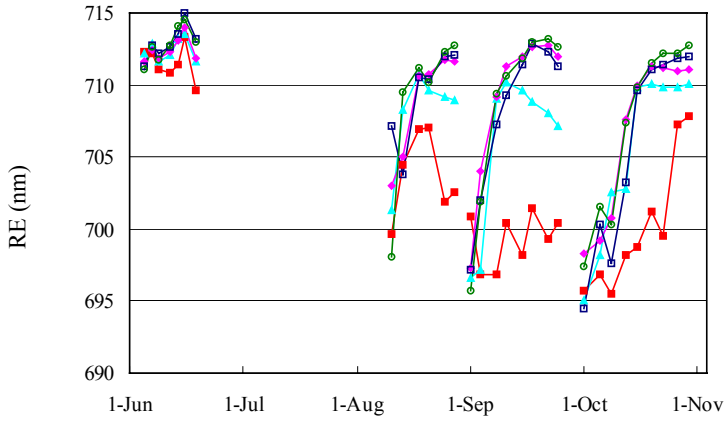


Figure 4.5 Development of red edge (RE) position for averaged sward curves 0N (■), 30N (▲), 60N (◆), 90N (□) and 120N (○).

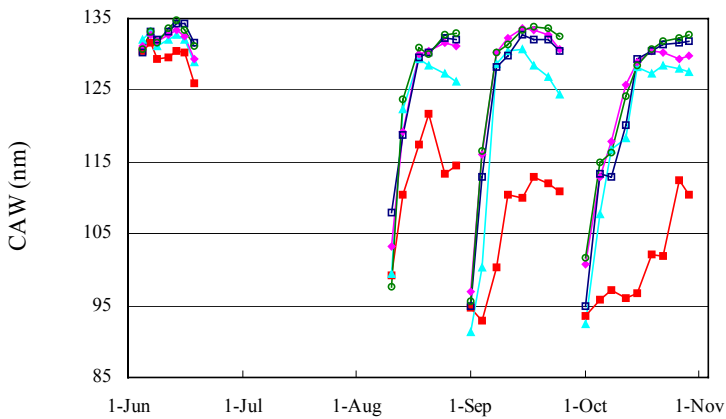


Figure 4.6 Development of chlorophyll absorption width (CAW) for averaged sward curves for 0N (■), 30N (▲), 60N (◆), 90N (□) and 120N (○).

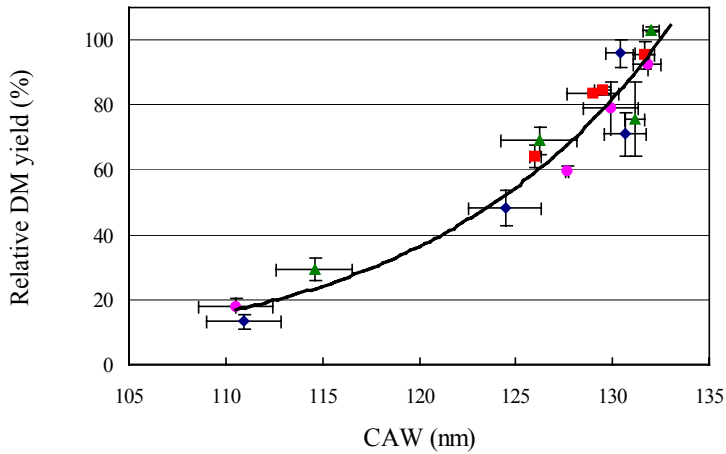


Figure 4.7 Dry matter yield relative to 120N dry matter yield as function of chlorophyll absorption width (CAW) for harvests on 20 June (■), 29 August (▲), 27 September (◆) and 31 October (●). Line: $y = 0.002e^{0.081x}$, $R^2=0.95$. Error bars indicate standard error of treatment means.

Table 4.3 Linear regression of principal components (PC) with DM yields, and DM, N and organic N concentrations, N yields and relative DM yields.

	Number of observations	PC in the regression model	R ²	SE observations
DM yield (kg ha ⁻¹)	60	PC1, PC3, PC5, PC6, PC7, PC8	0.87	377
DM (%)	60	PC2,PC3,PC4,PC9	0.61	1.66
N (%)	60	PC1, PC2, PC3, PC4, PC5, PC6, PC7	0.77	0.42
N org. (%)	60	PC1, PC2, PC3, PC5, PC6, PC7	0.75	0.35
Sugar (%)	60	PC1,PC2,PC7	0.78	3.89
N yield (kg ha ⁻¹)	60	PC1, PC2, PC3, PC4, PC5	0.77	13.3
RDM yield (%) [*]	20	PC1, PC2, PC3, PC4	0.93	7.5

* PC analysis performed on spectra averaged over N treatment replicates

4.3.3 Yield depression

The CAW parameter relates strongly to relative DM yield ($R^2=0.95$, Figure 4.7). Differences in CAW at high relative DM yields were smaller than at low relative DM yields. The CAW parameter outperformed RE ($R^2=0.78$) and GE ($R^2=0.78$) alone in the correlation with RDM yield.

4.3.4 Principal component analysis

The principal components were highly correlated with DM yield, N concentration and sugar concentration (Table 4.3). Total N was slightly stronger related to PC than organic N. Most PC were selected for more than one variable. RDM yield was strongly related to PC1 through PC5, with an R^2 value of 0.93.

4.3.5 Profiles of BE, GE and RE

As an example, profiles of BE, GE and RE were calculated from image lines recorded on 30 October. The profiles for BE (Figure 4.8) and GE (Figure 4.9) showed greater differences between low and high IC's than RE (Figure 4.10).

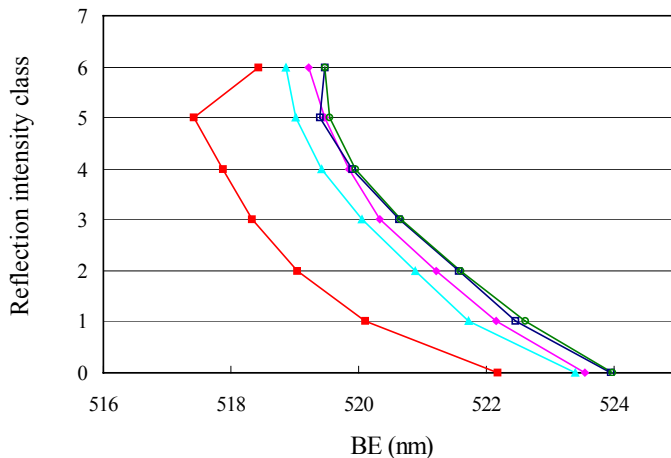


Figure 4.8 Blue edge (BE) position of leaf pixels per reflection intensity class for 0N (■), 30N (▲), 60N (◆), 90N (□) and 120N (○).

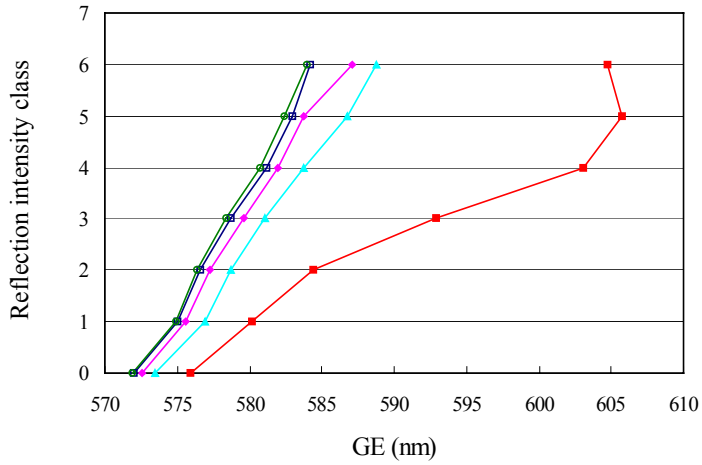


Figure 4.9 Green edge (GE) position of leaf pixels per reflection intensity class for 0N (■), 30N (▲), 60N (◆), 90N (□) and 120N (○).

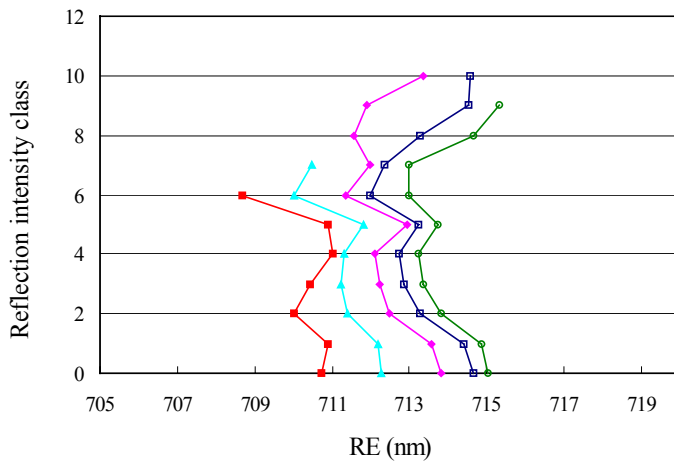


Figure 4.10 Red edge (RE) position of leaf pixels per reflection intensity class for 0N (■), 30N (▲), 60N (◆), 90N (□) and 120N (○).

The BE and GE showed a larger shift with IC than RE throughout growth periods. Changes of BE (4.5 - 4.8 nm) and GE (8 – 30 nm) with IC for the August, September and October harvests were larger than temporal changes of BE (1.3 - 3.5 nm) and GE (7 - 27 nm) of the MSS (compare Figure 4.3 with Figure 4.8 and Figure 4.4 with Figure 4.9). Differences between N treatments were more or less constant within the profile for the BE and RE. For the GE, the N0 treatment deviated more from all other treatments with increasing IC.

In the 2D classified image of Figure 4.11A it is shown that pixels with bright colours, and thus high reflection intensity, were from horizontally oriented leaves positioned in the top of the canopy. In general, pixels in lower IC's were nearer to the soil or stronger vertically orientated. Within the collection of pixels with identical IC, various edge positions occurred (Figure 4.11B and C). Nevertheless, changes in BE and GE position were, on average, correlated with IC (Figure 4.12).

In this figure, the MICS and the BE and GE position are shown from the Figure 4.11 image lines. The MICS differed in shape, affecting various curve-characteristics such as BE and GE position and position of maximum derivatives. The BE and GE position of MICS shifted 4.3 (BE) and 7 nm (GE) from Grass IC0 to Grass IC6 (Figure 4.12).

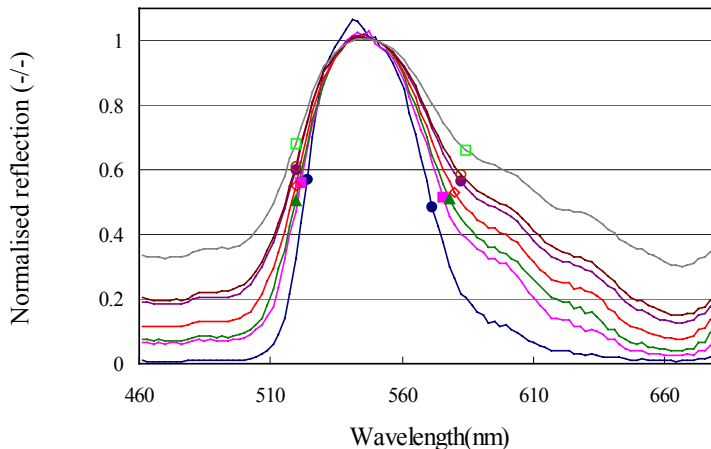


Figure 4.12 Normalised reflection curve, for the Figure 4.11 images, for GCG₀ (—), GCG₁ (—), GCG₂ (—), GCG₃ (—), GCG₄ (—), GCG₅ (—) and GCG₆ (—). The calculated BE and GE positions are indicated by markers on the curves.

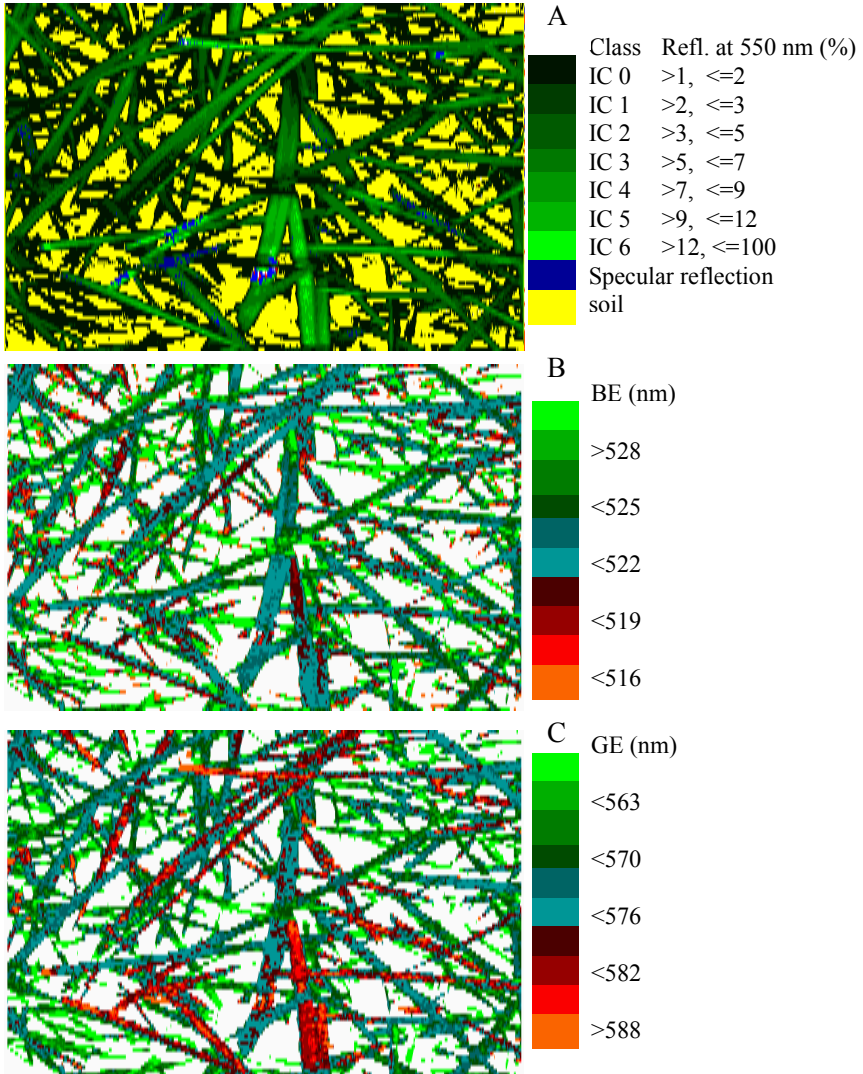


Figure 4.11 Image of 100 adjacent image lines with classified image (A), images with relative position of BE (B) and GE (C).

4.4 Discussion and conclusion

Nitrogen treatments differed in evolution of ground cover (GC), index of reflection intensity (IRI) and spectral characteristics. It was found earlier that GC and IRI are related to biomass and canopy geometry (Schut & Ketelaars, Chapter 3). Therefore, an indication of nitrogen (N) stress can only be given when actual values of GC and IRI can be compared with GC and IRI under optimal N supply.

Nitrogen treatments differed occasionally in spatial standard deviation of GC and logistically transformed values of GC. These differences arose from differences in GC dynamics. For all N treatments, GC-SSD and TGC-SSD values remained below 10 and 0.65 respectively. Schut & Ketelaars (Chapter 8) found that dense swards had GC-SSD values below 10.5 and TGC-SSD values below 0.6. Absolute differences between control and deteriorated swards were largest at 50% GC for GC-SSD and shortly after harvesting for TGC-SSD. Nitrogen treatments were not different in GC-SSD and TGC-SSD, neither at 50% GC nor shortly after harvesting, and it is concluded that nitrogen supply did not affect sward heterogeneity.

Leaf reflectance can indicate N stress in maize (Blackmer *et al.*, 1994; Schepers *et al.*, 1996; Masoni *et al.*, 1997). The dynamics of blue edge (BE), green edge (GE) and red edge (RE) at limited N supply differed from those at liberal N supply. The CAW (chlorophyll absorption width, calculated as the difference between RE and GE position) at limited N supply decreased in the second half of the growth period, in contrast to liberal N supply.

The CAW appeared to be strongly correlated with relative dry matter yield ($R^2=0.95$). This harvest-independent relation was stronger for the CAW parameter than for the GE or RE alone, and may therefore be the preferable parameter for N fine-tuning. The shape of the relation was exponential with smaller differences in CAW under near optimal N supply. Higher N treatments (60, 90 and 120 kg N ha⁻¹) could, therefore, not be separated from each other in all growth periods. The relation between N supply and chlorophyll (Chl) concentration has a curvilinear character (Wood *et al.*, 1992; Kantety *et al.*, 1996) and reflection decreases asymptotically with increasing Chl (Everitt *et al.*, 1985; Boochs *et al.*, 1990; Ercoli *et al.*, 1993; Schepers *et al.*, 1996). Therefore, identification of near-optimal N-fertilised swards with leaf reflectance alone is difficult. The same conclusion can be drawn from absorption measurements (with *e.g.* SPAD). In *Festuca arundinacea* Schreb., Kantety *et al.* (1996) found a maximum response for SPAD at 254 kg N supply,

while DM yield was highest at 290 kg N. Apparently, small changes in SPAD measurements were accompanied by relative large changes in DM yield. These findings, however, are in contrast with the results of Canova & Gaborcik (2000), who found a response in SPAD values up to the highest N supply. Likewise, Gaborcik *et al.* (1998) found linear relations between leaf colour, Chl concentration and N concentration in leaves of various grass species.

The linear regression between relative DM yield and principal components was strong ($R^2=0.93$). The principal components were also strongly related to DM yield and N concentration. The intertwined response of PC to DM yield, N concentration and leaf colour made interpretation difficult. Therefore, detection of N stressed swards under a range of harvesting frequencies requires extensive calibration and validation in order to correct for differences in DM yield related to the length of the growth period and not to N deficiency.

In literature, various methods are described for characterising reflection curves, such as fitting functions to edge regions and calculation of derivatives or indices. Fitting a Gaussian function to the edge region (Bonham-Carter, 1988) is limited to edges with a more or less Gaussian shape. Obviously, this approach is suitable for the BE and RE, but not for the GE. Polynomials (*e.g.* cubic splines) do not have this limitation (Railyan & Korobov, 1993). Derivatives are sensitive for the degree of smoothing (Rollin & Milton, 1998) and data noise and, therefore, require continuous curves. Indices use only a small part of the reflection curve. The method we used is hyperspectral, simple, fast and not limited to a specific edge shape.

Some remarks must be made with regard to the strong effect of reflection intensity on edge position. The observed profiles are presumably the result of a combination of sensor characteristics, canopy geometry and changes in leaf characteristics within the canopy.

Firstly, irradiance in our experimental system decreases with decreasing height positions in the canopy, despite the bar-lens in front of the light source (Schut *et al.*, Chapter 2). The imaging spectrograph requires high light input as it subdivides the incoming light over a large number of spectral bands and diffraction efficiency is smaller than 50% (Herrala & Okkonen, 1996). Therefore, lower boundaries of camera sensitivity in strong absorbing regions of the spectrum are reached earlier at low than at high canopy height positions. As this phenomenon will be less pronounced for strongly reflecting regions of the spectrum, the result may be changes in the shape of the reflection curve with reflection intensity.

Secondly, shadowed leaves will have reduced reflection intensity and will, therefore, be assigned to 'lower' IC's. Shadowed leaves receive greener light than leaves in full light, as leaves preferably absorb blue and red light. In the system used, however, only a narrow line is illuminated and reflection is measured under a narrow angle, minimising shadow effects. Light composition can only be altered by light scattered from neighbouring leaves within a few centimetres. In the recorded images only minor shadow effects were visible. Therefore, we expect that shadow had only a minor effect on spectral composition. In accordance with this, canopy edge profiles were also strong for treatments with low biomass and presumably a minimum of shadowed areas.

Thirdly, canopy geometry apparently affects the profiles. Profiles of clover swards differed from grass swards and diurnal changes in clover leaf-orientation affected profile slope (Chapter 7). Leaves with a vertical orientation will be assigned to 'lower' IC's (Schut *et al.*, Chapter 2). The amount of chlorophyll, expressed per pixel, will automatically increase when leaves become more vertically oriented. As a consequence, shifts of the red edge, at canopy level, have been observed in relation to leaf inclination angle (Asner, 1998; Guyot *et al.*, 1992). Yet an increase in the amount of pigment per pixel only affects the reflection curve when light absorption is below its maximum. Therefore, leaf angle will probably have a greater influence with leaves and canopies low in pigment concentration than with leaves and canopies high in pigment content.

Finally, leaf pigment composition within the canopy might change with leaf age, position on the leaf and growth conditions. During growth, leaves near the soil gradually become shaded and are exposed to greener light as a result of absorption of light by newly developing leaves. Both yellow light, when compared to red light (Liu *et al.*, 1993), and low light intensity induce lower Chl *a/b* ratios and higher Chl *a* and *b* contents (Evans, 1988; Watanabe *et al.*, 1993). Thus, the Chl *a* profile within a canopy is stronger than the Chl *b* profile, leading to a profile in Chl *a/b* ratios (Yamasaki *et al.*, 1996). Pigment composition also varies within a leaf, with lower pigment content near the leaf base and leaf tip than in the middle (Biswal *et al.*, 1994). Obviously, leaf tips are mostly found at the top of the canopy and leaf bases low in the canopy. Changing pigment content with position on the leaf may, therefore, lead to profiles of pigment content within the canopy.

In acetone, strong absorption peaks are found with an absorption maximum at 661.6 and 429.6 nm for Chl *a*, at 644.8 and 455.8 nm for Chl *b* and at 454 nm for β -carotene (Lichtenthaler, 1987). In vivo, peak positions are slightly

different with 680 nm and 440 nm for Chl *a* and 660 and 460 nm for Chl *b* (Maier *et al.*, 1999). Thus, changes in Chl *b* would have a stronger effect on GE, whereas changes in Chl *a* would primarily affect RE and changes in both Chl *a* and β -carotene would affect BE. We found that BE, GE and RE responded simultaneously during re-growth and were sensitive for the amount of N supplied. This can be understood when considering that Chl *a* and Chl *b* respond to similar environmental factors, *e.g.* nitrogen stress, and are, therefore, strongly correlated.

Imaging spectroscopy provides accurate means to monitor growth and growth retardation due to nitrogen deficiency. Treatments with different N-supply showed a strong correlation between relative DM yield and CAW, although discriminating ability of CAW was limited at higher levels of relative yield. The effects of sensor characteristics, canopy geometry, and pigment composition within the canopy on edge profiles require further study. For this, an experiment where images were recorded after removal of individual leaf-strata will be analysed and presented in future work.

5

Effects of angle, height, and pigment content of leaves on reflection characteristics of grass swards

A.G.T. Schut, J.J.M.H. Ketelaars & J.P.F.G. Helsper

5. Abstract

In this paper, effects of leaf angle, leaf height and pigment content of leaves on reflectance spectra of grass swards. were studied. Reflectance was measured with an experimental imaging spectroscopy system with high spatial (0.28-1.45 mm²) and spectral resolution (5-13 nm). An experiment was conducted with mini swards of *Lolium perenne* L. at 4 nitrogen (N) supply levels. Images were recorded twice a week, during two growth periods. Treatment effects on ground cover and changes in leaf spectral characteristics were studied separately. Leaf pixels with similar reflection intensity were grouped in intensity classes (IC). Blue edge, green edge (GE) and red edge (RE) positions were calculated for each IC. The width of the chlorophyll absorption band (CAW) was calculated as difference between RE and GE. At harvest, swards were harvested in three strata (>16 cm, 9-16 cm, and 4-9 cm) and strata were subjected to chemical analysis. Effects of leaf angle and height on spectral properties were studied independently with the help of detached leaves.

Contents of N and pigments, on average, increased with increasing N level and decreased downward into the sward. Edges showed strong, N treatment dependent, changes with IC. At harvest, CAW of intact swards increased with N level, with absolute values being similar to values measured at harvested material of the upper stratum. When upper strata were subsequently removed, CAW of the remaining sward decreased much less than expected from measurements at harvested material. Varying leaf angle from horizontal to nearly vertical increased CAW about 6 nm. Decreasing leaf height up to 20 cm decreased CAW with 2.6 nm. The ratio between red and blue reflectance was also strongly affected by leaf angle. The summed effects of leaf height and leaf angle could only partly explain changes of edge positions with IC, and may have been augmented by sensor characteristics. It is concluded that combinations of the red/blue ratio, shifts of GE with IC and CAW may be useful to separate effects of leaf angle on sward reflectance from effects of leaf pigment concentration *per se*.

5.1 Introduction

The interpretation of reflectance measured from leaves within a standing canopy requires a full understanding of the factors affecting the composition

and intensity of the reflected signal. The factors known to influence leaf reflectance are leaf pigment content, constituent composition, cellular arrangement and leaf angle. With close range sensing, the position of leaves in the canopy is of particular importance as reflectance intensity and characteristics depend on shadows and angle with incident light (Sandmeier *et al.*, 1998). The currently available imaging spectrometers combine a high spatial and spectral resolution (Herrala & Okkonen, 1996). This allows reflection measurements of individual leaves within a canopy (Borregaard *et al.*, 2000; Feyaerts & Van Gool, 2001; Schut *et al.*, Chapter 2). Schut & Ketelaars (Chapter 4) found that edge positions of reflection signals were related to reflection intensity. They discussed that shadow, pigment content gradient in the canopy, leaf angle and limitations in dynamic range of the sensor may affect this relation. Furthermore, this relation differed for clover and grass swards, and shifted with circadian changes in cloverleaf angle (Schut & Van den Berg, Chapter 7). It is yet unclear to what extent these factors affect the reflectance recorded.

The objective of this paper was to study factors affecting the relation between reflection characteristics and reflection intensity of grass canopies at harvest, and to quantify the effect of leaf angle, height position in the canopy and pigment content on reflectance of leaves within a canopy. To this end, spectroscopic images were recorded from intact grass swards with 4 different nitrogen (N) application levels. In addition, images were recorded before and after harvesting sward strata, and from detached harvested material per stratum. Finally, the influence of leaf angle and height in the canopy on reflection characteristics was quantified for detached leaves.

5.2 Materials and Methods

5.2.1 Experiment

In 2001, an experiment was conducted with 4 N supply levels of 0, 30, 60 and 90 kg N ha⁻¹ per growth period (referred to as N0, N1, N2 and N3 respectively) in 4 replicates. In late April 2001, a 1999 sown sward with a mixture of 4 *Lolium perenne* L. cultivars was transplanted into containers (0.4 m high, 0.9 m long and 0.4 m wide) filled with sandy topsoil material, which were placed outside, and weighed twice a week. These swards were fertilised with 100 kg N ha⁻¹ in March 2001. Water, potassium, phosphate and sulphur were kept at

sufficient levels. There were two intermediate harvests, without additional N fertilisation, on 28 May and 25 June. On 21-23 July and 21-23 August mini swards were hand cut at a height of 16 cm, 9 cm and 4 cm above soil surface, so that three strata were obtained. For each mini sward, fresh material was collected and weighed per stratum. Per treatment, fresh material of treatment replicates was combined per stratum and samples were taken for chemical analysis, including pigment analysis, and for determination of leaf area ratio (LAR). Six soil samples per container were mixed and sampled for analysis of soil mineral N content. Additional N supplies were given after the 25 June and 23 July harvest. The mineral N content in the soil was low after the July harvest. Therefore, extra N was supplied on 7 August, equivalent to 0 (N0), 10 (N1), 20 (N2), and 30 kg N ha⁻¹ (N3).

5.2.2 Measurements

On 42 positions in each container, from a height of 1.3 m above the soil, hyperspectral image lines were recorded with the V7 and N10 sensor (for details see Schut *et al.*, Chapter 2). The V7 sensor measures reflection between 404 and 709 nm and the N10 sensor between 680 and 970 nm. At soil level, an image line was 1.39 mm wide and 152.5 mm long, resulting in a spatial resolution of 0.28 mm² at. The spectral resolution was 5 nm. Light was focussed with a bar lens, and only a 2-4 cm wide strip was illuminated. Light was projected vertically onto the soil, and reflection was measured at an angle of 2 degree from nadir. Image lines were recorded twice a week during the growth periods. At harvest, image lines were recorded from intact canopies. Then strata were harvested. Before harvesting a stratum, image lines were recorded. In addition, for the August harvest some material from each stratum was placed on a black cloth, when sufficient material was available. The leaves were positioned horizontally under the imaging spectroscopy system, at a height equivalent to 18 cm above soil surface. Then, 50 images (each 1 mm apart) were recorded twice, and image analysis results were averaged. On 20 August, images were recorded from detached leaves under various angles. For this, three leaves of the N1 and N3 treatment were positioned under the imaging system at a height equivalent to 18 cm above soil surface. The leaves were fixed on a black cloth, which was connected to a rotating plate, with the adaxial side of the leaf on top. First, images of the reflection standard were recorded. Then, leaves were rotated around their shortest axis. Images were recorded twice, and image analysis results were averaged. The effects of leaf height were

evaluated by measuring reflectance of leaves at various distances from the sensor. From three sets of three leaves, reflectance was also measured between a height equivalent to 2-19 cm above the soil. Again, these leaves were placed on a black cloth on a horizontal plateau with their adaxial leaf side on top. Then, the height of the plateau was varied.

Image analysis

Schut *et al.* (Chapter 2) defined threshold values for soil, grass leaves (G), leaves with specular reflection (S), and dead material (D) classes and an intermediate class between soil and dead material. Separation between classes was based on ratios of reflectance (R) at 450, 550 and 680 nm. These classes are subdivided into reflection intensity classes (IC), based on the reflection intensity at predefined wavelengths of 550 nm for the V7 sensor and 746 nm for the N10 sensor. High-reflecting classes represent upper, more horizontally oriented leaves, while low reflecting classes represent lower, more vertically oriented leaves. The intensity classes for grass ranged from IC 0 up to and including IC 6 for the V7 sensor and from IC 0 up to and including IC 10 for the N10 sensor. For leaves with specular reflection, IC ranged from 0 up to and including 2, and for dead material from IC 0 up to and including 3. A large number of pixel reflection spectra in these intensity classes are stored in a spectral library. With this library, pixel spectra of the recorded image lines were classified with maximum likelihood procedures (Schut & Ketelaars, Chapter 3). The classification procedure was based on a limited number of wavelengths, selected according to a statistical function (Feyaerts & Van Gool, 2001) maximising class to class separation. After classification, spectra of pixels were normalised, according to equations in Schut *et al.* (Chapter 2). Normalisation means that reflection was divided by the mean reflection in the 550-555 nm range for the V7 sensor, and in the 800-850 nm range for the N10 sensor. Mean sward reflection spectra (MSS) were calculated from normalised spectra of all grass pixels, excluding grass IC 0. In addition, mean reflection spectra were calculated from normalised spectra for each IC (MICS). It is stressed that for this procedure only pixels containing grass were selected, thus eliminating pixels containing soil and dead material. Under the assumption that the data of the V7 and N10 sensors were from identical objects and that the sensitivity of the sensors in overlapping regions was comparable, the data of the V7 sensor were normalised to the 800-850 nm range (Schut *et al.*, Chapter 2). This resulted in continuous MSS for the spectral range from 405 to 970 nm. For the

recordings of individual leaves similar procedures were followed. The mean spectral curve was now calculated from all pixels in GCG and GCS classes, excluding GCG₀.

Ground cover, index of reflection intensity and spatial heterogeneity of GC

Ground cover was calculated per mini sward for each IC. Total image line (IL) ground cover (GC_{IL}, %) was calculated as the sum of ground cover of all grass IC (GCG) and IC of all specular classes (GCS) from the V7 sensor:

$$GC_{IL} = \sum_{ic=0}^6 GCG_{ic} + \sum_{ic=0}^2 GCS_{ic} \quad (1)$$

where *ic* is the index number of the intensity class. The mini sward GC was calculated as mean GC_{IL} over the 42 image lines. The index of reflection intensity (IRI, %) was then calculated as:

$$IRI = 100 \times \frac{\sum_{ic=3}^6 \frac{1}{42} \sum_{IL=1}^{42} GCG_{IL,ic}}{GC} \quad (2)$$

This IRI measures the presence of highly reflecting green pixels as a percentage of GC. A high value represents a relatively high canopy with horizontally oriented leaves (Schut & Ketelaars, Chapter 3). The spatial heterogeneity was quantified with the spatial standard deviation of GC (GC-SSD) and logistically transformed values of GC (TGC-SSD). These were calculated according to the equations in Schut & Ketelaars (Chapter 8), where the spatial standard deviation was calculated per mini sward as the standard deviation of the 42 GC_{IL} estimates. The GC-SSD can be best evaluated when GC is around 50%.

Calculation of edges

Reflectance spectra of green material typically have a sharp transition from minimum reflection around 680 and maximum reflection around 750 nm, known as the red edge (RE) (Horler *et al.*, 1983). Green material reflects more radiation in the green part than in blue or red parts of the spectrum, and a blue edge (BE) and a green-edge (GE) can be found around 520 and 600 nm respectively. In this study we used a simple method for determination of edge

position. From the normalised spectra, minimum (R_{\min}) and maximum (R_{\max}) reflection values were determined for BE, GE and RE regions within the spectral range of 472-800 nm. Then, a threshold value (T) was calculated according to:

$$T = R_{\min} + (R_{\max} - R_{\min}) \times C \quad (3)$$

where C is the critical value. At the RE, the transition between the V7 and N10 sensor typically occurs between a normalised reflection value of 0.35 and 0.5. To minimise effects of this transition, the C was set at 0.55. The reflection value of band i was calculated as the average of band i , band $i-1$ and band $i+1$. Then, the wavelength position with a reflection value equal to T was calculated. For this, two neighbouring bands were determined where reflection in one band was smaller, and in the other band was larger than T . The exact wavelength position of T was calculated by linear interpolation of reflection values and wavelength positions. Edges were calculated for MSS and for each MICS. For MSS, the chlorophyll dominated absorption width (CAW) around 680 nm was calculated as the difference between RE and GE.

Relation between IC number and edge position

Reflection intensity of leaves, measured with the system, is affected by leaf angle and leaf height (Schut *et al.*, Chapter 2). Each MICS was calculated as the mean over a large number of pixels and effects of angles of individual leaves and mixed pixels (for IC 0) on MICS were considered small. Therefore, differences between reflection characteristics of MICS may contain additional information about the canopy. IC number was plotted versus edge value. These relations were characterized by a regression of the function ($Y = a + b \times X$) through the GE parameters of GCG₀ up to and including GCG₅. The number of pixels in GCG₆ was low early in the growth period. Therefore, GCG₆ was not included in the regression as a few leaves can influence the reflection characteristics of GCG₆ strongly. The slope parameter b (IC nm⁻¹) was used to compare the relations between IC number and GE.

Chemical analysis

At harvest, fresh matter yield was weighed and samples were taken for analyses of dry matter (DM), total N, nitrate-N and sugar concentration. Total N was

determined with the Dumas method on a Vario EL (Elementar Analyse Systemen, GmbH Hanau), and nitrate-N on a Bran and Luebbe Traacs 800 continuous flow system (Maarsen, the Netherlands). Sugars were determined from dried material. Sugars were extracted by adding demineralised water to a ground sample. On a Bran and Luebbe AutoAnalyzerII (Maarsen, the Netherlands, Method NL213-89FT), the amount of reducing sugars (glucose and fructose) was measured as reduction in light absorbance at 420 nm and expressed as glucose equivalents. Total sugars was determined in the same extract after a hydrolysis-step of di- and oligosaccharides to glucose and fructose.

Pigment analysis

Chlorophylls *a* and *b*, carotenoids and total xanthophylls (neoxanthin, violaxanthin, antheraxanthin, zeaxanthin plus lutein and β -cryptoxanthin) were quantitatively determined using reversed phase high-performance liquid chromatography (RP-HPLC) according to Helsper *et al.* (2003).

5.3. Results

5.3.1 Experiment

Yields and chemical analysis

An increase in the amount of N supplied resulted in considerably higher FM yields. Yields were higher in the August than in the July harvest (Table 5.1). Differences between replicates were small. The mineral N content of the soil after harvest was low, even after the high N supply in the August growth period, with values of 1.9-3.3 mg kg⁻¹ dry soil in July and 1.6-3.0 mg kg⁻¹ dry soil in August. The harvested material also had low nitrate-N (0-0.01% in July and 0-0.04% in August) and low N concentrations (1.78-2.32% in July and 2.12-2.85% in August) in both harvests.

The low values of mineral N content in the soil, nitrate-N and total N indicate that even the highest N application was insufficient for maximum growth, especially for the July growth period. N deficiency resulted in high total sugar concentrations with mean values between 21.9-26.8% in the July harvest and 13.4-17.2% in the August harvest. In general, FM and DM yields and N and

nitrate-N content increased, whereas DM content and LAR decreased with N supply. Contents of total sugars were lowest for N3 in the August harvest, in contrast to the July harvest where N0 had lowest sugar contents. Differences in reducing sugar contents between treatments and harvest dates were small. In the August growth period, only swards of the N3 lodged from 16 August onwards. This did not occur in the July harvest.

Table 5.1 Fresh matter yield (FM) and mineral N content (N-min) of the soil after harvest \pm standard error of the treatment mean, total dry matter yield (DM), DM content and contents in DM of nitrate-N (NO₃-N), nitrogen (N), reducing sugars and total sugars, and leaf area ratio (LAR) per treatment.

	N0	N1	N2	N3
-----July 2001-----				
FM (t ha ⁻¹)	2.38 \pm 0.16	4.81 \pm 0.27	9.30 \pm 0.13	14.03 \pm 0.10
N-min (mg kg ⁻¹ dry soil)	3.3 \pm 1.2	2.7 \pm 0.6	1.9 \pm 0.1	2.3 \pm 0.1
DM (kg ha ⁻¹)	644	1212	2171	2944
DM (%)	27.5	25.2	23.4	21.0
NO ₃ -N (%)	0.0	0.0	0.0	0.003
N (%)	1.78	1.90	1.99	2.32
Reducing sugars (%)	2.97	2.83	3.35	3.11
Total sugars (%)	21.91	26.82	26.36	22.59
LAR (m ² g ⁻¹ DM)	0.023	0.011	0.012	0.008
-----August 2001-----				
FM (t ha ⁻¹)	2.74 \pm 0.13	8.45 \pm 0.26	14.27 \pm 0.38	16.94 \pm 0.98
N-min (mg kg ⁻¹ dry soil)	1.6 \pm 0.1	2.0 \pm 0.2	2.2 \pm 0.3	3.0 \pm 0.6
DM (kg ha ⁻¹)	688	1887	2791	3442
DM (%)	25.1	22.3	19.6	20.4
NO ₃ -N (%)	0.002	0.003	0.008	0.043
N (%)	2.12	2.17	2.44	2.85
Reducing sugars (%)	3.30	3.09	2.70	3.10
Total sugars (%)	17.15	16.81	14.30	13.43
LAR (m ² g ⁻¹ DM)	0.017	0.013	0.009	0.011

Ground cover, canopy structure and spatial GC standard deviation

The GC values were slightly higher in the August than in the July growth period (Figure 5.1). The GC ordering at harvest was in accordance with N supply. The IRI of the higher N supply levels strongly increased in the second half of the growth periods, with the N3 having the highest IRI values (Figure 5.2). The 50% GC was reached in the 5-8 day interval after harvest for N1, N2 and N3, whereas N0 reached 50% GC in the 9-13 day interval after harvest (Figure 5.1). There were minor differences between treatments in GC-SSD (Table 5.2), except just before harvest.

Characteristics of canopy strata

As expected, the lowest canopy strata had the highest DM yield (Table 5.3). Although total DM yield was higher in the August than in the July harvest, DM yields in the highest stratum were comparable for the N3, with 215 kg DM ha⁻¹

Table 5.2 Spatial standard deviation of ground cover (GC-SSD) and logistically transformed ground cover (TGC-SSD) \pm standard error of mean for intervals of days after harvest (DAH). Different uppercase letters within rows indicate significant ($\alpha=0.05$) differences between treatment means.

DAH	N0	N1	N2	N3
-----GC-SSD-----				
1-4	7.14 \pm 0.17 ^a	9.62 \pm 0.47 ^b	8.12 \pm 0.25 ^a	8.08 \pm 0.32 ^a
5-8	9.18 \pm 0.18 ^a	10.24 \pm 0.21 ^a	10.25 \pm 0.53 ^a	10.12 \pm 0.48 ^a
9-13	10.55 \pm 0.46 ^a	8.32 \pm 0.08 ^b	8.05 \pm 0.40 ^b	7.77 \pm 0.08 ^b
14-21	10.37 \pm 0.43 ^a	7.80 \pm 0.18 ^b	6.99 \pm 0.18 ^c	6.94 \pm 0.10 ^c
Day before harvest	10.32 \pm 0.29 ^a	6.63 \pm 0.14 ^b	6.63 \pm 0.28 ^c	5.57 \pm 0.30 ^c
-----TGC-SSD-----				
1-4	0.49 \pm 0.01 ^{ab}	0.54 \pm 0.03 ^a	0.50 \pm 0.02 ^{ab}	0.48 \pm 0.02 ^b
5-8	0.48 \pm 0.01 ^a	0.43 \pm 0.01 ^a	0.44 \pm 0.02 ^a	0.44 \pm 0.03 ^a
9-13	0.47 \pm 0.02 ^{ab}	0.41 \pm 0.01 ^a	0.45 \pm 0.02 ^a	0.53 \pm 0.02 ^b
14-21	0.43 \pm 0.02 ^a	0.41 \pm 0.01 ^a	0.43 \pm 0.01 ^a	0.48 \pm 0.02 ^b
Day before harvest	0.44 \pm 0.02 ^a	0.37 \pm 0.01 ^b	0.52 \pm 0.03 ^c	0.57 \pm 0.02 ^c

Table 5.3 Dry matter yield (DM), contents of DM, nitrate-N (NO₃-N), N, reducing sugars, total sugars and leaf area ratio (LAR) of sward strata.

	Stratum	N0	N1	N2	N3	N0	N1	N2	N3
		-----July 2001-----				-----August 2001-----			
DM (kg ha ⁻¹)	>16 cm		22	87	215		95	289	201
	9-16 cm	48	179	532	928	37	390	802	1212
	4-9 cm	596	1012	1553	1800	651	1402	1699	2030
DM (%)	>16 cm		22.1	24.6	23.2		24.1	21.5	23.5
	9-16 cm	27.5	26.3	23.0	20.7	28.1	21.0	18.1	19.6
	4-9 cm	27.5	25.1	23.4	20.9	25.0	22.6	20.0	20.5
NO ₃ -N (%)	>16 cm		0.002	0.000	0.000		0.003	0.001	0.008
	9-16 cm	0.000	0.000	0.000	0.000	0.014	0.000	0.006	0.018
	4-9 cm	0.000	0.000	0.000	0.005	0.001	0.004	0.010	0.061
N (%)	>16 cm		2.02	2.77	3.17		3.13	3.43	3.69
	9-16 cm	2.00	2.37	2.41	2.69	2.55	2.68	3.00	3.22
	4-9 cm	1.76	1.81	1.80	2.02	2.10	1.96	2.00	2.55
Red. sugars (%)	>16 cm		3.5	3.7	3.9		3.2	3.2	3.5
	9-16 cm	3.2	3.0	3.1	3.0	3.5	2.8	2.7	3.2
	4-9 cm	3.0	2.8	3.4	3.1	3.3	3.2	2.6	3.0
Total sugars (%)	>16 cm		14.1	19.8	17.9		17.5	16.1	11.6
	9-16 cm	17.1	22.1	24.5	21.5	16.0	15.8	11.4	13.9
	4-9 cm	22.3	27.9	27.4	23.7	17.2	17.0	15.4	13.4
LAR (m ² g ⁻¹ DM)	>16 cm		0.015	0.011	0.009		0.011	0.008	0.011
	9-16 cm	0.024	0.014	0.011	0.008	0.017	0.011	0.009	0.011
	4-9 cm	0.023	0.009	0.015	0.008	0.018	0.015	0.009	0.013

in July and 201 kg DM ha⁻¹ in August. This was due to lodging of the N3 sward in the August harvest. Leaves in the highest stratum tended to have a higher DM content, a higher concentration of N and reducing sugars and a lower concentration of nitrate-N and total sugars than leaves in the lowest stratum (Table 5.3). In August, LAR was larger for N0, N1, N2 and N3 in the 4-9 cm stratum than in the >16 cm stratum, whereas in July, this was only true for N2. The highest stratum of N1 in July contained mainly generative plant material, accompanied by lower DM and N content and larger LAR values.

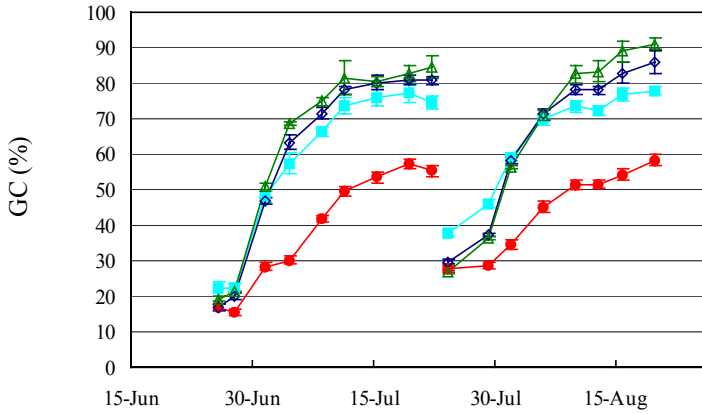


Figure 5.1 Development of image ground cover (GC) for N0 (●), N1 (■), N2 (◇) and N3 (△).

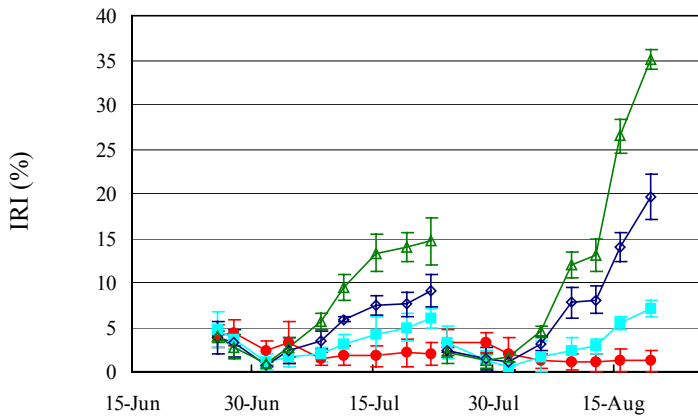


Figure 5.2 Development of index of reflection intensity (IRI) for N0 (●), N1 (■), N2 (◇) and N3 (△).

As expected, chl-*a*, chl-*b*, total xanthophylls and β -carotene concentrations increased with N supply and, on average, decreased with stratum height (Table 5.4). The pigment contents were higher in the August than in the July harvest. All pigment contents decreased more strongly with stratum height in the July than in the August harvest. In both harvests, chl-*a* concentration decreased more strongly with stratum depth than chl-*b*. As a result, the ratio between chl-*a* and chl-*b* was lower for the lowest stratum than for the upper stratum. The total

xanthophylls concentrations were higher in the >16 cm stratum than in the 9-16 cm and 4-9 cm stratum. Relative differences between the two lower strata were small. The relative decrease with stratum of β -carotene was comparable to the relative decrease of chl-*a*.

GC and IRI after harvest of strata material

The GC decreased slightly but progressively after removal of material in higher strata (Table 5.5). The response of GC to harvesting strata was slightly stronger in the August than in the July harvest. The IRI also decreased progressively after harvesting above 9 cm compared to 16 cm for the N2 and N3 (Table 5.6).

Table 5.4 Contents of chlorophyll *a* and *b*, total xanthofylls and β -carotene in harvested material of grass swards in strata above 16 cm, between 9-16 cm and between 4-9 cm.

Canopy stratum	July 2001				August 2001			
	N0	N1	N2	N3	N0	N1	N2	N3
Chlorophyll- <i>a</i> (mg g ⁻¹ DM)								
>16 cm		2.14	3.55	4.54		4.69	4.68	5.59
9-16 cm	1.99	2.45	2.71	3.52	3.25	3.04	4.08	4.71
4-9 cm	2.07	1.86	2.15	2.03	2.36	2.97	3.37	
Chlorophyll- <i>b</i> (mg g ⁻¹ DM)								
>16 cm		0.63	1.06	1.36		1.44	1.45	1.77
9-16 cm	0.58	0.73	0.87	1.14	0.96	0.98	1.35	1.65
4-9 cm	0.62	0.60	0.73	0.69	0.72	1.00	1.18	
Chlorophyll- <i>a</i> / Chlorophyll- <i>b</i>								
>16 cm		3.42	3.35	3.35		3.27	3.22	3.15
9-16 cm	3.44	3.36	3.13	3.09	3.40	3.10	3.02	2.86
4-9 cm	3.32	3.11	2.93	2.93	3.28	2.97	2.86	
Total xanthofylls (mg g ⁻¹ DM)								
>16 cm		0.33	0.47	0.69		0.73	0.74	0.81
9-16 cm	0.29	0.37	0.32	0.44	0.49	0.40	0.51	0.76
4-9 cm	0.31	0.27	0.43	0.31	0.38	0.50	0.54	
β -Carotene (mg g ⁻¹ DM)								
>16 cm		0.17	0.24	0.36		0.32	0.37	0.34
9-16 cm	0.17	0.20	0.19	0.27	0.21	0.24	0.28	0.36
4-9 cm	0.17	0.14	0.21	0.16	0.17	0.23	0.27	

Table 5.5 Ground cover (GC, %) \pm standard error of the mean before and after harvesting sward strata.

Canopy stratum	N0	N1	N2	N3
-----July 2001-----				
Complete canopy	55.3 \pm 2.1	74.7 \pm 0.7	80.8 \pm 0.4	84.4 \pm 0.8
<16 cm	55.2 \pm 1.9	75.0 \pm 0.6	79.3 \pm 1.1	81.4 \pm 1.5
<9 cm	52.1 \pm 1.8	72.0 \pm 1.2	72.5 \pm 1.6	70.9 \pm 1.8
<4 cm	27.7 \pm 1.8	37.9 \pm 2.9	29.8 \pm 1.8	26.9 \pm 1.5
-----August 2001-----				
Complete canopy		77.8 \pm 0.7	86.0 \pm 1.0	91.0 \pm 0.8
<16 cm	58.3 \pm 1.2	76.6 \pm 0.5	81.9 \pm 0.8	88.9 \pm 0.4
<9 cm	59.3 \pm 1.8	72.4 \pm 1.6	66.8 \pm 1.1	63.6 \pm 4.1

Table 5.6 Index of reflection intensity (IRI, %) \pm SE of the mean before and after harvesting sward strata.

Canopy stratum	N0	N1	N2	N3
-----July 2001-----				
Complete canopy	2.1 \pm 0.6	6.0 \pm 0.7	9.0 \pm 1.1	14.7 \pm 2.4
<16 cm	2.0 \pm 0.7	5.2 \pm 0.9	8.0 \pm 0.8	14.4 \pm 2.3
<9 cm	2.1 \pm 0.6	5.7 \pm 0.8	4.5 \pm 1.3	3.2 \pm 0.3
<4 cm	3.3 \pm 0.8	3.3 \pm 1.1	2.5 \pm 0.1	2.1 \pm 0.4
-----August 2001-----				
Complete canopy		7.1 \pm 0.5	19.7 \pm 2.3	35.1 \pm 1.3
<16 cm	1.2 \pm 0.4	6.1 \pm 0.4	13.7 \pm 1.2	27.0 \pm 0.4
<9 cm	1.4 \pm 0.4	2.3 \pm 0.2	3.0 \pm 0.2	5.3 \pm 0.1

5.3.2 Reflection characteristics of intact swards

The CAW increased up to 133.1 nm in the July growth period and 133.7 nm in the August growth period for the N3 and N2 (Figure 5.3). The N0 and N1 did not reach this maximum. In the second half of the growth period, the CAW decreased.

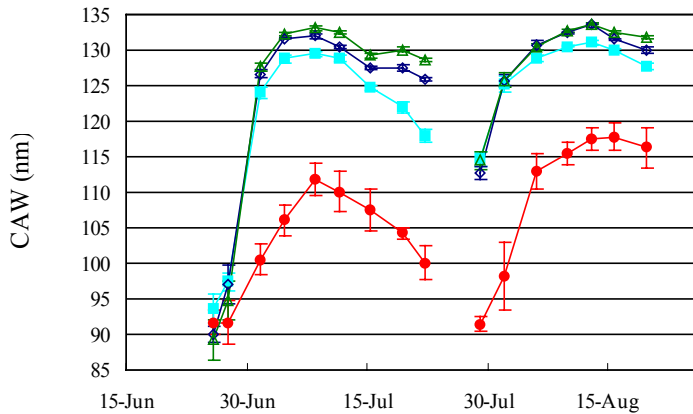


Figure 5.3 Development of chlorophyll absorption width (CAW) for averaged sward curves for N0 (●), N1 (■), N2 (◇) and N3 (△).

The decrease was strongest for the N1 and N2, although the N3 also decreased. In the July growth period the CAW of N3 decreased to 128.6 nm at harvest, whereas in the August growth period the CAW was 131.8 nm at harvest. This is in accordance with the higher N application in the August growth period and the low nitrate-N, N and soil mineral N contents of the July harvest. The CAW of N3 did not respond strongly to lodging.

The CAW for N1 in the August harvest was higher than for N2 in the July harvest and the CAW for the August N2 was higher than for the July N3 treatment, although the N application was equal. This is, however, in accordance with the slightly higher N and nitrate-N contents in the August than in the July harvest. The CAW just before harvest of the N0 treatment was considerably higher for the August (116.3 nm) than for the July harvest (100.1 nm). Again, this coincided with the higher N contents and the higher pigment contents of the August than of the July harvest (Tables 5.1 and 5.4). As an example, the relations between IC number and BE, GE and RE of 20 August are presented in Figures 5.4A, 5.4B and 5.4C, respectively. The differences in BE, GE and RE between N treatments were present in all intensity classes, yet the largest differences were found in the highest intensity classes. The edge positions tend to shift to shorter (GE) and longer wavelengths (BE, RE) for classes with a lower reflection intensity. Differences between intensity classes

ranged between 2.8-3.4 nm, 11.6-30.5 nm and 5.3-7.9 nm for BE, GE and RE, respectively. This range remained present after harvesting above 9 cm, with 2.3-4.6 nm, 23.7-31.5 nm and 3.2-5.3 nm for the BE, GE, and RE respectively. The value of the b parameter in the linear relation between GE position and reflection intensity class increased with N treatment (Figure 5.5), where N3 had the 'steepest' curve (Figure 5.4). Values for b increased for the N3 treatment from 0.1-0.2 shortly after cutting to 0.47-0.55 IC nm⁻¹ GE shift at harvest. The values for the parameter b (slope) for the N0 remained constant at 0.1-0.2 IC nm⁻¹ GE shift and did not respond to lodging of the N3 sward from 16 August onwards.

5.3.3 *Reflection characteristics of canopy strata*

After harvesting above 16 cm, the CAW increased slightly for the N1, N2 and N3 treatments in both harvests (Table 5.7). The CAW decreased after the intermediate stratum was harvested. The CAW decrease was smaller for the N0 and N1, than for the N2 and N3 treatments. The CAW is a combination of GE and RE position. The GE position of N2 and N3 shifted slightly to longer wavelengths after harvesting above 16 cm (0.4 nm (only N2) in July and 0-0.6 nm in August). The GE shifted further to longer wavelengths (3.4-4.7 nm in July and 3.9-6.4 nm in August) after harvesting above 9 cm, while shifts progressively increased with N supply. The RE of N2 and N3 shifted, remarkably, also to longer wavelengths, with 0.8-1.2 nm in July and 1.7-1.8 nm in August after harvesting above 16 cm and with 0.4-0.9 nm in July and 0.4 nm in August after harvesting above 9 cm. The RE shifted 2 nm to longer wavelengths after harvesting above 9 cm in August. Harvesting above 16 cm hardly changed the value of b in the July harvest (Table 5.8). In August, the value of b only changed for N1. This b value decreased to 0.21 (N1) 0.23 (N2) and 0.20 (N3) in the July cut and to 0.20 (N1), 0.19 (N2) and 0.20 (N3) after harvesting above 9 cm.

5.3.4 *Reflection characteristics of harvested material*

The CAW of harvested material progressively decreased with lower strata (Table 5.9). This is in accordance with the progressive decrease in pigment content for lower strata (Table 5.4). CAW values for the upper stratum of the August harvest were similar to the values measured at the intact canopy.

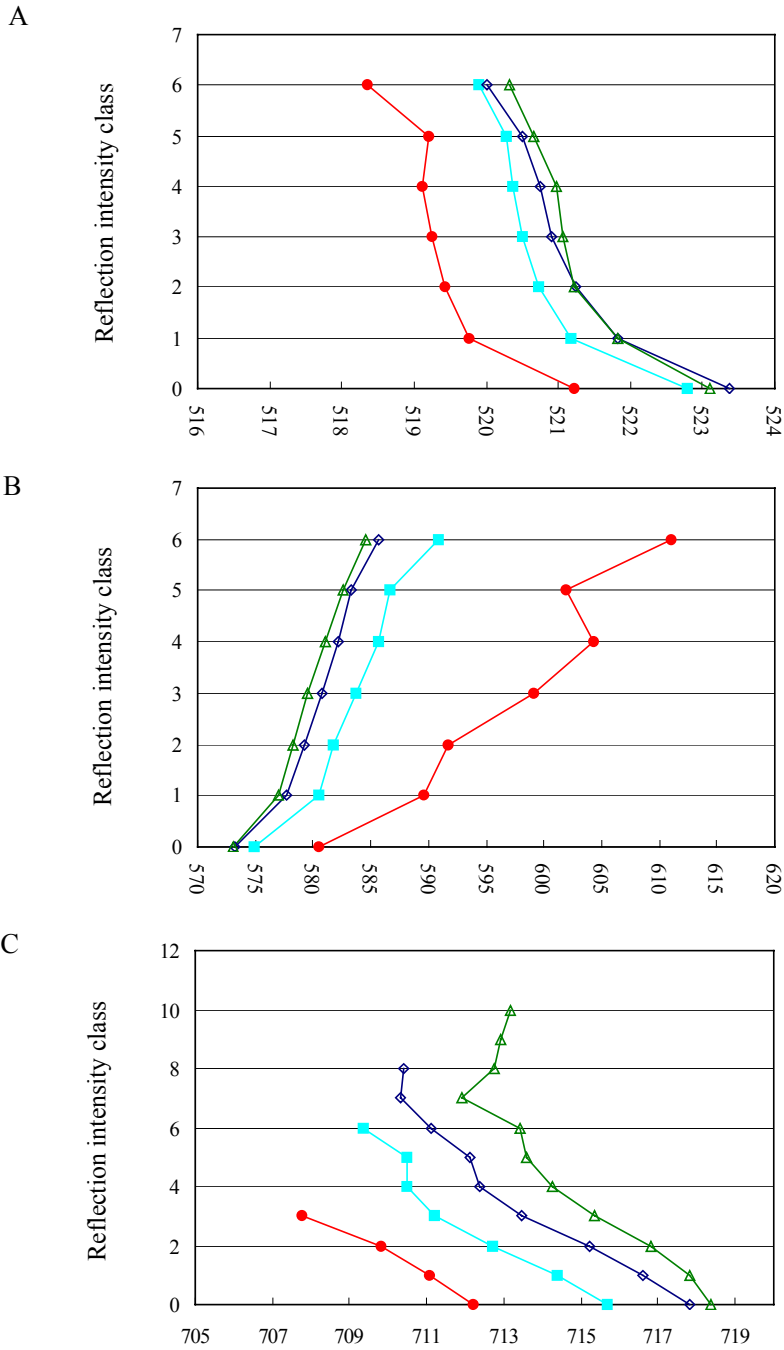


Figure 5.4 Edge position of leaf pixels per reflection intensity class for N0 (●), N1 (■), N2 (◇) and N3 (△) for BE (A), GE (B) and RE (C) on 20 August.

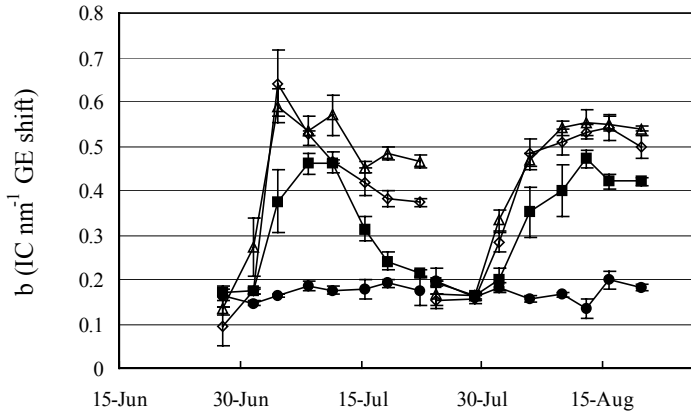


Figure 5.5 Evolution of parameter b (IC nm^{-1}) in the linear relation $GE = a + b \times \text{IC}$ for N0 (●), N1 (■), N2 (◇) and N3 (△).

Table 5.7 Chlorophyll absorption width (CAW) \pm standard error of the mean of MSS before harvesting sward strata. Different uppercase letters within a column indicate significant differences between strata means ($p < 0.05$).

Canopy stratum	N0	N1	N2	N3
-----July 2001-----				
Complete canopy	100.1 \pm 2.4 ^a	118.1 \pm 0.9 ^a	125.8 \pm 0.2 ^{ab}	128.6 \pm 0.3 ^a
<16 cm	107.2 \pm 1.9 ^b	119.6 \pm 0.4 ^a	126.9 \pm 0.2 ^b	129.4 \pm 0.4 ^a
<9 cm	104.7 \pm 1.9 ^{ab}	118.5 \pm 0.8 ^a	124.3 \pm 0.8 ^a	125.1 \pm 0.7 ^b
<4 cm	96.7 \pm 2.6	107.3 \pm 1.4	105.0 \pm 0.9	99.9 \pm 1.1
-----August 2001-----				
Complete canopy		127.7 \pm 0.4 ^a	130.0 \pm 0.5 ^a	131.8 \pm 0.2 ^a
<16 cm	116.4 \pm 2.8 ^a	128.8 \pm 0.5 ^a	131.2 \pm 0.2 ^a	133.4 \pm 0.2 ^a
<9 cm	117.8 \pm 2.2 ^a	128.6 \pm 0.8 ^a	127.8 \pm 0.6 ^b	125.1 \pm 1.8 ^b

Table 5.8 Mean values and standard error of the mean for parameter b (IC nm⁻¹) in the linear relation IC = a + b * GE.

Canopy stratum	N0	N1	N2	N3
-----July 2001-----				
Complete canopy	0.17 ± 0.03	0.21 ± 0.01	0.37 ± 0.01	0.46 ± 0.01
<16 cm	0.16 ± 0.03	0.20 ± 0.01	0.36 ± 0.02	0.45 ± 0.01
<9 cm	0.20 ± 0.03	0.21 ± 0.02	0.23 ± 0.01	0.20 ± 0.01
<4 cm	0.20 ± 0.03	0.19 ± 0.01	0.15 ± 0.01	0.17 ± 0.03
-----August 2001-----				
Complete canopy		0.42 ± 0.01	0.50 ± 0.03	0.54 ± 0.01
<16 cm	0.18 ± 0.01	0.36 ± 0.01	0.49 ± 0.01	0.54 ± 0.03
<9 cm	0.19 ± 0.01	0.21 ± 0.01	0.19 ± 0.02	0.20 ± 0.02

Table 5.9 Chlorophyll absorption width (CAW) ± standard error of the mean of harvested material of the August harvest. Different uppercase letters within a column indicate significant differences between strata means (p < 0.05).

Canopy stratum	N0	N1	N2	N3
>16 cm		128.3 ± 1.4 ^a	129.3 ± 0.3 ^a	132.8 ± 0.6 ^a
9-16 cm		126.1 ± 1.7 ^a	126.5 ± 1.2 ^a	129.0 ± 1.1 ^a
4-9 cm	120.0 ± 0.1	114.5 ± 1.5 ^b	111.7 ± 1.1 ^b	114.0 ± 2.8 ^b

5.3.5 *Reflection characteristics of detached leaves in relation to system properties*

The CAW showed a strong response when leaves were rotated around their shortest axis (Figure 5.6). Edges shifted towards longer (BE and RE) or shorter (GE) wavelengths for upwards oriented leaves when compared to horizontally oriented leaves. The GE shifted to longer and BE and RE to shorter wavelengths for downwards oriented leaves when compared to horizontally oriented leaves. There is a clear effect of specular reflectance visible for

horizontal leaves, approximately decreasing BE with 0.5 nm and RE with 0.5-1.0 nm and increasing GE with 3-4 nm. This resulted in a net decrease in CAW of approximately 3.5-4.5 nm. Changing leaf angle from 0 to 60 degree with the horizontal plane shifted edges with a maximum of 2, 6 and 2 nm for the blue, green and red edge, respectively, resulting in a net CAW increase of 5.9-7.3 nm. Leaves of *Lolium perenne* L. under an angle reflect relatively more light in the blue than in the red wavelength range (Figure 5.7). Nutrient supply also affected this ratio (Figure 5.8). The ratio remained above 0.8 throughout the growth period. The ratio remained above 1 after harvesting strata, although leaves were clearly more vertically oriented in the lower strata, but probably due to lower pigment contents (Table 5.4).

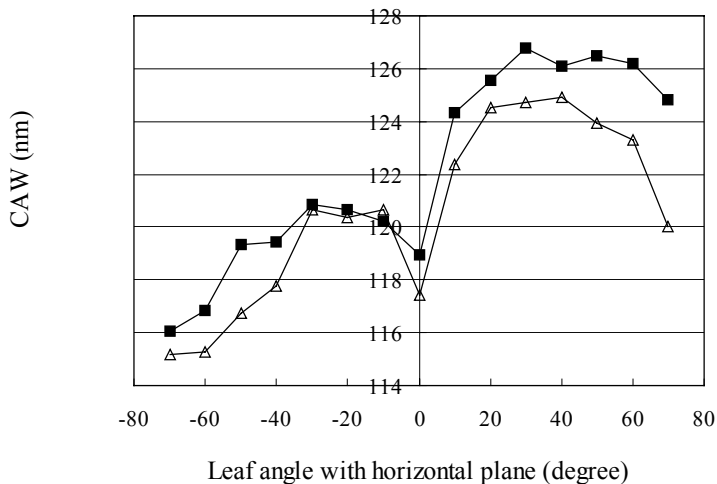


Figure 5.6 Width of the chlorophyll absorption band (CAW) as function of leaf angle with the horizontal plane for leaves from the N1 (■) and N3 (△). The leaf tip is oriented upwards at 80 degree.

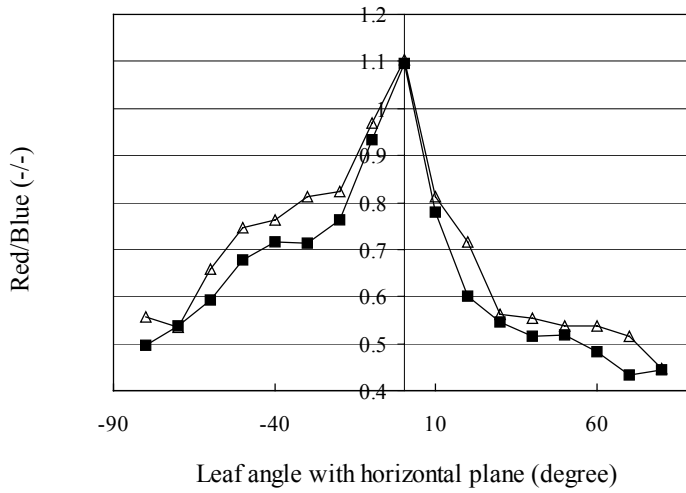


Figure 5.7 Ratio between the mean reflection from 657-664 nm (Red) and 411-463 nm (Blue) for leaves of the N1 (■) and N3 (△) treatment.

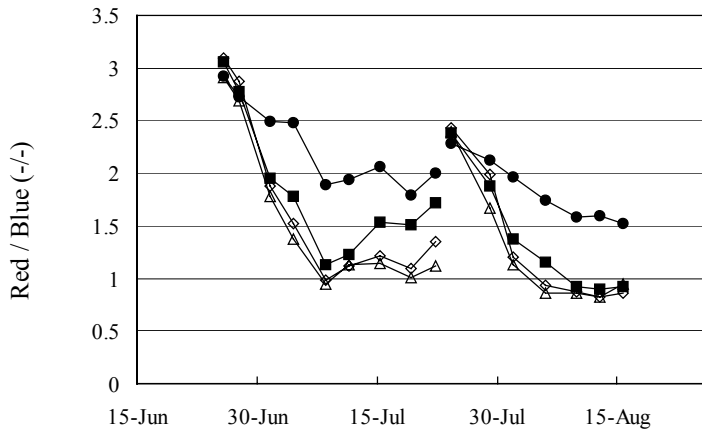


Figure 5.8 Ratio between the mean reflection from 657-664 nm (Red) and 411-463 nm (Blue) for N0 (●), N1 (■), N2 (◇) and N3 (△).

CAW in leaves showed a tendency to decrease with height above the soil surface (Figure 5.9). The BE position hardly changed with leaf height position. GE shifted to slightly shorter wavelengths when leaves were closer to the soil surface, with a net shift of 2.3 nm for a 20 cm decrease in height. There was a clear linear effect of height on RE, with RE shifting 4.9 nm to shorter wavelengths with a decrease in height of 20 cm. This resulted in a net CAW decrease of 2.6 nm with a decrease in height of 20 cm. The red/blue ratio linearly decreased for leaves with a higher position in the canopy (Red / Blue = $1.19 - 0.009 \times \text{leaf height (cm)}$). This indicates that the relation between leaf angle and red/blue ratio and the CAW must change with leaf height, *i.e.* distance to the sensor.

5.4. Discussion and conclusion

5.4.1 Experiment

It was intended to create grass swards with a wide range of N statuses, from strongly N deficient to N saturated. In the July harvest, the highest N supply treatment was certainly not fully N saturated, as indicated by the low mineral N content in the soil after harvest, low nitrate-N and N concentration and high sugar content in harvested material.

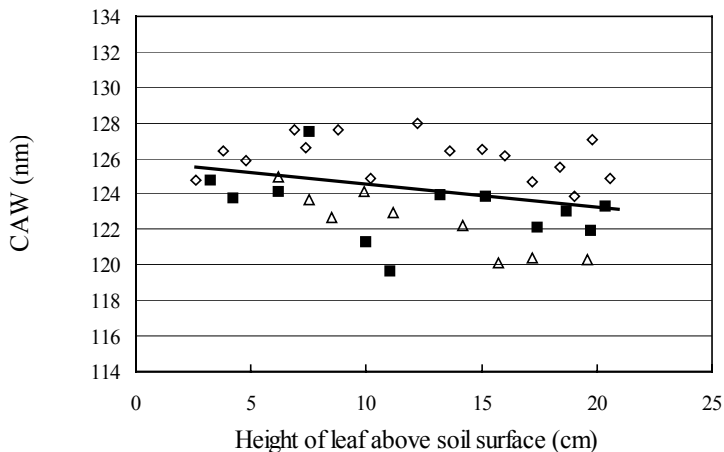


Figure 5.9 Width of chlorophyll absorption band (CAW, B) as function of leaf height above soil surface for leaves from 3 sets of 3 leaves (■, △, ◇).

The CAW also indicated that N supply for the July harvest was insufficient for a saturated N status. More N was supplied for the August growth period. In the August harvest, the highest N supply was probably nearly N saturated, as indicated by higher values for nitrate-N and N and lower sugar contents in harvested material and higher CAW values.

The values for LAR were relatively low as compared to the 2000 experiment (Schut and Ketelaars, Chapter 4), where LAR values under a high N supply ranged from 0.010-0.019 m² g⁻¹ DM for various harvests. The GC-SSD is closely related to the spatial heterogeneity of tiller density. Schut & Ketelaars (Chapter 8) found that seasonal mean GC-SSD ranged between 9.2-10.8% and TGC-SSD below 0.6 within the first to weeks after harvest for dense swards. Deteriorated swards had a GC-SSD between 10.3-15.0% and a TGC-SSD above 0.7 within the first two weeks after harvest. In the experiment presented here, values of GC-SSD remained below 11% and values of TGC-SSD remained below 0.6 at all intervals. There were no significant differences in GC-SSD and TGC-SSD between treatments at 50% GC. Therefore, it is concluded that all treatments were spatially homogeneous and that N application did not affect spatial heterogeneity of grass swards. This is in accordance with findings of an N experiment in 2000 (Schut & Ketelaars, Chapter 4).

5.4.2 Characteristics of canopy strata

The lowest canopy strata had the highest DM yield. In general, leaves in higher strata had a higher DM content, a higher concentration of N and a lower concentration of nitrate-N than leaves in the lower strata. Pigment concentrations were higher for the >16 cm stratum than for 9-16 cm and 4-9 cm strata. The differences between strata were larger in the July than in the August harvest. The GC progressively decreased after harvest of higher strata, except for N1 in July. The leaves in the higher two strata were more horizontally orientated, whereas leaves in the lowest strata were more vertically orientated. This effect was even stronger for the N3 treatment in the August harvest, as swards had lodged from 16 August onwards. The IRI decreased to values below 6% after harvesting material above 9 cm. The response of IRI was much stronger after harvesting above 9 cm than above 16 cm. This indicates that IRI is very sensitive for changes in leaf angle. It was found that pigment contents progressively decreased for strata lower in the canopy. The decrease in chl-*a* content with stratum was stronger than the decrease in chl-*b* content. Therefore

chl-*a* / chl-*b* ratios slightly decreased with height, in accordance with findings of Yamasaki *et al.* (1996).

5.4.3 *Reflection characteristics of intact canopies*

The CAW increased up to 133.1 nm in the July growth period and 133.7 nm in the August growth period for the N3 and N2 treatments. In the second half of the growth period CAW decreased, while the decrease was stronger in the July harvest than in the August harvest. This is in accordance with the higher N application and N status in the August than the July harvest. The CAW hardly responded to lodging. Treatment differences were clearly present in the slope of the relation between GE and reflection intensity. The range in GE values (12-30 nm) was smaller for high N than for low N application levels.

5.4.4 *Reflection characteristics of canopies after harvesting strata*

The CAW of grass swards increased slightly in both harvests for the N1, N2 and N3 treatments after harvesting above 16 cm with 0.8-1.5 nm in July and 1.1-1.6 nm in August. The CAW decreased after harvesting above 9 cm, slightly for the N0 and N1 and more significantly for the N2 and N3. This changing CAW was, remarkably, the net result of shifts to longer wavelengths of both GE and RE. The RE shift was larger than GE shift after harvesting above 16 cm, resulting in a net CAW increase. After harvesting above 9 cm the GE responded stronger than RE, resulting in a net CAW decrease. In swards harvested at 16 cm, the range in GE values within reflection intensity classes did not change much as compared to those for the intact canopy. In swards harvested above 9 cm, the GE ranges converged and treatment differences disappeared.

5.4.5 *Reflection characteristics of harvested material*

The CAW of harvested material above 16 cm was similar to the CAW measured at intact grass swards, with differences of 0.6-1.0 nm for various N application levels. The differences between CAW of harvested material and grass swards became progressively larger when strata were removed. Considering the limited height difference, and the minor effect of height on CAW, it is concluded that a change of leaf angle distribution was the determining factor for this trend.

5.4.6 Reflection characteristics of detached leaves in relation to system properties

Normally, leaf angle distribution of perennial ryegrass swards changes from erectophyle to plagiophyle during growth. Therefore, mean leaf angle with the horizontal plane in the sward varies roughly between 70° shortly after harvest and 30° at high DM yields (De Wit, 1965). Changing leaf angle from 0 to 60 degree with the horizontal plane increased CAW with maximally 7.3 nm. This was probably caused by an increase in pigment content in the pixel field of view.

The CAW increased 2.6 nm when leaf position decreased 20 cm in height. It is yet unclear what caused this shift. Probably, it can be attributed to wavelength dependent limitations in dynamic range of the sensor *i.e.* relative changes for weak signals in regions of the spectrum with a low reflection are lower than in regions with a high reflection.

5.4.7 Towards understanding of the reflected signal of canopies

Decreasing reflection intensity could, as combined result of more vertically oriented leaves and lower leaf height position within the canopy increase CAW with maximally 9.9 nm. In more vertically oriented leaves low in the canopy this range may still further increase, as the dynamic range of the sensor may become a severely limiting factor, augmenting the effect of leaf angle. The observed ranges in GE position with intensity classes were much larger than can be explained by leaf angle and height position. This indicates that the interaction between leaf angle and height position was important for leaves low in the canopy. This interaction will also affect BE and RE position, although the observed BE and RE ranges were similar to the ranges found for leaf angle and leaf height. From the pigment profile, it can be expected that CAW progressively decreased with strata lower in the canopy. For harvested material, the CAW indeed progressively decreased with stratum, in contrast to the CAW of grass swards. For the lowest stratum, CAW differences between harvested material and (remaining) grass swards were 11 and 16 nm. A CAW difference of approximately 10 nm can be explained when considering the horizontal leaf orientation of harvested material and the more vertical leaf orientation for the lower canopy strata, in combination with differences in height position. The remaining difference might then result from the interaction between leaf height position and leaf angle. The slope of the relation between reflection intensity

and GE position did not change strongly after harvesting above 16 cm, indicating that this slope was not sensitive for small changes in canopy height, biomass or pigment content. The slope changed strongly after harvesting above 9 cm. This can be understood when considering that leaf angles of treatments were comparable for the lowest stratum (more vertically oriented leaves), and that for this stratum the interaction between leaf angle and low height position was most important. Schut and Van den Berg (Chapter 7) found that clover swards, with horizontally oriented leaves, had a smaller GE range than grass swards. The GE range of clover swards strongly increased when leaf angle with the horizontal plane increased, due to the circadian rhythm of leaf opening and closure. For grass swards they found values for the GE range and for the slope of IC number over GE comparable with values found in our experiment. Therefore, it is concluded that a large range in GE values over intensity classes (and hence, a lower value for the slope parameter) coincides with an erectophyle leaf angle distribution and that a relatively small range coincide with a plagiophyle leaf angle distribution.

It was found that the ratio between reflection in the red and blue parts of the spectrum decreased from 1.1 for horizontally oriented leaves to 0.4 for more vertically oriented leaves. Unfortunately, N supply and sensor limitations (observed when decreasing leaf height) also affected this ratio. The ratio between red and blue reflectance remained above 0.8 throughout the growth period. Ratios were lower in the August harvest (where swards were lodged) than in the July harvest.

Schut & Ketelaars (Chapter 4) found that the discriminating ability of leaf reflectance between treatments with high N supply was limited. The discriminating ability may be improved when effects of leaf angle and pigment content on reflectance signals can be separated. This study indicates that for the experimental system leaf angle is one of the most important factors in the relation between reflection intensity and edge position, and that also the ratio between red and blue reflectance is affected by leaf angle. Therefore, effects of leaf angle and pigment content on sward reflectance may be further separated when considering together the red/blue ratio, the range in GE values and CAW.

6

Early detection of drought stress in grass swards with imaging spectroscopy

A.G.T. Schut & J.J.M.H. Ketelaars

Submitted to Netherlands Journal of Agricultural Science

6. Abstract

The potential of an experimental imaging spectroscopy system, with high spatial (0.28-1.45 mm²) and spectral resolution (5-13 nm) is explored for early detection of drought stress in grass. A climate chamber experiment was conducted with 9 *Lolium perenne* L. mini swards with drought stress treatments in two N levels. Images were recorded twice a week. Growth was monitored by changes in ground cover (GC) and index of reflection intensity (IRI) and wavelength position of and gradient at inflection points, as estimated from images. Drought stress increased leaf dry matter content and sugar concentration. Drought stress decelerated and ultimately reversed GC evolution, and kept IRI at low values. In contrast to unstressed growth, all absorption features narrowed and became shallower under drought stress. The inflection points near 1390 and 1500 nm were most sensitive to drought stress. Differences between drought stress and control swards were detected just before leaf water content dropped below 80%. The evolution of inflection point wavelength positions reversed under drought stress, except for the inflection point at the red edge where the shift to longer wavelengths during growth accelerated. The relation between inflection points at 705 and 1390 nm differentiated unstressed swards in an early growth stage from drought-stressed swards in a later growth stage.

6.1 Introduction

Water resources for agriculture are limited, urging optimisation of irrigation water use. Irrigation optimisation strategies include temporal- and spatial differentiation. In grassland, duration and intensity of drought stress influences tiller survival (Grashoff *et al.*, 2001). Therefore, an accurate timing of irrigation may prevent sward deterioration. In grass swards under drought stress, first growth rate decreases and in more advanced stages of drought stress, morphological changes and eventually leaf senescence and leaf death take place (Jones & Lazenby, 1988). With accurate drought stress detecting sensors, new irrigation management tools can be developed, limiting irrigation water use and preventing long term production loss.

Dehydration of leaves decreases light absorption by water and severe dehydration affects pigment light-absorption. Dehydration also changes internal leaf structure. However, changes in internal leaf structure are less important

than effects of pigment and water absorption (Carter, 1991). Therefore, reflectance of leaves increases when water is lost, in both visible and infrared wavelengths (Ripple, 1986; Bowman, 1989; Inoue *et al.*, 1993; Penuelas & Inoue, 1999). For passive sensors, only wavelengths with abundant natural light can be used for stress detection, eliminating the use of strong water absorption bands. Remote sensing of drought stress in crops is further complicated by changes in LAI and ground cover, canopy geometry, fraction of dead leaf material and background soil reflectance (Jackson & Ezra, 1985; Ripple, 1986; Hunt *et al.*, 1987; Penuelas *et al.*, 1993; Fernández *et al.*, 1994).

With a recently developed imaging spectroscopy system, new and automatic means for grass sward characterisation become available (Schut *et al.*, Chapter 2). Reflection intensity measured with this system is related to leaf height and leaf angle. With this character, image ground cover (GC) can be differentiated into reflection intensity classes, where the pixel distribution over intensity classes relates to canopy geometry (Schut *et al.*, Chapter 2). The non-destructive nature of reflection measurements allows the study of the evolution of GC, canopy geometry and leaf pixel spectra in intact swards. From GC data light interception, leaf area index (LAI) and biomass can be estimated (Schut & Ketelaars, Chapter 3). Sward heterogeneity can be quantified with spatial GC variability and is related to production capacity (Schut & Ketelaars, Chapter 8).

In this paper, the potential of this experimental system is explored for early detection of drought stress in grass swards. For this, a climate chamber experiment was conducted with 9 *Lolium perenne* L. mini swards from 1 through 27 November 2000. Evolution of ground cover (GC), spatial GC variability and spectral characteristics in response to drought stress were studied. To this end images of drought-stressed swards with low and high N supply were recorded throughout one growth period, and shifts of and gradients near inflection points were studied with derivative spectra.

6.2 Materials and methods

6.2.1 Experiment

From 1 - 27 November 2000, 9 mini swards of *Lolium perenne* L. were grown under abundant light (16 hours under HPI 400 light source (120 W m^{-2}) and 8 hours dark). Temperatures were kept at 20° C during the day and 15° C during the night, with 65% relative humidity during the day and 80% during the night.

Swards were grown in containers (0.9 m long, 0.7 m wide, 0.4 m high). The mini sward containers were taken from a nitrogen experiment (Schut & Ketelaars, Chapter 4). Only containers with mini swards were used which previously had received adequate N nutrition (3 mini swards with 60, 3 with 90 and 3 with 120 kg N ha⁻¹ per harvest). These containers were evenly divided over the treatments: control with high N supply (Co), drought-stressed with high N supply (DS-HN) and drought-stressed with low N supply (DS-LN), with three replicates per treatment. There were not enough mini swards available to include also a control with low N supply. At the start of the experiment, the high N treatments were fertilised with 120 kg N ha⁻¹ and the low N with 30 kg N ha⁻¹.

Mini swards started with 20% (volume) soil moisture. After the start of the experiment, no extra water was supplied to the DS-LN and DS-HN mini swards. The Co mini swards were kept at 20% soil moisture, water being supplied through perforated drains. These drains were placed on top of the soil and under the canopy, minimising changes in canopy geometry. Once every two days containers were weighed. Leaf dry matter (DM) content was measured for monitoring the degree of drought stress. For this, ten top canopy leaves per mini sward were sampled and dried (105^o) overnight for DM content determination.

6.2.2 *Chemical analysis*

At harvest (27 November), fresh matter was weighed and samples were taken for analyses of dry matter, total N, nitrate and (soluble) sugar content. Total N was determined with the Dumas method on a Vario EL (Elementar analyse systemen GmbH Hanau), nitrate on a Bran and Luebbe Traacs 800 continuous flow system (Maarsen, the Netherlands). Sugars were extracted from dried material by adding demineralised water to a ground sample. On a Bran and Luebbe AutoAnalyzerII (Maarsen, the Netherlands, Method NL213-89FT), reducing sugars were measured by reaction with ferricyanide which is reduced to colourless ferrocyanide. The reduction in absorbance at 420 nm was used to calculate the amount of sugars as glucose equivalents. Total sugars after hydrolysis were determined in the same extract but the autoanalyser was now equipped with a hydrolysis-step to convert di- and oligosaccharides to glucose and fructose.

6.2.3 Images

Image recording

On 42 positions in each mini sward, image lines were recorded once every two days. On each position, reflection was measured with three sensors (V7, N10 and N17), in the wavelength range from 405-710 nm (V7), 675-970 nm (N10) and 960-1659 nm (N17), for details see Schut *et al.* (Chapter 2). At soil level, an image line recorded by the V7 and N10 was 1.39 mm wide and 152.5 mm long. For the N17 sensor, an image line was 1.39 mm wide and 133.1 mm long. There were 768 (V7 and N10) and 128 (N17) pixels per image line for the spatial dimension, resulting in a spatial resolution of 0.28 mm² (V7 and N10) and 1.45 mm² (N17) per pixel at the soil. Per pixel, radiance was measured in 565 (V7 and N10) and 128 (N17) spectral bands. The spectral resolution was 5 nm for the V7 and N10 sensor and 13 nm for the N17 sensor. The system used xenon and halogen light sources with lenses illuminating only the area (2-4 cm wide strip) where an image line was recorded. Light was projected vertically to the soil, and reflection was measured under an angle of 2 degree from nadir, minimising shadow effects. The imaging spectroscopy system recorded per sensor a single image line with the light sources switched off and 5 image lines from a 50% reflection standard as part of the sampling routine. With these standard image lines, reflection was calculated from the radiance data.

Classification

Schut *et al.* (Chapter 2) defined threshold values for soil, grass leaves (G), leaves with specular reflection (S), and dead material (D) classes and an intermediate class between soil and dead material. Separation between classes was based on ratios of reflectance (R) at 450, 550 and 680 nm. These classes were subdivided into reflection intensity classes (IC), based on the reflection intensity at predefined wavelengths (550 nm for the V7, 746 nm for the N10 and 1100 nm for the N17 sensor). The intensity classes ranged for grass from IC 0 up to and including IC 6 for the V7 sensor and from IC 0 up to and including IC 10 for the N10 and N17 sensor. For leaves with specular reflection, IC ranged from 0 up to and including 2, and for dead material from IC 0 up to and including 3. A large number of pixel reflection spectra per intensity class are stored in a spectral library. With this library, pixel spectra of the recorded image lines were classified with maximum likelihood procedures

(Schut & Ketelaars, Chapter 3). The classification procedure was based on a limited number of wavelengths, selected according to a statistical function maximising class to class separation (Feyaerts & Van Gool, 2001).

After classification, spectra of pixels were normalised, according to equations in Schut *et al.* (Chapter 2). Normalisation means that reflection was divided by the mean reflection in the 550-555 nm range for the V7 sensor, 800-850 nm range for the N10 sensor and 1070-1130 nm for the N17 sensor. Mean sward reflection spectra (MSS) were calculated from normalised spectra of all pixels in grass IC 1 trough 10. In addition, mean reflection spectra were calculated from normalised spectra for each IC. It is stressed that for this procedure only grass pixels were selected, eliminating pixels containing soil and dead material. Under the assumption that the data of the V7 sensor and the N10 sensor were from identical objects and that the sensitivity of the sensors in overlapping regions was comparable, the data of the V7 sensor were normalised to the 800-850 nm range (Schut *et al.*, Chapter 2). These assumptions seem valid for MSS.

Ground cover, index of reflection intensity and spatial variability of GC

Ground cover was calculated per mini sward for each IC. Total image line (IL) ground cover (GC_{IL} , %) was calculated as sum of ground cover of all grass IC (GCG) and IC of all specular classes (GCS) from the V7 sensor:

$$GC_{IL} = \sum_{ic=0}^6 GCG_{ic} + \sum_{ic=0}^2 GCS_{ic}$$

where ic is the index number of the intensity class. The mini sward GC was calculated as the average of the GC_{IL} over the 42 image lines. This mini sward GC estimate underestimates visually scored GC, visually scored GC equals $8.63 + 1.076 \times GC$ (Schut *et al.*, Chapter 2). The index of reflection intensity (IRI, %) was then calculated as:

$$IRI = 100 \times \frac{\sum_{ic=3}^6 \frac{1}{42} \sum_{IL=1}^{42} GCG_{IL,ic}}{GC}$$

This IRI measures the presence of highly reflecting green pixels as a percentage of GC. A high value represents a dense canopy with horizontally oriented leaves (Schut & Ketelaars, Chapter 3).

The spatial heterogeneity was quantified with the spatial standard deviation of GC (GC-SSD) and logistically transformed values of GC (TGC-SSD). These were calculated according to the equations in Schut & Ketelaars (Chapter 8), and the spatial standard deviation was calculated per mini sward as the standard deviation of the 42 GC_{IL} estimates.

Calculation of chlorophyll absorption width (CAW)

Reflectance spectra of green material typically have a sharp transition from minimum reflection around 680 nm and maximum reflection around 750 nm, known as the red edge (RE) (Horler *et al.*, 1983). Green material reflects more radiation in the green part than in blue or red parts of the spectrum, and a blue edge (BE) and a green-edge (GE) can be found around 520 and 600 nm. In earlier work, Schut & Ketelaars (Chapter 4) used a CAW distance measure between the half height of the green and red edge. This CAW was strongly related to relative growth deficit due to nitrogen shortage.

Calculation of derivative spectra

The MSS spectra were smoothed with cubic splines. Splines are non-parametric regressions functions, mostly third order polynomials, where a regression curve is calculated for each interval between knots. The regression curve is continuous between intervals at the first and second derivative (Silverman, 1985). The number of knots was arbitrarily set to one third of the number of spectral bands. Decreasing the number of knots smoothes the spectral curve more strongly, and small features will be removed. The effects of the choice of the number of knots on the selected features were evaluated by setting the number of knots to one ninth of the number of spectral bands. From the resulting regression curves, first and second derivatives were determined. The minimum or maximum derivative wavelength was defined as the point of intersection of the second derivative with the abscissa (Railyan & Korobov, 1993). These points of intersection will be referred to as inflection points (IP, nm). The gradient values, calculated as Δ reflection per Δ nm over the two nearest bands at the IPs, were also determined. The gradients and IP only slightly changed with the choice of number of knots. Therefore, the values of the IP and gradients presented were calculated with the number of knots set to one third of the number of spectral bands.

6.2.4 Statistics

The statistical differences were evaluated with analysis of variance. The null hypothesis was that treatment means did not differ on the same date. This hypothesis was tested with a two-sided t-test ($p < 0.05$).

6.3 Results

6.3.1 DM yield and chemical analysis

The DM yield of drought-stressed treatments was significantly lower than control (Table 6.1). Drought stress affected all variables, only nitrate of DS-HN and control were not significantly different. Drought stress increased DM content and concentration of reducing and total sugars. The concentration of long chained sugars increased from 14.7% for Co to 23.8% for DS-HN and 25.5% for DS-LN. The DS-LN had lower N- and nitrate concentrations than DS-HN and Co. The N concentration of DS-HN was slightly lower than Co, but there was no difference in nitrate concentration (Table 6.1). During growth, leaf DM content of Co increased, but did not exceed 21% (Figure 6.1). From 13 November onwards, DM contents of DS-HN and DS-LN were higher than Co.

Table 6.1 Means and standard deviations of DM yield and concentrations of DM, N, nitrate and reducing sugars and total sugars for control (Co), and drought-stressed swards with high (DS-HN) and low (DS-LN) N supply. Different uppercase letters within rows indicate significant ($p < 0.05$) differences between treatment means.

	Co	DS-HN	DS-LN
Yield (kg DM ha ⁻¹)	2000 ± 108 ^a	761 ± 276 ^b	649 ± 122 ^b
DM (%)	16.93 ± 0.8 ^a	39.13 ± 7.3 ^b	34.37 ± 2.9 ^b
Reducing sugars (%)	3.22 ± 0.26 ^a	4.39 ± 0.55 ^b	4.50 ± 0.26 ^b
Total sugars (%)	14.7 ± 1.8 ^a	23.8 ± 3.5 ^b	25.5 ± 1.3 ^b
N (%)	3.81 ± 0.09 ^a	3.40 ± 0.20 ^b	2.26 ± 0.17 ^c
Nitrate (%)	0.51 ± 0.05 ^a	0.51 ± 0.04 ^a	0.04 ± 0.01 ^b

The DM content of DS-HN significantly differed from Co for the first time on 13 November and DS-LN significantly differed from Co for the first time on 17 November. The soil moisture content of DS-HN dropped two days earlier below 11% than DS-LN. Therefore, DM content of DS-HN also responded slightly earlier than DS-LN.

6.3.2 *Image analysis*

GC, IRI and spatial GC standard deviation

The GC of Co increased steadily up to 27 November (Figure 6.2). The DS-LN had a slightly higher initial GC. The growth rates of GC of DS-HN and DS-LN decreased after 9 November and became negative after 17 November, resulting in a decrease in GC due to folding and eventually dying of leaves. From 15 November onwards, error bars of drought stressed treatments are longer. This indicates that differences between replicates of drought stressed swards increased. The IRI of Co increased strongly after 17 November, whereas the IRI of DS-HN and DS-LN remained constant (Figure 6.3). Drought stress visibly changed leaf angle to a more horizontal orientation, but also decreased mean leaf height. Due to these two opposite effects IRI values increased only slightly. The GC-SSD of Co remained below 11% in all intervals, where the GC-SSD first increased and then decreased (Table 6.2). The GC-SSD values of DS-LN and DS-HN remained fairly constant after 8 days from the start of the experiment. Therefore, the significant differences in GC-SSD between DS-LN and DS-HN and Co just before harvest (27 days of growth) mainly resulted from differences in GC evolution. The TGC-SSD remained below 0.6 for all intervals and treatments, except for DS-HN at 27 growth days with a value of 0.66. Only one of the three DS-HN replicates showed a strong TGC-SSD increase towards harvest. This indicates that the GC decrease was not evenly distributed over this container. The differences in TGC-SSD between the drought-stressed swards and Co were not significant.

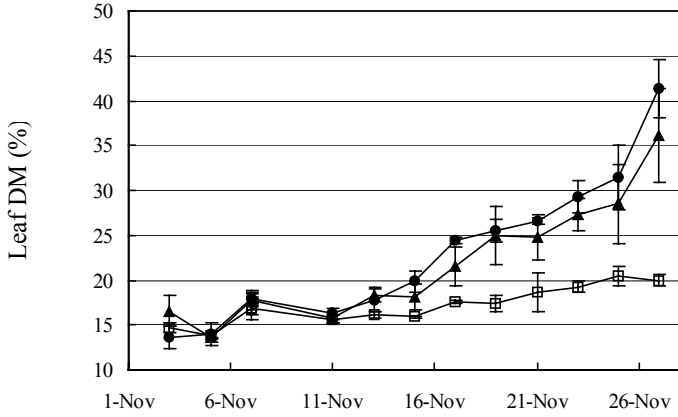


Figure 6.1 Development of leaf dry matter content for control swards (□), drought-stressed swards with high N supply (●) and drought-stressed swards with low N supply (▲). Error bars indicate standard error of means.

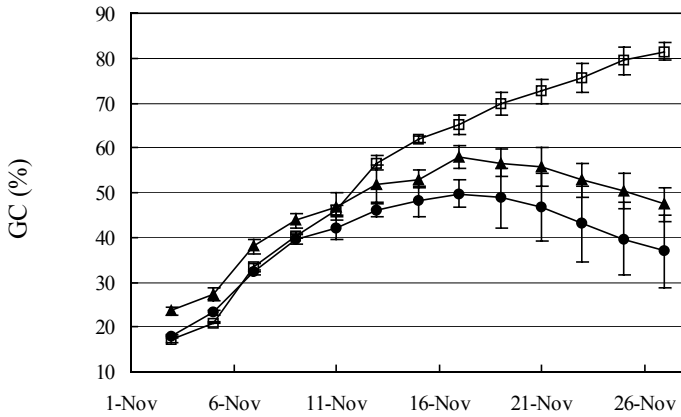


Figure 6.2 Development of image ground cover (GC) for control swards (□), drought-stressed swards with high N supply (●) and drought-stressed swards with low N supply (▲). Error bars indicate standard error of means.

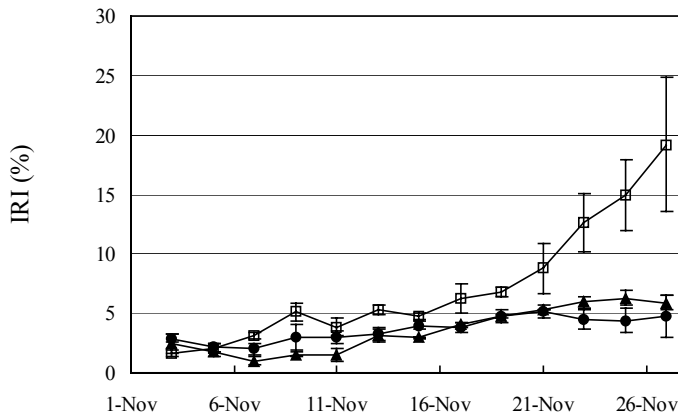


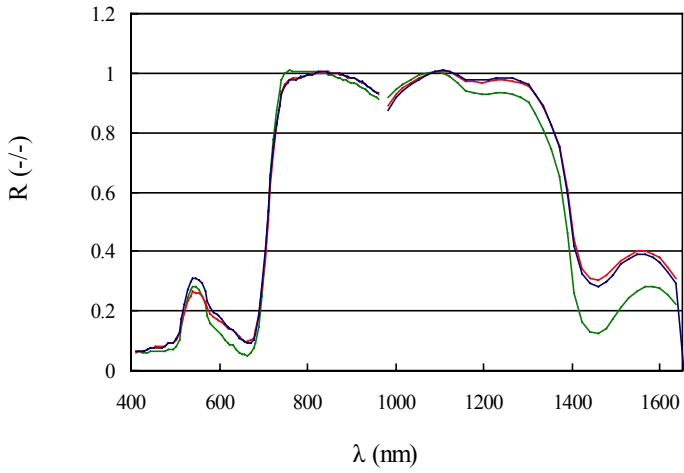
Figure 6.3 Development of index of reflection intensity (IRI) for control swards (□), drought-stressed swards with high N supply (●) and drought-stressed swards with low N supply (▲). Error bars indicate standard error of means.

Derivative spectra

The drought-stressed swards had higher normalised reflection than Co in the visible wavelength range and in the range above 1100 nm than control, whereas reflection was lower in the 730-830 nm range (Figure 6.4A). The amplitude of the derivatives of DS-HN and DS-LN were lower than Co throughout the spectral range measured. The dots in Figure 6.4B indicate that there were 17 IPs identified (at 463, 480, 485, 519, 570, 595, 608, 624, 640, 705, 768, 960, 990, 1140, 1220, 1390 and 1510 nm). The IPs at 519, 570, 705, 990, 1140, 1390 and 1510 nm corresponded to clearly visible slopes (Figure 6.4) that were also selected with the number of knots set to one ninth of the number of spectral bands. The IPs at 463, 480, 485, 595, 608, 624 and 640 nm corresponded to absorption features that were not as strong, although these features were present in spectra of all data.

During unstressed growth, absorption features became deeper and wider, resulting in IP shifts. Under drought stress, water absorption features became narrower, resulting in reversed IP shifts. In Table 6.3, the pigments and chemical bonds with light absorbing or emitting features near the IP and the evolution of IPs with significant effects of drought stress are presented. On 17 November, all IPs detected with the N17 sensor, and the IP near 960 nm of the N10 sensor responded to drought. The IPs near the strongest water

A



B

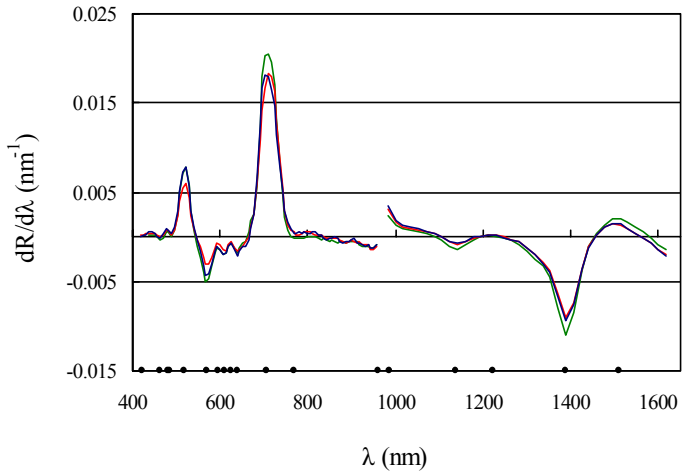


Figure 6.4 Normalised reflection (R) curve (A) and first derivative (B) for control (—), DS-HN (—) and DS-LN (—) swards on 23 November. Dots indicate wavelengths of selected minima and maxima of the first derivative.

Table 6.2 Spatial standard deviation of ground cover (GC-SSD, %) and logistically transformed ground cover (TGC-SSD, -/-) and standard error of replicate mean for intervals of growth days (GD) for control (Co), and drought-stressed swards with high (DS-HN) and low (DS-LN) N supply. Different uppercase letters within rows indicate significant ($p < 0.05$) differences between treatment means.

GD	Co	DS-LN	DS-HN
-----GC-SSD-----			
1-4	8.1 ± 0.9 ^a	8.6 ± 0.8 ^a	8.1 ± 0.1 ^a
5-8	9.3 ± 0.6 ^a	10.0 ± 0.5 ^a	10.7 ± 0.4 ^a
9-13	11.0 ± 0.6 ^{ab}	10.3 ± 0.3 ^a	12.3 ± 0.4 ^b
14-21	9.1 ± 0.7 ^a	10.8 ± 1.1 ^a	11.8 ± 1.1 ^a
27	6.5 ± 0.8 ^a	11.0 ± 1.8 ^b	12.8 ± 0.8 ^b
-----TGC-SSD-----			
1-4	0.57 ± 0.04 ^a	0.51 ± 0.03 ^a	0.53 ± 0.02 ^a
5-8	0.51 ± 0.05 ^a	0.47 ± 0.03 ^a	0.56 ± 0.01 ^a
9-13	0.47 ± 0.03 ^{ab}	0.43 ± 0.01 ^a	0.53 ± 0.02 ^b
14-21	0.46 ± 0.03 ^a	0.47 ± 0.04 ^a	0.51 ± 0.06 ^a
27	0.47 ± 0.06 ^a	0.47 ± 0.09 ^a	0.66 ± 0.09 ^a

absorption feature, around 1390 and 1500 nm responded earliest to drought stress. The evolution of IPs of DS-HN and DS-LN at 1140, 1390 and 1500 reversed after 11 November under drought stress, whereas the IP positions near 960 and 990 nm remained stable.

Drought stress accelerated shifts of IPs around 485, 707 and 768 nm, whereas the IPs around 624 and 570 nm shifted in opposite direction after 17 November (Table 6.3). The IPs around 480, 640 and 519 nm did not change significantly under drought stress.

There were no differences between DS-LN and DS-HN in IP position in the near infrared (NIR) region. The IPs around 485 for DS-LN shifted less to shorter wavelengths than DS-HN, and the IPs around 624 and 705 shifted less to longer wavelengths.

The slopes of nearly all IPs became steeper during unstressed growth (Table 6.4). Under drought stress, slopes became less steep for all IPs around water absorption features. In contrast to IP position, the gradient around 518 nm

of DS-HN was significantly different from Co just before harvest. Under moderate drought stress, slopes became less steep for most IPs. The accelerated shift of the IP position near 707 nm towards longer wavelengths under drought stress coincided with a decreased slope gradient. The gradient near 767 nm became negative under unstressed growth, whereas under drought stress gradients remained positive. This can be understood when considering the differences in general gradients between 740 and 800 nm of drought-stressed and unstressed leaves (Figure 6.4). In this range, unstressed leaves had a nearly flat reflection curve whereas drought-stressed leaves showed a slight increase in reflection with wavelength. The chlorophyll fluorescence feature in unstressed leaves has a distinct right shoulder, whereas this shoulder is flat for drought-stressed leaves and the IP is then located to the first maximum derivative thereafter.

The N supply affected gradients at the IPs around 485, 517, 570, 624 and 640 nm, whereas the gradients at NIR IPs for DS-LN were not different from DS-HN. The evolution of the IP position near 1390 nm during growth requires a reference to separate unstressed swards in an early growth stage (shortly after harvest) from stressed swards later in the growth period. The relation between the IP position near 705 and 1390 nm provided such a reference (Figure 6.5). The measurements at the beginning of a growth period are located at the left top, and points from measurements later in the growth period are located more to the right of the relation. The slope of the relation between the 705 nm and 1390 nm IP position for low ($\lambda_{1390} = 1495 - 0.15 \times \lambda_{705}$, $R^2=0.78$) and high N supply during unstressed growth differed significantly, with the slope for low N supply (-0.15) being less negative than for high N supply (-0.20). The combination of IPs larger than 706 and 1390.2 nm identified drought-stressed swards.

Chlorophyll absorption width

Under severe drought stress, DS-LN and DS-HN had a lower CAW than Co (Figure 6.6). CAW decreased when leaves started to shrink and GC decreased (Figure 6.2). Under drought stress, the RE shift to longer wavelengths became more pronounced and the normal GE shift to shorter wavelengths reversed. This increase in RE is caused by a shift of the position of the first derivative maximum. The DM yield of DS-HN was 38.1% of Co, and of DS-LN 32.5% of Co with a CAW of 120.2 (DS-HN) and 126.8 (DS-LN) at harvest.

Table 6.3 Mean inflection points (IP, nm) for control (Co), and drought-stressed swards with high (DS-HN) and low (DS-LN) N supply. Different uppercase letters indicate significant ($p < 0.05$) differences between means. Significant differences with control are printed in boldface. The indicated pigments (β -carotene (Car), chlorophyll a (Chla) and b (Chlb) and chemical bonds have an absorption or emission maximum near IPs (Curran, 1989; Lichtenthaler, 1987; Zarco Tejada *et al.*, 2000).

Pigment or bond		3/11	9/11	11/11	13/11	17/11	23/11	27/11
Co	Chlb+Car	481.2 ^a	479.3 ^a	479.2 ^a	479.0 ^a	478.3 ^a	480.2 ^a	479.7 ^a
DS-LN	Chlb+Car	480.0 ^a	478.9 ^a	478.1 ^a	479.2 ^a	479.7^b	479.4 ^{ab}	478.1 ^a
DS-HN	Chlb+Car	480.2 ^a	478.6 ^a	478.1 ^a	478.6 ^a	479.3 ^{ab}	478.7^b	478.6 ^a
Co	Car	484.2 ^a	485.6 ^a	486.4 ^{ab}	486.7 ^a	486.5 ^a	486.4 ^a	485.5 ^a
DS-LN	Car	484.9 ^a	486.6 ^a	486.6 ^a	487.4 ^a	487.2 ^a	486.7 ^a	487.7 ^{ab}
DS-HN	Car	485.5 ^a	485.9 ^a	485.6 ^b	487.3 ^a	488.2 ^a	488.3^b	489.2^b
Co	Car+Chlb	516.4 ^a	518.4 ^a	519.1 ^a	519.1 ^a	519.6 ^a	519.6 ^a	519.6 ^a
DS-LN	Car+Chlb	516.7 ^a	518.8 ^b	519.2 ^a	519.2 ^a	519.2^b	519.4 ^a	519.7 ^a
DS-HN	Car+Chlb	516.5 ^a	518.6 ^c	519 ^a	519.2 ^a	519.5 ^a	519.5 ^a	519.4 ^a
Co	Chlb	571.9 ^a	569.5 ^a	569.5 ^a	569.3 ^a	569.1 ^a	569.1 ^a	569.2 ^a
DS-LN	Chlb	571.2 ^a	569.8 ^a	569.5 ^a	569.5 ^a	569.8 ^a	570.1^b	570.4^b
DS-HN	Chlb	572.0 ^a	570.0 ^a	569.6 ^a	569.5 ^a	569.8 ^a	570.2^b	571.1^b
Co	Chla	622.8 ^a	625.0 ^a	625.2 ^a	624.5 ^a	625.4 ^a	625.1 ^a	624.4 ^a
DS-LN	Chla	622.6 ^a	624.9 ^a	624.9 ^a	625.2 ^a	624.7 ^{ab}	623.7 ^{ab}	623.9 ^{ab}
DS-HN	Chla	622.5 ^a	624.6 ^a	624.1 ^a	624.9 ^a	623.4^b	623.4^b	622.0^b
Co	Chlb	639.3 ^a	640.8 ^a	640.9 ^a	639.4 ^a	639.5 ^a	639.6 ^a	638.9 ^a
DS-LN	Chlb	640.7 ^a	640.9 ^a	639.4 ^a	640.7 ^a	640.3 ^a	638.4 ^a	640.2 ^a
DS-HN	Chlb	641.5 ^a	638.6 ^a	638.1 ^a	638.9 ^a	637.7^b	639.2 ^a	638.9 ^a
Co	Chla	696.2 ^a	703.3 ^a	706.5 ^a	706.3 ^a	706.9 ^a	708.1 ^{ab}	709.6 ^{ab}
DS-LN	Chla	695.0 ^a	705.9 ^b	705.8 ^a	707.8^b	707.8 ^a	707.0 ^a	708.7 ^a
DS-HN	Chla	694.9 ^a	704.6 ^{ab}	707.8 ^a	708.5^b	709.5 ^a	710.6^b	711.7^b
Co	Fluorescence	763.5 ^a	765.8 ^a	766.1 ^a	767.0 ^a	771.6 ^a	770.5 ^a	770.6 ^a
DS-LN	Fluorescence	763.5 ^a	766.2 ^a	766.9 ^a	767.7 ^a	770.9 ^a	775.1 ^a	776.3 ^{ab}
DS-HN	Fluorescence	762.4 ^a	767.6 ^a	765.8 ^a	767.6 ^a	771.1 ^a	774.9 ^a	781.6^b
Co	O-H	962.6 ^a	961.6 ^a	961.1 ^a	960.2 ^a	959.6 ^a	959.1 ^a	957.6 ^a
DS-LN	O-H	962.6 ^a	962.0 ^b	961.9 ^a	961.4^b	961.6^b	962.0^b	961.6^b
DS-HN	O-H	962.6 ^a	961.9 ^{ab}	961.4 ^a	961.2 ^{ab}	961.4^b	962.0^b	961.4^b
Co	O-H	996.6 ^a	992.6 ^a	992.0 ^a	989.8 ^a	987.6 ^a	986.8 ^a	981.9 ^a
DS-LN	O-H	996.6 ^a	994.1 ^b	993.6 ^a	992.3 ^a	992.8^b	993.5^b	992.9^b
DS-HN	O-H	996.6 ^a	993.2 ^a	992.6 ^a	991.8 ^a	992.4^b	993.7^b	992.8^b
Co	O-H	1142.9 ^a	1139.2 ^a	1139.3 ^a	1139.4 ^a	1138.6 ^a	1137.9 ^a	1138.4 ^a
DS-LN	O-H	1139.7 ^a	1139.6 ^a	1140.1 ^a	1139.4 ^a	1140.5^b	1141.1^b	1144.1^b
DS-HN	O-H	1142.4 ^a	1139.2 ^a	1138.7 ^a	1139.5 ^a	1141.1^b	1142.4^b	1143.3^b
Co	O-H, C-H	1391.8 ^a	1390.2 ^a	1389.7 ^a	1389.7 ^a	1389.6 ^a	1389.0 ^a	1389.4 ^a
DS-LN	O-H, C-H	1391.8 ^a	1390.7 ^a	1390.0 ^a	1390.4^b	1390.4^b	1390.9^b	1392.9^b
DS-HN	O-H, C-H	1391.8 ^a	1390.3 ^a	1390.1 ^a	1390.2^b	1391.0^c	1391.8^b	1393.2^b
Co	O-H, N-H	1499.8 ^a	1500.3 ^a	1504.7 ^a	1504.5 ^a	1506.4 ^a	1508.0 ^a	1506.6 ^a
DS-LN	O-H, N-H	1499.0 ^a	1499.1 ^a	1501.0^b	1502.9 ^{ab}	1503.6^b	1500.9^b	1496.4^b
DS-HN	O-H, N-H	1498.5 ^a	1501.4 ^a	1502.8 ^{ab}	1502.0^b	1502.6^b	1499.7^b	1497.0^b

Table 6.4 Mean derivatives ($\times 10^{-3}$, in Δ reflection per Δ nm) near the inflection points for control (Co), and drought-stressed swards with high (DS-HN) and low (DS-LN) N supply. Different uppercase letters indicate significant ($p < 0.05$) differences between means. Significant differences with control are printed in boldface.

	Typical pos. (nm)	3/11	9/11	11/11	13/11	17/11	23/11	27/11
Co	480	1.53 ^a	0.88 ^a	0.74 ^a	0.77 ^a	0.62 ^a	0.56 ^a	0.51 ^a
DS-LN	480	1.50 ^a	0.91 ^a	0.81 ^a	0.79 ^a	0.84^b	0.83^b	1.00^b
DS-HN	480	1.48 ^a	0.84 ^a	0.71 ^a	0.77 ^a	0.82^{ab}	0.84^b	1.01^b
Co	485	1.41 ^a	0.61 ^a	0.38 ^a	0.36 ^a	0.21 ^a	0.33 ^a	0.31 ^a
DS-LN	485	1.28 ^a	0.47^b	0.32 ^a	0.30 ^a	0.42^b	0.50^b	0.41 ^a
DS-HN	485	1.12 ^a	0.46^b	0.40 ^a	0.26 ^a	0.25 ^{ab}	0.28 ^a	0.33 ^a
Co	517	8.5 ^a	8.81 ^a	8.15 ^a	8.19 ^a	8.02 ^a	7.69 ^a	7.59 ^a
DS-LN	517	8.26 ^a	7.84^b	8.03 ^a	7.62^b	7.70 ^a	7.50 ^a	6.97 ^a
DS-HN	517	8.67 ^a	8.48 ^{ab}	7.57 ^a	7.45^b	6.80^b	5.81^b	5.08^b
Co	570	-3.59 ^a	-5.15 ^a	-4.87 ^a	-5.03 ^a	-5.03 ^a	-4.81 ^a	-4.69 ^a
DS-LN	570	-3.62 ^a	-4.59^b	-4.86 ^a	-4.64^b	-4.57 ^a	-4.14 ^{ab}	-3.61^b
DS-HN	570	-3.80 ^a	-5.07 ^{ab}	-4.45 ^a	-4.50^b	-4.02^b	-3.14^b	-2.51^c
Co	623	-1.05 ^a	-1.37 ^a	-1.30 ^a	-1.31 ^a	-1.29 ^a	-1.23 ^a	-1.18 ^a
DS-LN	623	-1.08 ^a	-1.14 ^a	-1.22 ^a	-1.19 ^a	-1.20 ^a	-1.07 ^{ab}	-0.98 ^a
DS-HN	623	-1.02 ^a	-1.24 ^a	-1.30 ^a	-1.23 ^a	-1.02 ^a	-0.73^b	-0.60^b
Co	640	-2.36 ^a	-2.52 ^a	-2.24 ^a	-2.21 ^a	-2.11 ^a	-1.99 ^a	-1.98 ^a
DS-LN	640	-2.28 ^a	-2.23 ^a	-2.16 ^a	-2.13 ^a	-2.01 ^a	-1.93 ^{ab}	-1.70 ^a
DS-HN	640	-2.46 ^a	-2.41 ^a	-1.96 ^a	-2.03 ^a	-1.93 ^a	-1.56^b	-1.26^b
Co	707	16.41 ^a	20.30 ^a	20.70 ^a	20.63 ^a	20.56 ^a	20.40 ^a	20.18 ^a
DS-LN	707	16.51 ^a	19.41^b	20.32 ^a	19.93 ^a	19.26 ^a	18.46^b	17.43^b
DS-HN	707	16.74 ^a	20.12 ^a	20.18 ^a	19.99 ^a	18.96 ^a	18.04^b	17.09^b
Co	767	1.07 ^a	0.14 ^a	-0.19 ^a	-0.09 ^a	-0.22 ^a	-0.27 ^a	-0.27 ^a
DS-LN	767	1.06 ^a	0.30 ^a	0.16^b	0.06 ^a	0.04 ^a	0.19^b	0.34^b
DS-HN	767	0.98 ^a	0.05 ^a	-0.01 ^{ab}	0.04 ^a	-0.02 ^a	0.28^b	0.44^b
Co	963	-23.29 ^a	-13.11 ^a	-10.13 ^a	-7.13 ^a	-4.71 ^a	-3.37 ^a	-1.51 ^a
DS-LN	963	-23.17 ^a	-14.59 ^a	-13.43 ^a	-10.80^b	-11.32^b	-12.56^b	-11.26^b
DS-HN	963	-22.65 ^a	-14.06 ^a	-11.63 ^a	-10.35 ^{ab}	-10.32^b	-11.89^b	-9.07^b
Co	997	2.60 ^a	2.58 ^a	2.36 ^a	2.35 ^a	2.27 ^a	1.96 ^a	0.75 ^a
DS-LN	997	2.59 ^a	2.49 ^a	2.38 ^a	2.26 ^a	2.25 ^a	2.31^b	2.14 ^a
DS-HN	997	2.53 ^a	2.58 ^a	2.36 ^a	2.37 ^a	2.20 ^a	2.1 ^{ab}	1.84 ^a
Co	1140	-0.26 ^a	-0.93 ^a	-0.98 ^a	-1.08 ^a	-1.26 ^a	-1.43 ^a	-1.47 ^a
DS-LN	1140	-0.17 ^a	-0.65^b	-0.81 ^a	-0.91^b	-0.98^b	-0.81^b	-0.66^b
DS-HN	1140	-0.23 ^a	-0.79^c	-0.93 ^a	-0.92^b	-0.88^b	-0.78^b	-0.63^b
Co	1392	-7.69 ^a	-10.39 ^a	-10.64 ^a	-10.62 ^a	-10.74 ^a	-10.92 ^a	-10.22 ^a
DS-LN	1392	-7.69 ^a	-8.90^b	-9.29^b	-9.32^b	-9.78 ^{ab}	-9.25^b	-7.56^b
DS-HN	1392	-7.10 ^a	-9.79 ^{ab}	-9.77 ^{ab}	-9.49^b	-9.20^b	-8.36^b	-6.89^b
Co	1500	1.30 ^a	1.93 ^a	1.89 ^a	1.91 ^a	1.97 ^a	2.10 ^a	2.13 ^a
DS-LN	1500	1.55^b	1.64^b	1.60 ^a	1.74^b	1.69^b	1.54^b	1.32^b
DS-HN	1500	1.23^c	1.78 ^{ab}	1.70 ^a	1.68^b	1.64^b	1.34^b	1.19^b

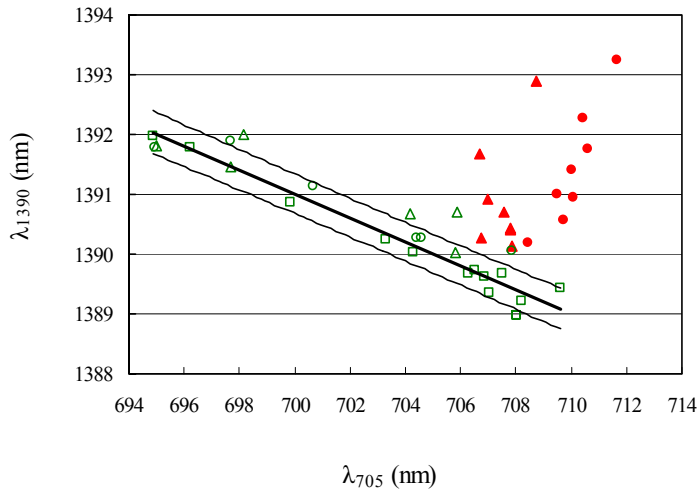


Figure 6.5 Relation between evolution of edges near 705 and 1390 nm. Open symbols indicate measurements of control (\square) and drought-stressed with high N (\circ) and low N supply (\triangle) before 12 November (no drought stress), closed symbols in red indicate measurements after 12 November (drought stressed). The bold line ($\lambda_{1390} = 1531 - 0.2 \times \lambda_{705}$, $R^2 = 0.92$) is fitted through all points of the control. The thin lines indicate the 99% confidence interval for 1 new observation.

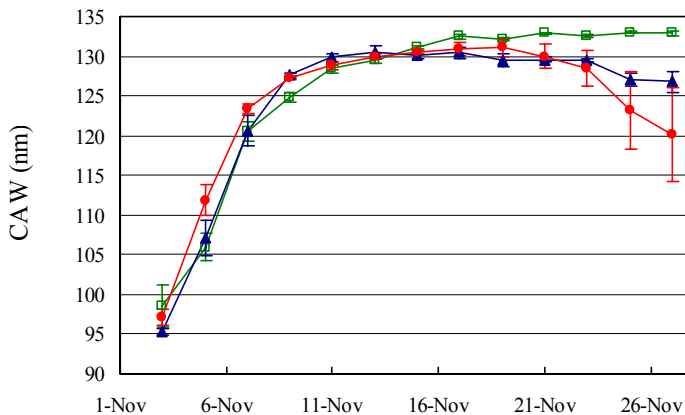


Figure 6.6 Development of chlorophyll absorption width (CAW) for control swards (\square), drought-stressed swards with high N supply (\bullet) and drought-stressed swards with low N supply (\blacktriangle). Error bars indicate standard error of means.

6.4 Discussion and conclusion

Drought stress increased leaf dry matter content and sugar concentration, decelerated and ultimately reversed ground cover (GC) evolution and kept index of reflection intensity (IRI) at low values. This GC development can be understood when considering that drought stress first decreases leaf photosynthesis and, in a more advanced stage of drought stress, specific leaf area (Jones *et al.*, 1980a; b). Thomas (1991) and Van Loo (1992) found earlier that sugar content under drought stress strongly increased in *Lolium perenne* L. Drought stress became first visible in slower GC development. The GC estimates are linearly related to the light intercepting capacity of the sward. The IRI is a measure of canopy geometry and with the combination of GC and IRI, dry matter (DM) yield can be determined (Schut & Ketelaars, Chapter 3). Spatial GC standard deviation slightly increased under drought stress, whereas spatial GC standard deviation of control swards decreased towards harvest. The spatial standard deviation of logistically transformed GC values just before harvest was not significantly different from control. Schut & Ketelaars (Chapter 8) found that at GC values between 30-50%, spatial GC standard deviation of deteriorated swards ranged from 12.6 to 15.0% and spatial GC standard deviation of logistically transformed GC values ranged from 0.72 to 0.85. Drought-stressed swards with similar GC values remained well below these values, and it is concluded that drought stress did not significantly increase sward heterogeneity.

Within a growth period, all absorption features visible in reflectance spectra between 400-1650 nm deepened and widened. The positions of the detected inflection points (IP) corresponded with locations of specific absorption features of carotenoids, chlorophylls and stretching and bending of O-H, C-H and N-H bonds as reported by Lichtenthaler (1987) and Curran (1989). The minor IPs detected in the visible part of the spectrum corresponds with intersections with the abscissa of the second derivative found by Buschmann & Nagel (1993). The reflection curves had a small peak around 740 nm, corresponding with the location of the chlorophyll fluorescence peak (Zarco Tejada *et al.*, 2000). This resulted in a detected IP around 770 nm.

Under drought stress, all absorption features became shallower and narrower again, which is in agreement with Ripple (1986), Bowman (1989), Inoue *et al.* (1993) and Penuelas & Inoue (1999). Water absorption features (with maximum absorption around 970, 1200 and 1450 nm) responded earlier to drought stress than absorption features in the visible wavelength range,

agreeing with Carter (1991, 1993). In the VIS wavelength range, the position of IPs near 570 nm and 623 nm responded strongest to drought stress, agreeing with Carter (1993) who found that sensitivity is largest near 584 nm. The IPs near 960, 990, 1140, 1390 and 1500 nm of drought-stressed swards significantly deviated from control swards, from the moment that leaf DM content of drought-stressed swards increased.

Moderate drought stress did not change the position of IPs in the green and red area's of the spectrum, but clearly changed the slope near the IPs, agreeing with data of Penuelas *et al.* (1994). The absorption features in visible wavelengths responded at more advanced stages of drought when GC already decreased. This is probably due to chlorophyll breakdown and decreased light absorption of chlorophyll (Carter, 1991).

Zarco Tejada *et al.* (2000) showed that chlorophyll fluorescence emission contributes to apparent reflectance spectra of leaves with distinct peaks at 690 and 740 nm. In later growth stages of our experiment, leaves clearly showed an additional feature on the reflection curve, with a maximum around 740 nm. In drought-stressed swards, this feature was also present but detection was difficult, due to changes in the character of the underlying reflection curve. The curve in the 740-800 nm range is nearly flat for control swards, but increasing for drought-stressed swards. Carter (1991) also found flat reflection curves in this range for fresh leaves, but increasing reflection with wavelength for dehydrated and rehydrated leaves.

The position of the IPs around 485, 624 and 705 nm also responded to N supply level. The shift of IPs positions in the visible wavelength range during growth and under drought stress was not as strong for low N supply than for high N supply. The gradients at the IPs around 485, 517, 570, 624, 640 nm were lower for low N supply than for high N supply. In the NIR region, there were no differences found in positions and gradients of IPs between low and high N supply.

The CAW parameter reached a maximum value of 133 nm for control swards, corresponding with Schut & Ketelaars (Chapter 4). In grass swards under moderate N stress, both GE as RE showed a reversed development in the second half of a growing period, whereas GE and RE at high N showed a stable maximum. Severe drought stress also decreased CAW, with the decrease being stronger for high N supply. The relative yield of DS-HN fits well within the relation between CAW and relative yield as found earlier for N stress, whereas relative yield of DS-LN does not (Schut & Ketelaars, Chapter 4).

Under drought stress, the IP position near 570 nm reversed in the second half of the growth period for both low and high N, in parallel with GC decrease, leaf death and chlorophyll breakdown. Drought stress accelerated the increase of IP position near 705 nm up to harvest. Horler *et al.* (1983) also reported a shift of the IP at the red edge to longer wavelengths with leaf drying. This shift to longer wavelengths can also be found in spectra of dehydrated leaves (Penuelas *et al.*, 1993). Horler *et al.* (1983) discussed that this shift might result from changes in internal leaf structure.

In remote sensing with natural light, atmospheric absorption limits the detection of changes in canopy water content. Therefore, applicability of most remote sensed indices is limited to relative water concentrations below 80-85% (Penuelas *et al.*, 1993). In our research, the combination of an active sensor and a limited distance between detector and object allowed accurate reflection measurements in strong water absorbing spectral regions. At these regions, early drought stress could be detected just before leaf water content dropped below 80%.

In the presence of a control, drought stress can be identified by means of comparison of GC and IP position. With repeated measurements in time, the reversed shift of IP position can identify drought-stressed swards. The position of IP showed a clear evolution during unstressed growth. Therefore, growth stage should be taken into consideration when interpreting IP positions without a control.

The relation between the IP position near 705 and 1390 nm provided such a growth stage reference, and with this relation, unstressed swards shortly after harvest can be differentiated from drought-stressed swards in a later growth stage.

7

Detection of clover cover in grass swards with imaging spectroscopy

A.G.T. Schut & J.C. van den Berg

7. Abstract

The potential of an experimental imaging spectroscopy system, with high spatial (0.28-1.45 mm²) and spectral resolution (5-13 nm), is explored for robust discrimination between grass, clover and mixed mini swards at various growth stages. For this, spectra of grass and clover swards were compared and image line texture was analyzed using *spatial correlation*, a *special filter* and *wavelet entropy*. In 2000, an experiment with mini swards was conducted including two white clover (*Trifolium repens*, cv. *Blanca*) swards, three perennial ryegrass (*Lolium perenne* L.) swards and four swards with a grass and white clover mixture. The average spectral curves of pixels of grass and clover swards differed throughout the spectral range of 405 up to 1650 nm, but differences were smaller than one standard deviation of grass spectra. No specific discriminating spectral feature was found. Differences in edge positions between grass and clover swards were not consistent within growth periods. With image line texture, pure grass and clover swards could be separated with the filter, spatial correlation and wavelet entropy. Only wavelet entropy resulted in robust discrimination on all recording dates. In all three discriminating methods, results of mixed swards were intermediate between pure swards. It is concluded that imaging spectroscopy provides new means for quantification of clover cover in mixed swards.

7.1 Introduction

The reduction of fertiliser nitrogen (N) inputs in agricultural systems accrues the importance of symbiotically N₂ fixing white clover (*Trifolium repens* L.) as N source. White clover is most commonly grown with a companion grass, in cultivated pastures mostly perennial ryegrass (*Lolium perenne* L.). Swards with a mixture of grass and clover will be referred to as mixed swards. A stable mixture is required in order to minimize bloat hazards for grazing ruminants, and to maximize N₂ fixation. The optimal value for the fraction of clover ranges from 20 up to 40% (Baars & Van Dongen, 1989). The fraction of legume content in mixed swards is, however, highly variable in time (Elgersma & Schlepers, 1997; Elgersma *et al.*, 2000; Loiseau *et al.*, 2001; Schils, 1997) and space (Locher *et al.*, 2001; Schils *et al.*, 2000). Up till now, fast and adequate techniques to record this temporal and spatial heterogeneity and to study their responses to environmental factors are not available (Schulte, 2001, p.4).

A rapid assessment of N₂ fixation by clover is required to calculate farm N balances correctly (Velthof *et al.*, 2000). The annual N₂ fixation per unit clover dry matter (DM) is rather stable with reported values between 40 to 55 kg ton⁻¹ DM (Velthof *et al.*, 2000), irrespective of N application (Van der Meer & Baan Hofman, 2000). For pure clover swards, ground cover (GC) is linearly related to DM yield (Schils *et al.*, 1999). Parameters derived from imaging spectroscopy were successfully related to grass biomass, explaining 75 up to 82 % of the variation in DM yield. The estimates were significantly improved by including the index of reflection intensity (IRI, a parameter related to canopy geometry) (Schut & Ketelaars, Chapter 3). Including reflection intensity information might also improve the relation between GC and clover DM yield. For mixed swards, clover and grass DM yield can only be estimated with GC when clover GC is differentiated from grass GC. In this paper, the potential of an experimental imaging spectroscopy system (Schut *et al.*, Chapter 2) is explored for its applicability to discriminate between grass, clover and mixed mini swards at various growth stages. For this, a small container experiment was conducted with grass, clover and mixed swards. Spectral discrimination at leaf and canopy scale and three textural classification methods will be examined. A successful classification method should be robust, which means that it should be applicable throughout growth periods.

7.2 Materials and Methods

7.2.1 Experiment

In the summer of 2000, a container experiment was conducted from 28 August up to 30 October with 2 clover swards, 3 grass swards and 4 mixed swards. Containers were 90 cm long, 70 cm wide and 40 cm deep, and were filled with a sandy soil with 3% organic matter. For the pure clover swards, large-leaved white clover (*Trifolium repens* L., *cv. Blanca*) was sown on 10 June. The perennial ryegrass swards (*Lolium perenne* L.) were transplanted on 10 June from a 2nd year grass sward. The mixed swards were constructed with transplanting best parts of existing mixed swards, sown in March (50 kg ha⁻¹ grass (*Lolium perenne* L.) and 5 kg ha⁻¹ clover seed (*Trifolium repens* L., *cv. Blanca*)). Two swards contained more grass than clover (mixture 1) and two swards contained more clover than grass (mixture 2), but within both mixtures grass was intermingled with clover. These mixed swards were harvested on

July 25. Grass swards received 120 kg N per growth period, clover swards received no additional N. For the mixtures N application was limited to control grass growth (for maintaining a mixture). Mixture 1 swards received 30 kg N per growth period, and mixture 2 swards received 60 kg N per growth period. All swards received additional P, K and S after each harvest. Soil water content was maintained at field capacity. On August 29 and October 30, swards were hand-cut, fresh material was weighed and analyzed for dry matter content. On September 22 and October 13 cover fractions of the mixtures were visually scored at 300 raster intersects per sward, using the method of Korva (1996).

7.2.2 Images

Twice a week image lines were recorded with the experimental imaging spectroscopy system. The image lines were 15.3 cm long and 1.39 mm wide, and were recorded in a regular pattern with 3 bands next to one other per mini sward. In each band 14 image lines were recorded each 5 cm apart, see (Schut *et al.*, Chapter 2) for details. The system combines high spatial (0.28-1.45 mm² per pixel) and high spectral resolution (5-13 nm). Three imaging spectrographs (V7, N10 and N17) are used, measuring reflectance (R) in the spectral range from 400 up to 1650 nm. Additionally, 200 adjacent image lines were recorded in 2001 of grass and mixed swards, fertilized with 90 and 60 kg N ha⁻¹ and sufficient P, K and S, to be able to construct and display two-dimensional (2D) images.

7.2.3 Image analysis

The image lines were classified with maximum likelihood procedures (Schut & Ketelaars, Chapter 3). The spectral library contained classes for soil, grass, leaves with specular reflection, dead material and an intermediate class between soil and dead material. Reflection intensity recorded with the system is a function of leaf angle and leaf height in the canopy (Schut *et al.*, Chapter 2). Therefore, the grass and specular classes in the spectral library were further subdivided into reflection intensity classes (IC), ranging from 0 up to and including 6 for grass and from 0 up to and including 2 for leaves with specular reflection. Image ground cover was calculated per intensity class. Total image line (IL) ground cover (GC_{IL}, %) was calculated as the sum of grass (GCG) and specular classes (GCS):

$$GC_{IL} = \sum_{ic=0}^6 GCG_{ic} + \sum_{ic=0}^2 GCS_{ic} \quad (1)$$

where ic is the index number of the intensity class. The mini sward GC was calculated as the average of the GC_{IL} over the 42 image lines. The index of reflection intensity (IRI) was then calculated as:

$$IRI = 100 \times \frac{\sum_{ic=3}^6 \frac{1}{42} \sum_{IL=1}^{42} GCG_{IL,ic}}{GC} \quad (2)$$

This IRI measures the presence of highly reflecting green pixels as a percentage of the ground cover. A higher value represents a higher canopy with more horizontally oriented leaves (Schut & Ketelaars, Chapter 3). After classification, reflection spectra of pixels were normalised (\tilde{R}), according to equations in (Schut *et al.*, Chapter 2) Average sward spectra were calculated from all classified grass pixels, where $0 < IC \leq 6$. In addition, a reflection curve was calculated for each IC separately. Reflectance spectra of green material typically have a sharp transition from minimal reflection at 680 nm and maximal reflection at 750 nm, known as the red edge (RE) (Horler *et al.*, 1983). Green material reflects more radiation in the green part than in blue or red parts of the spectrum, and a blue edge (BE) and a green edge (GE) can be found around 520 and 600 nm respectively (Figure 7.3). In this study a simple hyperspectral method for determination of edge parameters was used. From the normalised spectra, the minimum (\tilde{R}_{min}) and maximum (\tilde{R}_{max}) reflection value was determined within the spectral range of 472-800 nm for the BE, GE and RE. Then, a threshold value (T) was calculated according to:

$$T = \tilde{R}_{min} + (\tilde{R}_{max} - \tilde{R}_{min}) \times CV \quad (3)$$

where CV is the critical value. At the RE, the transition between the V7 and N10 sensor typically occurs between a normalised reflection value of 0.35 and 0.5. To minimise effects of this transition, the CV was set at 0.55. The reflection value of band i was calculated as the average of band i , band $i-1$ and band $i+1$. Then, the wavelength position with a reflection value equal to T was calculated. For this, two neighbouring bands were determined where reflection in one band is smaller, and in the other band is greater than T . The exact wavelength position of T was calculated by linear interpolation of reflection values and wavelength positions. Edges were calculated for each IC reflection curve, and for the field average reflection curve.

7.2.4 *Discrimination of clover and grass*

Species discrimination with imaging systems can be based on numerous characteristics, *e.g.* growth characteristics, canopy geometry, spectral characteristics of leaves or canopies, leaf size or leaf shape. With 1D image lines, information on GC and IRI development, leaf and canopy spectra and image line texture was available. Image line texture is defined as the sequence of pixel reflection values.

Spectral discrimination

Species can be recognised, based on their spectral characteristics, if inter-species variability is larger than intra-species variability (Skidmore *et al.*, 1988). Spectral variability depends on scale. On canopy scale, geometric properties (*e.g.* plant-physiology, leaf angle and plant-density), background together with colour and leaf properties of plants determine reflectance measurements. On this scale, hyperspectral data can be used to discriminate several species (Hahn & Muir, 1993; Daughtry & Walthall, 1998; Moshou *et al.*, 2001; Schmidt & Skidmore, 2001). Reflectance measured with imaging spectrographs permit measurement at sub-leaf scale (Borregaard *et al.*, 2000; Feyaerts & Van Gool, 2001). At this scale, canopy geometry becomes less important, but within species variability increases since variation between leaves and shadow effects (when measured under sunlight conditions) are also included. In this experiment, spectral measurements at sub-leaf and canopy scale are compared for clover and grass. To do so, pixel spectra were collected per sensor and per intensity class from image lines of grass and clover swards, recorded on 30 October. From these spectra, averages and standard deviations were calculated per spectral band. Additionally, edge positions in three images of mixed grass/clover swards and grass swards were analysed (Figure 7.5). The edge positions in these images were calculated as explained above, where wavelength position of the minimum and maximum reflection value were fixed at 550 and 680 nm for the green edge (GE). At the canopy scale, sward average spectra (calculated as described above) of clover and grass were compared. The spectral curve shows a remarkable shift over intensity classes, resulting in profiles of edge positions that may result from canopy geometry (Schut & Ketelaars, Chapter 4). To minimise geometry effects, results are shown for an intermediate intensity class (IC 3). Edge positions are related to reflection intensity (see *e.g.* Figure 7.7), which might result from the combination of

sensor characteristics, changes in pigment composition within a canopy, leaf angle and lighting conditions (Schut & Ketelaars, Chapter 4). Therefore, the resulting edge profiles might be characteristic for an individual crop. Linear regression was performed between edge position and intensity class for IC 0 through IC 5, where the slope was used as profile descriptor.

Textural discrimination

Trifolium repens leaves are composed of 3 leaf blades, and have an oval shape with a typical diameter between 1 cm and 5 cm. Clover leaves are mostly horizontally orientated, but orientation changes towards a more vertical direction during the night. Leaf angle distribution is of a planophile type (De Wit, 1965). *Lolium perenne* L. leaves are narrow and long, typically less than 1 cm wide and up to 40 cm long. Leaf angles of individual leaf sheets change from almost vertically oriented at the leaf base to more horizontally oriented at the leaf top. Leaf angle distribution within a grass canopy is of a spherical type, changing towards plagiophile leaf angle distribution at higher amounts of biomass (De Wit, 1965). Reflection intensity recorded with the experimental imaging spectroscopy system is a function of both leaf angle and leaf height position in the canopy (Schut *et al.*, Chapter 2). Both leaf height and leaf angle vary less for a single leaf in clover than in grass. Therefore, the reflection intensity pattern in “clover” image lines may be different from “grass” image lines. Three methods were used to extract textural information from the image lines: a filter, spatial correlation and wavelet transformation.

Filter

Based on the difference in leaf width of grass and clover, a filter was constructed to distinguish both leaf types. First, to find green pixels, image lines are classified using simple thresholds and ratios, as defined in Schut *et al.* (Chapter 2). Then classification results were used to connect leaf pixels on a single image line. For clover and grass, two types of filters were defined, to assign a pixel to a connected area. The first filter considers a pixel as part of a connected area if all pixels in a 10 and 25 mm range are classified as green material and have a classification between IC 2 and IC 6, while classification may deviate only 1 unit from the starting pixel. The connected areas in the second filter must at least be 5 mm long, and IC may deviate 2 classes from the starting pixel. The filters are consecutively applied to each pixel.

For the 2D images, pixels classified as green material, with an IC between 2 and 6 are represented by a green color. However, when the pixel passes a filter and is, therefore, considered as part of a connected region, it is colored red. In all other cases pixels are uncolored. The percentage of leaves within the threshold sizes (L) were calculated as:

$$L (\%) = 100 * (\text{red pixels}) / (\text{red} + \text{green pixels}) \quad (4)$$

Spatial correlation

Spatial relations can be studied with correlation, semivariograms or covariance functions (Stein *et al.*, 1999). Here, the spatial correlation between pixels at a specific distance is calculated. First, image lines are classified. If a pixel is classified as green material, the average reflection value (\bar{R}) in the 550-555 nm region is calculated. Then, correlation is calculated according to:

$$\sigma_h = \frac{\text{Cov}(\bar{R}_x, \bar{R}_{x+h})}{\sigma_x \sigma_{x+h}}, \quad (5)$$

where h ($h = 1, 2 \dots$ number of pixels per image line) represents the lag or distance between the pixels x and $x+h$ on a image line, and σ is the standard deviation. The covariance between pixel reflection values at 550-555 nm at distance h is calculated as:

$$\text{Cov}(\bar{R}_x, \bar{R}_{x+h}) = \frac{1}{n} \sum_{j=1}^n ((\bar{R}_{x,j} - \hat{R}_x)(\bar{R}_{x+h,j} - \hat{R}_{x+h})), \quad (6)$$

where \hat{R} is the mean reflection value and n the number of pixel pairs.

Wavelet transformation

Let us consider the reflection response \bar{R} on an image line with x positions. This response (of any type) may be oscillating on a large or small scale, with high or low amplitudes. The wavelet is a smooth and quickly vanishing oscillating function with good localization in both frequency and location (*e.g.* in time or space). A wavelet family $\psi_{a,b}$ is the set of elementary functions generated by dilations and translations of a unique mother wavelet $\psi(x)$:

$$\psi_{a,b}(x) = |a|^{-1/2} \psi\left(\frac{x-b}{a}\right) \quad (7)$$

where $a, b \in R, (a \neq 0)$ are the scale parameter and the translation parameter respectively, and x the position on the image line. As a decreases, the wavelet becomes narrower, and as b changes the center of the wavelet $\psi_{a,b}$ shifts along the x -axis. The continuous wavelet transform (CWT) of \bar{R} is defined as the inner product of the function $\bar{R}(x)$ with the wavelet $\psi_{a,b}(x)$ for each a and b :

$$W_{\psi}\bar{R}(a, b) = |a|^{-1/2} \int_{-\infty}^{\infty} \bar{R}(x) \psi^*\left(\frac{x-b}{a}\right) dx = \langle \bar{R}, \psi_{a,b} \rangle \quad (8)$$

The Wavelab802 CWT command (Buckheit *et al.*, 1995) was used with the Morlet function as mother wavelet:

$$\psi(x) = \frac{1}{\sqrt[4]{\pi}} e^{-x^2/2} (e^{-i\xi_0 x} - e^{-\xi_0^2/2}) \quad (9)$$

where ξ_0 indicates the modulation frequency, usually taken to be 5.33 (Daubechies, 1992, p76). The CWT transformation yields the signal in the wavelet domain in 96 frequency scales (12 voices per octave with 8 octaves), for each transect x -position. The question is whether the distribution of transformation values over the scales is different for clover and grass image lines. There may even be unique scales with a specific response for clover or grass. To identify these, the relative wavelet energy might be a good measure. Rosso *et al.* (2001) calculated the *relative wavelet energy* p_a in scale a for each scale as:

$$p_a = \frac{E_a}{E_{tot}}, \quad (10)$$

where E_a is the energy per scale,

$$E_a = \sum_b |W_{\psi}y(a, b)|^2, \quad (11)$$

and E_{tot} the total energy in the image line,

$$E_{tot} = \sum_a E_a. \quad (12)$$

The parameters a and b in these summations range over all scales and translations occurring in the Wavelab802 CWT algorithm as applied in the signal $y(x)$. The distribution of energy over the scales can be characterized by the total wavelet entropy (Rosso *et al.*, 2001), defined as the Shannon entropy of the relative energy distribution p_a :

$$S_{CWT} = -\sum_a p_a \ln(p_a). \quad (13)$$

Lower values of this wavelet entropy represent higher degrees of order, which means that all energy is concentrated in a limited number of scales. The sward average wavelet entropy is then calculated as the average over all the image lines in a container:

$$S_{sward} = \frac{1}{n} \sum_{j=1}^n S_{CWT}(j), \quad (14)$$

where n represents the number of image lines. The sensitivity of wavelet entropy estimates for various degrees of sward damage was evaluated. For this, 9 individual mini swards were selected from a sward damage experiment (Schut & Ketelaars, Chapter 3). For reasons of clarity, only data of the September growth period were used. At harvest, the DM yield in the sward damage experiment varied between 1660 and 2302 kg DM ha⁻¹, whereas dense swards here yielded 2696 kg DM ha⁻¹ and clover swards yielded 2368 kg DM ha⁻¹ (Table 7.1).

7.3 Results

7.3.1 Growth

Dry matter yields of the September harvest were higher than for the October harvest (Table 7.1). Yield depression in the last harvest was larger for white clover swards than for grass swards. Mixtures had lower N contents than either clover or grass, probably as a result of lower N applications. Mixture 2 contained a higher fraction of clover than mixture 1 in both growing periods (Table 7.2). After harvest, clover GC was much higher than grass GC (Figure 7.1). During the growth period, GC increase was higher for grass than for clover swards, resulting in minor differences at harvest. The three GC dips, on 13, 16 and 23 October in clover and mixtures, were caused by early morning measurements. On these three dates, a cloudy sky caused low light levels at the time of measurement (08.30 hour), and clover leaves were still dark-adapted (leaves in almost vertical position). The strong decline in clover DM yield in late autumn (Table 7.1) is also reflected in slow vertical growth and consequently in low IRI values (Figure 7.2).

Table 7.1 Treatments in the experiment and treatment averages for dry matter (DM) yield, dry matter content and total nitrogen (N) content.

Treatment	DM yield (kg ha ⁻¹)	DM content (%)	Total N content (N kg DM ⁻¹ , %)
-----September harvest-----			
White clover	2368	12.30	4.19
Grass/ clover mixture 1	2542	14.70	2.92
Grass /clover mixture 2	1885	13.35	3.65
Grass	2696	14.30	3.84
-----October harvest-----			
White clover	879	14.50	4.61
Grass/ clover mixture 1	1222	14.75	3.52
Grass /clover mixture 2	1488	14.05	4.01
Grass	1403	12.97	4.88

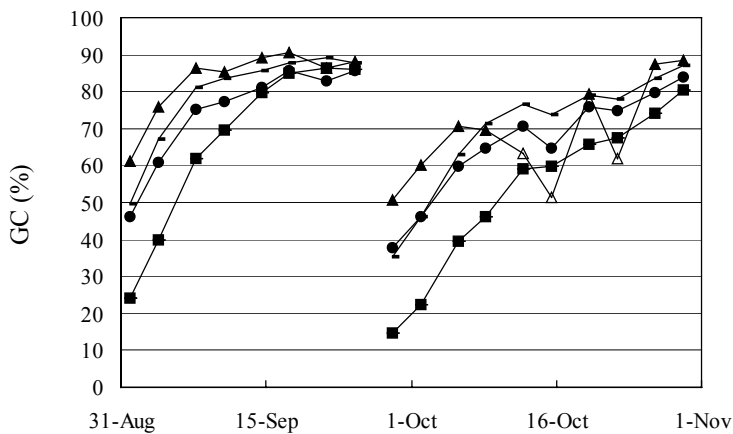


Figure 7.1 Image ground cover evolution for grass swards (■), clover swards (▲), where (Δ) indicate folded leaves, mixture 1 (●) and mixture 2 (○).

Table 7.2 Visual scores of ground cover of white clover (GCc) and grass (GCg) in mixed white clover / grass swards.

Treatment	22 September		13 October	
	GCc (%)	GCg (%)	GCc (%)	GCg (%)
Grass / clover mixture 1	26	70	31	58
Grass / clover mixture 2	53	46	36	53

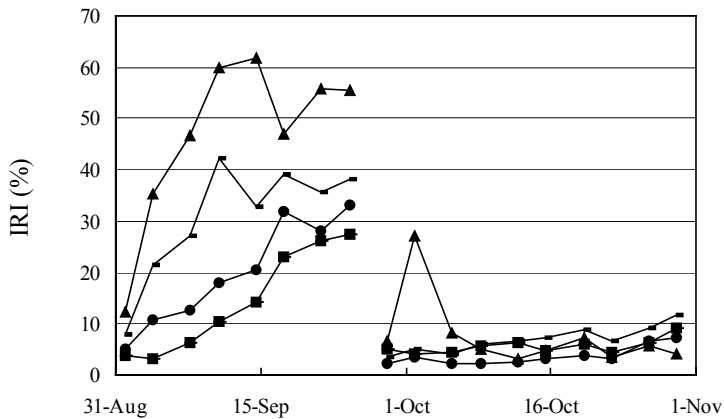


Figure 7.2 Index of reflection intensity (IRI) evolution for grass swards (■), clover swards (▲), where (Δ) indicate folded leaves, mixture 1 (●) and mixture 2 (-).

Spectral discrimination

On pixel scale, the spectral curve differed between grass and clover in all three spectral domains (Figure 7.3). No specific absorption feature could be identified on which separation could be based. The difference in average curve of grass and clover was smaller than the standard deviation of grass pixels, throughout the range from 400 nm up to 1650 nm. The differences in spectra were also present in the position of the BE, GE and RE.

On canopy scale, the average spectral curves for IC 3 showed differences between grass and clover in GE position before harvest (Figure 7.4), where white clover had a lower GE position than grass. Mixtures had intermediate

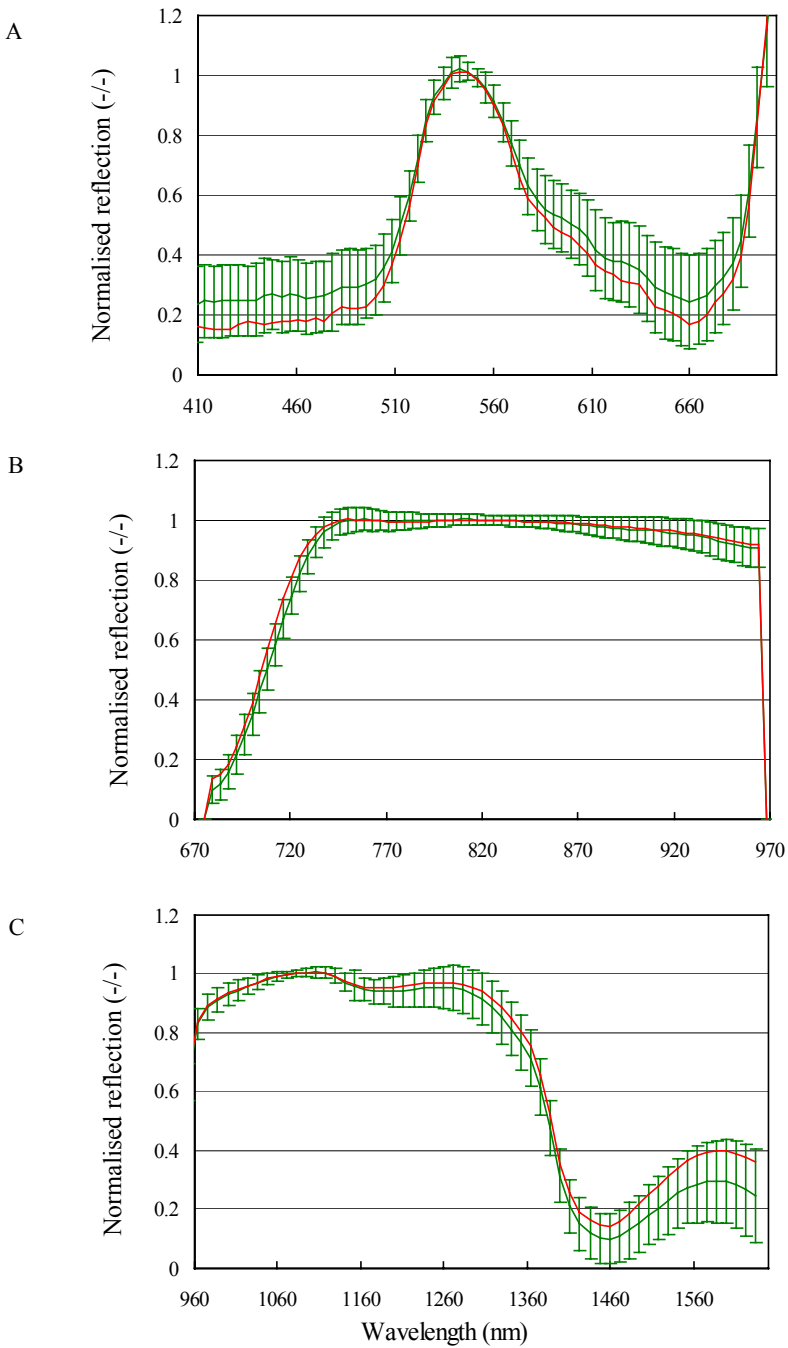


Figure 7.3 Average reflection curves for grass (-) and clover (-) pixels for the V7 (A), N10 (B) and N17 (C) sensor. Error bars indicate standard deviation for grass curves.

values. The GE position showed a clear evolution during growth, while changes were stronger for grass swards. In Figure 7.5, 2-Dimensional images are shown for mixtures and grass swards, recorded on three dates within one growth period. On pixel basis, variability in GE position within a small area is large (Figure 7.6), the same holds for BE and RE position (not shown). When the GE was calculated for each IC, it appeared that differences between grass and white clover were larger for higher IC's than for lower IC's (Figure 7.7). The shift in GE with IC was larger in grass and mixture swards than in white clover swards. The slope of the profiles distinguished grass from clover swards throughout the two growing periods (Figure 7.8), except for 23 October. The mixtures showed intermediate slope values.

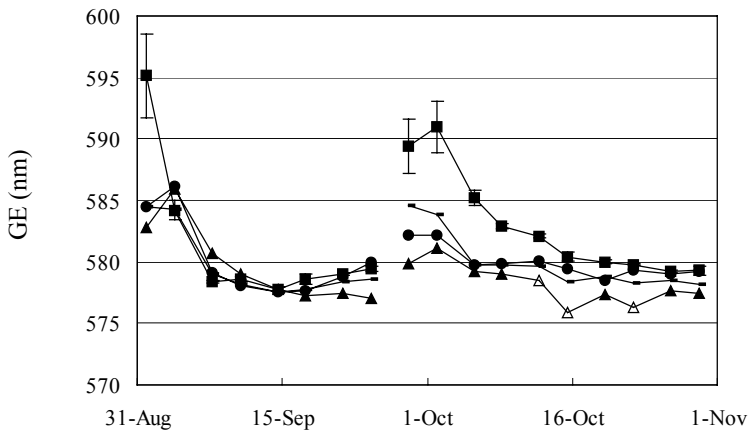


Figure 7.4 Evolution of green edge position (GE) for reflection intensity class 3 for grass swards (■), clover swards (▲), where (Δ) indicate folded leaves, mixture 1 (●) and mixture 2 (○).

7.3.2 *Discrimination of clover and grass*



Figure 7.5 Images of a sward with a grass clover mixture (top) and a pure grass sward (bottom), taken on 6 (left), 13 (middle) and 21 (right) July 2000.

Textural discrimination

Filter

In Figure 7.9, reflection at 550 nm is shown for two image lines, with typical patterns for white clover and grass swards. The grass image line has a strong peaky pattern, whereas the clover image line has a more step-wise pattern, resulting from differences in leaf width and leaf orientation. The developed filter could distinguish these differences in pattern (Figure 7.10). In this figure, most white clover leaves were correctly marked. However, not all pixels on white clover leaves were recognised as such, and mistakes were made within grass swards when leaves were either clustered or lay parallel to the image line. In Figure 7.11, cover estimates are given for leaves larger than 10 mm

(Figure 7.11 A) and larger than 5 mm (Figure 7.11 B). In both figures, clover swards showed a larger cover of pixels above threshold size than grass swards, while mixtures were intermediate. Differences between grass and clover swards were larger than the variation within the mean of the grass swards. On 16 and 23 October no differences were visible, presumably due to folded leaves.

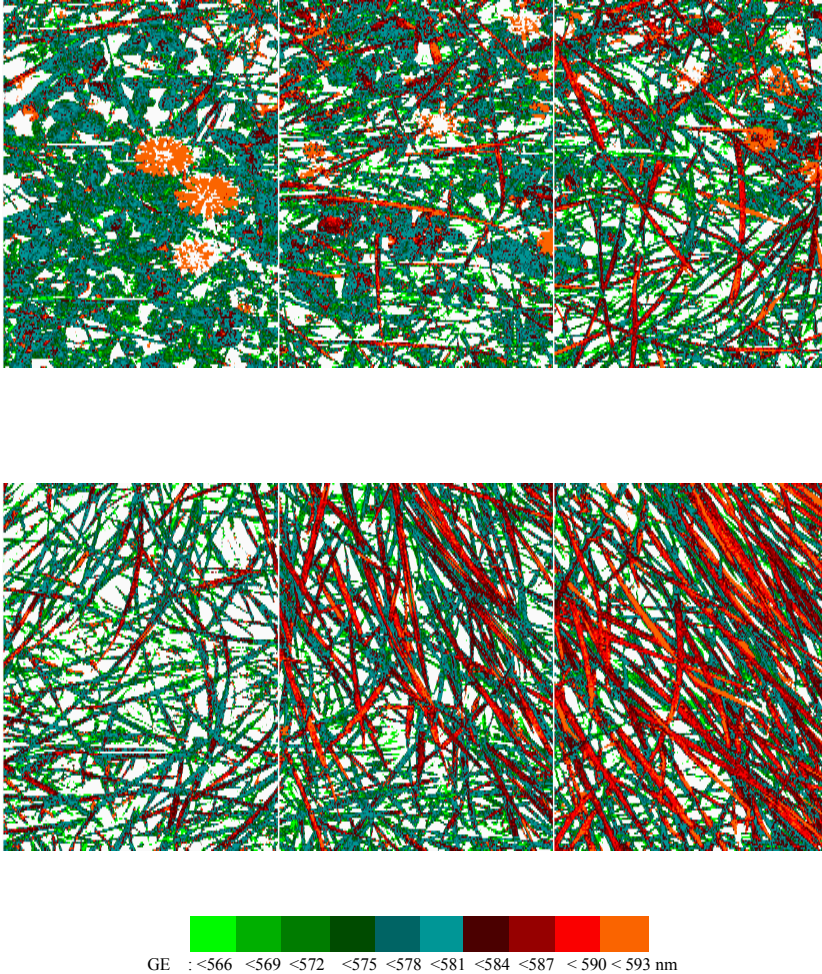


Figure 7.6 Images based on green edge (GE) classification for the Figure 7.5 images.

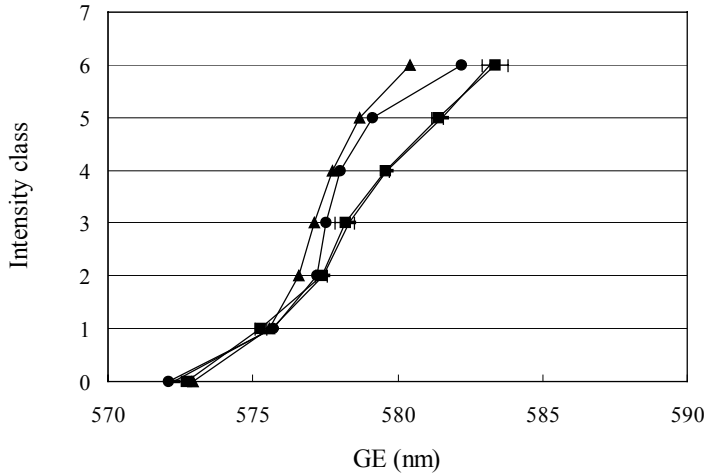


Figure 7.7 Green edge (GE) position profiles for grass swards (■), clover swards (▲), where (Δ) indicate folded leaves, mixture 1 (●) and mixture 2 (–) on 30 October.

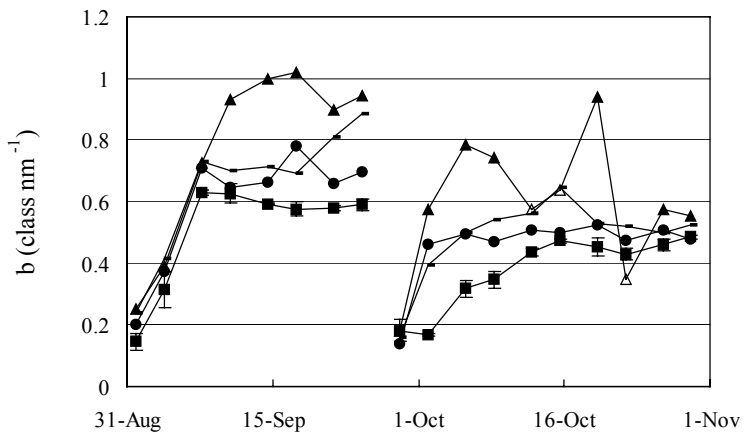


Figure 7.8 Slope estimates of a linear fit ($IC = a + b GE$) through green edge position profiles (see Figure 7.7), for classes IC 0 up to and including IC 5, for grass swards (■), clover swards (▲), where (Δ) indicate folded leaves, mixture 1 (●) and mixture 2 (–).

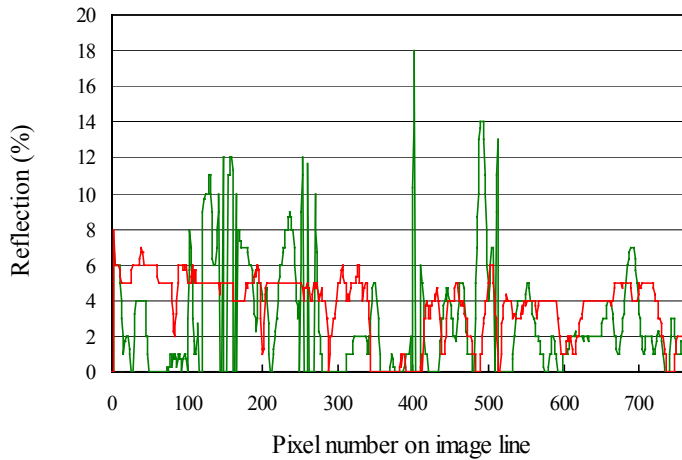


Figure 7.9 Typical image line patterns for average reflection value between 550- 555 nm for a clover (—) and grass sward (—)

Spatial correlation

In Figure 7.12, as an example, the correlation coefficient of pixel reflection values at 500-550 nm is given for each sward type as function of distance. In this figure, differences between grass and clover are present between 2 and 12 mm distance, with largest absolute differences on shorter distances. At distances beyond 20 mm, correlation coefficient was below 0.1. This is in correspondence with the differences between grass and clover in Figure 7.9. Within the mixed swards, both leaf types will occur within the 42 image lines, resulting in an intermediate spatial correlation between the pure swards. In Figure 7.13, the correlation coefficient at a distance of 3 mm is depicted. Again, differences between grass and clover swards were clearly present. The value of the correlation coefficient varies within growth periods, especially for the mixtures. Shortly after harvest, the correlation coefficient of mixtures was similar to clover, but decreased towards values for grass swards at harvest.

Wavelet transformation

In Figure 7.14, examples of the distribution of relative wavelet energy over the wavelet scales are shown, for a single date, for 3 grass and 2 white clover swards. High frequencies correspond with great detail. At low frequency scales

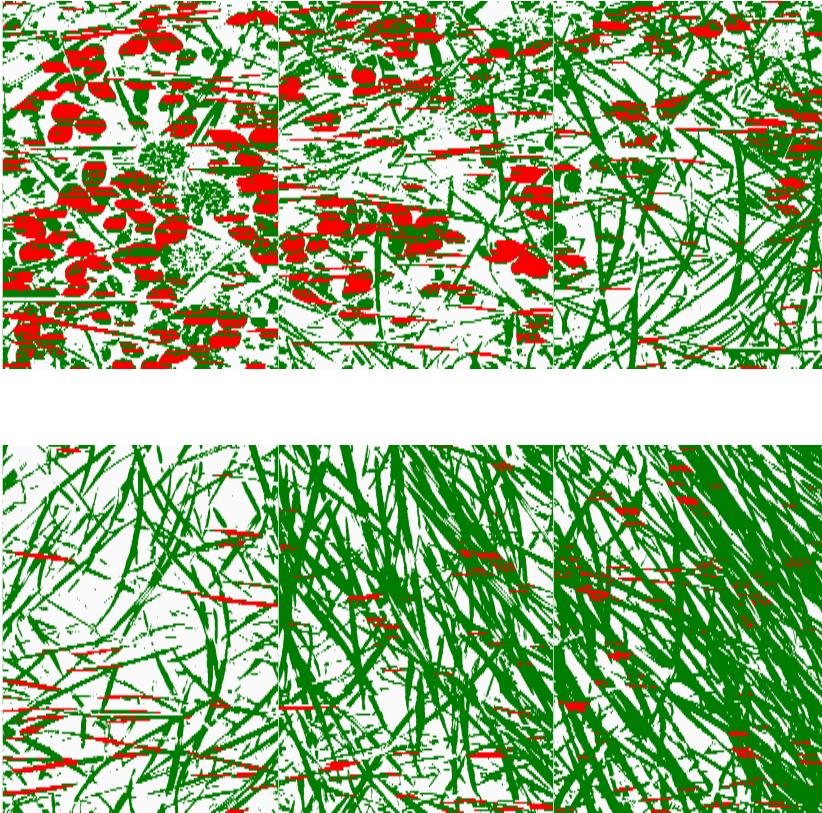


Figure 7.10 Images with pixels on a large leaf (between 10-25 mm wide in horizontal direction and with maximum 1 IC class deviation) for grass pixels with an intensity class 3 or higher. Pixels on a large leaf are coloured red and all other pixels within the grass classes with an intensity class 3 or higher are coloured green.

small details are less important, although details have a cone of influence on lower frequencies (Mallat, 1999). In the grass swards, relative energy decreased more or less linearly with frequency. The clover decreased in an exponential fashion with frequency. This difference is characterised by the wavelet entropy value (Figure 7.15), where clover swards had a lower wavelet entropy value than grass swards. Again, mixtures were intermediate. Wavelet entropy of mixture 1 was more similar to grass swards, whereas mixture 2 wavelet entropy was more similar to clover swards. This is in agreement with a higher clover fraction of mixture 1 when compared to mixture 2 (see Table 7.2).

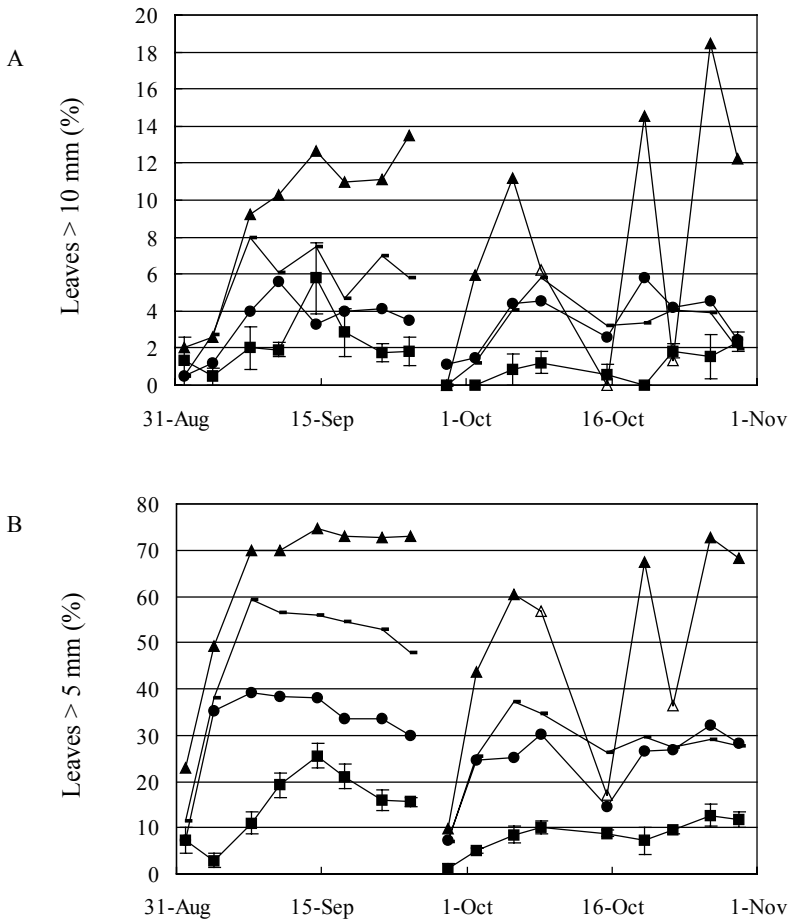


Figure 7.11 Evolution of the percentage of large leaves, wider than 10 mm (A) and wider than 5 mm (B) within pixels with an intensity class of 3 or higher for grass swards (■), clover swards (▲), where (△) indicate folded leaves, mixture 1 (●) and mixture 2 (—).

Although the white clover sward wavelet entropy increased on 13 and 16 October, differences with grass swards were still large enough for separation. A single threshold was defined for separation of clover and grass swards, a wavelet entropy value of 3.4 discriminated between pure grass and pure clover during the entire period of observation, except within the first days after harvest. This value was, therefore, defined as the threshold value. The response

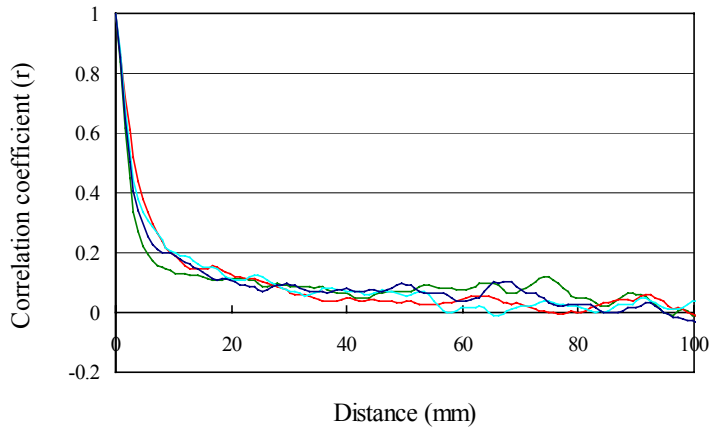


Figure 7.12 Correlation coefficient between reflection value (averaged between 550 and 555 nm) on position x on the image line and on position $x + \text{distance}$ on the image line for grass swards (—), clover swards (—), mixture 1 (—) and mixture 2 (—).

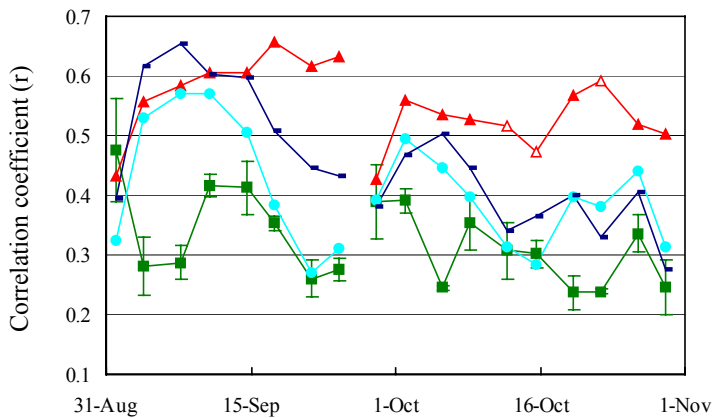


Figure 7.13 Correlation coefficient between pixel reflection values (averaged between 550-555 nm) at a distance of 3mm for grass swards (■), clover swards (▲), where (△) indicate folded leaves, mixture 1 (●) and mixture 2 (—).

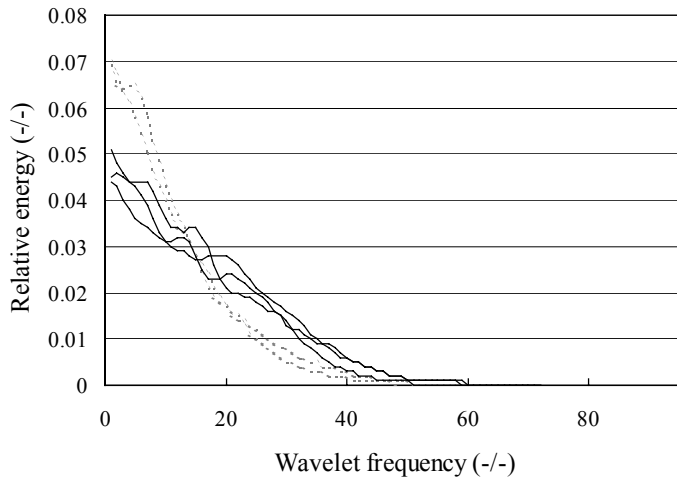


Figure 7.14 Relative wavelet energy as function of the frequency scale for three grass (—) and two clover swards (····).

of wavelet entropy of grass swards varies only slightly within a growth period, and it seems that wavelet entropy was specific for leaf shape within an image line. This is illustrated in Figure 7.16, where the wavelet entropy value for individual mini swards with various degrees of sward damage is depicted. The summed wavelet energy does show a clear evolution (not shown), similar to the evolution of IRI (Figure 7.2).

7.4 Discussion

The strong decrease in DM yield for white clover and the lower clover contents of the mixtures in the October growth period can be understood from the stronger temperature response of clover than of grass (Baker & Williams, 1987, p 133). Measurements of clover GC were also clearly disturbed by the circadian rhythm of leaf opening and closure (Baker & Williams, 1987, p 126). Our results showed that pixel spectra are highly variable, even within single intensity classes where effects of plant geometry are limited. Zwiggelaar (1998) discussed that this large variability is a common problem in spectral species recognition. Potentially, combinations of a number of wavelengths can reduce

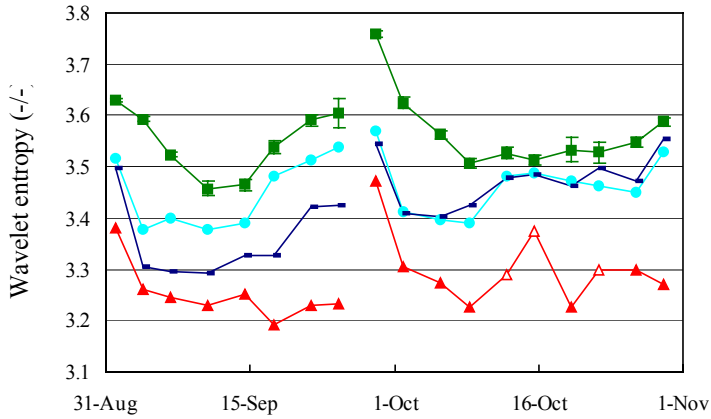


Figure 7.15 Evolution of wavelet entropy for grass swards (■), clover swards (▲), where (△) indicate folded leaves, mixture 1 (●) and mixture 2 (●).

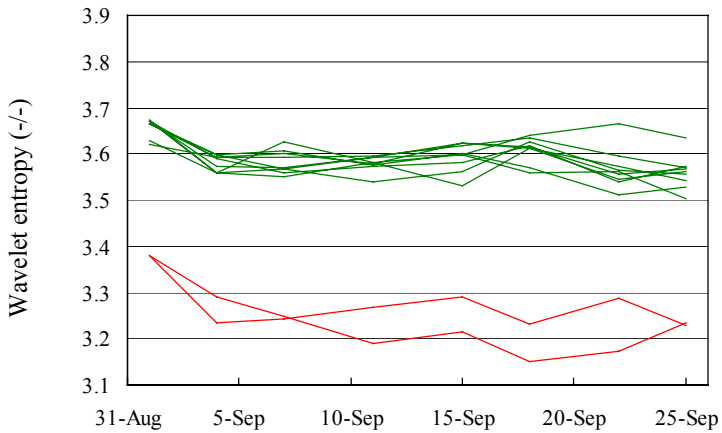


Figure 7.16 Evolution of wavelet entropy for individual grass swards with various degree of sward damage (—), and clover swards (—). For clarity only the September growth period is depicted.

this variability, but then results might not be robust in time or in space (Zwiggelaar, 1998). On a higher aggregation level (sward), differences in spectral characteristics existed between grass and clover, but differences varied within growth cycles and with nutrient supply. Schut & Ketelaars (Chapter 4) found that edge profiles were present within grass canopies, which might have been the combined effect of sensor characteristics, leaf angle and differences in biochemical properties within a canopy. Edge profiles of grass and clover were clearly different and changed remarkably when clover leaves were folded, indicating that these profiles are indeed affected by changes in canopy geometry. Differences in image line texture were quantified with a filter, spatial correlation as well as with wavelet analysis. Grass swards and white clover could be successfully discriminated by all these methods. Estimates of clover content within a mixture varied within a growing period, as clover leaves dominated (when projected horizontally) shortly after harvest and grass leaves dominate in the second half of the growth period.

Amongst the three methods studied, the wavelet entropy method was least sensitive for temporal changes in canopy geometry. Additionally, wavelet entropy was insensitive for the degree of sward damage. This indicates that wavelet entropy responds specifically to textural differences, rather than differences in density. Each method has pros and cons. The filter and spatial correlation can only be used in situations where leaf sizes are clearly different, within a limited growth period. Both methods are fast and simple but have to be used with caution. Ideally, measurement direction has to be adjusted according to (grass) leaf orientation, appropriate thresholds have to be selected, and the filter width has to be adjusted according to leaf size in the field.

Bradshaw & Spies (1992) showed that different canopy types had different patterns of wavelet variance. Therefore, it was expected that specific wavelet scales could be used to uniquely identify specific leaf types. The results show that in general there is a clear difference between grass and clover, but that no specific wavelet scale dominates. This means that the occurrence of other species in the sward may affect the wavelet entropy. Further studies may look into whether or how these results change when instead of continuous wavelet transform as used here, some form of discrete wavelet transform is used. It is expected that it will speed up calculations considerably, but one may lose some advantage of the redundancy in the continuous wavelet transform. Of course the approach is severely limited by the format of our basic data. If 2D images were available one could try and use a 2D wavelet transform, and exploit its sensitivity to direction (Van den Berg, 1999; Schut *et al.*, Chapter 2).

Mixed swards usually consist of either clover or grass dominated patches. The fraction of clover in these patches show typical temporal oscillations (Schulte, 2001), resulting from delayed N transfer (Loiseau *et al.*, 2001). Therefore, it is probably sufficient to separate clover dominated patches from grass dominated patches. The clover fraction in the field can then be calculated from the relative cover of clover dominated patches. Within the farm N balance, little knowledge is available on N input from clover N₂ fixation (Velthof *et al.*, 2000). The N yield per unit mass of clover DM is rather stable, for pure clover swards values of 39-43 kg N t⁻¹ clover DM are reported (Elgersma *et al.*, 2000). Values of 49-63 kg N t⁻¹ clover DM are reported for mixtures (Elgersma & Hassink, 1997; Elgersma *et al.*, 1997). Additionally, the N₂ fixation per unit of clover DM is rather stable, around 40-55 kg N t⁻¹ DM (Velthof *et al.*, 2000), even under varying N application (Van der Meer & Baan Hofman, 2000). These values are annual means, and may vary within the growing season, although ‘Seasonal patterns of nitrogen fixation by white clover follow fairly closely the clover growth curve’ (Baker & Williams, 1987, p.192). Heuwinkel *et al.* (2000) reported that ‘N₂-fixation could be calculated by multiplying the legume N-yield by a factor of 0.9’. Watson & Goss (1997) reported a linear relationship between extra DM production of mixed swards, compared to grass swards, and N₂ fixation. Clover DM can be determined with near-infrared reflectance spectroscopy (Heuwinkel *et al.*, 2000; Wachendorf *et al.*, 1999) and with clover GC (Schils *et al.*, 1999). For grass, good estimates of DM yield, N content (Schut *et al.*, Chapter 9), as well as N stress and N yield (Schut and Ketelaars, Chapter 4) can be made with imaging spectroscopy. From this, we hypothesise that with imaging spectroscopy grass N yield can be quantified within reasonable limits.

Results in this paper show that texture of 1D images provide enough information for separation of clover and grass swards. There were 42 image lines available per 0.63 m². Possibly, the number of image lines required for patch characterization can be reduced, depending on the method used. Spatial correlation and the filter method are more sensitive to leaf-orientation than wavelet entropy and, therefore, require more image lines for a robust estimate. Further study may reveal the minimum number of image lines per patch.

When using 2D images, spatial and spectral information can be combined, improving classification results (Zhou & Robson, 2001). This may improve robustness, as textural analysis then becomes less sensitive to leaf-orientation. For practical purposes (recording speed, data volume), 2D images permit only a limited number of spectral bands. Only three spectral bands are required for

discrimination between soil and green material (Schut *et al.*, Chapter 2). Estimates of N content in grass were based on a large number of spectral bands (Schut *et al.*, Chapter 9) Therefore, simplifying the sensor might limit its applicability to ground cover estimates. Combined use of a hyperspectral sensor and a 2D sensor with three spectral bands for GC estimates could improve robustness and amplify processing speed. Processing speed can be further amplified with combination of the filter and wavelet entropy. The filter can be used on all images for spatial distribution of clover cover and results can then be validated with wavelet entropy, calculated for only a limited number of 2D images or hyperspectral image lines.

7.5 Conclusion

With imaging spectroscopy, a clear distinction was made between image lines of grass and clover swards. Based on image line texture, pure grass and clover swards could be separated with a simple filter, with correlation between single band reflection values of pixels at a small distance, and with wavelet entropy. Discrimination between grass and clover swards with wavelet entropy was robust throughout growth periods. Wavelet entropy was insensitive for various degrees of sward damage. In all textural methods, results of mixed swards of grass and clover were intermediate between grass and clover swards.

The mean spectral curves of grass and clover swards differed throughout the spectral range of 405 up to 1650 nm, but differences were smaller than one standard deviation. In general, absorption features of grass and clover are similar and, therefore, no specific discriminating feature was found. At higher aggregation level (a sward) differences in blue, green and red edge positions were present. These differences were not consistent throughout re-growth periods and varied with N supply. Therefore, spectral discrimination will not result in a simple and robust discrimination method.

Imaging spectroscopy provides new tools for quantification of clover cover. Based on literature, we conclude that accurate estimates of clover cover can be translated to estimates of clover N yield and N₂ fixation. For field applications, a two-sensor system is proposed, combining 2D images with three spectral bands and a hyperspectral sensor. For analysis, joint use of the filter and wavelet entropy combines high processing speed and high information content, and ensures accurate measurements.

8

Assessment of seasonal dry matter yield and grass sward quality with imaging spectroscopy

A.G.T. Schut & J.J.H.M. Ketelaars

Provisionally accepted at Grass and Forage Science

8. Abstract

This paper describes the potential of imaging spectroscopy for assessment of seasonal dry matter yield (SDM) and sward quality. For this, relations between spatial heterogeneity of tiller density, light interception (LI), ground cover (GC) and SDM were studied. Sward heterogeneity was quantified with spatial GC standard deviation (GC-SSD) and logarithmically transformed GC (TGC-SSD), and patterns in GC transects were quantified with wavelet entropy. An experiment was conducted with 8 control swards (CS), 8 naturally damaged swards (NDS) and 12 artificially damaged swards (ADS). Swards were established in containers and spectroscopic images were recorded twice a week in a regular pattern. SDM was linearly related to a combination of means of GC and index of reflection intensity ($R^2 = 0.93$). Spatial variation of tiller density was larger for ADS and NDS than for CS. Values of GC-SSD and wavelet entropy were larger for ADS and NDS than for CS. GC-SSD of CS remained below 13% throughout the season, in contrast to values of NDS and ADS. Absolute differences in TGC-SSD between CS, ADS and NDS were largest within 8 days after harvest. Seasonal means of wavelet entropy ($R^2 = 0.70$) and GC-SSD ($R^2 = 0.63$) at harvest were linearly related to SDM. It is concluded that imaging spectroscopy can provide accurate means for assessment of SDM and sward heterogeneity. Effects of sward management and botanical composition on heterogeneity require further study, before conclusions can be drawn with regard to the implications of sward heterogeneity for sward reseeded or renovation.

8.1 Introduction

8.1.1 *Sward quality and problem definition*

Grassland is with 880 884 ha of permanent grassland and 112 090 ha of grassland in rotation (CBS, 2001) the crop with the largest cultivated area in the Netherlands. Annually about 62 500 ha grassland is reseeded and 12 500 ha grassland is renovated. Reseeding is more frequent on sandy soils, in order to improve sward quality (Keuning & Vellinga, 1986; Anonymous, 2001; Aarts *et al.*, 2002). Sward quality is defined as the production capacity of a sward as determined by botanical composition and sward density (Lantinga, 1986). This study focuses on the spatial aspects of sward density, *i.e.* the number and distribution of productive plants and tillers. Production capacity was measured

by seasonal dry matter yield (SDM). Grassland renovation is expensive, and can only be economically justified when swards are heavily deteriorated (Elsässer, 1991; Keuning & Vellinga, 1986; MacCarthy, 1982; Smith & Allcock, 1985; Spatz *et al.*, 1981). Therefore, sward renovation should be evaluated on its economical merits, and assessments of potential yield improvements are required before reseeding or renovation.

8.1.2 Determination of sward quality

Sward quality deteriorates in case of local tiller or plant death as a result of *e.g.* frost or drought damage, urine scorch, treading, poaching or heavy cuts (*e.g.* Deenen, 1990; Keuning & Vellinga, 1986). Local tiller or plant death creates gaps, which may be filled with weeds (Keuning & Vellinga, 1986; Marriott *et al.*, 1997). All this leads to heterogeneous swards, in terms of dry matter yield (DM) and feeding quality. This deterioration can be monitored and quantified either visually or by the absence frequency method, in which the absence frequency of tillers in rings of different sizes is recorded (Neuteboom *et al.*, 1992). Dry matter yield is strongly related to absence frequency, but genotype and sward management, such as harvest frequency and grazing, affect this relation (Van Loo, 1992). Absence frequencies provide valuable information on sward structure, but this method is laborious and difficult to automate. Aarts *et al.* (2002) concluded that there were no good judgement criteria for economically justified grassland renovation or reseeding.

8.1.3 Alternatives with images

Sward quality is related to the ability of a sward to convert solar radiation into dry matter with a high feeding value. Swards with gaps or a low tiller density are limited in their ability to intercept light. Swards with poor botanical composition are limited in the conversion from intercepted light energy to DM. Invasion of weed species and local tiller death increase spatial variability, in terms of light interception (LI) and DM yield. Therefore, we hypothesize that this spatial sward heterogeneity can be used as measure of LI capacity and, therefore, sward quality. Imaging spectroscopy provides accurate means to monitor growth, estimate DM yield, leaf area index (LAI) and LI. Light interception is strongly related to ground cover (GC), although sward density and weather conditions (clear or cloudy sky) affect this relation (Schut & Ketelaars, Chapter 3). Therefore, spatial sward heterogeneity may be directly related to spatial GC variability.

8.1.4 Objectives

The first objective is to assess SDM of mini swards with imaging spectroscopy. The second objective is to explore the relation between spatial variability and sward quality and to quantify sward quality with imaging spectroscopy techniques. Spatial variability was studied in terms of variation of tiller density, variation of LI, variation of GC and spatial GC patterns. Spatial GC patterns were studied with wavelet entropy. SDM was used as a quantitative measure of sward quality. To this end images of damaged grass swards, due to drought damage or artificially created gaps, were recorded throughout the growing season of 2000.

8.2 Materials and Methods

8.2.1 Experiment

In 2000, 28 mini swards were measured with a wide range of production capacities. These mini swards were available from experiments in which effects of drought on sward damage and production recovery was investigated. Natural and artificial sward damage was created in 1999.

Mini swards

Mini swards were established from seed in April 1999 using a mixture of 4 *Lolium perenne* L. cultivars. Mini swards were grown in containers of 0.9 m long, 0.7 m wide and 0.4 m high, filled with a sandy soil with 3% organic matter. Throughout the growing season, containers were kept under a rain shelter, covered with foil (1999: 70% transparent, new foil in 2000: 80% transparent) and wind breaking fences at the sides. Water was supplied through perforated drains at 10 cm depth. Soil moisture content was monitored by weighing containers twice a week. During winter, containers were placed outside the greenhouse.

Mini swards 1999

In 1999, mini swards from a drought experiment were available (Grashoff *et al.*, 2001). In April, mini swards received 8.1 g m⁻² N, 13.8 g m⁻² P₂O₅ and

24 g m⁻² K₂O. At harvesting, mini swards were hand cut to a stubble height of 4 cm. After every harvest 9.4 g m⁻² N (dissolved in water) was supplied. After 15 September this dose was reduced to 5.1 g m⁻² N. Drought stress was created during two periods (T1 and T2) and differed in length (control, 10, 20, 30 and 40 days without extra water). The T1 drought period created sward damage with severe tiller death for the 40 days treatment, whereas the T2 period did not create any sward damage (Grashoff *et al.*, 2001). From this drought experiment, only the control and the 40 days drought mini swards were used, see Table 8.1. For 12 of the T2 mini swards, artificial sward damage was created. Before this, any sward damage already present due to sampling for tiller analysis in the drought experiment was repaired. Then, an area of approximately 25%, 50% and 70% of the sward was removed with small rings of 12.5 cm or with large rings of 22.5 cm in diameter. The locations of gaps in the sward were selected by picking cross-points at random on a grid, restricted to non-overlapping gaps.

Mini swards 2000

On 17 March 2000, above ground fertiliser was supplied with 8.1 g m⁻² N, 6.6 g m⁻² P₂O₅ and 12 g m⁻² K₂O. On the 11th of July 3 g m⁻² P₂O₅, 20 g m⁻² K₂O and 6 g m⁻² S was supplied. On 30 August an additional 6.3 g m⁻² K₂O was supplied. The mini swards were hand cut to a stubble height of 4 cm. After every harvest 9.4 g m⁻² N (dissolved in water) was supplied. After 15 September this dose was reduced to 5.1 g m⁻² N. In 2000, another drought experiment was conducted. From the 1999 experiment, mini swards without sward damage were selected and assigned at random to 5 drought treatments. These treatments were control, and 10, 20, 30 and 40 days without water in the period from 1 June to 10 July. The 20 days without water treatment did not create any sward damage, and SDM was not significantly different from control ($p < 0.05$). From this experiment, the control and 20 days without water were used, see Table 8.1. There were three sward quality groups: dense swards from control treatments (CS), artificially damaged swards (ADS, swards with created gaps), and naturally damaged swards (NDS, drought-damaged swards) (Table 8.1). Not just the mini swards of control, but also the swards that were without extra water during 20 days in 2000 were considered as control swards since the 2000 drought period did not affect sward quality. All treatments had identical harvest regimes.

Table 8.1 Treatments and number of replicates for control swards (CS), naturally damaged swards (NDS) and artificially damaged swards (ADS).

Treatment	Replicates (#)	Sward quality group
20 days drought from June 21 – 10 July 2000	4	CS
Control	4	CS
Drought damaged swards	8	NDS
25% of sward removed, small gaps created	2	ADS
47% of sward removed, small gaps created	2	ADS
68% of sward removed, small gaps created	2	ADS
25% of sward removed, large gaps created	2	ADS
55% of sward removed, large gaps created	2	ADS
75% of sward removed, large gaps created	2	ADS

8.2.2 *Measurements*

At harvest, fresh matter yield was determined and samples were taken for analysis of DM and N content. Swards were harvested on 25 April, 12 May, 30 May, 20 June, 11 July, 8 August, 29 August, 27 September, and 31 October 2000. For two ADS swards, samples of one harvest were lost. These swards were excluded in the regression of SDM data. For the Figures 8.2 and 8.3, missing values were replaced by the mean value of ADS.

Tillers

Tillers were counted just after harvest on 20 September or 1 October 1999, and between 26 and 28 April 2000. Counts were made in 10 cm long and 15 cm wide grid cells. These grid cells were positioned within two (2000) or three (1999) 15 cm wide and 70 cm long bands with 7 grid cells each. For each mini sward the mean and tiller standard deviation over grid cells were calculated. The tiller coefficient of variation (CV) was calculated as the (spatial) standard deviation divided by the mean.

Light interception

Light interception was measured by hand with a DECAGON LI-meter twice a week. This LI-meter has 80 light sensitive cells of 1 cm² on a 1 m long and 1 cm high stick. The LI-stick is longer than the container width. For below canopy measurements, the LI-stick was placed on the container sides. Per mini swards 7-14 alternating measurements above and below canopy were made. Afterwards, LI was calculated per cell by 100% * below / above canopy readings. Results were averaged per 15 cm, matching bands of spectroscopic image recording, excluding positions outside scanned areas. This resulted in 21-42 LI estimates per mini sward. From these LI measurements, means, standard deviations and CVs were calculated.

Images and image analysis

Twice a week, image lines were recorded with the experimental imaging spectroscopy system (Schut *et al.*, Chapter 2). The image lines were 15.3 cm long and 1.39 mm wide, and were recorded in a regular pattern with 3 bands next to one another per mini sward. In each band 14 image lines were recorded, each 5 cm apart, resulting in 42 image lines per mini sward (see Figure 8.1). The system combines high spatial (0.28-1.45 mm² per pixel) and high spectral resolution (5-13 nm). Three imaging spectrographs (V7, N10 and N17) were used, measuring reflectance in the spectral range from 400 up to 1650 nm. The image lines were classified with maximum likelihood procedures (Schut & Ketelaars, Chapter 3). The spectral library contained classes for soil, grass, leaves with specular reflection, dead material and an intermediate class between soil and dead material. Reflection intensity is a function of leaf angle and position of the reflecting surface in the canopy (Schut *et al.*, Chapter 2). Therefore, the grass and specular classes in the spectral library were further subdivided into reflection intensity classes (IC), ranging from 0 up to and including 6 for grass and from 0 up to and including 2 for leaves with specular reflection. Image line ground cover was calculated per intensity class. Total image line ground cover (GC_{IL}) was calculated as the sum of grass (GCG) and specular classes (GCS):

$$GC_{IL} = \sum_{ic=0}^6 GCG_{ic} + \sum_{ic=0}^2 GCS_{ic} \quad (1)$$

where ic is the index number of the intensity class.

Sward GC was calculated as mean over the 42 GC_{IL} estimates. The index of reflection intensity (IRI) is then calculated as:

$$IRI = 100 \times \frac{\sum_{ic=3}^6 \frac{1}{42} \sum_{IL=1}^{42} GCG_{IL,ic}}{GC} \quad (2)$$

This IRI measures the presence of highly reflecting green pixels as a percentage of ground cover. A higher value represents a higher canopy with more horizontally oriented leaves (Schut *et al.*, Chapter 2). Relations between DM yield and GC in the first harvest of 2000 strongly deviated from other cuts (Schut & Ketelaars, Chapter 3). This was due to camera saturation of the V7 sensor in high swards, *e.g.* swards with generative tillers. Therefore, only image recordings after 26 April were included in the analysis.

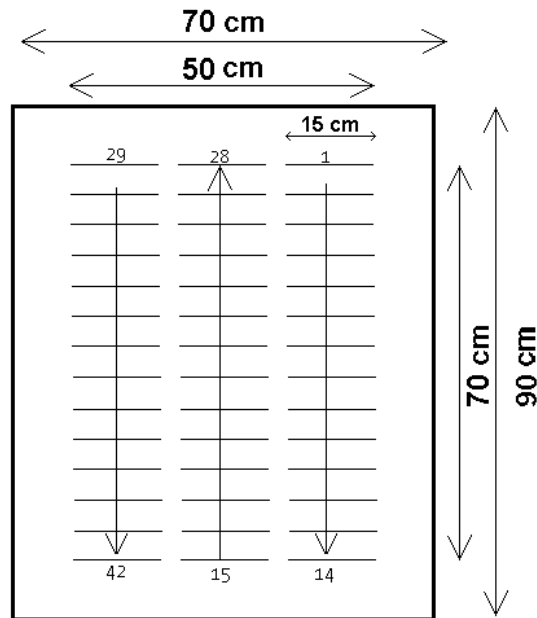


Figure 8.1 Position of 42 image lines in container mini sward.

8.2.3 Sward heterogeneity

Sward heterogeneity can be considered as the variation within a sward in terms of the spatial distribution of plants, tillers and leaves. Heterogeneity may also be present in image GC. Image GC is strongly related with LI, LAI and DM yield (Schut & Ketelaars, Chapter 3). Heterogeneity can then be defined as the spatial variation of measured GC values. This GC variation may also have a spatial context, GC_{IL} of neighbouring image lines are probably more alike than GC_{IL} of image lines on a greater distance. The GC_{IL} estimates can also be considered as transect signal itself. In a homogeneous sward, deviations in GC_{IL} estimates are randomly distributed, whereas in heterogeneous sward deviations are clustered. These clusters may be of varying sizes. These aspects of heterogeneity were studied in terms of spatial GC variation, and wavelet entropy. Wavelets decompose a signal into signals of different frequencies. The wavelet entropy is a measure of the number of spatial frequencies needed to describe the signal.

Spatial GC variation

The spatial GC standard deviation (GC-SSD) was used as measure for the spatial variation, and was calculated as standard deviation of the 42 image line GC estimates. It is likely that GC variation decreases towards GC values of 0 or 100%. Therefore, image line GC values are transformed (TGC) with a logistic function:

$$TGC_{IL} = \ln\left(\frac{GC_{IL}}{101 - GC_{IL}}\right) \quad (3)$$

The value of 101 is chosen in order to maximize relative differences near 100 and 0% GC and to avoid divisions by zero. A high GC value will result in positive TGC values, and a low value will result in negative TGC values. Again spatial TGC standard deviation (TGC-SSD) was calculated over the 42 TGC_{IL} estimates.

Wavelet transformation

Schut & Van den Berg (Chapter 7) found that wavelet entropy is a useful measure for discrimination of grass and clover image lines, based on

differences in spatial patterns of reflectance within an image line. The wavelet analysis used here is very similar, although other signals are studied and parameter settings were slightly changed. Let us consider a sward with N GC estimates on a transect. This response (of any type) may be oscillating on a large or small scale, with high or low amplitudes. The wavelet is a smooth and quickly vanishing oscillating function with good localization in both frequency and location (*e.g.* in time or space). A wavelet family $\psi_{a,b}$ is the set of elementary functions generated by dilations and translations of a unique mother wavelet $\psi(x)$:

$$\psi_{a,b}(x) = |a|^{-1/2} \psi\left(\frac{x-b}{a}\right) \quad (4)$$

where $a, b \in R$, ($a \neq 0$) are the scale parameter and the translation parameter respectively, and x the (image line) position within the transect. As a decreases, the wavelet becomes narrower, and as b changes the center of the wavelet $\psi_{a,b}$ shifts along the x -axis. The continuous wavelet transform (CWT) of GC is defined as the inner product of the function $GC(x)$ with the wavelet $\psi_{a,b}(x)$ for each a and b :

$$W_{\psi} GC(a,b) = |a|^{-1/2} \int_{-\infty}^{\infty} GC(x) \psi^*\left(\frac{x-b}{a}\right) dx = \langle GC, \psi_{a,b} \rangle \quad (5)$$

The Wavelab802 CWT command (Buckheit *et al.*, 1995) was used with the Morlet function as mother wavelet:

$$\psi(v) = \frac{1}{\sqrt[4]{\pi}} e^{-v^2/2} (e^{-i\xi_0 v} - e^{-\xi_0^2/2}) \quad (6)$$

where ξ_0 indicates the modulation frequency, usually taken to be 5.33 (Daubechies, 1992, p76). Here, the modulation frequency was arbitrarily set to 2.5, to limit the amplitude and number of oscillations of the mother wavelet. The CWT transformation yields a signal in the wavelet domain in 48 frequency scales (12 voices per octave with 4 octaves), for each transect x -position. The question is whether the distribution of transformation values over frequency scales is different with varying sward quality. To identify the important scales, the relative wavelet energy might be a good measure. Rosso *et al.* (2001) calculated the *relative wavelet energy* p_a in scale a for each scale as:

$$p_a = \frac{E_a}{E_{tot}}, \tag{7}$$

where E_a is the energy per scale,

$$E_a = \sum_b |W_\psi y(a, b)|^2, \tag{8}$$

and E_{tot} the total energy in the image line,

$$E_{tot} = \sum_a E_a. \tag{9}$$

The parameters a and b in these summations range over all scales and translations occurring in the Wavelab802 CWT algorithm as applied in the signal $y(x)$. The distribution of energy over the scales can be characterized by the total wavelet entropy (Rosso *et al.*, 2001), defined as the Shannon entropy of the relative energy distribution p_a :

$$S_{CWT} = -\sum_a p_a \ln(p_a). \tag{10}$$

Lower values of this wavelet entropy (S) represent higher degrees of order, which means that energy is concentrated in a smaller number of scales. The wavelet entropy is calculated in three different ways per mini sward. First, wavelet entropy was calculated for the transect of 42 GC estimates in the order indicated in Figure 8.1. The second transect consisted of 42 TGC estimates. The concatenation of the three bands in Figure 8.1 introduced a discontinuity in the transect signal. Thirdly, therefore, wavelet entropy was calculated per band, with 14 GC estimates per transect. The mini sward wavelet entropy was then calculated as mean of these estimates per band.

8.3 Results

8.3.1 DM yield, tiller counts and LI measurements

The CS had a higher SDM yield and a lower N concentration than ADS and NDS, see Table 8.2. For the 28 mini swards, there was a linear decrease

Table 8.2 Means and standard deviations of dry matter yield (kg ha^{-1}), seasonal dry matter yield (SDM) and seasonal mean N concentration for control swards (CS), artificially damaged swards (ADS) and naturally damaged swards (NDS). Different uppercase letters within a row indicate significant differences between means ($p < 0.05$).

	CS	ADS	NDS
25 April	3222 \pm 266	2940 \pm 355	3335 \pm 453
12 May	1914 \pm 150	1452 \pm 227	1631 \pm 244
30 May	832 \pm 154	566 \pm 197	635 \pm 148
20 June	1523 \pm 242	1147 \pm 376	1322 \pm 228
11 July	958 \pm 278	820 \pm 177	992 \pm 156
8 August	2691 \pm 445	1811 \pm 655	2314 \pm 374
29 August	2368 \pm 338	1620 \pm 247	1791 \pm 234
27 September	2403 \pm 193	1947 \pm 278	1979 \pm 222
31 October	1166 \pm 144	845 \pm 316	920 \pm 161
SDM ($\text{t ha}^{-1} \text{ yr}^{-1}$)	17.08 \pm 1.36 ^a	13.67 \pm 1.67 ^b	14.92 \pm 1.39 ^b
*N (%)	3.66 \pm 0.11 ^a	3.93 \pm 0.10 ^b	3.93 \pm 0.14 ^b

* Regression on individual mini swards: $N (\%) = 4.9 - 0.069 * \text{SDM}$, $R^2 = 0.60$, SE observations = 0.11.

Table 8.3 Means and standard errors of tiller density (T) in October 1999 and April 2000 and light interception at harvest (LI) for dense control swards (CS), artificially damaged swards (ADS) and naturally damaged swards (NDS).

	T-1999 (#/m ²)	T-2000 (#/m ²)	LI (%)
CS	5330 \pm 250	6250 \pm 360	84 \pm 1.0
ADS	2610 \pm 270	3860 \pm 240	67 \pm 2.2
NDS	3600 \pm 340	3660 \pm 390	74 \pm 1.8

Table 8.4 Means and standard errors of coefficient of variations of tiller density (T) in October 1999 and April 2000 and light interception just before harvest (LI) for control swards (CS), artificially damaged swards (ADS) and naturally damaged swards (NDS).

	T-1999 CV*	T-2000 CV*	LI CV*
CS	0.23 ± 0.02	0.19 ± 0.02	0.05 ± 0.003
ADS	0.66 ± 0.05	0.52 ± 0.03	0.12 ± 0.019
NDS	0.83 ± 0.08	0.74 ± 0.08	0.13 ± 0.013

* CV calculated as spatial standard deviation divided by mean per mini sward

($R^2 = 0.60$) in N content with higher SDM yield. This higher N content in ADS and NDS can originate from higher N availability per plant. Treatment differences in DM yields were relatively small in the first cut, in which NDS had highest yields. In all other cuts, except 11 July, CS had highest yields (Table 8.2). The CS had higher tiller densities and LI just before harvest than the ADS and NDS (Table 8.3). In spring 2000, tiller density was higher when compared to the fall of 1999. In spring, tiller density of CS ranged from 4893 – 8127 tillers m^{-2} . The increase in tiller density was lower for NDS than for CS and ADS. Spatial coefficient of variation of tiller density and LI was higher for ADS and NDS than for CS (Table 8.4). The coefficient of variation of tiller density in 1999 was higher than in 2000 with reductions of 17% (CS), 21% (ADS) and 11% (NDS).

8.3.2 *Relation between SDM yield and mean GC and IRI*

Control swards had a higher seasonal mean GC than ADS and NDS (Figure 8.2). The seasonal mean GC values ranged from 36% to 56%. These GC values are linearly related to visually scored GC (GC_v) estimates, where GC_v equals $8.63 + 1.076 \times GC$ (Schut & Ketelaars, Chapter 3), leading to GC_v ranges of 47% to 69%. A decrease of GC by 1% decreased SDM by $0.31 t ha^{-1}$ (Table 8.5). This slope changes to 0.35 when the intercept was not set to zero. The ranges in Figure 8.2 reveal that the relative decrease was stronger for SDM than for GC.

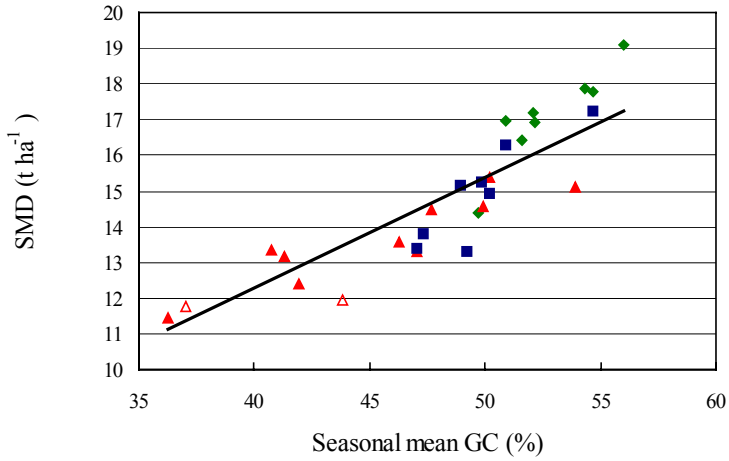


Figure 8.2. Seasonal mean GC versus Seasonal DM (SDM) yield in 2000 for control swards (◆), artificially damaged swards (▲), artificially damaged swards with missing observation (△) and naturally damaged swards (■). See Table 8.5 for equation of fitted line.

Table 8.5 Linear regression of ground cover (GC) and index of reflection intensity (IRI) with seasonal dry matter yield (SDM, t ha⁻¹ yr⁻¹).

Model	a	b	c	R ²	SE observations
SDM = a + b GC ₂	0	0.31		0.77	0.97
SDM = a + b IRI ₂	10.7	1.02		0.77	0.97
SDM = a + b GC ₂ + c IRI ₂	2.8	0.2	0.58	0.89	0.69
SDM = a + b GC ₁	-4.32	0.29		0.87	0.74
SDM = a + b IRI ₁	10.8	0.51		0.82	0.86
SDM = a + b GC ₁ + c IRI ₁	1.17	0.17	0.24	0.93	0.56

¹ Calculated as mean over observations just before harvest

² Calculated as mean over all observations

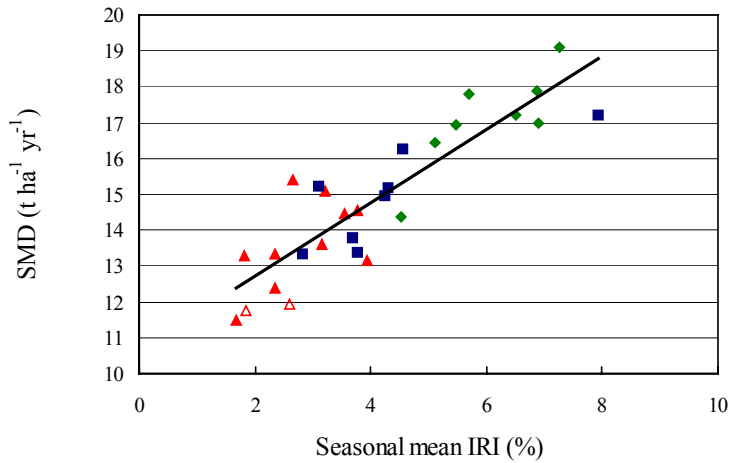


Figure 8.3 Seasonal mean index of reflection intensity (IRI) versus seasonal dry matter yield (SDM) yield for control swards (♦), artificially damaged swards (▲), artificially damaged swards with missing observation (△) and naturally damaged swards (■). See Table 8.5 for equation of fitted line.

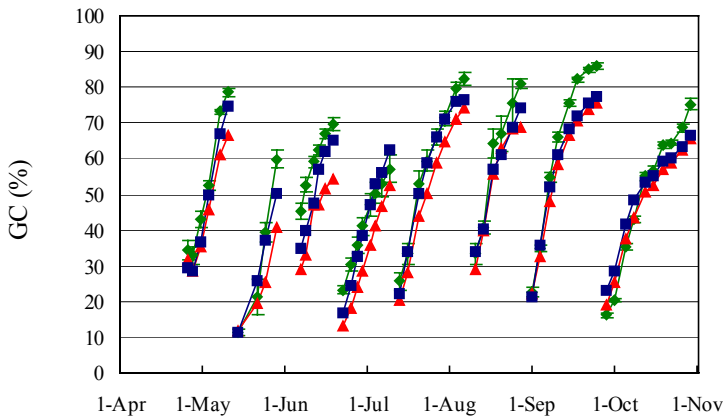


Figure 8.4 Evolution of ground cover (GC) for control swards (♦), artificially damaged swards (▲) and naturally damaged swards (■). Error bars indicate standard error of the mean for control swards.

High yielding swards had a higher mean IRI (Figure 8.3). Relative differences in IRI were larger than in GC (compare Figures 8.2 and 8.3). The combination of GC and IRI ($R^2=0.89$) explained more SDM variation than GC ($R^2=0.77$) or IRI alone ($R^2=0.70$) (Table 8.5). Even more SDM variation was explained with means of GC and IRI measurements just before harvest ($R^2=0.93$, Table 8.5).

The GC of ADS and NDS was lower than CS throughout the season, with exception of the June-July growth period where NDS had a higher GC than CS (Figure 8.4). In this growth period, the DM yields of CS were also lower than NDS. The highest positive correlations between GC and SDM were found in the summer period, whereas in the first and last growth period of 2000 correlations were weak or even negative (Figure 8.5). In general, the correlation between GC and SDM was weaker just after than just before harvest.

8.3.3 *Heterogeneity in relation to sward quality*

Spatial GC patterns were consistently present in ADS and NDS. This is illustrated in Figure 8.6, where means were calculated over all measurements from days just before harvest for three individual mini swards. There were only small variations in GC for the dense sward, but the ADS and NDS clearly had locations within the sward with a lower GC throughout the year. Although GC level between NDS image lines 12 and 33 were on a similar GC level as CS, there were two peaks present at image lines 19 and 25. These peaks could be identified as two distinct plants. The dips in the ADS image line were locations where round gaps with a 22.5 cm diameter were created.

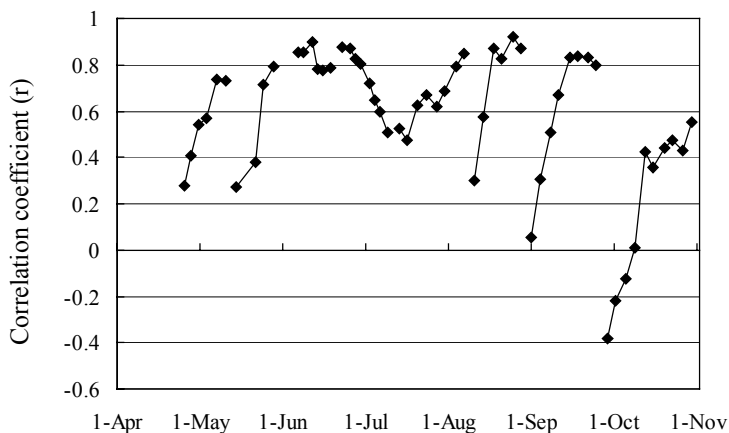


Figure 8.5 Pearson correlation coefficient between ground cover and seasonal dry matter yield.

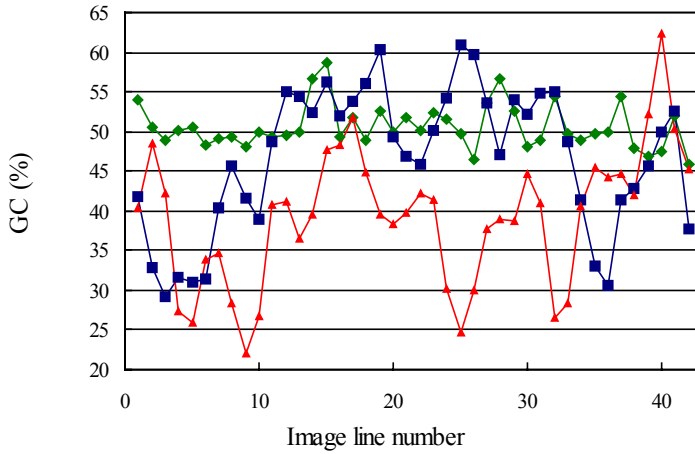


Figure 8.6. Transects of mean ground cover (GC) at harvest for a dense sward (◆), an artificially damaged sward (▲), and a naturally damaged sward (■)

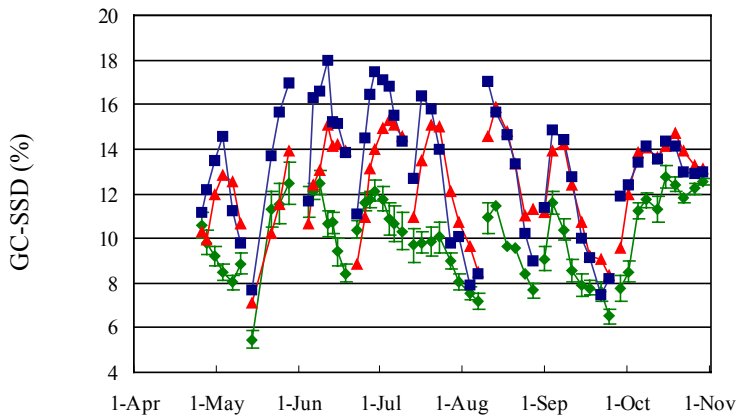


Figure 8.7 Evolution of spatial ground cover standard deviation (GC-SSD) for control swards (◆), artificially damaged swards (▲), and naturally damaged swards (■). Error bars indicate standard error of the mean for control swards.

Spatial GC and TGC variation

Spatial GC variability throughout the season was smaller for CS than for ADS and NDS (Figure 8.7). Variability automatically decreases as GC estimates approach 100%. This effect is evident in Figure 8.7, where GC-SSD decreased stronger towards 7 and 29 August and 27 September when DM yields (Table 8.2) and GC estimates were high. The maximum GC-SSD was reached when mean GC ranged between 40 and 60% (compare Figure 8.4 and 8.7). The relation between GC and GC-SSD is illustrated in Figure 8.8. Mini swards within ADS and NDS strongly varied in GC-SSD value. On nearly all dates, GC-SSD of ADS and NDS was higher than for CS (Figure 8.7). GC-SSD of CS remained below 13% throughout the season, where ADS and NDS exceeded this threshold almost every growth period. The logistic transformation of GC strongly affected TGC-SSD values just after harvest (compare Figure 8.7 and Figure 8.9). The transformation did not enlarge sward quality differences just before harvest. The changes within a growth period in GC-SSD and TGC-SSD were larger for NDS and ADS than CS (Figure 8.7 and 8.9). Seasonal means of GC-SSD and TGC-SSD showed that NDS had larger heterogeneity than ADS just after harvest, whereas ADS had higher or equal heterogeneity than NDS just before harvest (Table 8.6). TGC-SSD of CS was fairly constant at the different intervals, whereas TGC-SSD of ADS and NDS decreased strongly within the growing period. Absolute differences in TGC-SSD between damaged swards and CS were largest 5-8 days after harvest. Correlation between SDM and GC-SSD was weak just after harvest (Figure 8.10). The correlation became stronger up to GC values of 50-60% (Figure 8.4), reaching strong negative values in the second half of the growth period. This can be understood when considering the differences in evolution of GC-SSD for the sward quality groups. The SDM of CS was highest and ADS lowest (Table 8.2), whereas CS had lowest and NDS highest GC-SSD values just after harvest (Table 8.6). The correlation between SDM and TGC-SSD (Figure 8.11) just after harvest was more negative when compared to GC-SSD (Figure 8.10). The correlation became weaker when GC values approached 80% (compare Figure 8.4 with Figure 8.10).

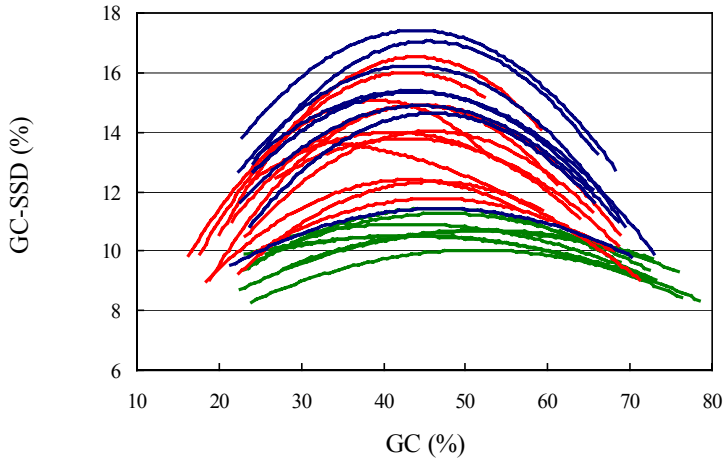


Figure 8.8 Ground cover spatial standard deviation (GC-SSD) as function of GC value for control swards (—), artificially damaged swards (—) and naturally damaged swards (—). Lines correspond to measurements of individual mini swards throughout the season.

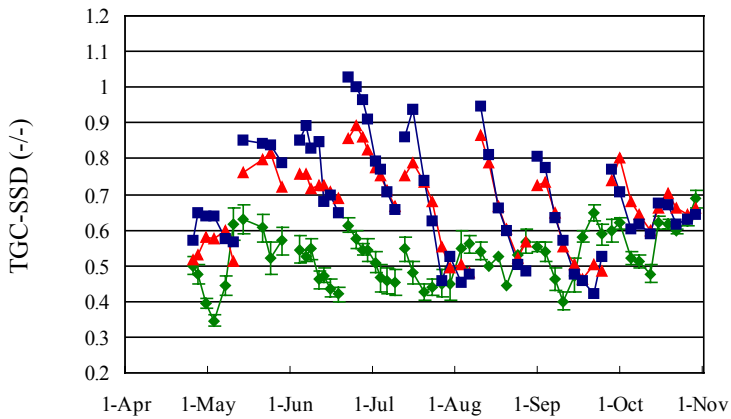


Figure 8.9 Evolution of spatial standard deviation of logistically transformed ground cover (TGC-SSD) for control swards (◆), artificially damaged swards (▲), and naturally damaged swards (■). Error bars indicate standard error of the mean for control swards.

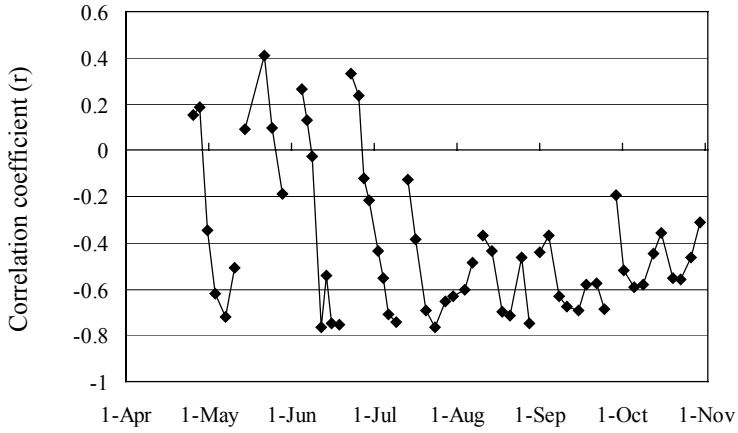


Figure 8.10 Pearson correlation coefficient between ground cover spatial standard deviation and seasonal dry matter yield.

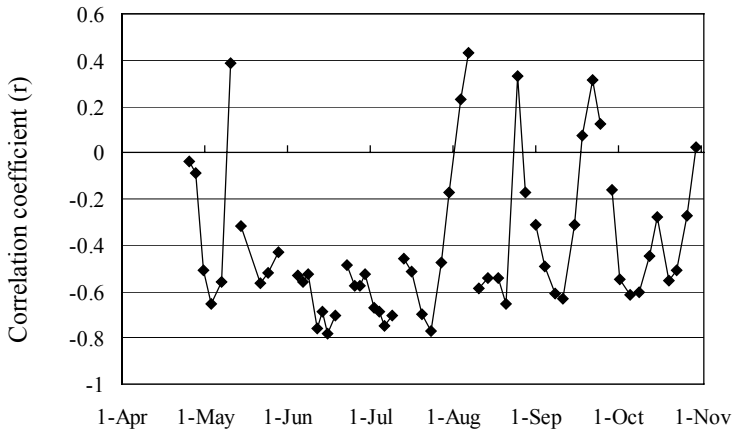


Figure 8.11 Pearson correlation coefficient between logistically transformed ground cover spatial standard deviation and seasonal dry matter yield.

Wavelet entropy

On most measurement dates, the wavelet entropy value, calculated over 42 GC estimates per mini sward, of NDS and ADS was higher than for CS (Figure 8.12). This means that, indeed, there were fewer frequencies (or scales) needed to describe the GC transect for CS than for ADS and NDS. Wavelet entropy values were slightly higher in summer than in spring or fall, and the greatest differences between treatments were found in the summer. Within a growth period, the wavelet entropy value strongly decreased. Wavelet entropy does not respond to the amplitude of the signal, but responds to relative amplitude changes. Towards the end of a growth period, absolute variability decreased and GC increased. This results in smaller relative amplitude changes, and decreased wavelet entropy values. The TGC wavelet entropy ($R^2 = 0.60$) were slightly weaker related to SDM than GC wavelet entropy ($R^2 = 0.70$, Table 8.7). The wavelet entropy calculated per band did not improve predictions ($R^2 = 0.59$). Therefore, wavelet entropy values were not strongly affected by concatenation of GC estimates recorded in three bands.

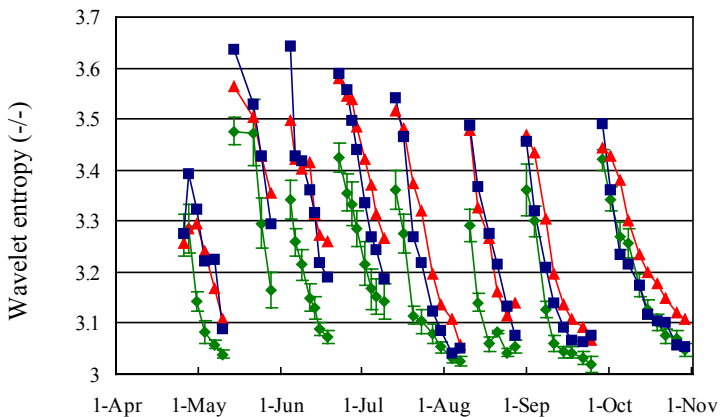


Figure 8.12 Evolution of wavelet entropy of 42 GC estimates for control swards (♦), artificially damaged swards (▲), and naturally damaged swards (■). Error bars indicate standard error of the mean for control swards.

Table 8.6 Seasonal means and standard error of ground cover (GC), GC spatial standard deviation (GC-SSD) and logistically transformed values of GC (TGC-SSD) for intervals of days after harvest (DAC). Different uppercase letters within a row indicate significant differences between means ($p < 0.05$).

Interval	CS	ADS	NDS
-----GC-----			
1-4 DAC	24.90 ± 0.82 ^a	22.03 ± 1.23 ^a	23.20 ± 0.36 ^a
5-8 DAC	34.87 ± 0.81 ^a	28.03 ± 1.59 ^b	32.89 ± 0.92 ^{ab}
9-13 DAC	51.38 ± 1.25 ^a	41.47 ± 2.30 ^b	48.51 ± 1.26 ^a
14-21 DAC	66.25 ± 1.01 ^a	56.18 ± 1.98 ^b	62.75 ± 1.00 ^a
At harvest	73.75 ± 1.06 ^a	62.30 ± 1.83 ^b	68.29 ± 0.93 ^c
-----GC-SSD-----			
1-4 DAC	9.22 ± 0.23 ^a	10.30 ± 0.42 ^{ab}	11.93 ± 0.45 ^b
5-8 DAC	10.77 ± 0.16 ^a	12.56 ± 0.42 ^b	14.65 ± 0.71 ^b
9-13 DAC	10.50 ± 0.18 ^a	13.44 ± 0.39 ^b	15.00 ± 0.59 ^b
14-21 DAC	9.78 ± 0.15 ^a	12.67 ± 0.39 ^b	12.64 ± 0.53 ^b
At harvest	9.25 ± 0.21 ^a	11.79 ± 0.52 ^b	11.70 ± 0.45 ^b
-----TGC-SSD-----			
1-4 DAC	0.56 ± 0.01 ^a	0.72 ± 0.02 ^b	0.82 ± 0.03 ^b
5-8 DAC	0.53 ± 0.01 ^a	0.77 ± 0.03 ^b	0.85 ± 0.05 ^b
9-13 DAC	0.48 ± 0.01 ^a	0.70 ± 0.04 ^b	0.72 ± 0.04 ^b
14-21 DAC	0.51 ± 0.01 ^a	0.61 ± 0.03 ^b	0.60 ± 0.02 ^b
At harvest	0.56 ± 0.01 ^a	0.60 ± 0.03 ^a	0.60 ± 0.02 ^a

Linear regressions relating heterogeneity parameters to SDM and tiller CV

The within mini sward LI standard deviation was linearly related to SDM ($R^2 = 0.5$, Table 8.7). The GC coefficient of variation ($R^2 = 0.71$) and TGC wavelet entropy ($R^2 = 0.70$) explained more SDM variation than the spatial GC standard deviation did ($R^2 = 0.63$). The tiller coefficient of variation (TCV) was linearly related ($R^2 = 0.69$) to spatial GC standard deviation, calculated as mean over all measurements within the growing season. At harvest, this spatial variation faded, and this resulted in a weakened relation between TCV and spatial GC standard deviation if only observations just before harvest were taken into consideration ($R^2 = 0.33$, Table 8.7).

Table 8.7 Linear regressions of heterogeneity variables with seasonal dry matter yield (SDM, t ha⁻¹ yr⁻¹) and the spatial tiller coefficient of variation (TCV) in 2000.

Model	a	b	R ²	SE observations
SDM = a + b LI-SD ₁	18.5	-0.40	0.50	1.32
SDM = a + b GC-CV ₁	20.5	-30.5	0.71	1.10
SDM = a + b GC-SSD ₁	25.0	-0.92	0.63	1.23
SDM = a + b GC-WE ₁	100.1	-27.3	0.70	1.11
SDM = a + b TGC-WE ₁	91.7	-22.0	0.60	1.28
SDM = a + b GC-WE _{1,3}	131.8	-37.7	0.59	1.30
GC-SSD ₂ = a + b TCV	9.4	5.2	0.69	0.89
GC-SSD ₁ = a + b TCV	9.0	4.11	0.33	1.45

₁ Calculated as mean over observations just before harvest

₂ Calculated as mean over all observations

₃ Calculated as mean of three wavelet entropy estimates per mini sward, one for each band

8.4 Discussion and conclusion

As expected, artificially damaged swards (ADS) and naturally damaged swards (NDS) had lower seasonal dry matter yield (SDM) than control swards (CS). In the first cut, yield differences were small, with highest yields for NDS. The largest differences in DM yield arose in summer. The N content of ADS and NDS was higher than for CS, indicating luxury consumption. This reflects the higher N availability per unit DM produced. This is in agreement with Richards & Wolton (1975), who found that grazing damage affected the DM to N ratio. Deenen (1994, p38) concluded that ‘sward quality strongly affects the absolute and marginal response of herbage and implicitly animal production to fertiliser N applied’. Therefore, it is concluded that N supply requires fine-tuning for differences in sward quality (Mooij & Vellinga, 1993).

8.4.1 Ground cover

The control swards had a seasonal mean ground cover (GC) between 36% and 56%, which correspond to visually scored GC values of 47% and 69%. These values are similar to data from Alberda (1968), from which mean GC values of 67% for hay type and 65% for pasture type were calculated for the 4 weeks harvest intervals. Longer harvest intervals decreased mean GC in the first four

weeks after harvest by 20% (Alberda, 1968). An increase of 1% GC rose SDM with 0.31 t DM ha⁻¹. Over the growth period from 26 April through 30 October (186 days), the nearby meteorological station of Wageningen received on average 13.83 MJ m⁻² d⁻¹ solar radiation. The rain shelter foil transmitted 80% of solar radiation. The fraction photosynthetically active radiation is equal to 50% of the total solar radiation. Therefore, mini swards received a total of 5.6 MJ PAR m⁻² d⁻¹. In the GC range around 50% GC, increasing GC with 1% increases LI with 1.42% under a cloudy and clear sky (Schut & Ketelaars, Chapter 3). In the LINGRA growth model (Schapendonk *et al.*, 1998), *Lolium perenne* L. has a maximum light use efficiency of 3.0 g DM MJ⁻¹ (PAR, calibrated value for Northern Europe) and a fraction of 0.165 for root growth (Bouman *et al.*, 1996). The maximum light use efficiency is corrected for intense radiation resulting in a light use efficiency of 2.694 g DM MJ⁻¹ (PAR). From this, it was calculated that an increase of 1% GC would increase SDM with 0.33 t DM ha⁻¹, a value similar to the regression coefficient found for the relation between GC and SDM. The relative range in SDM (11.4-19.2 t DM ha⁻¹) was larger than the relative range in seasonal mean GC (36-56%). Open swards have a lower light interception capacity per unit GC under clear sky conditions (Schut & Ketelaars, Chapter 3). The relatively strong response of SDM to changes in GC can be attributed to these changes in light interception capacity per unit GC. This also means that plants surrounding gaps did not compensate for yield loss. This in contrast to Fehmi *et al.* (2001), who found in California annual grassland that plants surrounding gaps partly compensated yield loss, as 0.75-1.50 dm² size gaps did not limit the realised productivity.

8.4.2 *Relation between image parameters and SDM*

The linear regression between SDM and repeated measurements of ground cover (GC) and index of reflection intensity allowed accurate SDM prediction ($R^2 = 0.93$). Correlation between GC and SDM showed strong changes within a growing period. Correlations were strongest just before harvest ($r = 0.55-0.87$). Therefore, it is concluded that growth capacity of a sward can best be judged after a period of growth.

8.4.3 *Spatial variability in relation to sward quality groups*

The spatial variation in tiller density and light interception was larger for ADS and NDS than for CS. This spatial heterogeneity was also present in the images of ADS and NDS, although image heterogeneity faded during growth.

Transects of GC estimates revealed that the variability was clustered, as shown by wavelet entropy. Both spatial GC standard deviation (GC-SSD) and patterns in GC estimates were stronger for ADS and NDS than for CS, especially during summer. The GC-SSD reached its maximum value when GC values were between 40 and 60%. The spatial standard deviation of the logistically transformed GC values (TGC-SSD) amplified differences between CS, ADS and NDS just after harvest. In the second half of the growth period GC-SSD and TGC-SSD decreased and GC increased, although patterns remained visible. Therefore, relative variability decreased, diminishing also the importance of clusters. As a result, wavelet entropy values strongly decreased within a growth period. Sward heterogeneity showed a seasonal pattern, with maximum heterogeneity in the summer period for the ADS and NDS.

8.4.4 Discrimination of sward quality groups

Calculating seasonal means of GC-SSD and TGC-SSD improved discrimination of ADS and NDS from CS. The GC-SSD showed maximum differences between groups at 50% GC. Discrimination at low GC values strongly improved with a logistic conversion of GC values. The seasonal mean TGC-SSD of the CS remained below 0.6 in all harvest intervals, whereas ADS and NDS had a TGC-SSD value equal or greater than 0.6. The absolute differences between seasonal means of CS, ADS and NDS were largest 9-13 days after harvest for GC-SSD and 5-8 days after harvest for TGC-SSD. In contrast to this, correlation between SDM and GC-SSD and TGC-SSD became stronger towards harvest. This was caused by differences in the dynamics of heterogeneity for CS, ADS and NDS. The NDS showed a stronger decrease in seasonal mean GC-SSD and TGC-SSD within a re-growth period than ADS, whereas seasonal mean GC-SSD and TGC-SSD of CS changed only slightly during re-growth.

8.4.5 Assessment of sward quality with image parameters

In this study, seasonal dry matter yield (SDM) was used as quantitative measure of sward quality. The combination of seasonal mean GC and IRI proved to be the best predictor of SDM. However, values of SDM and seasonal mean GC and IRI are strongly affected by sward management, *e.g.* grazing, harvest intervals and nutrient application. Therefore, assessment of sward quality with seasonal means of GC and IRI requires an accurate reference, *i.e.* an estimate of optimal seasonal mean values of GC and IRI for the given sward management.

This reference may be derived from the best field or the best location within a field or from accurate predictions of yield potential by grass growth models.

The spatial heterogeneity of swards was expected to be less sensitive to changes in sward management than SDM or seasonal mean GC. The spatial variation present in tiller density and light interception was also present in GC estimates. Unfortunately, the accumulation of biomass masked spatial heterogeneity, strongly decreasing spatial GC heterogeneity above 50% GC. Although spatial GC heterogeneity was related to SDM ($R^2=0.59-0.71$), discriminating power of this relationship was unsatisfactory with standard errors of observations between 1.1 and 1.3 t DM ha⁻¹ yr⁻¹. The dynamic aspects of heterogeneity may affect the relations between heterogeneity and production capacity found in this study. Management practices, such as grazing, may temporarily increase or decrease heterogeneity. Dung and urine patches increase heterogeneity (Keuning & Vellinga, 1986). Dung and urine may also create gaps in the canopy (Lantinga, 1986), especially under high stocking rates (Wolton, 1978). Small and medium sized gaps in the canopy are rapidly filled by vegetative expansion or seedlings (Marriott *et al.*, 1997). Therefore, the dynamics of heterogeneity should be incorporated in a sward quality assessment, and this requires repeated measurements during the growing season.

It is concluded that imaging spectroscopy provides means for accurate SDM assessment. Differences in TGC-SSD between sward quality groups were largest within 8 days after harvest, whereas the correlation between SDM of individual swards and GC-SSD became stronger negative towards harvest. Grassland renovation is expensive, and may only be economically justified when swards are heavily deteriorated (Elsässer, 1991; Keuning & Vellinga, 1986; MacCarthy, 1982; Smith & Allcock, 1985; Spatz *et al.*, 1981). Sward renewal is economically attractive when the production increase compensates the cost of reseeding or renovation. Reseeding is beneficial at 18-23% yield increase for 5 year reseeding intervals and 10-15% for 10 year reseeding intervals (Aarts *et al.*, 2002). The actual production can be quantified with imaging spectroscopy. The calculation of the potential increase of production requires an additional reference for comparison with actual production. Mini sward heterogeneity was well quantified with imaging spectroscopy. The effects of botanical composition and management strategies on image heterogeneity characteristics, and the self-recovery capacity of deteriorated swards require further study before conclusions can be made with regard to the implications of sward heterogeneity for sward reseeding or renovation.

9

Potential of imaging spectroscopy as tool for pasture management

A.G.T. Schut, C. Lokhorst, M.M.W.B. Hendriks,
J.G. Kornet & G. Kasper

Submitted to Grass and Forage Science

9. Abstract

The potential of imaging spectroscopy (IS) was explored as a robust tool for pasture management. The experimental IS system measured reflectance between 404-1650 nm with three sensors at high spatial (0.28-1.45 mm²) and spectral (5-13 nm) resolution. The prediction accuracy of dry matter (DM) yield, mineral concentration (N, P, K, S, Ca, Mg, Mn, Zn and Fe), crude fiber (CF), ash, sugar and DM content of grass swards was evaluated. Two data sets were used from *Lolium perenne* L. mini sward experiments, conducted in 2000 in containers under a rain shelter. The first data set included up to 300 observations from 9 harvests of mini swards with adequate N supply that varied in sward damage. The second data set included up to 100 observations from 6 harvests of an experiment where N application varied from 0 up to 120 kg N ha⁻¹ harvest⁻¹. Partial least square (PLS) regression models were built from the leaf reflectance data, and were calibrated and validated per data set. PLS models were evaluated per sensor and for a combination of 2 sensors. The 2-sensor PLS models were combined with ground cover (GC) and index of reflection intensity (IRI). The potential reduction in model error was explored for 10, 25 and 50 observations per field for a large and small model bias contribution. The 2-sensor PLS model including GC and IRI performed best. The mean prediction errors for exp. 1 and 2 were 268 and 235 kg DM ha⁻¹, 0.24 and 0.34 N (%), 1.68 and 0.96 DM (%), 16.2 and 27.7 sugar (g kg⁻¹ DM), 6.5 and 5.8 ash (g kg⁻¹ DM) and 10.4 and 8.36 CF (g kg⁻¹ DM). The predictions for P, K, S, and Mg allowed identification of deficiency levels, in contrast to Na. Predictions were poor for Zn, Mn and Ca. With 25 replicate measurements, the calculated prediction error of DM yield may be maximally reduced to 95-142 kg ha⁻¹ for fields with a within-field standard deviation of 300 kg ha⁻¹. It is concluded that imaging spectroscopy provides robust and accurate means for assessment of DM yield and feeding quality of standing grass. This opens up new means for improvement of grassland and dairy farm management. The methodology requires further evaluation under field conditions, including a range of grass species and management practices.

9.1 Introduction

In the Netherlands more than 1 million ha of grass is used for the feeding of dairy cows. Optimisation of the grassland management by dairy farmers will

help to reduce the cost price of milk and reduce emissions to the environment. Planning of grassland use, timing and quantity of manuring and fertilising, timing of grazing and mowing and adaptation of parcel size are at hand to improve the quantity and quality of own produced roughage. A prerequisite for all these management options is to estimate or measure the production capacity of the land (Hack-ten Broeke, 2000). Potential deficiencies or excesses of minerals in grassland are important, and mostly related to the use of fertilisers (Hopkins *et al.*, 1994). Adequate concentrations of mineral contents in the grass influence the efficiency of the grass growth (McKenzie & Jacobs, 2002). Therefore it might be of interest to be able to measure the mineral content of the grass. Dutch farmers are used to calculate the ration for cows based on feed information. Dry matter content, mineral content, and feeding value are important. Feeding values of grass and maize silage and concentrates are mostly available, but feeding value of fresh grass is mostly unknown. Farmers have the possibility to collect a sample of fresh grass, based on 25 hand plucks per parcel, and send it to the Dutch Laboratory for Soil and Crop Testing (BLGG) where it is analysed for dry matter content, sugar content, feeding values and mineral contents. The time delay between sampling and return of laboratory results is a disadvantage of this method. Within the concept of Precision Agriculture, very little research has been focused on grassland yield mapping. Lokhorst & Kasper (1998) performed a field test in 1997 to get insight in the measuring capabilities of existing measuring techniques and in the spatial and temporal variation in grass yield under Dutch conditions. The main conclusion from that work was that available techniques were not suitable to measure accurately and non-destructively grass yield and quality. Therefore, new measuring techniques should be developed. With the recently developed system for hyperspectral imaging spectroscopy, new automatic means for grass sward characterisation are available (Schut *et al.*, Chapter 2). Reflection intensity measured by the system is related to position in the canopy and leaf angle. With this feature, image ground cover (GC) can be differentiated into reflection intensity classes, where the distribution of pixels over the intensity classes is indicative for canopy geometry. Due to the non-destructive nature of reflection measurements, evolution of GC, canopy geometry and leaf spectra can be studied. GC estimates are strongly related to light interception, leaf area index and biomass (Schut & Ketelaars, Chapter 3). The objective of the study is to establish relations between information from imaging spectroscopy, obtained from direct non-destructive measurement of the grass and various grass quality parameters, which are determined after harvesting of the grass. The objective of the analyses is to: 1)

predict values of these quality parameters solely based on image information, with the help of calibrated relationships, 2) to estimate the precision with which these parameters can be predicted, and 3) to identify important image parameters and spectral regions, that are highly predictive for these quality parameters. This information can possibly be used in future applications of the technique for practical use in the field. This paper describes the test results in which the imaging spectroscopy system was tested in two experiments under laboratory conditions. Grass characteristics that were studied with the system were yield, dry matter content, sugar, N, nutrient concentrations and feeding values.

9.2 Materials and Methods

9.2.1 Experiments

In 2000, two experiments were conducted with mini swards of *Lolium perenne* L., grown in containers of 0.9 m long, 0.7 m wide and 0.4 m high, filled with a sandy soil (3% organic matter). The containers were placed under a rain shelter covered with 80% light-transparent foil, with wind breaking fencing at the sides. Soil moisture content was maintained at field capacity by weighing twice a week. Data from two experiments (where the degree of sward damage and N application varied) were used as a representation of Dutch grasslands.

Experiment 1

This experiment is described in detail in Schut & Ketelaars (Chapter 3). In short, a total of 36 mini swards were available from a two year drought experiment (Grashoff *et al.*, 2001). There were 8 mini swards with damaged swards, due to a period of 40 days without additional water. Artificial sward damage was created in 12 mini swards. On random locations in the sward, circular patches of 12.5 and 22.5 cm diameter were removed with a total area of 25, 50 or 75% of the sward. The remaining 16 swards were part of an drought-stress experiment, with control swards and swards where no extra water was supplied for 20, 30 and 40 days in the period from 1 June through 10 July. Harvests from severely dried out swards were excluded from the data set. On 17 March 2000, fertiliser was supplied with $8.1 \text{ g m}^{-2} \text{ N}$, $6.6 \text{ g m}^{-2} \text{ P}_2\text{O}_5$ and $12 \text{ g m}^{-2} \text{ K}_2\text{O}$. On the 11th of July, $3 \text{ g m}^{-2} \text{ P}_2\text{O}_5$, $20 \text{ g m}^{-2} \text{ K}_2\text{O}$ and $6 \text{ g m}^{-2} \text{ S}$ was supplied, with an additional $6.3 \text{ g m}^{-2} \text{ K}_2\text{O}$ on 30 August. After every cut

9.4 g m⁻² N (dissolved in water) was supplied. After 15 September the N dose was reduced to 5.1 g m⁻².

Experiment 2

The second experiment is described in detail in Schut & Ketelaars (Chapter 4). In this experiment, nitrogen (N) application varied in 5 levels, equivalent to 0, 30, 60, 90 and 120 kg N ha⁻¹. This experiment consisted of two observation periods. For the first period, a mixture of *Lolium perenne L.* cultivars (BG3, Barenburg) was sown in April 2000. Before sowing, 8.1 g m⁻² N, 13.8 g m⁻² P₂O₅ and 24 g m⁻² K₂O was applied. Once a good sward was established, grass was cut (30 May) and the day after, N was supplied according to the treatments. For the second observation period, 5-10 cm thick grass swards (sown in autumn 1999) were transplanted into containers on 6 July. After a two-month start-up period without additional N, N was supplied after each harvest from 8 August onwards. Swards were harvested on 25 July, 8 August, 29 August, 27 September, and 31 October. Because of the time of the year, N levels were reduced to 0, 20, 40, 60 and 90 kg N per ha⁻¹ after the 27 September harvest. Application of N was further reduced with one N level when N-min content was higher than 22.5 kg ha⁻¹.

9.2.2 *Measurements*

Laboratory analysis

At harvest, swards were hand-cut to a stubble height of 4 cm. In Table 9.1, harvest dates and DM yields are given. At harvest, fresh material was collected and weighted and samples were taken. These samples were analysed at the Dutch Laboratory of Soil and Crop Research (BLGG) for chemical analysis. From each sample, dry matter (DM) yield, fresh matter (FM) yield and DM content (DMc) was determined by weighing, sugar and N content and feeding value was determined using NIRS, and mineral composition (P, K, S, Ca, Mg, Mn, Zn, Fe) was determined using ICP-OES. The feeding value of fresh grass can be calculated with estimates of N content, DMc, ash content, crude fiber (CF) content and sugar content. The ash content is the residue of ash after heating (550°C), and the CF is the amount lost after boiling in an acid and

Table 9.1 Harvest dates and treatment mean DM yield (kg DM ha⁻¹) in experiment 1 and 2.

Treatment	Experiment 1		Experiment 2			
	control	N0	N30	N60	N90	N120
25 April	3308	-	-	-	-	-
12 May	1953	-	-	-	-	-
30 May	912	-	-	-	-	--
20 June	1643	2430	3161	3198	3612	3786
11 July	1156	-	-	-	-	-
25 July*	-	1471	1488	1418	1439	1361
8 August*	2941	916	1030	948	1053	918
29 August	2348	591	1381	1514	2066	2001
27 September	2358	356	1304	1913	2587	2696
31 October	1115	253	836	1109	1298	1403

* In experiment 2: intermediate harvests without N supply

caustic solution (Anonymous, 1998). In Table 9.2, the repeatability of the BLGG measurement procedure is given for each variable, with mean and standard deviation values in fresh grass samples analysed in 2001.

Imaging spectroscopy

The experimental system used is described in detail elsewhere (Schut *et al.*, Chapter 2). In short, image lines were recorded with three sensors: the V7, N10 and N17. The V7 sensor detects reflectance between 404-709 nm, the N10 sensor between 680-970 nm and the N17 sensor between 960-1650 nm. The sensors have a spectral resolution of 5 nm (V7 and N10) and 13 nm (N17), and a spatial resolution at soil level of 0.28 mm² (V7 and N10) and 1.45 mm² (N17). At soil level, an image line is 1.39 mm wide and 152.5 mm long for the V7 and N10 sensor, and 1.39 mm wide and 133.1 mm long for the N17 sensor. Per image line, reflection was measured in 768 (V7 and N10) and 128 (N17) picture elements (pixels). Light is focussed with a bar lens, and only a 2-4 cm wide strip is illuminated. Light is projected vertically to the soil, and reflectance is measured under an angle of 2 degree from nadir. On 42 positions per mini-

Table 9.2 Confidence boundary for repeatability ($p < 0.05$) of duplicate samples at the Dutch Laboratory for Soil and Crop Research (BLGG), mean values and standard deviations of fresh grass analysis in 2001 (BLGG, personal communication).

	Repeatability	Mean values in 2001
Ash (g kg ⁻¹ DM)	11	107 ± 12
CF (g kg ⁻¹ DM)	13	228 ± 21
Sugar (g kg ⁻¹ DM)	14	93 ± 53
N (g kg ⁻¹ DM)	1.8	37 ± 8
K (g kg ⁻¹ DM)	1	36 ± 7
P (g kg ⁻¹ DM)	0.1	4.3 ± 0.8
S (g kg ⁻¹ DM)	0.2	4.1 ± 1.3
Mg (g kg ⁻¹ DM)	0.2	2.6 ± 0.5
Ca (g kg ⁻¹ DM)	NA	5.8 ± 1.7
Na (g kg ⁻¹ DM)	0.2	2.4 ± 1.3
Mn (mg kg ⁻¹ DM)	3	98 ± 57
Zn (mg kg ⁻¹ DM)	3	44 ± 20
Fe (mg kg ⁻¹ DM)	9	155 ± 143

sward, image lines were recorded in a regular pattern. In general, image lines were recorded two times per week. Swards were harvested a day after image recording, with exception of the 27 September harvest, which was harvested two days after image recording. Schut *et al.* (Chapter 2) defined threshold values for soil, grass leaves (G), leaves with specular reflection (S), and dead material (D) classes and an intermediate class between soil and dead material. Separation between classes was based on ratios of reflectance (R) at 450, 550 and 680 nm. These classes are subdivided into reflection intensity classes (IC), based on the reflection intensity at predefined wavelengths (550 nm for the V7, 746 nm for the N10 and 1100 nm for the N17 sensor). The intensity classes ranged for grass from IC 0 up to and including IC 6 for the V7 sensor and from IC 0 up to and including IC 10 for the N10 and N17 sensor. For leaves with specular reflection, IC ranged from 0 up to and including 2, and for dead material from IC 0 up to and including 3. A large number of pixel reflection spectra per intensity class are stored in a spectral library. With this library, pixel spectra of the recorded image lines were classified with maximum likelihood procedures (Schut & Ketelaars, Chapter 3). The classification procedure was

based on a limited number of wavelengths, selected according to a statistical function maximising class to class separation (Feyaerts & Van Gool, 2001). After classification, spectra of pixels were normalised, according to equations in Schut *et al.* (Chapter 2). Normalisation means that reflection was divided by the mean reflection in the 550-555 nm range for the V7 sensor, 800-850 nm range for the N10 sensor and 1070-1130 nm for the N17 sensor. Mean sward reflection spectra were calculated per sensor from normalised spectra of all pixels in grass IC 1 through 10. It is stressed that with this procedure only grass pixels were selected, eliminating pixels with soil and dead material. Ground cover was calculated per mini sward for each IC. Total image line (IL) ground cover (GC_{IL} , %) was calculated as sum of ground cover of all grass IC (GCG) and IC of all specular classes (GCS) from the V7 sensor:

$$GC_{IL} = \sum_{ic=0}^6 GCG_{ic} + \sum_{ic=0}^2 GCS_{ic}$$

where ic is the index number of the intensity class. The mini sward GC was calculated as the average of the GC_{IL} over the 42 image lines. The index of reflection intensity (IRI, %) was then calculated as:

$$IRI = 100 \times \frac{\sum_{ic=3}^6 \frac{1}{42} \sum_{il=1}^{42} GCG_{il,ic}}{GC}$$

This IRI measures the presence of highly reflecting green pixels as a percentage of GC. A high value represents a dense canopy with more horizontally oriented leaves (Schut & Ketelaars, Chapter 3).

Partial least squares

The available spectral information is highly multivariate and (in general) very co-linear, *i.e.* the information in single wavelengths is usually highly correlated with information in other wavelengths. Furthermore, the number of observations is smaller than the number of wavelengths detected by the sensors. Partial least squares (PLS) regression is most suitable for these two data-properties. PLS combines data reduction with a regression model:

$$Y = \beta X + e,$$

where Y is vector with the measured variables of interest, X is the matrix with reflection values per spectral band and β is the matrix with coefficients

estimated with PLS and e is the error vector. PLS searches for latent variables (LVs) in the spectral space that explain as much variation as possible in both the spectral data and the variable of interest. The minimum prediction error sum of squares of the (leave one-out) cross-validated predictions was used as criterion to select the appropriate number of LVs. As an example, Figure 9.1 shows the minimum prediction error sum of squares, as function of the number of LVs included in the PLS model for DM yield in experiment 1. For each variable per experiment, the optimum number of LVs was determined. An extensive introduction to PLS regression can be found in Geladi & Kowalski (1986). Data were analysed using Matlab version 6.0 with the Matlab PLS-toolbox (Matlab, 2000; PLS_Toolbox, 2000).

9.2.3 Model evaluation

The data were, per experiment and per sensor, pseudo-randomly divided, *i.e.* with regard to treatment and cutting date, into calibration and validation sets with a ratio of 2:1. All spectra were visually inspected for each sensor and excluded from the data set when abnormal or missing. The N17 sensor was defect from 14th August up to 15th October 2000 and, therefore, data of the 29 August and 27 September harvests were not available. In experiment 1,

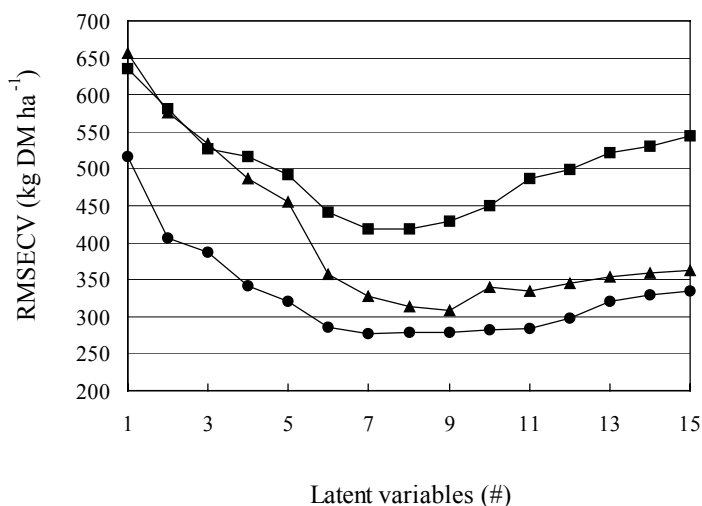


Figure 9.1 Root means square error of cross validation (RMSECV) as function of number of latent variables included in the PLS calibration model for DM yield in experiment 1 for sensor 1 (●), 2 (■) and 3 (▲).

293 to 307 (V7 and N10 sensor) and 220 observations (N17 sensor) were available and in experiment 2 95-100 (V7 and N10 sensor) and 57 observations (N17 sensor) were available. PLS models were constructed with the calibration set. These PLS models were used to generate predictions of the response variables in the validation set. To evaluate the calibration models the following criteria were used:

$$R^2 = 1 - \sum_i \frac{(\hat{y}_i - y_i)^2}{(\hat{y}_i - \bar{y})^2}, \quad (1)$$

where \hat{y}_i and y_i were respectively the leave-one-out predictions and measured values of the variable of interest, while \bar{y} was the average value of the variable of interest in the calibration set. The root mean squared error of cross-validation (RMSECV) was calculated as:

$$RMSECV = \sqrt{\frac{\sum_i (\hat{y}_i - y_i)^2}{n}}. \quad (2)$$

The validation models were evaluated with:

$$Q^2 = 1 - \sum_i \frac{(\hat{y}_i^v - y_i^v)^2}{(\hat{y}_i^v - \bar{y})^2}, \quad (3)$$

where \hat{y}_i^v and y_i^v were the predicted and measured values of the variable of interest in the validation set and \bar{y} the average value of the variable of interest in the calibration set. The Q^2 can be interpreted as the fraction of variation explained by the model. The Q^2 is (as in R^2), therefore, strongly sensitive to the variation within the data set. Therefore, one should be careful when looking at Q^2 values. The root mean squared standard error of prediction (RMSEP) was calculated as:

$$RMSEP = \sqrt{\frac{\sum_i (\hat{y}_i^v - y_i^v)^2}{n}}. \quad (4)$$

With imaging spectroscopy, the number of samples for analysis can easily be expanded without additional costs. Increasing the number of observations (N) per field will reduce the variance (random error component) of the model prediction error (RMSEP_M) of imaging spectroscopy (S_{IS}) according to:

$$S_{IS} = \sqrt{RMSEP_B^2 + \frac{RMSEP_M^2 + S_x^2}{N}} \quad (5)$$

The S_x^2 is the sampling error due to within-field variation. This does not reduce the model bias (RMSEP_B, the systematic error component). Van der Voet (personal communication) found that the ratio between RMSEP_B and RMSEP_M was between 0.03 and 0.30 for NIRS determination of N and CF content in samples of ensiled grass. Therefore, potential reductions in RMSEP were calculated with an intermediate and high estimate of the ratio of RMSEP_B / RMSEP_M of 0.25 and 0.50, under 10, 25 and 50 observations in the field. For this, the RMSEP of the best model averaged over two experiments were used. The S_x was estimated from the within-field standard deviation of a data set with 100 subplots of 4 m², within a newly sown field of 1.2 ha. Each plot had three harvests (Lokhorst & Kasper, 1998). The within-field standard deviations, averaged over three harvests, were: 5.09 t ha⁻¹ FM yield, 660 kg ha⁻¹ DM yield, in the FM 12.8 g kg⁻¹ DMc, and in the DM 6.9 g kg⁻¹ ash, 12.9 g kg⁻¹ CF, 3.7 g kg⁻¹ N, 4.6 g kg⁻¹ K, 0.51 g kg⁻¹ P, 1.0 g kg⁻¹ Ca, 0.34 g kg⁻¹ Mg and 2.0 g kg⁻¹ Na. These estimates are conservative, as the large subplot size is expected to average out small-scale variation, which do contribute to the variation in a composite sample of hand-plucks. The calculated S_{IS} was compared with the total error of laboratory fresh grass analysis and within field variation (S_{FG}). Laboratory analysis is performed on one composite sample per field, where sub-samples are collected in a regular pattern over the field. Due to sampling, the S_{FG} error is the combination of the laboratory error S_{lab} and the error originating from analysing only one composite sample per field:

$$S_{FG} = \sqrt{S_{lab}^2 + \frac{S_x^2}{N}} \quad (6)$$

The S_{lab} multiplied with 2.8 indicates the repeatability of laboratory measurements, which is presented in Table 9.2. The number of observation (N) equalled 25 (Anonymous, 1998). The ratio between standard deviation in the data set and RMSECV was calculated. It has been suggested that for near infrared spectroscopy, a ratio above 2.5 indicate that the calibration is adequate for quality screening purposes. A ratio above 3.0 indicate that the calibration should perform well for quantitative analysis (Sinnaeve *et al.*, 1994; Park *et al.*, 1998).

9.2.4 *Data sets*

At first, spectra were analysed for each sensor separately, resulting in three different calibration models for each variable of interest.

Combination of sensors

For each experiment, a large data set was constructed in which spectra of sensors were combined. PLS models attempt to describe all variability in spectra as well as in the variable of interest. Variable predictability with PLS models only improve when including spectral bands describing yet unexplained variation. Therefore, only the V7 and N17 data sets are combined, as predictability with spectra of the N10 sensor was limited. Again, calibration and validation models were constructed for this 2-sensor data set and tested according to the methodology described above.

Including ground cover and IRI parameters

Schut & Ketelaars (Chapter 3) showed that GC was strongly related to light interception and LAI in grass swards. The IRI was related to canopy geometry, and there was a linear relation between GC, IRI and DM yield ($R^2_{\text{adj}} = 0.75$). Therefore, three additional models (A, B and C) were constructed. Model A included GC and model B included GC and IRI. Model C included all GC estimates of GCG and GCS classes, containing detailed information about the relative importance of various classes. The 2-sensor spectra were combined with these additional variables. The models were block-scaled, which implied that both blocks, spectra and additional variables contributed equally to the total sum of squares. With these combined data new PLS models were built, according to procedures described above.

9.3 Results

9.3.1 *Data sets*

In Table 9.3, means and standard deviations for the calibration and validation data sets for the V7 sensor are presented. The two experiments had similar DM yields, but differed considerably in DMc and concentrations of CF, ash, sugar and minerals. The variability of N and sugar was smaller and variability of K

and Ca was considerably larger in experiment 1 than in experiment 2. The high N concentration in experiment 1 indicated that N application was sufficient, whereas in experiment 2 N deficiency occurred. In general, there were no large differences between the calibration and validation sets. There were strong correlation coefficients found between variables within the data sets (Table 9.4). Based on previous studies, good predictability was expected for DM yield, N and DMc when combining GC, IRI and reflectance. Therefore, high correlation with one of these variables may be important for the predictability. Pearson correlation coefficients (r) above 0.5 in both data sets were found for DM yield and FM yield ($r=0.98$), N ($r<-0.5$), P ($r>0.52$), K ($r>0.64$), S ($r>0.66$), Mg ($r<-0.55$), Ca ($r<-0.71$) and Na ($r=-0.81$). The correlation was also strong between DMc and FM ($r<-0.54$), K ($r<-0.54$), Mg ($r>0.67$) and Ca ($r=0.81$) and between N and Na ($r>0.61$), Zn ($r>0.61$) and Fe ($r>0.55$).

Table 9.3 Means and standard deviations (SD) for variables in calibration and validation data sets of the V7 sensor.

	Experiment 1				Experiment 2			
	Calibration(n=207)		Validation(n=100)		Calibration (n=66)		Validation(n=34)	
	Mean	SD	Mean	SD	Mean	SD	Mean	SD
FM yield (t ha ⁻¹)	10.0	5.9	10.3	6.4	9.6	5.7	9.8	4.8
DM yield (kg ha ⁻¹)	1731	840	1752	902	1634	939	1694	832
Ash (g kg ⁻¹ DM)	84.8	9.8	86.4	9.0	97.1	10.9	96.9	11.4
CF (g kg ⁻¹ DM)	217	12	218	13	244	16	242	12
DMc (g kg ⁻¹ FM)	187	37	184	29	177	25	176	28
Sugar (g kg ⁻¹ DM)	123	26	119	26	147	64	148	67
N (g kg ⁻¹ DM)	39	4	39	4	28	8	29	7
K (g kg ⁻¹ DM)	26.0	10.9	26.5	11.2	34.4	5.5	35.2	5.4
P (g kg ⁻¹ DM)	3.7	1.2	3.8	1.1	4.3	0.8	4.2	0.9
S (g kg ⁻¹ DM)	4.1	1.0	4.2	1.1	5.2	1.4	5.1	1.4
Mg (g kg ⁻¹ DM)	3.0	0.8	3.0	0.8	3.2	0.6	3.2	0.6
Ca (g kg ⁻¹ DM)	12.1	4.1	11.9	3.6	6.7	1.6	6.6	1.4
Na (g kg ⁻¹ DM)	2.5	0.9	2.5	0.8	2.5	1.4	2.4	1.1
Mn (mg kg ⁻¹ DM)	170	51	175	51	158	57	157	38
Zn (mg kg ⁻¹ DM)	98	15	100	17	45	10	45	9
Fe (mg kg ⁻¹ DM)	116	22	116	25	122	38	124	43

9.3.2 Spectra per sensor

In general, the R^2 and Q^2 values were higher for the V7 and N17 sensor than for the N10 sensor (Table 9.5). The mean Q^2 value of the N10 sensor was extremely low in experiment 2, whereas mean Q^2 value was comparable with the N17 sensor in experiment 1. The V7 sensor responded strongest to CF and nutrients, whereas the N17 sensor responded strongest to FM and DM yield, DMc and sugar. Remarkably, the N17 sensor had high Q^2 values for the nutrients in experiment 1, but low Q^2 values in experiment 2. The Q^2 values of the N17 sensor for DM (0.85 and 0.84) and FM (0.93 and 0.89) yield and DMc (0.61 and 0.60) were high in both experiments. The V7 sensor had higher Q^2 values in experiment 1 than in experiment 2 for DM (0.89 vs. 0.41) and FM (0.88 vs. 0.45) yield and DMc (0.71 vs. 0.38), whereas Q^2 values for N, P, S, Mg and Zn were comparable. This indicates that the high Q^2 values for these nutrients did not result from auto-correlation with DM and FM yield or DMc alone.

Table 9.4 Pearson correlation coefficient (r) between variables for experiment 1 in the upper right half, and experiment 2 in the lower left half in *Italic*.

	FM	DM	Ash	CF	DMc	Sugar	N	K	P	S	Mg	Ca	Na	Mn	Zn	Fe
FM		0.98	0.51	0.35	-0.54	0.21	-0.53	0.72	0.56	0.73	-0.62	-0.78	-0.82	-0.05	-0.39	-0.25
DM	<i>0.98</i>		0.49	0.41	-0.42	0.35	-0.50	0.68	0.52	0.68	-0.55	-0.71	-0.81	-0.02	-0.38	-0.25
Ash	<i>0.60</i>	<i>0.55</i>		0.67	-0.35	-0.06	0.31	0.80	0.52	0.77	-0.35	-0.46	-0.19	-0.04	0.11	0.32
CF	<i>0.43</i>	<i>0.44</i>	<i>0.59</i>		0.18	0.27	0.33	0.38	0.43	0.47	0.16	-0.01	-0.01	0.36	0.26	0.27
DMc	<i>-0.63</i>	<i>-0.53</i>	<i>-0.53</i>	<i>-0.05</i>		0.42	0.31	-0.54	-0.40	-0.42	0.74	0.81	0.42	0.39	0.37	0.16
Sugar	<i>-0.12</i>	<i>0.03</i>	<i>-0.38</i>	<i>-0.09</i>	<i>0.52</i>		-0.24	-0.01	-0.23	-0.10	0.22	0.11	-0.27	0.13	-0.03	-0.26
N	<i>-0.54</i>	<i>-0.56</i>	<i>0.14</i>	<i>-0.02</i>	<i>0.27</i>	<i>-0.21</i>		-0.15	0.03	-0.06	0.44	0.52	0.73	0.18	0.64	0.64
K	<i>0.67</i>	<i>0.64</i>	<i>0.80</i>	<i>0.33</i>	<i>-0.62</i>	<i>-0.26</i>	<i>-0.13</i>		0.38	0.78	-0.63	-0.72	0.72	-0.32	-0.27	-0.04
P	<i>0.64</i>	<i>0.56</i>	<i>0.59</i>	<i>0.40</i>	<i>-0.53</i>	<i>-0.47</i>	<i>-0.08</i>	<i>0.38</i>		0.71	-0.37	-0.58	0.56	0.31	-0.02	0.17
S	<i>0.73</i>	<i>0.66</i>	<i>0.75</i>	<i>0.41</i>	<i>-0.52</i>	<i>-0.35</i>	<i>-0.09</i>	<i>0.66</i>	<i>0.78</i>		-0.58	-0.61	0.73	-0.01	-0.12	0.17
Mg	<i>-0.67</i>	<i>-0.62</i>	<i>-0.53</i>	<i>-0.11</i>	<i>0.67</i>	<i>0.34</i>	<i>0.37</i>	<i>-0.69</i>	<i>-0.41</i>	<i>-0.55</i>		0.85	-0.62	0.49	0.58	0.18
Ca	<i>-0.81</i>	<i>-0.75</i>	<i>-0.60</i>	<i>-0.19</i>	<i>0.81</i>	<i>0.28</i>	<i>0.49</i>	<i>-0.70</i>	<i>-0.61</i>	<i>-0.66</i>	<i>0.75</i>		-0.78	0.32	0.52	0.24
Na	<i>-0.78</i>	<i>-0.81</i>	<i>-0.33</i>	<i>-0.08</i>	<i>0.42</i>	<i>-0.12</i>	<i>0.61</i>	<i>-0.62</i>	<i>-0.30</i>	<i>-0.51</i>	<i>0.60</i>	<i>0.67</i>		-0.05	-0.39	-0.25
Mn	<i>-0.12</i>	<i>-0.15</i>	<i>-0.07</i>	<i>0.14</i>	<i>0.16</i>	<i>-0.09</i>	<i>0.18</i>	<i>-0.34</i>	<i>0.31</i>	<i>0.07</i>	<i>0.49</i>	<i>0.17</i>	<i>0.28</i>		0.53	0.25
Zn	<i>-0.48</i>	<i>-0.51</i>	<i>-0.07</i>	<i>0.04</i>	<i>0.36</i>	<i>-0.04</i>	<i>0.61</i>	<i>-0.32</i>	<i>-0.08</i>	<i>-0.14</i>	<i>0.51</i>	<i>0.54</i>	<i>0.60</i>	<i>0.43</i>		0.49
Fe	<i>-0.06</i>	<i>-0.12</i>	<i>0.34</i>	<i>0.12</i>	<i>-0.08</i>	<i>-0.43</i>	<i>0.55</i>	<i>0.14</i>	<i>0.29</i>	<i>0.32</i>	<i>-0.06</i>	<i>0.05</i>	<i>0.29</i>	<i>0.16</i>	<i>0.42</i>	

The mean R^2 and Q^2 values were on average higher in experiment 1 than in experiment 2. PLS model performance was directly related to the amount of variation in the data set (compare Tables 9.3 and 9.5).

9.3.3 Spectra of 2 sensors combined

In Table 9.6, the R^2 , RMSECV, Q^2 and RMSEP of the 2-sensor model are presented. When compared to the single V7 and N17 sensor models (Table 9.5), Q^2 values of sugar, Ca, Na and Mn improved slightly in experiment 1.

Table 9.5 Calibration and validation results for the V7, N10 and N17 sensor.

	Experiment 1						Experiment 2					
	Calibration, (n=150), R^2			Validation, (n=74), Q^2			Calibration, (n=39), R^2			Validation, (n=21), Q^2		
	V7	N10	N17	V7	N10	N17	V7	N10	N17	V7	N10	N17
FM yield	0.92	0.69	0.92	0.88	0.67	0.93	0.78	0.80	0.99	0.45	-0.39	0.89
DM yield	0.92	0.82	0.89	0.89	0.83	0.85	0.74	0.51	0.95	0.41	0.23	0.84
Ash	0.72	0.57	0.73	0.64	0.42	0.46	0.61	0.21	0.42	0.42	0.04	0.57
CF	0.72	0.48	0.58	0.30	0.36	0.04	0.78	0.59	0.57	0.63	0.44	0.53
DMc	0.87	0.77	0.83	0.71	0.64	0.61	0.59	0.69	0.75	0.38	0.19	0.60
Sugar	0.50	0.57	0.68	0.53	0.57	0.44	0.88	0.22	0.69	0.47	-0.04	0.64
N	0.62	0.44	0.60	0.64	0.54	0.45	0.93	0.46	0.71	0.61	0.00	0.24
K	0.78	0.75	0.83	0.77	0.63	0.67	0.63	0.47	0.31	0.21	0.38	0.16
P	0.71	0.69	0.85	0.68	0.71	0.71	0.64	0.71	0.93	0.59	0.43	-1.79
S	0.66	0.64	0.73	0.63	0.58	0.68	0.85	0.77	0.99	0.66	0.46	-0.99
Mg	0.70	0.72	0.78	0.54	0.49	0.72	0.82	0.22	0.82	0.42	-0.17	0.06
Ca	0.89	0.79	0.83	0.74	0.62	0.72	0.52	0.48	0.77	0.15	-0.30	-0.08
Na	0.85	0.75	0.74	0.74	0.71	0.62	0.80	0.41	0.83	0.46	0.05	0.07
Mn	0.32	0.20	0.24	0.23	0.02	-0.01	0.82	0.92	0.98	0.01	0.08	0.12
Zn	0.51	0.36	0.50	0.37	0.27	0.12	0.63	0.62	0.64	0.35	-0.36	0.53
Fe	0.19	0.22	0.34	0.15	0.22	0.27	0.76	0.49	0.05	0.45	-0.56	0.07
Mean	0.68	0.59	0.69	0.59	0.52	0.52	0.74	0.54	0.71	0.42	0.03	0.15

In experiment 2, Q^2 values improved considerably for sugar, N, K, Mg, Na and Mn, whereas results improved only slightly for DMc, S and Zn. The mean Q^2 value was higher for the 2-sensor model than for separate sensors (compare Table 9.5 and 9.6). This indicates that the different parts of the spectra indeed contained additional information.

9.3.4 Regression results of 2-sensor spectra combined with GC, GC and IRI or all GCG and GCS classes

Including GC as variable (model A) did not further improve Q^2 values much in experiment 1 and improved slightly in experiment 2 (Table 9.7). The predictions for experiment 2 further improved for both data sets when

Table 9.6 Calibration and validation results for the 2-sensor PLS model.

	Experiment 1				Experiment 2			
	Calibration (n=138)		Validation (n=68)		Calibration (n=37)		Validation (n=21)	
	R ²	RMSECV	Q ²	RMSEP	R ²	RMSECV	Q ²	RMSEP
FM yield (t ha ⁻¹)	0.96	1.36	0.93	1.83	0.97	0.91	0.80	1.99
DM yield (kg ha ⁻¹)	0.96	188	0.91	286	0.90	322	0.85	344
Ash (g kg ⁻¹ DM)	0.80	4.7	0.55	6.4	0.51	8.5	0.47	8.3
CF (g kg ⁻¹ DM)	0.63	7.8	0.31	10.8	0.56	8.9	0.28	8.6
DMc (g kg ⁻¹ FM)	0.90	12	0.71	16	0.83	8	0.63	10
Sugar (g kg ⁻¹ DM)	0.68	15	0.57	16	0.81	32	0.87	25
N (g kg ⁻¹ DM)	0.74	2	0.64	3	0.84	3	0.77	4
K (g kg ⁻¹ DM)	0.88	4.0	0.72	6.5	0.97	1.0	0.38	5.2
P (g kg ⁻¹ DM)	0.89	0.4	0.85	0.4	0.66	0.4	-0.10	0.6
S (g kg ⁻¹ DM)	0.79	0.5	0.68	0.6	0.93	0.4	0.72	0.8
Mg (g kg ⁻¹ DM)	0.79	0.4	0.58	0.5	0.95	0.2	0.69	0.4
Ca (g kg ⁻¹ DM)	0.89	1.5	0.77	1.9	0.87	0.7	0.15	1.3
Na (g kg ⁻¹ DM)	0.89	0.3	0.78	0.4	0.91	0.5	0.64	0.8
Mn (mg kg ⁻¹ DM)	0.39	42	0.24	44	0.87	14	0.35	27
Zn (mg kg ⁻¹ DM)	0.61	9	0.20	14	0.77	4	0.62	6
Fe (mg kg ⁻¹ DM)	0.41	17	0.33	21	0.55	29	0.43	36
Mean	0.76		0.61		0.81		0.53	

including both GC and IRI. The largest improvements, as expected, were found for FM and DM yields. Including all GCG and GCS variables did not further improve Q^2 , *i.e.* the extra information provided in model C when compared to model B did not compensate the decrease in degrees of freedom in the model.

9.3.5 Best predictive models

In general, Q^2 values were highest for the model with GC and IRI included (model B, Table 9.7). It was, therefore, concluded that model B had the best overall performance. In Table 9.8, the RMSEP and Q^2 of this model B can be found. This model performed reasonably well for most variables. The Q^2 values

Table 9.7 Validation Q^2 results for the 2-sensor PLS model (2-SM) extended with ground cover (A), ground cover and index of reflection intensity (B) and GCG and GCS classes (C).

Model	Experiment 1				Experiment 2			
	2-SM	A	B	C	2-SM	A	B	C
FM yield	0.93	0.94	0.94	0.94	0.80	0.80	0.91	0.93
DM yield	0.91	0.93	0.93	0.93	0.85	0.85	0.93	0.94
Ash	0.55	0.52	0.53	0.58	0.47	0.65	0.76	0.47
CF	0.31	0.19	0.36	0.35	0.28	0.46	0.57	0.41
DMc	0.71	0.66	0.69	0.74	0.63	0.80	0.65	0.44
Sugar	0.57	0.55	0.58	0.60	0.87	0.84	0.84	0.64
N	0.64	0.64	0.67	0.69	0.77	0.91	0.80	0.79
K	0.72	0.72	0.75	0.76	0.38	0.26	0.37	0.05
P	0.85	0.85	0.82	0.85	-0.10	0.44	0.45	0.44
S	0.68	0.66	0.67	0.72	0.72	0.80	0.82	0.64
Mg	0.58	0.58	0.57	0.61	0.69	0.66	0.69	0.55
Ca	0.77	0.81	0.84	0.83	0.15	0.28	0.09	0.03
Na	0.78	0.78	0.78	0.75	0.64	0.56	0.58	0.66
Mn	0.24	0.18	-0.01	-0.00	0.35	0.68	0.77	0.66
Zn	0.20	0.17	0.14	0.12	0.62	0.63	0.65	0.08
Fe	0.33	0.39	0.42	0.38	0.43	0.59	0.61	0.62
Mean	0.61	0.60	0.61	0.62	0.53	0.64	0.66	0.52

for Ca in experiment 2 and Mn and Zn in experiment 1 were low. These variables had a poor predictability in all models (Table 9.5 and 9.7). The Q^2 values for DMc, sugar, N, S, Mg and Na were well above 0.5 in both experiments. The RMSEP of FM and DM yield were low with values of 1.64 t ha⁻¹ FM and 268 kg ha⁻¹ DM for experiment 1 and 1.44 t ha⁻¹ FM and 235 kg ha⁻¹ DM for experiment 2. The RMSEP includes the error of the reference method. Therefore, the RMSEP is by definition larger than the standard deviation of laboratory analysis. Although Q^2 values of ash and CF were 0.53 and 0.36 in experiment 1, RMSEP (6.46 and 10.4 g kg⁻¹ DM for ash and CF) was only 1.6 and 2.2 times larger than standard deviation of laboratory analysis (3.93 and 4.64 g kg⁻¹ DM for ash and CF, values of repeatability in Table 9.2 divided by 2.8). The RMSEP of N was a factor 4-6 larger, S, Mg, Na and Fe were a factor 5-11 larger and K and P were a factor 11-17 larger. The ratio between standard deviation and RMSECV was larger than 3.5 for FM yield, DM yield and sugar content in experiments 1 and 2. This ratio was larger than 2.5 for DMc, ash and S in experiments 1 and 2. In experiment 1, this ratio was

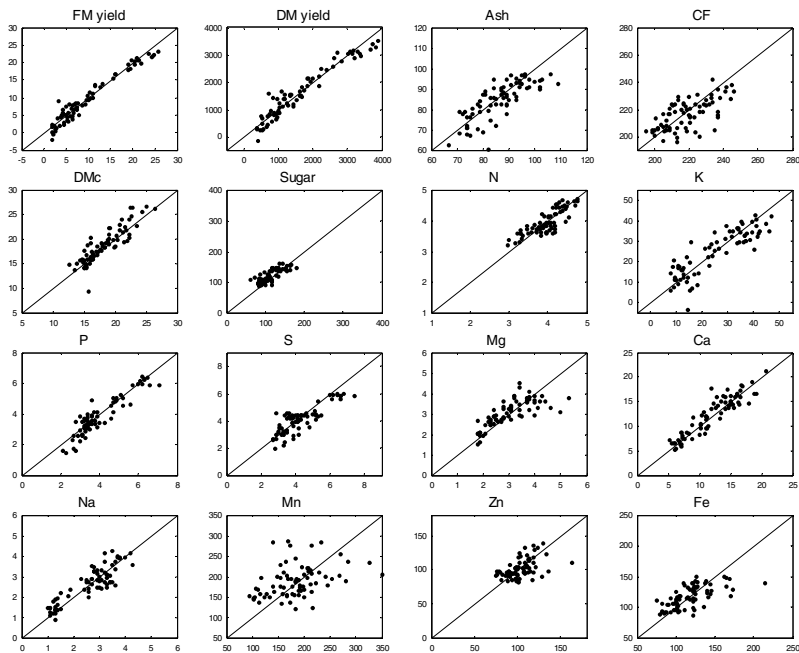


Figure 9.2 Measured values (on the x-axis) versus predicted values (on the y-axis) for experiment 1. The units can be found in Table 9.3.

lower than 2.5 for N, Na and Fe, whereas all other variables had a ratio above 2.5. In experiment 2, only N and Na had a ratio larger than 2.5. In figures 9.2 and 9.3, scatter plots are presented of model B with measured vs. predicted values of variables in experiments 1 and 2. In general, the predictions were reasonably well distributed around the 1:1 lines. This indicates that there was no discrepancy between the calibration and validation data sets, see also results of individual sensors in Table 9.5.

Table 9.8 Measurement accuracy of fresh grass analysis in the field (S_{FG}), Q^2 , root mean squared error of prediction (RMSEP) and the ratio between SD within the data set and root mean squared error of cross validation (RMSECV) for model B.

	Experiment 1				Experiment 2		
	S_{FG}	Q^2	RMSEP	SD/RMSECV	Q^2	RMSEP	SD/RMSECV
FM yield (t ha ⁻¹)	-	0.94	1.64	10.4	0.91	1.44	4.5
DM yield (kg ha ⁻¹)	-	0.93	268	7.7	0.93	235	5.1
Ash (g kg ⁻¹ DM)	4.2	0.53	6.46	2.9	0.76	5.84	2.5
CF (g kg ⁻¹ DM)	5.3	0.36	10.4	4.6	0.57	8.36	2.2
DMc (g kg ⁻¹ FM)	*	0.69	16.8	9.8	0.65	9.6	2.7
Sugar (g kg ⁻¹ DM)	*	0.58	16.2	6.5	0.84	27.7	4.4
N (g kg ⁻¹ DM)	1.0	0.67	2.4	1.4	0.80	3.4	4.0
K (g kg ⁻¹ DM)	1.0	0.75	6.01	6.0	0.37	5.12	1.4
P (g kg ⁻¹ DM)	0.11	0.82	0.50	5.3	0.45	0.62	2.4
S (g kg ⁻¹ DM)	*	0.67	0.66	3.3	0.82	0.70	2.7
Mg (g kg ⁻¹ DM)	0.10	0.57	0.53	4.2	0.69	0.37	1.7
Ca (g kg ⁻¹ DM)	*	0.84	1.55	7.2	0.09	1.34	1.4
Na (g kg ⁻¹ DM)	0.41	0.78	0.43	2.4	0.58	0.81	4.8
Mn (mg kg ⁻¹ DM)	*	-0.01	50.8	4.2	0.77	16.0	1.4
Zn (mg kg ⁻¹ DM)	*	0.14	14.7	3.9	0.65	5.67	1.2
Fe (mg kg ⁻¹ DM)	*	0.42	19.5	1.4	0.61	29.3	2.4

* No BLGG repeatability data available

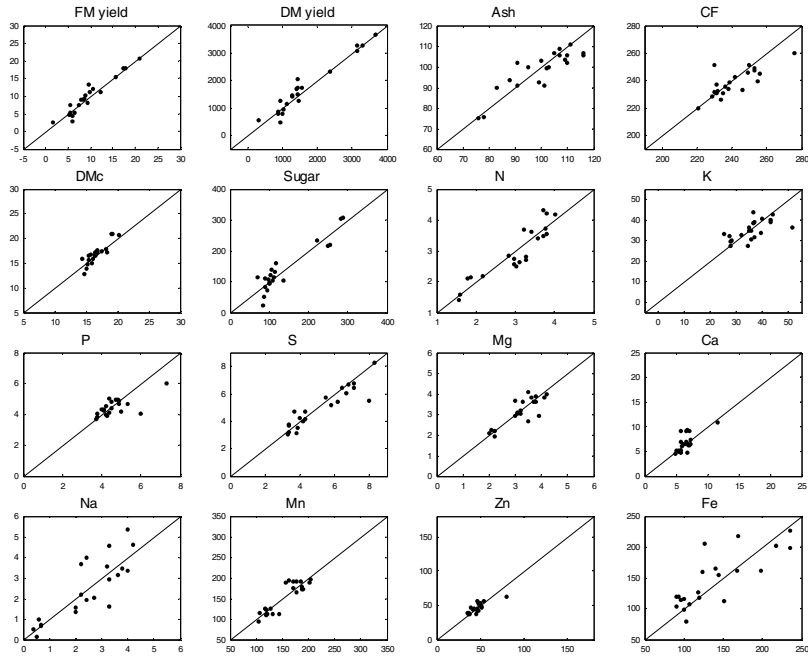


Figure 9.3 Measured values (on the x-axis) versus predicted values (on the y-axis) for experiment 2. The units can be found in Table 9.3.

9.3.6 Potential reduction in model errors for an example field

Under the assumption that the ratio between $RMSEP_B / RMSEP_M$ equaled 0.25 with 10 replicate measurements for an example field in the Netherlands (Table 9.9), S_{IS} was smaller than S_{FG} for ash, CF and N, whereas K, P, Mg and Na were slightly larger than S_{FG} (compare Table 9.8 and 9.9). When the ratio between $RMSEP_B / RMSEP_M$ was 0.5, the error for CF became also slightly larger than S_{FG} . Although the spatial variation in the field considered was high ($660 \text{ kg DM ha}^{-1}$), the prediction error was low with 226 and $247 \text{ kg DM ha}^{-1}$ for a $RMSEP_B / RMSEP_M$ ratio of 0.25 and 0.5 respectively. Increasing the number of observations to 25 may further reduce this error to $151\text{--}184 \text{ kg DM ha}^{-1}$. For more homogeneous fields, e.g. with a standard deviation of $300 \text{ kg DM ha}^{-1}$, this error may be reduced to $128\text{--}162 \text{ kg DM ha}^{-1}$ for 10 observations, $95\text{--}142 \text{ kg DM ha}^{-1}$ for 25 observations and $80\text{--}134 \text{ kg DM ha}^{-1}$ for 50 observations.

Table 9.9 Potential RMSEP values (averaged over experiment 1 and 2) for imaging spectroscopy measurements in the field for two ratios (R) between $RMSEP_B$ and $RMSEP_M$ and three observation frequencies (N).

	R = 0.25			R = 0.5		
	N=10	N=25	N=50	N=10	N=25	N=50
FM yield (t ha ⁻¹)	1.69	1.11	0.83	1.80	1.29	1.06
DM yield (kg ha ⁻¹)	226	151	116	247	184	158
Ash (g kg ⁻¹ DM)	3.04	2.26	1.93	3.89	3.43	3.26
CF (g kg ⁻¹ DM)	5.21	3.76	3.14	6.40	5.44	5.08
DMc (g kg ⁻¹ DM)	6.1	4.6	4.0	8.0	7.2	6.9
N (g kg ⁻¹ DM)	1.6	1.1	0.9	1.9	1.7	1.6
K (g kg ⁻¹ DM)	2.41	1.87	1.65	3.27	2.98	2.89
P (g kg ⁻¹ DM)	0.25	0.19	0.17	0.33	0.30	0.29
Mg (g kg ⁻¹ DM)	0.19	0.15	0.13	0.26	0.24	0.23
Ca (g kg ⁻¹ DM)	0.30	0.19	0.13	0.30	0.19	0.13
Na (g kg ⁻¹ DM)	0.67	0.44	0.33	0.72	0.51	0.42

9.3.7 PLS β coefficient weights

There were broad spectral regions with high absolute values for PLS β coefficients (Figure 9.4, 9.5 and 9.6). For the 404-709 nm wavelength range, there were large differences in PLS β coefficient values between the experiments. For experiment 2, the patterns of the 404-709 nm wavelength range for N and DMc are similar, but mirrored with the abscissa. For DMc (Figure 9.5), weights were quite similar for the 960-1650 nm wavelength range in both experiments. The pattern of PLS β coefficients for DM yield was very irregular in experiment 1. For experiment 2, the higher (absolute) values were located at equivalent wavelengths as N concentration (Figure 9.4 and 9.6).

9.4 Discussion and conclusion

The partial least square models accurately predicted herbage mass, with a Q^2 value of 0.93. The mean prediction errors of the partial least square models for dry matter (DM) yield, using only spectral information from the wavelength range of 404-709 nm and 960-1650 nm, were 286 and 344 kg ha⁻¹ for

respectively experiments 1 and 2. This error was further reduced to 268 and 235 kg ha⁻¹ for experiment 1 and 2 when including (image estimates of) ground cover (GC) and index of reflection intensity (IRI) in the models.

The accurate predictions of herbage mass with only spectral information ($Q^2 = 0.85-0.91$) can be understood when considering the influence of canopy geometry, *i.e.* the horizontal and vertical arrangement of plant parts, on the measured reflection. Reflection intensity of leaf pixels is directly related to height in the canopy and leaf angle, as result of the specific characteristics of the imaging spectroscopy system (Schut *et al.*, Chapter 2). Reflection curve characteristics, measured with the system, are directly related to reflection intensity (Schut & Ketelaars, Chapter 4). Schut & Van den Berg (Chapter 7) found that this relation differentiated clover (with more horizontally oriented leaves) from grass swards.

The predictive power of spectra in the 404-709 nm wavelength range was higher than in the 960-1650nm range. Predictive power was poor for the 680-970 nm wavelength range. The combination of 404-709 nm and 960-1650 nm spectra improved predictive power slightly, when compared to separate wavelength ranges. Including GC and IRI further improved predictive power.

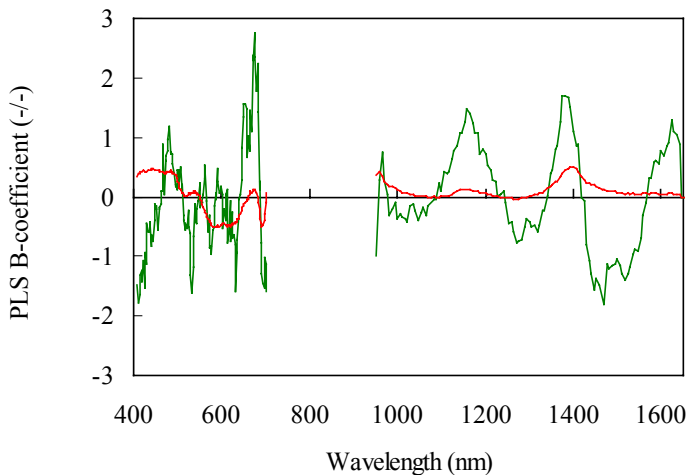


Figure 9.4 Values for PLS beta coefficient for N concentration regression in experiments 1 (green line) and 2 (red line) for the combined sensor model.

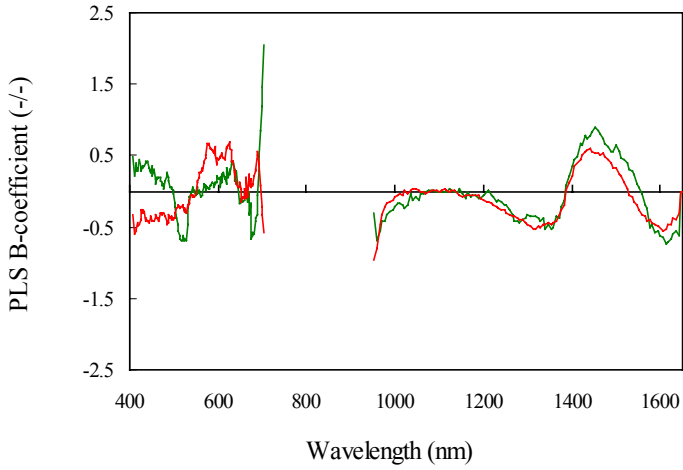


Figure 9.5 Values for PLS beta coefficient for DM content regression in experiments 1 (green line) and 2 (red line) for the combined sensor model.

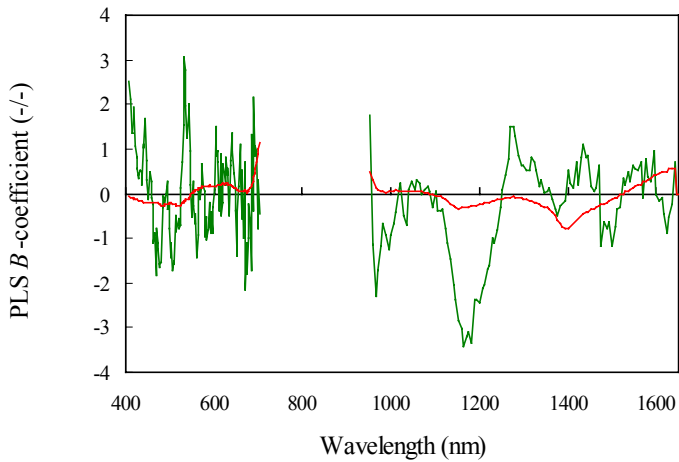


Figure 9.6 Values for PLS beta coefficient for DM yield regression in experiments 1 (green line) and 2 (red line) for the combined sensor model.

Schut & Ketelaars (Chapter 3) found that GC was curvilinearly related to herbage mass, where sensitivity was highest at low amounts of herbage mass. The combination of GC and IRI was linearly related to herbage mass. Including GC and IRI improved predictions more than including GC only.

The feeding value of fresh grass can be calculated with content estimates of N, DM content, ash, CF and sugar (Anonymous, 1998). The mean prediction errors for the best model in experiments 1 and 2 were: 2.4 and 3.4 g kg⁻¹ DM N, 16.8 and 9.6 g kg⁻¹ FM DMc, 16.2 and 27.7 g kg⁻¹ DM sugar, 6.46 and 5.84 g kg⁻¹ DM ash and 10.4 and 8.36 g kg⁻¹ DM CF. The mean prediction errors of the best model for experiment 1 and 2 were 6.0 and 5.1 g kg⁻¹ DM K, 0.5 and 0.6 g kg⁻¹ DM P, 0.7 and 0.7 g kg⁻¹ DM S, 0.5 and 0.4 g kg⁻¹ DM Mg, 0.4 and 0.8 g kg⁻¹ DM Na and 19.5 and 29.3 mg kg⁻¹ DM Fe. Predictions of Ca, Mn and Zn were poor. This predictive power resulted mainly from reflectance in the 404-709 nm wavelength range. The ratio between standard deviation in the data set and RMSECV of sugar was larger than 3.5 in experiments 1 and 2. This ratio was larger than 2.5 for ash, DMc and S in both experiments, and larger than 2.5 for N, K, P, Mg, Na in either experiment 1 or 2. Obviously, this ratio depends strongly on the variation within the data set. A ratio above 3.5 indicates that the calibrations can be used for quantitative analysis and a ratio above 2.5 indicates that the calibrations can be used for qualitative analysis (Sinnaeve *et al.*, 1994; Park *et al.*, 1998). It is concluded that calibrations of sugar allow quantitative analysis and calibrations of ash, DMc, N, K, P, S, Mg and Na allow qualitative analysis.

The predictability of nutrient contents can be understood when considering the accurate predictions of NIRS on undried grass silage (Sinnaeve *et al.*, 1994; Park *et al.*, 1998) and the strong correlations found with other variables such as DM yield and N concentration. These strong correlations originate from the dilution of nutrients when DM accumulates (Greenwood *et al.*, 1990; Lemaire *et al.*, 1989; Peeters & Van Bol, 1993). Prummel (1973), Hopkins *et al.* (1994) & McKenzie & Jacobs (2002) showed that N supply also affects nutrient concentration. Many authors found strong relations between reflectance and N supply at the leaf and canopy scale (Blackmer *et al.*, 1996; Daughtry *et al.*, 2000; Ercoli *et al.*, 1993; Everitt *et al.*, 1985; Pinar & Curran, 1996; Schepers *et al.*, 1996). Concentrations of Mg, Zn, Fe and Mn are also closely related to chlorophyll content and leaf reflectance (Adams *et al.*, 2000a; b; Mariotti *et al.*, 1996; Milton *et al.*, 1991; Gáborčík *et al.*, 2000). Gausman *et al.* (1973) & Graeff *et al.* (2001) found that with specific wavelength ranges deficiencies of N, Mg, Fe, P and S can be identified from leaf reflectance.

It is, therefore, concluded that the high predictability of nutrient concentrations were most likely the result of interactions between these nutrients and DM yield, DM content, N concentration and canopy geometry. Nevertheless, the Q^2 values of FM and DM yield, and contents of DM, ash, CF, sugar, N, K, P, S, Mg, Na and Fe allowed robust predictions in both experiments, in contrast to Mn, Zn and Ca.

In this study, there were no wavelength regions identified of particular importance for the prediction of a single variable. There were spectral regions with stronger positive or negative values for the estimated PLS coefficients, but the weights and locations of these regions differed between experiments and between DM yield, DM content and N concentration. Seasholtz & Kowalski (1990) concluded that ambiguities exist in the β coefficients of the PLS model as a result of interference with multiple absorbing constituents. Therefore, multiple spectral regions are required for the PLS model in order to extract the response of a single variable from the matrix of all variables that affect leaf reflectance.

It was calculated that with replicate measurements, the accuracy of imaging spectroscopy for field application considerably improved. Replicate measurements average out the random error component of the predictions, whereas the model bias does not change. Van der Voet (personal communication) found that the model bias contributed a fraction of 0.03 to 0.3 to the total model error. The amount of noise in the spectra recorded with the experimental system is likely to be larger than in spectra recorded with instruments under controlled laboratory conditions. Smoothing of the spectral data (with cubic splines) hardly changed the results (mean Q^2 value deviation between smoothed spectra and raw spectra of 0.008 and 0.005 in experiment 1 and 2 respectively). It is, therefore, unlikely that spectral noise is an important factor for the analysis in this paper. Under the assumption that this model bias contributed an intermediate (0.25) and high (0.5) fraction to the total model error, it was shown that capability of replicate measurements within one field reduced prediction error strongly. Increasing the number of measurements reduces prediction error stronger when model bias is low. It was calculated for a specific field that imaging spectroscopy with a low fraction of model bias and 50 replicate measurements was more accurate for ash, CF, N and Na than laboratory analysis of a single, composite fresh grass sample. Laboratory analysis was more accurate for K, P and Mg. Economic considerations limit the laboratory analysis of fresh grass to one composite sample per field. Therefore, large spatial variability will considerably decrease accuracy of laboratory

determination. Imaging spectroscopy does not have this disadvantage as the number of observations can be expanded without additional cost for analysis.

Nutrient concentrations are considered sufficient for both grass and animal production when above 25 g kg⁻¹ DM K, 3 g kg⁻¹ DM P and 2 g kg⁻¹ DM for Na, Mg and S (Anonymous, 1999; Bakker *et al.*, 2000). The difference between these thresholds and the 2001 nutrient means in fresh grass (measured by BLGG) equaled 1.8 and 2.1, 2.6 and 2.1, 3.2 and 3.0, 1.1 and 1.6 and 0.9 and 0.5 times RMSEP for K, P, S, Mg and Na in experiment 1 and 2 respectively. These distances increased with 50 observations and low model bias to 6.7, 7.6, 2.3 and 1.2 times RMSEP for K, P, Mg and Na respectively. It is concluded that for practical purposes with replicate measurements the accuracy for K, P and Mg permits, therefore, identification of deficiency levels, in contrast to Na.

The required accuracy of DM yield predictions for fertilisation and planning practices on the farm amounts to 10% (mean deviation from the actual yield) (Sanderson *et al.*, 2001; Lokhorst & Kasper, 2001). The mean prediction error found for DM assessment (<270 kg DM ha⁻¹) is promising for development of on-farm applications, especially when considering that these errors may be strongly reduced. With 25 replicate measurements within one field, the error could be reduced to 151-184 kg DM ha⁻¹ for fields with a standard deviation of 660 kg DM ha⁻¹ and 95-142 kg DM ha⁻¹ for fields with a standard deviation of 300 kg DM ha⁻¹. These results are an improvement over other, currently available non-destructive methods. Gabriels & Van den Berg (1993) reported a residual standard error of about 450 kg DM ha⁻¹ at 1600 kg DM yield for a combination of the capacitance probe and rising plate meter in *Lolium perenne* L. swards, while errors further increased at higher DM yields. Harmoney *et al.* (1997), Sanderson *et al.* (2001) & Virkajärvi (1999) found an even lower accuracy for various methods.

It is concluded that imaging spectroscopy provides robust and accurate means for assessment of DM yield and feeding quality of standing grass. The potential assessment accuracy with replicate measurements in the field of crude fiber and ash content, N and Na concentration in the field is satisfactory. The accuracy of K, P, S and Mg allows identification of nutrient deficiency. This opens up new means for improvement of grassland management and fine-tuning of rations of dairy cattle in the grazing season. The data sets were obtained from experiments with only *Lolium perenne* L., without grazing. Therefore, the methodology requires further testing under field conditions, including a range of grass species and management practices.

10

General discussion

10. General discussion

In this Chapter, the results from the previous Chapters will be evaluated and discussed. Some general conclusions are drawn relating to the objectives stated in the general introduction concerning system design and operation (10.1), information from imaging spectroscopy (10.2) and imaging spectroscopy in grass swards (10.3). In section 10.4 perspectives of imaging spectroscopy and recommendations for field-based systems are discussed.

10.1 System design and operation

The system for imaging spectroscopy designed operates within the 405-1659 nm range, with spectral resolutions between 5 and 13 nm and spatial resolutions ranging from 0.28 - 1.45 mm² at soil level. This spectral range was chosen to include various absorption features responsive to changes in pigment and O-H, C-H or N-H bonds. The combination of dispersing elements with charge coupled devices (CCD), allowed instantaneous measurements in combination with high spatial and high spectral resolution with a large number of spectral bands (Herrala and Okkonen, 1996).

The system design was strongly determined by the high irradiation requirements of the sensors. Therefore, light-sources in combination with bar lenses and nadir illumination were used, positioned relatively close to the crop for adequate irradiation levels. The small angle between projected light and reflected light that was detected by the system determined that the system records reflection in the hotspot.

Spatial resolution

In most periods of the growing season, ground cover of grass swards is incomplete (Chapter 2; Alberda, 1968). Therefore, remote sensing applications with a low resolution contain pixels of grass swards that are a mixture of soil, grass leaves and dead material. In the described imaging spectroscopy system, pixel width is much smaller than leaf width of *Lolium perenne* L., strongly reducing the number of pixels affected by background characteristics (dead material in the sward and soil). As shown in Appendix I, increasing pixel width (lowering spatial resolution) not only increased background influence, but also altered various spectral characteristics. The amplitude of this effect depended

on the width of the pixels on the image line, wavelength and background characteristics. The effects of pixel width were larger for stressed swards than for control swards.

Classification procedure

In Chapter 2, thresholds were defined for identification of classes differentiating soil, dead material and green material with and without specular reflection. Based on the spectral characteristic, grass could be easily distinguished from soil and dead material by simple thresholds and ratios. Pixels were further subdivided into intensity classes. The distribution of pixels over these intensity classes differentiated images of a production sward from sports-field images. The fraction of pixels in intensity classes with high reflection intensity, which is called the index of reflection intensity (IRI), responded to vertical sward geometry. There were no improvements in the predictions of the variables studied in Chapter 9 when including cover fractions of all intensity classes when compared to including only GC and IRI. Therefore, it is concluded that IRI described most of the relevant information present in the distribution of pixels over intensity classes. It must be noted that IRI is sensitive to the choice of intensity class boundaries. Another approach would be to functionally characterise the distribution of pixel reflection intensity in a specific spectral band within image lines, without prior classification, but this possibility was not further investigated.

The classification procedure with simple thresholds and ratios resulted in satisfactory classification results, although pixels with erroneous spectra were not excluded. These erroneous pixel spectra can strongly influence the mean spectral curve of a sward. Therefore, maximum likelihood procedures were used, selecting spectra within explicit ranges of acceptance.

Sampling pattern

One of the objectives of this thesis was to characterise grass swards. A sampling scheme per mini sward was chosen in order to record representative figures and reduce sampling time and disk space. The choice of this sampling scheme was to a certain extent arbitrarily. However, the outer 10 cm from each mini sward was excluded from the sampling scheme, in order to minimise biased observations arising from side effects. Image lines were recorded from the inner part (50 cm wide and 70 cm long) of mini swards in a regular pattern,

with 5 cm distance between image lines. Recordings were made in three lanes, resulting in 42 image lines per mini sward. This sampling pattern excluded a full hyperspectral analysis in 2 spatial dimensions. In Appendix I, it is shown that the inaccuracy resulting from the sampling scheme was limited for dense swards, when compared to adjacent image lines. This inaccuracy was larger for heterogeneous swards.

It is important to consider that the choice of sampling pattern definitely influenced the heterogeneity measures described, although repeatability of GC estimates was high with a coefficient of variance of 1.9% for GC (Appendix I).

System characteristics

Reflection intensity increased with leaf height position in the canopy, resulting from the combination of distance and the effects of a slightly diverging light beam (Chapter 2). With this feature, images of a production sward could be easily distinguished from images of sports-field swards. Reflection intensity was also strongly affected by leaf angle. Body reflection of nearly vertical leaves is a factor 4 lower when compared to horizontal leaves. The intertwined effects of leaf angle, irradiation-level and leaf height position in the canopy required a large dynamic range of the camera. Unfortunately, the peaky pattern of (xenon) light sources consumed part of the available dynamic range. This resulted in limited sensor sensitivity, which affected various image parameters. The resulting variation in reflection masked intrinsic spectral differences between leaves. Normalisation, taking ratios at pre-defined wavelengths, was expected to remove most of this intensity variation. Polder *et al.* (2002) described a colour-constancy method, *i.e.* taking ratios of the sum of the complete spectrum per sensor. This method and *e.g.* base-line correction could not be used, due to limitations in dynamic range of the sensors *i.e.* there was not sufficient signal at all wavelengths in “dark” pixels. Therefore, ratios were taken at wavelengths with high reflectance that were minimally affected by absorption features.

Error sources in imaging spectrometry systems

Jørgensen (2002) identified and summarized a large number of potential error sources with imaging spectroscopy systems. The most important error sources were related to distortions in the horizontal and vertical direction of the image and noise. Therefore, neighboring pixels have effect on the spectral information

of the pixel under consideration. The influence of this image-distortion is expected to be relatively small, as spectral information was averaged over a large number of pixels on various image line positions. These image-distortions become important when considering spectra of single pixels, and appropriate calibrations should be performed with regard to x and y location on the CCD (Jørgensen, 2002; Polder & Van der Heijden, 2001). The approach of Borregaard *et al.* (2000), of using only spectra of those pixels at the centre of leaves, may decrease the importance of this error source.

10.2 Information from imaging spectroscopy

From our experimental imaging spectroscopy system, we had 4 different types of information available: ground cover, reflection intensity, spectra and image texture. Spectral information was available per intensity class. Texture was quantified on the scale of an image line and on the scale of a mini sward. Due to the sampling scheme used, resulting in collections of image lines rather than images, object shape could not be used as information source. Various parameters were identified to quantify these information sources (Table 10.1).

GC and IRI

Variation in crop density is reflected in GC and IRI. The GC estimated from images was an underestimation of the visually estimated GC. In the lower GC range, this was probably due to the overestimation of the fraction of dead material, and in the higher range due to limited exposure times when the camera was light saturated. The IRI strongly responded to changes in leaf angle and crop height.

Texture

In this thesis, texture analysis was limited to sequences of parameter-values within and between image lines. This resulted in transects with various sampling patterns and frequencies. Transects were quantified in terms of correlation between spatially separated pixels with a defined distance and wavelet entropy of reflection intensity. Wavelet entropy is defined as Shannon entropy of the relative wavelet energy distribution over various wavelet

Table 10.1 Identified and studied image parameters.

Parameter description	Abbreviation	Unit	Chapter
-----ground cover-----			
Ground cover of green material	GC	%	2-9
Ground cover 1 th intensity class	GCG ₁ / GCS ₁	%	2
Ground cover dead material	GCD	%	2, 8
Logistically transformed GC	TGC	-/-	4, 5, 6, 8
-----reflection intensity-----			
Mean sward reflection in <i>n</i> bands	MSS	%	2-9
Mean sward reflection in <i>n</i> bands per intensity class	MICS	%	2-7
Index of reflection intensity	IRI	%	2-9
-----texture-----			
GC-Spatial standard deviation	GC-SSD	%	4, 5, 6, 8
TGC-Spatial standard deviation	TGC-SSD	-/-	4, 5, 6, 8
GC-wavelet entropy	GC-WE	-/-	8
Image line - wavelet entropy	IL-WE	-/-	7
Correlation between pixel reflection intensity within an image line	IL-corr	-/-	7
Cover of continuous green area with minimum width	IL-filter	%	7
-----spectra characteristics-----			
Half height position on blue, green and red edge	BE, GE, RE	nm	4, 5
Ratio between red and blue reflectance	<i>R</i> / <i>B</i>	-/-	5
Slope of relation between intensity class and edge position	<i>b</i>	Class nm ⁻¹	5, 7
Position of minimum or maximum derivatives	λ_i	nm	6
Slope at position of minimum or maximum derivatives	$d\lambda_i$	nm	6

frequencies (Rosso *et al.* 2001). Sequences in reflection intensity within image lines are related to leaf-orientation and leaf-size, and can be used to quantify canopy types (grass, clover and mixtures of grass and clover). Sequences of image line GC were used to quantify patchiness. GC values are bounded between zero and one hundred with low variation at both low and high crop

densities, masking variation in plant and tiller density. Therefore, values of $GC / (1 - GC)$ were logarithmically transformed in order to increase variation at high and low GC values.

Spectral information

In the recent past, understanding of the effect of cellular arrangement, water- and pigment content on leaf reflectance has resulted in accurate reflectance models (Jacquemoud *et al.*, 1996; Maier *et al.*, 1999). These models do not include pigments other than chlorophyll and require information about leaf structure. Fourty (1996) found that leaf optical properties of dry leaves may be modeled from explicit description of leaf biochemistry with sugar, cellulose and hemicellulose as main components. The effects of leaf dry matter components and leaf water content were, however, less clear for fresh leaves (Baret & Fourty, 1997).

Information from the spectral curves available was described with various methods. Spectral bands were recombined with principal component analysis and partial least squares, including all spectral bands available in the analysis. These approaches are statistical by nature, and require relatively large data sets as reference to understand parameter responses.

The spectral edges (BE, GE and RE) were defined as the wavelength at which reflection is equal to a predefined fraction of the difference between the minimum and maximum reflection of the edge. This provided a robust estimate of edge position, responsive to changes at both minimum and maximum, and the curvature of the edge. In literature, various methods are described for characterising reflection curves, such as fitting functions to edge regions and calculation of derivatives or indices. Fitting a Gaussian function to the edge region is limited to edges with a more or less Gaussian shape (Bonham-Carter, 1988). Obviously, this approach is suitable for the BE and RE, but not for the GE. Polynomials (*e.g.* cubic splines) do not have this limitation (Railyan & Korobov, 1993). Horler *et al.* (1983) used derivative analysis to characterise spectral changes in the red edge region. In Chapter 6, derivative analysis was used on MSS (transformed with cubic splines) to quantify changes in spectral characteristics. It was found that position of minimum and maximum derivatives depends on the degree of smoothing, agreeing with Rollin & Milton (1998). The half-height red edge and maximum derivative at the red edge were closely correlated ($r=0.95$, Table 10.2). The relative low correlation coefficients between BE, GE and RE (and also between λ_{517} , λ_{570} , and λ_{705}) indicate that

these spectral regions contain different information. In Chapter 6, it was found that response of λ_{570} and λ_{705} was very different under severe drought stress, where λ_{705} increased and λ_{570} decreased. The edge half-height is closely related to the position of maximum derivatives with correlation values of 0.89, 0.80 and 0.95 for the BE, GE and RE respectively. The CAW is slightly stronger affected by GE than RE, whereas the difference between λ_{705} and λ_{570} is stronger affected by λ_{705} than λ_{570} .

There exists a strong relation between spectral characteristics and reflection intensity (*i.e.* intensity classes) in data recorded with the experimental system (Chapter 4, 5 and 7). Leaf angle distribution was probably the most important factor affecting this relation, reinforced by system specific limitations in dynamic range. This is illustrated by the clear differences in the relation between spectral characteristics and reflection intensity between grass and clover swards with contrasting leaf angle distributions and the strong response to the circadian rhythm of cloverleaf opening and closure (Chapter 7).

The ratio between reflection at red and blue wavelengths responded to leaf angle and nitrogen supply (Chapter 5). Combinations of this ratio, the relation between reflection intensity and edge position, and CAW may be useful to separate effects of leaf angle from pigment concentration.

Table 10.2 Correlation coefficients between spectral parameters of edge half-height (BE, GE, RE) and position of minimum or maximum derivatives (λ_{517} , λ_{570} , λ_{705}) at these edges of mean sward spectra recorded just before harvest in the drought- and nitrogen experiments in 2000 and 2001.

	BE	GE	RE	λ_{517}	λ_{570}	λ_{705}	CAW
GE	-0.47						
RE	0.56	-0.49					
λ_{517}	0.89	-0.77	0.62				
λ_{570}	-0.18	0.80	-0.45	-0.55			
λ_{705}	0.54	-0.51	0.95	0.61	-0.51		
CAW	0.58	-0.93	0.78	0.82	-0.77	0.78	
$\lambda_{705} \cdot \lambda_{570}$	0.50	-0.65	0.91	0.66	-0.70	0.97	0.86

10.3 Imaging spectroscopy in grass swards

Light interception

In grass swards, GC was strongly related to light interception (for dense swards: $R^2_{\text{adj}}=0.87-0.94$). The relation between GC and light interception was a function of cloudiness, linear under a cloudy sky and more logistic under a clear sky. Haverkort *et al.* (1991) found a linear relationship between GC and LI for potatoes, whereas Van der Zaag (1984) described a non-linear relation. Van Delden (2001) argued that for potatoes, light interception was non-linearly related to GC and that ‘this non-linearity can be explained by clustering of the leaves’. It must be noted that these authors did not differentiate between recordings at cloudy and clear sky conditions.

The parameters in the relations between GC and light interception under clear and cloudy sky conditions differed for heterogeneous and homogeneous swards. At similar GC values, heterogeneous swards had a lower light interception than homogeneous swards under clear sky conditions. Under a cloudy sky, heterogeneous swards intercepted more light than homogeneous swards when GC was below 55% and less when above 55%. This may be understood when considering that swards are taller within a patch in heterogeneous swards than in homogeneous swards at similar GC values. When considering multiple angles of incident light, occurring under a cloudy sky, taller swards may compensate for the fraction of light that falls on bare soil. The total leaf surface exposed to sunlight may then be larger for heterogeneous swards than for homogeneous swards in the lower GC range, *i.e.* it is less important where leaf elements are located. Goudriaan & Van Laar (1994) proposed a clustering factor that lowers the extinction coefficient in the relation between LAI and light interception. This clustering factor should, therefore, also depend on the directional distribution of the radiation reaching the crop.

Horizontal sward structure and canopy geometry

The canopy structure is defined as the distribution and arrangement of the above ground plant parts within a plant community (Davies *et al.*, 1993). Laca & Lemaire (2000) distinguished horizontal and vertical sward structure. The horizontal sward structure was described with GC and the spatial distribution of GC. The vertical sward structure was partly described with IRI, although IRI responded primarily to height position and orientation of the top leaf layer.

Therefore, it is more appropriate to relate IRI to canopy geometry rather than to vertical sward structure.

The LAI is most commonly used to describe the horizontal and vertical sward structure (Laca & Lemaire, 2000; Denison & Russotti, 1997). Alternatively, relations between GC, IRI and LAI can be used. The LAI was curvilinearly related to GC ($R^2_{\text{adj}}=0.88$), limiting reliability of LAI estimates in the higher LAI range. The relation between logarithmically transformed LAI and GC, IRI and LAR was linear and slightly stronger ($R^2_{\text{adj}}=0.91$). Combining multiple viewing angles may further improve LAI estimates (Laca & Lemaire, 2000 and references therein).

Growth monitoring

It was found that the GC was a very sensitive parameter for monitoring growth under various conditions, GC differentiated mini swards in initial status, growth and growth rate. The sensitivity of GC for growth monitoring may be illustrated with stressed swards: drought stress decreased GC 'growth rate' even before changes in leaf water content were noticeable (Figure 6.2). Another example is the steady increase in GC at consecutive measurements and the similar changes in GC growth rate for various treatments in response to weather changes (Figures 3.7, 4.1, 5.1 and 8.4).

Seasonal mean ground cover was strongly related ($R^2_{\text{adj}}=0.77$, Figure 8.2) to seasonal dry matter yield (SDM). These seasonal mean GC values were similar to data from Alberda (1968). An increase of 1% GC raised SDM with 0.31 t DM ha⁻¹, corresponding with a value that can be expected (0.33 t DM ha⁻¹ per percent GC increase) from an increase in light interception.

Within a growing period, IRI values strongly increased when GC values were above 60% for homogeneous swards (Figure 3.11). Therefore, IRI values could be used to monitor and differentiate mini sward in the higher DM yield range. Seasonal mean IRI was strongly related to seasonal dry matter yield. Even more variation was explained when combining seasonal means of GC and IRI ($R^2_{\text{adj}}=0.89-0.93$). Therefore, it is concluded that GC and IRI contain additive information about the process of biomass accumulation.

Dry matter yield

Obviously, the relation between dry matter yield and GC had a curvilinear nature ($R^2_{\text{adj}}=0.82-0.91$, Chapter 3 and Appendix II). It was concluded that IRI

is sensitive to lodging (Appendix II). Combining GC and IRI yielded stronger relations with DM yield ($R^2_{\text{adj}} = 0.82\text{-}0.95$, Chapter 2, 4 and Appendix II).

The mean deviation from the regression line equalled 305-340 kg DM (within the range of 292-4075 kg DM ha⁻¹). Mean sward spectra from the V7 and N17 sensors also contained information about DM yield (Chapter 9). In the validation sets, mean errors of prediction for the sward damage and nitrogen experiment in 2000 were 286 - 344 kg DM ha⁻¹. Combining spectral information with GC and IRI further reduced these prediction errors to 235 - 268 kg DM ha⁻¹.

These prediction errors were much smaller than the errors in the relation between DM yield and crop height or CropsScan NDVI and WDWI. The discriminating ability of NDVI is severely limited above 1800-2000 kg DM ha⁻¹. The WDWI and crop height were linearly related to DM yield, but a large amount of variation remained unexplained (Appendix II; King *et al.* 1986; Lokhorst & Kasper, 2001). Including all available CropsScan bands in the regression equations increased the amount of explained variation, although even more variation was explained with the experimental imaging spectroscopy system.

The required accuracy of DM yield predictions for fertilization and planning practices on the farm is about 10% (mean deviation from the actual yield) (Sanderson *et al.*, 2001; Lokhorst & Kasper, 2001). The mean prediction error found for yield assessment is promising for development of on-farm applications, especially when considering that these errors may be reduced by 27 to 40% with 25 replicate observations. These results are an improvement over other, currently available non-destructive methods such as rising plate meter or capacitance probe (Gabriels & Van den Berg, 1993; Harmoney *et al.*, 1997; Murphy *et al.*, 1995; Sanderson *et al.*, 2001; Stockdale & Kelly, 1984; Virkajärvi, 1999).

Sward spatial heterogeneity

Sward heterogeneity was studied for three types of swards: (dense) control swards, artificially damaged swards, and naturally damaged swards. These groups differed significantly in mean tiller density and in spatial variation of tiller density and light interception. This spatial heterogeneity was also present in the images, although image heterogeneity faded during growth. This means that growth stage or GC has to be taken in consideration for interpretation of

image heterogeneity measures (Figure 8.8). Both spatial GC-SSD and patterns in GC estimates were stronger for damaged swards than for control swards.

Calculating seasonal means over intervals after harvest of GC-SSD and TGC-SSD significantly differentiated damaged from control swards. The heterogeneity measures were found to be insensitive for the short term effects of drought- and nitrogen stress, as GC-SSD and TGC-SSD in these experiments were comparable to the values for CS in the sward damage experiment and nitrogen treatments were not different in GC-SSD and TGC-SSD (Chapter 4, 5 and 6).

Ground cover transects of highly yielding swards had a lower wavelet entropy than transects of poorly yielding swards. This indicates that the GC variation present was distributed over more wavelet frequencies (read scales) in low yielding swards than in high yielding swards. It must be noted that there is a strong resemblance between the GC wavelet entropy derived from images and the tiller absence frequency distribution over core samples of various sizes (Neuteboom *et al.*, 1992), as both methods quantify differences in tiller density over multiple scales.

In this thesis, seasonal dry matter yield (SDM) was used as quantitative measure of sward quality. As mentioned above, a combination of seasonal mean GC and IRI explained more variation in SDM than heterogeneity parameters. However, values of SDM and seasonal mean GC and IRI are expected to be sensitive to sward management such as grazing, cutting frequency and nutrient application level, in contrast to spatial heterogeneity measures. Although spatial GC heterogeneity was related to SDM ($R^2 = 0.59-0.71$), discriminating power of this relationship was unsatisfactory with standard errors of observations between 1.1 and 1.3 ton DM ha⁻¹ yr⁻¹. Alternatively, assessment of sward quality with seasonal means of GC and IRI can be done with a reference, *i.e.* an estimate of optimal seasonal mean values of GC and IRI for the given sward management. This reference may be derived from the best field on a farm, from the best location within a field or from accurate predictions of yield potential by grass growth models.

Detection of nitrogen deficiency

Nitrogen treatments differed in evolution of GC, IRI and spectral characteristics. The dynamics of edges (BE, GE and RE) at limited N supply differed from those at liberal N supply, agreeing with Blackmer *et al.* (1994), Schepers *et al.* (1996) and Masoni *et al.* (1997). The CAW at limited N supply

decreased in the second half of the growth period, in contrast to liberal N supply. The CAW was strongly exponentially related to relative dry matter yield at harvest ($R^2=0.95$, Chapter 5). The data points of the second harvests of the 2001 N experiment fitted well within this relationship, with relative yields of 20, 55 and 81% and a CAW of 116.4, 127.7 and 130.0 nm. The relative yields in the first harvest of 2001 were relatively low when compared to their CAW value (21.9, 41.2, 73.3% with a CAW of 100.1, 118.1, 125.8 nm for low, intermediate and high N supply respectively). This was probably due to N deficiency of the highest N supply treatment (Chapter 6), as indicated by low CAW values, low N contents in harvested material and low mineral N contents of the soil after harvest.

The differences in CAW were small under near optimal N supply. Higher N supply treatments (60, 90 and 120 kg N ha⁻¹) could, therefore, not be separated from each other for all growth periods. The relation between N supply and chlorophyll (Chl) concentration has a curvilinear character (Wood *et al.*, 1992; Kantety *et al.*, 1996) and reflection decreases asymptotically with increasing Chl (Everitt *et al.*, 1985; Boochs *et al.*, 1990; Ercoli *et al.*, 1993; Schepers *et al.*, 1996). Gitelson *et al.* (1996) found that 'variation of inflection point position with change in chlorophyll content was small for yellow-green to dark green leaves'. Therefore, identification of near-optimally N-fertilised swards with leaf reflectance alone remains difficult.

The relative DM yield was also strongly related to principal components of mean sward spectra. However, principal components were also strongly related to DM yield and N concentration. This intertwined response of principal components to DM yield, N concentration and leaf colour made interpretation difficult. Therefore, detection of N stressed swards under a range of harvesting frequencies requires extensive calibration and validation in order to correct for differences in DM yield, related to the length of the growth period rather than N deficiency.

Horizontally oriented leaves had lower CAW values than vertically oriented leaves (Chapter 5). CAW values increased slightly after harvesting at 16 cm above the soil, resulting in a larger fraction of vertical canopy elements becoming visible (Chapter 5). The decrease in CAW in the second half of the growth period resulted, therefore, from an intertwined response of changes in leaf angle and leaf color, although the strongest changes in leaf angle (due to lodging, see Appendix II) occurred under high N supply where decrease in CAW was smaller than at low N supply. Discriminating power of reflectance measurements may, therefore, be improved when combining red/blue ratio,

slope of the relation between reflection intensity and edge position, and CAW in order to separate effects of leaf angle from effects of pigment concentration.

Detection of drought stress

Drought stress became first visible in retarded GC development. Within a growth period, all absorption features visible in reflectance spectra between 400-1650 nm deepened and widened in unstressed swards. Under drought stress, all absorption features became shallower and narrower again (Chapter 6, Ripple, 1986; Bowman, 1989; Inoue *et al.*, 1993; Penuelas & Inoue, 1999). Water absorption features (with maximum light absorption near 970, 1200 and 1450 nm) responded earlier to drought stress than absorption features in the visible wavelength range, agreeing with Carter (1991, 1993). From the moment that leaf DM content of drought-stressed swards deviated from unstressed swards, also inflection points near 960, 990, 1140, 1390 and 1500 nm differed significantly.

Moderate drought stress did not change the position of inflection points in the green and red wavelength ranges, in contrast to the slope near these inflection points, agreeing with data of Penuelas *et al.* (1994). These absorption features did respond at more advanced stages of drought when GC already decreased. This was probably due to chlorophyll breakdown and decreased light absorption of chlorophyll (Carter, 1991). Drought stress accelerated the increase of IP position near 705 nm up to harvest (Chapter 6; Penuelas *et al.*, 1993; Horler *et al.* 1983). Horler *et al.* (1983) discussed that this shift might result from changes in internal leaf structure.

In presence of a control, drought stress can be identified by means of comparison of GC and IP position. With repeated measurements in time, the reversed shift of IP position can identify drought-stressed swards. The IP position showed a clear evolution during unstressed growth. Therefore, growth stage should be taken into consideration when interpreting IP positions without a control. The relation between the IP position near 705 and 1390 nm provided such a growth stage reference, and with this relation, unstressed swards shortly after harvest can be differentiated from drought-stressed swards in a later growth stage.

Estimation of clover content in swards with white clover and grass

Mixed swards have a patchy character, where both grass and white clover dominated patches oscillate (Schulte, 2001), resulting from delayed N transfer (Loiseau *et al.*, 2001). For an estimate of white clover content in mixed swards, it is probably sufficient to count the area in a limited number of classes *e.g.* clover and grass dominated patches and mixed patches.

Separation of white clover from grass swards based on spectral characteristics was unsuccessful. Pixel spectra were highly variable, even within single intensity classes where variations in leaf angle are limited. Zwiggelaar (1998) argued that combinations of a number of wavelengths can reduce this variability, but then results might not be robust in time or in space. Differences in characteristics of the mean sward spectra occurred between grass and clover. Unfortunately, these differences varied in time and responded to nutrient supply.

The relation between reflection intensity and (GE) edge position was clearly different for grass and clover swards. This relation changed remarkably for white clover swards when leaves folded, due to the circadian rhythm of leaf opening and closure (Baker & Williams, 1987). In Chapter 5 it is concluded that leaf angle is the most important factor in the relation between edge position and reflection intensity.

Alternatively, image line texture can be used to identify white clover and grass dominated patches. Grass and white clover swards were successfully discriminated by correlation of reflection intensity of distant pixels, a filter and wavelet entropy. Estimates of clover content within a mixture varied within a growing period, as clover leaves dominate shortly after cutting and grass leaves in the second half of the growth period. Amongst the three methods studied, the wavelet entropy method was least sensitive to temporal changes in canopy geometry. Bradshaw & Spies (1992) showed that different canopy types had different patterns of wavelet variance. Therefore, it was expected that specific wavelet scales could be used to uniquely identify specific leaf types. The results show that, in general, there is a clear difference between grass and clover, but that no specific wavelet scale dominates. This means that the occurrence of other species in the sward may affect the wavelet entropy. The value of wavelet entropy was found to be insensitive to the degree of sward damage.

Estimation of feeding value and nutrient content

The feeding value of fresh grass can be calculated with content estimates of N, DM, ash, CF and sugar (Anonymous, 1998). The prediction errors relative to the mean (of validation sets) in the sward damage and N experiment were 6.2-11.7% for N content, 5.5-9.1% for DM content, 13.6-18.7% for sugar content, 6.0-7.5% for ash content, and 3.5-4.8% for CF content (Chapter 9).

The difference between nutrient means in fresh grass samples and critical concentrations for cattle grass growth were, when compared to the prediction errors for nutrient concentrations, large enough to identify nutrient deficiency (Chapter 9). The predictability of nutrient contents can be understood when considering the accurate predictions of NIRS on undried grass silage and the strong correlations found with *e.g.* DM yield, N concentration and chlorophyll content (Chapter 9; Sinnaeve *et al.*, 1994; Park *et al.*, 1998; Prummel, 1973; Hopkins *et al.*, 1994; McKenzie & Jacobs, 2002; Adams *et al.*, 2000a; b; Mariotti *et al.*, 1996; Milton *et al.*, 1991; Gáborčík *et al.*, 2000). It was concluded that the high predictability of nutrient concentrations were most likely the result of interactions between these nutrients and DM yield, DM content, N concentration and canopy geometry. Nevertheless, the predictions of DMc, ash, CF, sugar and concentrations of N, K, P, S, Mg, Na and Fe were robust, in contrast to those for Mn, Zn and Ca.

It was calculated for a specific field that estimates with a low fraction of model bias combined with 50 replicate measurements were probably more accurate for ash, CF, N and Na content than laboratory analysis of a single, composite fresh grass sample. Laboratory analysis was more accurate for K, P and Mg. Economic considerations limit the laboratory analysis of fresh grass to one composite sample per field. Therefore, large spatial variability will considerably decrease accuracy of determination. Imaging spectroscopy does not have this disadvantage as the number of observations can be expanded without additional cost for analysis.

Selected image parameters for various agronomic variables of interest

Selected image parameters for various agronomic variables of interest are given in Table 10.3. It must be noted that not all (available) image parameters were compared for each agronomic variable, although the selected variables explained most of the variation.

Table 10.3 Selected image parameters for various agronomic variables of interest.

Agronomic variable of interest	Selected image parameters	Chapter
Growth, LI, LAI	GC, IRI	2
DM yield at harvest	GC, IRI, MSS	2, 9, Appendix II
Seasonal yield	Seasonal means of GC and IRI at harvest	8
N deficiency	CAW, edge position VIS	4, 5
Drought stress	Edge position NIR, edge position VIS, CAW	6
Clover content	Wavelet-IL, MICS-b	7
Spatial heterogeneity	GC/TGC-SSD	8
Feeding value and nutrient content	MSS, GC, IRI	9

10.4 Imaging spectroscopy in the field

Imaging spectroscopy can be a valuable tool for monitoring and evaluating experimental fields and comparison of treatments in research. The non-invasive character permits growth monitoring on individual experimental plots or fields and quantification of light interception, N and drought stress, spatial heterogeneity, dry matter yield and clover content of (grass) swards.

Imaging spectroscopy systems may also be useful in other agricultural crops. Obviously, growth monitoring, yield and nutrient content estimation and detection of deficiencies is important for management of most agricultural crops. The approach developed may be used for other crops, although applications in other crops again require calibration and validation for most relations described. In principle, imaging spectroscopy systems provides eyes to vision systems capable of detecting reflection in any wavelength, as long as a sensor and radiator are available. For example, ultraviolet reflection may be used to detect urine tracks of animals (Viitala *et al.*, 1995). The combination of high spatial resolution in 2D and hyperspectral information is highly suitable for detection of patterns within crops and even within leaves. An example of such a pattern is the nerve system within a leaf, clearly visible in strong water absorbing wavelengths. Also patterns within a plant or within a plant community or planting row can be made “visible” with such a system (Moshou *et al.*, 2001). These patterns may be linked to foliar pests and diseases and may be used to separate species or types of species, important for weed control and selective herbicide application.

Imaging spectroscopy may also be an important information source for fine-tuning grassland management on dairy farms. Grass sward management on farms largely depends on qualitative expert knowledge, which is derived from guidelines and rules of thumb. In the absence of measurement methods, farmers lack reliable feedback for evaluation and optimisation of various management decisions. For example, comparison of fields on and between farms may identify weak and strong points in sward management.

Imaging spectroscopy may also be used in a decision support system. Under pressure of environmental legislation, farmers will reduce N fertilisation levels to approximately 250 to 300 kg ha⁻¹ (Smit *et al.*, 2003). In this moderate N supply range, leaf reflection is responsive to changes in N supply. Then, differences between and within fields in N availability due to *e.g.* N mineralisation, delayed N release from previous slurry applications and urine and dung depositions during grazing, may be quantified. This provides means for fine-tuning timing and amount of N supplied to field, site or even spot specific conditions.

Important in this respect is the quantification of spatial (and temporal) heterogeneity and the relation between heterogeneity and reduction in dry matter yield and nutrient use efficiency. Spatial heterogeneity within a mini sward was well quantified with imaging spectroscopy. However, effects of botanical composition, management strategies and the self-recovery capacity of deteriorated swards require further study before conclusions can be made with regard to the implications for necessity of sward reseeding or renovation.

The successful separation of image lines recorded in white clover- and grass dominated swards and mixed swards allows quantification and monitoring of the fraction of white clover in a mixed sward (Chapter 7). The N yield (Elgersma *et al.*, 2000; Elgersma & Hassink, 1997; Elgersma *et al.*, 1997) and N₂ fixation per unit mass of clover dry matter is rather stable, even under varying N application (Velthof *et al.*, 2000; Van der Meer & Baan Hofman, 2000). Quantification of white clover content in mixed swards may, therefore, be linked with N₂ fixation and clover dry matter yield through its relation with ground cover (Schils *et al.*, 1999).

Calculations revealed that replicate measurements should allow accurate assessments of feeding value and nutrient contents. The accuracy of estimation of K, P, S and Mg content allows identification of nutrient deficiency. This opens up new means for improvement of grassland management and fine-tuning of rations of dairy cattle in the grazing season. Despite these encouraging results, it must be noted that the methodology requires further

testing under field conditions, including a range of grass species and management practices before final conclusions can be drawn.

System requirements

Application of an imaging spectroscopy system in fields on farms require a mobile system that allows fast and accurate image recording with high spatial coverage. The type of sensor depend on the use envisaged for the system. For quantification of GC, IRI and texture (with *e.g.* wavelet entropy) a simple 2D camera with *e.g.* 3 bands with high contrast between green material and soil will probably suffice. For instance, a 2D camera with spectral bands at 600, 710 and 800 combines a high contrast between green material and background and permits, therefore, easy recognition of green material. It is also sensitive for changes in chlorophyll content (600 and 710 nm) and leaf stacking (800 nm).

Such a sensor would be useful for *e.g.* the assessment of growth, light interception, clover content, yield level, and probably also of N stress. With a 2D system, classification routines based on object shape (*e.g.* clover or weed leaves) can be included.

Quantification of nutrient and drought stress and prediction of DM yield, feeding value and mineral content require hyperspectral sensors. Such a hyperspectral system must be able to record reflection in the 400-1650 nm range, preferably in image lines to maintain high spectral and spatial resolution within a spatial context. Ideally, both 2D and hyperspectral sensors are combined in one system, allowing both high spatial coverage and high spatial and spectral resolution. The system should be equipped with a global positioning system for visualisation of data and quantification of patterns on a spatial scale larger than one image line or 2D image.

Working speed and the advantages of replicate observations make image recording while driving attractive. Measurements under motion ask for special attention for exposure times of the cameras, in order to maintain high spatial resolution. Brief exposure requires high irradiation levels.

When using sunlight instead of artificial light sources, reflection intensity of leaves will vary with sky conditions and with the position relative to other leaves in the canopy, due to shadow en multiple reflections. This disturbs the relation between reflection intensity and height position. Therefore, the amount of light from the light sources on the crop should dominate the amount of light from the sun, and the system should exclude solar influence by working under dark or shadowed conditions. In the experimental system, the halogen light

source produces around $265 \mu\text{mol APAR m}^{-2} \text{ s}^{-1}$. At an solar angle of 42° with the horizon, the sun produces between 200 and $1400 \mu\text{mol APAR m}^{-2} \text{ s}^{-1}$ under cloudy and clear sky conditions respectively (J. Kornet, pers. comm.).

The specific character of the light conditions used in the experimental system provided valuable information about vertical canopy geometry. Canopy geometry was an important information source for various variables of interest. The light sources used in the experimental system had a vertically projected and slightly diverging light beam, resulting in lower irradiation close to the soil surface. In the experimental system, the dynamic range and sensitivity at low irradiation levels was limited. Therefore, it is required that the dynamic range of the cameras is large enough to measure the full spectrum of vertically oriented leaves, including those in low canopy positions. Currently, the Institute of Agricultural and Environmental Engineering together with Plant Research International are building such a mobile imaging spectroscopy system.



References

-
- Aarts H.F.M., D.W. Bussink, I.E. Hoving, H.G. Van Der Meer, R.L.M. Schils and G.L. Velthof, 2002. *Milieutechnische en landbouwkundige effecten van graslandvernieuwing*. Wageningen, Plant Research International, report 41A
- Adams M.L., W.A. Norvell, W.D. Philpot and J.H. Peverly, 2000a. Spectral detection of micronutrient deficiency in 'Bragg' soybean. *Agronomy Journal*, **92**, 261-268
- Adams M.L., W.A. Norvell, W.D. Philpot and J.H. Peverly, 2000b. Toward the discrimination of manganese, zinc, copper, and iron deficiency in 'Bragg' soybean using spectral detection methods. *Agronomy Journal*, **92**, 268-274
- Alberda T., 1968. Dry matter production and light interception of crop surfaces. IV. Maximum herbage production as compared with predicted values. *Netherlands Journal of Agricultural Science*, **16**, 142-153
- Anonymous, 1998. *Handleiding voederwaardeberekening ruwvoerders : richtlijnen voor de bemonstering van ruwvoerders en vochtrijke krachtvoerders en voor de berekening van de voederwaarde voor herkauwers*. Lelystad, the Netherlands, Centraal Veevoederbureau.
- Anonymous, 1999. *Tabellenboek veevoeding 1999 : voedernormen landbouwhuisdieren en voederwaarde veevoerders*. Lelystad, the Netherlands, Centraal Veevoederbureau.
- Asner G.P., 1998. Biophysical and biochemical sources of variability in canopy reflectance. *Remote Sensing of Environment*, **64**, 234-253
- Baars T. and M.J.H. Van Dongen, 1989. *Graslandbeheer gericht op optimalisering van witte klaver : een literatuurstudie*. Driebergen, Louis Bolk Instituut.
- Baker M.J. and W.M. Williams, 1987. *White clover*. Wallingford, United Kingdom, C.A.B. International.

- Bakker J., E. Van Huet Lindeman and W. Koopman, 2000. *Kuilen met kwaliteit*. Zutphen, the Netherlands, Roodbont Uitgeverij.
- Baret F., J.G.P.W. Clevers and M.D. Steven, 1995. The robustness of canopy gap fraction estimates from red and near-infrared reflectances: a comparison of approaches. *Remote Sensing of Environment*, **54**, 141-151
- Baret F. and T. Fourty, 1997. Estimation of leaf water content and specific leaf weight from reflectance and transmittance measurements. *Agronomie*, **17**, 455-464
- Baret F. and G. Guyot, 1991. Potentials and Limits of Vegetation Indexes for LAI and APAR Assessment. *Remote Sensing of Environment*, **35**, 161-173
- Bausch W.C., K. Diker, A.F.H. Goetz and B. Curtis, 1998. Hyperspectral characteristics of nitrogen deficient corn. In: *ASAE Annual International Meeting, Orlando, Florida, USA, 12-16 July*, Paper no. 983061 pp.
- Birnie R.V., P. Millard, M.J. Adams and G.G. Wright, 1987. Estimation of percentage ground cover in potatoes by optical radiance measurements. *Research and Development in Agriculture*, **4**, 33-35
- Biswal B., L.J. Rogers, A.J. Smith and H. Thomas, 1994. Carotenoid composition and its relationship to chlorophyll and D1 protein during leaf development in a normally senescing cultivar and a stay-green mutant of *Festuca pratensis*. *Phytochemistry*, **37**, 1257-1262
- Blackburn G.A., 1998a. Quantifying chlorophylls and carotenoids at leaf and canopy scales: an evaluation of some hyperspectral approaches. *Remote Sensing of Environment*, **66**, 273-285
- Blackburn G.A., 1998b. Spectral indices for estimating photosynthetic pigment concentrations: a test using senescent tree leaves. *International Journal of Remote Sensing*, **19**, 657-675

-
- Blackmer T.M., J.S. Schepers and G.E. Varvel, 1994. Light reflectance compared with other nitrogen stress measurements in corn leaves. *Agronomy Journal*, **86**, 934-938
- Blackmer T.M., J.S. Schepers, G.E. Varvel and E.A. Walter Shea, 1996. Nitrogen deficiency detection using reflected shortwave radiation from irrigated corn canopies. *Agronomy Journal*, **88**, 1-5
- Bonham-Carter G.F., 1988. Numerical procedures and computer program for fitting an inverted gaussian model to vegetation reflectance data. *Computers and Geosciences*, **14**, 339-356
- Boochs F., G. Kupfer, K. Dockter and W. Kuhbauch, 1990. Shape of the red edge as vitality indicator for plants. *International Journal for Remote Sensing*, **11**, 1741-1753
- Booij R., D. Uenk, C. Lokhorst and C. Sonneveld, 2001. Monitoring crop nitrogen status in potatoes, using crop light reflection. In: S. Blackmore, and G. Grenier (eds.). *Third European Conference on Precision Agriculture, Montpellier, France*, pp. 893-898
- Borregaard T., H. Nielsen, L. Norgaard and H. Have, 2000. Crop-weed discrimination by line imaging spectroscopy. *Journal of Agricultural Engineering Research*, **75**, 389-400
- Bouman B.A.M., A.H.C.M. Schapendonk and W. Stol, 1996. *Description of the growth model LINGRA as implemented in CGMS*. Wageningen, The Netherlands, DLO Research Institute for Agrobiological and Soil Research, quantitative approaches in system analysis, report 7
- Bouman B.A.M., H.W.J. Van Kasteren and D. Uenk, 1992. Standard relations to estimate ground cover and LAI of agricultural crops from reflectance measurements. *European Journal of Agronomy*, **1**, 249-262
- Bowman W.D., 1989. The relationship between leaf water status, gas exchange, and spectral reflectance in cotton leaves. *Remote Sensing of Environment*, **30**, 249-255

- Bradshaw G.A. and T.A. Spies, 1992. Characterizing canopy gap structure in forests using wavelet analysis. *Journal of Ecology*, **80**, 205-215
- Buckheit J., S. Chen, D. Donoho and I. Johnstone, 1995. *Wavelab reference manual*. Available on web page: <http://www-stat.stanford.edu/~wavelab/>.
- Büker C. and J.G.P.W. Clevers, 1992. *Imaging spectroscopy for agricultural applications*. Wageningen, the Netherlands, Wageningen Agricultural University,
- Buschmann C. and E. Nagel, 1993. In vivo spectroscopy and internal optics of leaves as basis for remote-sensing of vegetation. *International Journal of Remote Sensing*, **14**, 711-722
- Canova I. and N. Gaborcik, 2000. Chlorophyll and fluorescence of cocksfoot (*Dactylis glomerata* L.) and tall fescue (*Festuca arundinacea* Schreb.) leaves grown under different conditions of mineral nutrition. In: E. Uhliarova, M. Zimkova, and N. Gáborcik (eds.). *Grassland ecology V., Banska Bystrica, Slovakia 23-25 November 1999*, pp. 22-29
- Carter G.A., 1991. Primary and secondary effects of water content on the spectral reflectance of leaves. *American Journal of Botany*, **78**, 916-924
- Carter G.A., 1993. Responses of leaf spectral reflectance to plant stress. *American Journal of Botany*, **80**, 239-243
- Chappelle E.W., M.S. Kim and J.E. Mcmurtrey, 1992. Ratio analysis of reflectance spectra (RARS) - an algorithm for the remote estimation of the concentrations of chlorophyll-a, chlorophyll-B, and carotenoids in soybean leaves. *Remote Sensing of Environment*, **39**, 239-247
- Clevers J.G.P.W., 1989. The application of a weighted infra-red vegetation index for estimating leaf area index by correcting for soil moisture. *Remote Sensing of Environment*, **29**, 25-37

-
- Clevers J.G.P.W. and C. B ker, 1991. Feasibility of the red edge index for detection of nitrogen deficiency. In: *the 5th International colloquium - Physical measurements and signatures in remote sensing, Courchevel, France, 14-18 January*, pp. 165-168
- Clevers J.G.P.W. and W. Verhoef, 1993. LAI estimation by means of the WDVI: a sensitivity analysis with a combined PROSPECT-SAIL model. *Remote Sensing Reviews*, **7**, 43-64
- Critten D.L., 1997. Fractal dimension relationships and values associated with certain plant canopies. *Journal of Agricultural Engineering Research*, **67**, 61-72
- Curran P.J., 1989. Remote sensing of foliar chemistry. *Remote Sensing of Environment*, **30**, 271-278
- Curran P.J., J.L. Dungan, B.A. Macler, S.E. Plummer and D.L. Peterson, 1992. Reflectance spectroscopy of fresh whole leaves for the estimation of chemical concentration. *Remote Sensing of Environment*, **39**, 153-166
- Danson F.M., M.D. Steven, T.J. Malthus and J.A. Clark, 1992. High-spectral resolution data for determining leaf water content. *International Journal of Remote Sensing*, **13**, 461-470
- Daubechies I., 1992. *Ten lectures on wavelets*. Philadelphia, USA, Society for Industrial and Applied Mathematics.
- Daughtry C.S.T. and C.L. Walthall, 1998. Spectral discrimination of Cannabis sativa L. leaves and canopies. *Remote Sensing of Environment*, **64**, 192-201
- Daughtry C.S.T., C.L. Walthall, M.S. Kim, E.B.D. Colstoun, J.E. McMurtrey, Iii and E.B. De Colstoun, 2000. Estimating corn leaf chlorophyll concentration from leaf and canopy reflectance. *Remote Sensing of Environment*, **74**, 229-239
- Davies A., R.D. Baker and S.A. Grant, 1993. *Sward measurement handbook*. Reading, United Kingdom, British Grassland Society.

- De Wit C.T., 1965. *Photosynthesis of leaf canopies*. Wageningen, Pudoc.
- Deenen P.J.A.G., 1994. *Nitrogen use efficiency in intensive grassland farming*. Thesis, Wageningen Agricultural University, Wageningen, the Netherlands.
- Elgersma A. and J. Hassink, 1997. Effects of white clover (*Trifolium repens* L.) on plant and soil nitrogen and soil organic matter in mixtures with perennial ryegrass (*Lolium perenne* L.). *Plant and Soil*, **197**, 177-186
- Elgersma A., F. Li and F.R. Li, 1997. Effects of cultivar and cutting frequency on dynamics of stolon growth and leaf appearance in white clover grown in mixed swards. *Grass and Forage Science*, **52**, 370-380
- Elgersma A. and H. Schlepers, 1997. Performance of white clover/perennial ryegrass mixtures under cutting. *Grass and Forage Science*, **52**, 134-146
- Elgersma A., H. Schlepers and M. Nassiri, 2000. Interactions between perennial ryegrass (*Lolium perenne* L.) and white clover (*Trifolium repens* L.) under contrasting nitrogen availability: productivity, seasonal patterns of species composition, N₂ fixation, N transfer and N recovery. *Plant and Soil*, **221**, 281-299
- Ercoli L., M. Mariotti, A. Masoni and F. Massantini, 1993. Relationship between nitrogen and chlorophyll content and spectral properties in maize leaves. *European Journal of Agronomy*, **2**, 113-117
- Evans J.R., 1988. Acclimation by the thylakoid membranes to growth irradiance and the partitioning of nitrogen between soluble and thylakoid proteins. *Australian Journal of Plant Physiology*, **15**, 93-106
- Everitt J.H., A.J. Richardson and H.W. Gausman, 1985. Leaf reflectance-nitrogen-chlorophyll relations in buffelgrass. *Photogrammetric Engineering and Remote Sensing*, **51**, 463-466
- Ewing R.P. and R. Horton, 1999. Quantitative color image analysis of agronomic images. *Agronomy Journal*, **91**, 148-153

-
- Fehmi J.S., E.A. Laca and K.J. Rice, 2001. The effect of small gaps in California annual grassland on above-ground biomass production. *Grass and Forage Science*, **56**, 323-329
- Fernández S., D. Vidal, E. Simon and L. Sole Sugranes, 1994. Radiometric characteristics of *Triticum aestivum* cv. Astral under water and nitrogen stress. *International Journal of Remote Sensing*, **15**, 1867-1884
- Feyaerts F. and L. Van Gool, 2001. Multi-spectral vision system for weed detection. *Pattern Recognition Letters*, **22**, 667-674
- Fourty T. and F. Baret, 1998. On spectral estimates of fresh leaf biochemistry. *International Journal of Remote Sensing*, **19**, 1283-1297
- Franz E., M.R. Gebhardt and K.B. Unklesbay, 1991a. Shape-description of completely visible and partially occluded leaves for identifying plants in digital images. *Transactions of the ASAE*, **34**, 673-681
- Franz E., M.R. Gebhardt and K.B. Unklesbay, 1991b. The use of local spectral properties of leaves as an aid for identifying weed seedlings in digital images. *Transactions of the ASAE*, **34**, 682-687
- Gaborcik N., B. Boller and F.J. Stadelmann, 1998. The content of chlorophyll - a trait applicable in grass breeding. In: *Breeding for a multifunctional agriculture. Proceedings of the 21st Meeting of the Fodder Crops and Amenity Grasses Section of EUCARPIA, Kartause Ittingen, Switzerland, 9-12 September 1997*, pp. 50-53
- Gabriels P.C.J. and J.V. Van Den Berg, 1993. Calibration of two techniques for estimating herbage mass. *Grass and Forage Science*, **48**, 329-335
- Gausman H.W., D.E. Escobar and R.R. Rodriguez, 1973. Discriminating among plant nutrient deficiencies with reflectance measurements. In: *Fourth Biennial Workshop on aerial color photography in the plant sciences, University of Maine, Orono, Maine, July 10-11-12.*, pp. 13-27
- Gausman H.W., R.R. Rodriguez and A.J. Richardson, 1976. Infinite reflectance of dead compared with live vegetation. *Agronomy Journal*, **68**, 295-296

- Geladi P. and B.R. Kowalski, 1986. Partial least squares regression: a tutorial. *Analytica Chimica Acta*, **185**, 1-17
- Gerhards R., A. Nabout, M. Sokefeld, W. Kuhbauch and H.A.N. Eldin, 1993. Automatic identification of 10 weed species in digital images using fourier descriptors and shape-parameters. *Journal of Agronomy and Crop Science*, **171**, 321-328
- Gitelson A.A., M.N. Merzlyak and H.K. Lichtenthaler, 1996. Detection of red edge position and chlorophyll content by reflectance measurements near 700 nm. *Journal of Plant Physiology*, **148**, 501-508
- Goetz A.F.H., 1992. Imaging spectrometry for earth remote sensing. In: F. Toselli, and J. Bodechtel (eds) *Imaging spectroscopy : fundamentals and prospective applications* pp. 266. Dordrecht, the Netherlands, Kluwer Academic Publishers.
- Gonzalez M.A., M.A. Hussey and B.E. Conrad, 1990. Plant Height, Disk, and Capacitance Meters Used to Estimate Bermudagrass Herbage Mass. *Agronomy Journal*, **82**, 861-864
- Goudriaan J. and H.H. Van Laar, 1994. *Modelling potential crop growth processes : textbook with exercises*. Dordrecht, the Netherlands, Kluwer Academic Publishers.
- Graeff S., D. Steffens and S. Schubert, 2001. Use of reflectance measurements for the early detection of N, P, Mg, and Fe deficiencies in *Zea mays* L. *Journal Of Plant Nutrition And Soil Science Zeitschrift Fur Pflanzenernahrung Und Bodenkunde Aug*, **164**, 445-450
- Grashoff C., H.F.M. Aarts, H.G. Smid, R.H.E.M. Geerts and D.M. Jansen, 2001a. Effect of spatial and temporal variation in drought on sward quality of grass: the need for precision irrigation. In: S. Blackmore, and G. Grenier (eds.). *Third European conference on precision agriculture, Montpellier, France*, pp. 665-670

-
- Grashoff C., H.F.M. Aarts, H.G. Smid, R.H.E.M. Geerts and D.M. Jansen, 2001b. Towards minimized irrigation: an algorithm to prevent permanent drought damage in grassland. In: S. Blackmore, and G. Grenier (eds.). *Third European conference on precision agriculture, Montpellier, France*, pp.
- Greenwood D.J., G. Lemaire, G. Gosse, P. Cruz, A. Draycott and J.J. Neeteson, 1990. Decline in percentage N of C3 and C4 crops with increasing plant mass. *Annals of Botany*, **66**, 425-436
- Groot J.C.J., 1999. *Modelling grass digestibility on the basis of morphological and physiological plant characteristics*. Thesis, Wageningen Agricultural University, Wageningen.
- Guyer D.E., G.E. Miles, M.M. Schreiber, O.R. Mitchell and V.C. Vanderbilt, 1986. Machine vision and image processing for plant identification. *Transactions of the ASAE American Society of Agricultural Engineers*, **29**, 1500-1507
- Guyot G. and F. Baret, 1988. Utilisation de la haute résolution spectrale pour suivre l'état des couverts végétaux [Utilisation of high spectral resolution for monitoring vegetation condition]. In: T.D. Guyenne, and J.J. Hunt (eds.). *Signatures Spectrales d'Objects en Télédétection: 4eme Colloque International, Aussois (Mondane), 18-22 Jan., France*, pp. 279-286
- Guyot G., F. Baret and S. Jacquemoud, 1992. Imaging spectroscopy for vegetation studies. In: F. Toselli, and J. Bodechtel (eds) *Imaging Spectroscopy: fundamentals and prospective applications* pp. 145-165. Dordrecht, the Netherlands, Kluwer.
- Hack-Ten Broeke M.J.D., 2000. *Nitrate leaching from dairy farming on sandy soils. Case studies for experimental farm De Marke*. Thesis, Wageningen Agricultural University, Wageningen, the Netherlands.
- Hahn F. and A.Y. Muir, 1993. *Discrimination of weeds in cabbage, leek, potato and turnip crops*. Scottish Centre of Agricultural Engineering, Note 62,

- Harmoney K.R., K.J. Moore, J.R. George, E.C. Brummer and J.R. Russell, 1997. Determination of pasture biomass using four indirect methods. *Agronomy Journal*, **89**, 665-672
- Haverkort A.J., D. Uenk, H. Veroude and M. Van De Waart, 1991. Relationships between ground cover, intercepted solar-radiation, leaf-area index and infrared reflectance of potato crops. *Potato Research*, **34**, 113-121
- Helsper J.P.F.G., C.H.R. De Vos, F.M. Maas, H.H. Jonker, H.C. Van Den Broeck, W. Jordi, C.S. Pot, L.C.P. Keizer and A.H.C.M. Schapendonk, 2003. Response of selected antioxidants and pigments in tissues of *Rosa hybrida* and *Fuchsia hybrida* to supplemental UV-A exposure. *Physiologia Plantarum*, **In Press**,
- Herrala E. and J. Okkonen, 1996. Imaging spectrograph and camera solutions for industrial applications. *International Journal of Pattern Recognition and Artificial Intelligence*, **10**, 43-54
- Heuwinkel H., F. Locher, T. Alfoldi, W. Lockeretz and U. Niggli, 2000. An approach to describe the variability of nitrogen fixation by a clover-grass mixture within a field. In: *IFOAM 2000: the world grows organic, Basel, Switzerland, 28 to 31 August*, pp. 90
- Hopkins A., A.H. Adamson and P.J. Bowling, 1994. Response of permanent and reseeded grassland to fertilizer nitrogen. 2. Effects on concentrations of Ca, Mg, K, Na, S, P, Mn, Zn, Cu, Co and Mo in herbage at a range of sites. *Grass and Forage Science*, **49**, 9-20
- Horler D.N.H., M. Dockray and J. Barber, 1983. The red edge of plant leaf reflectance. *International Journal of Remote Sensing*, **4**, 273-288
- Hunt E.R.J., B.N. Rock and P.S. Nobel, 1987. Measurement of leaf relative water content by infrared reflectance. *Remote Sensing of Environment*, **22**, 429-435

-
- Hutchings N.J., 1991. Spatial Heterogeneity and Other Sources of Variance in Sward Height as Measured by the Sonic and Hfro Sward Sticks. *Grass and Forage Science*, **46**, 277-282
- Hutchings N.J., 1992. Factors Affecting Sonic Sward Stick Measurements - the Effect of Different Leaf Characteristics and the Area of Sward Sampled. *Grass and Forage Science*, **47**, 153-160
- Hutchings N.J., A.H. Phillips and R.C. Dobson, 1990. An Ultrasonic Rangefinder for Measuring the Undisturbed Surface Height of Continuously Grazed Grass Swards. *Grass and Forage Science*, **45**, 119-127
- Ichoku C. and A. Karneilli, 1996. A review of mixture modelling techniques for sub-pixel land cover estimation. *Remote Sensing Reviews*, **13**, 161-186
- Inoue Y., S. Morinaga and M. Shibayama, 1993. Non-destructive estimation of water status of intact crop leaves based on spectral reflectance measurements. *Japanese Journal of Crop Science*, **62**, 462-469
- Jackson R.D. and C.E. Ezra, 1985. Spectral response of cotton to suddenly induced water stress. *International Journal of Remote Sensing*, **6**, 177-185
- Jacquemoud S., S.L. Ustin, J. Verdebout, G. Schmuck, G. Andreoli and B. Hosgood, 1996. Estimating leaf biochemistry using the PROSPECT leaf optical properties model. *Remote Sensing of Environment*, **56**, 194-202
- Jacquemoud S., J. Verdebout, G. Schmuck, G. Andreoli and B. Hosgood, 1995. Investigation of leaf biochemistry by statistics. *Remote Sensing of Environment*, **54**, 180-188
- Jones M.B. and A. Lazenby, 1988. *The grass crop: the physiological basis of production*. London, United Kingdom, Chapman and Hall.

- Jones M.B., E.L. Leafe and W. Stiles, 1980a. Water stress in field-grown perennial ryegrass. 1. Its effect on growth, canopy photosynthesis and transpiration. *Annals of Applied Biology*, **96**, 87-101
- Jones M.B., E.L. Leafe and W. Stiles, 1980b. Water stress in field-grown perennial ryegrass. 2. Its effect on leaf water status, stomatal resistance and leaf morphology. *Annals of Applied Biology*, **96**, 103-110
- Jørgensen R.N., 2002a. *Development and design of a line imaging spectrometer sampler (LISS) - a user manual*. Roskilde, Denmark, Risø National Laboratory, Report 1189
- Jørgensen R.N., 2002b. *The VTTVIS line imaging spectrometer - principles, error sources, and calibration*. Roskilde, Denmark, Risø National Laboratory, Report 1302
- Kantety R.V., E. Vansanten, F.M. Woods and C.W. Wood, 1996. Chlorophyll meter predicts nitrogen status of tall fescue. *Journal of Plant Nutrition*, **19**, 881-899
- Keuning J.A. and T.V. Vellinga, 1986. Zodekwaliteit en botanische samenstelling bij intensieve graslandexploitatie. *Verslagen Nederlandse Vereniging voor Weide en Voederbouw*, **27**, 1-14
- King J., E.M. Sim and G.T. Barthram, 1986. A comparison of spectral reflectance and sward surface height measurements to estimate herbage mass and leaf area index in continuously stocked ryegrass pastures. *Grass and Forage Science*, **41**, 251-258
- Kokaly R.F., G.T. Barthram, D.A. Elston and G.R. Bolton, 2001. Investigating a physical basis for spectroscopic estimates of leaf nitrogen concentration. *Remote Sensing of Environment*, **75**, 153-161
- Korva J.T., 1996. Grids in ground cover measurements. *Potato Research*, **39**, 533-540

-
- Laca E.A. and G. Lemaire, 2000. Measuring sward structure. In: L. 't Mannetje, and R.M. Jones (eds) *Field and laboratory methods for grassland and animal production research* pp. Wallingford, United Kingdom, CAB International.
- Lazenby A., 1988. The grass crop in perspective: selection, plant performance and animal production. In: M.B. Jones, and A. Lazenby (eds) *The grass crop : the physiological basis of production* pp. 311-360. London, United Kingdom, Chapman and Hall.
- Lemaire G., F. Gastal and J. Salette, 1989. Analysis of the effect of N nutrition on dry matter yield of a sward by reference to potential yield and optimum N content. In: *The XVI International Grassland Congress, Nice, France*, pp. 179-180
- Lichtenthaler H.K., 1987. Chlorophylls and carotenoids: pigments of photosynthetic biomembranes. In: L. Packer, and R. Douce (eds) *Methods in enzymology* pp. 350-382. New York, USA, Academic Press.
- Liu L.X., W.S. Chow and J.M. Anderson, 1993. Light quality during growth of *Tradescantia albiflora* regulates photosystem stoichiometry, photosynthetic function and susceptibility to photoinhibition. *Physiologia Plantarum*, **89**, 854-860
- Locher F., H. Heuwinkel, R. Gutser and U. Schmidhalter, 2001. Near infrared reflectance spectroscopy. A tool to estimate N₂- fixation. In: S. Blackmore, and G. Grenier (eds.). *Third European conference on precision agriculture, Montpellier, France*, pp. 941-945
- Loiseau P., J.F. Soussana, F. Louault and R. Delpy, 2001. Soil N contributes to the oscillations of the white clover content in mixed swards of perennial ryegrass under conditions that simulate grazing over five years. *Grass and Forage Science*, **56**, 205-217
- Lokhorst C. and G.J. Kasper, 1998. Site specific grassland management: measuring techniques, spatial- and temporal variation in grass yields. *VDI berichte*, **1449**, 209-214

- Lokhorst C. and G.J. Kasper, 2001. Feasibility of non-destructive grass yield measuring techniques for the support of precision grassland management. In: *Third European Conference on Precision Agriculture, Montpellier, France*, pp.
- Lukina E.V., M.L. Stone and W.R. Raun, 1999. Estimating vegetation coverage in wheat using digital images. *Journal of Plant Nutrition*, **22**, 341-350
- Maier S.W., W. Ludeker and K.P. Gunther, 1999. SLOP: a revised version of the stochastic model for leaf optical properties. *Special issue: Seventh International Symposium on Physical Measurements and Signatures in Remote Sensing, Courchevel, France, 7-11 April 1997*, **68**, 273-280
- Mallat S., 1999. *Wavelet tour of signal processing*. San Diego, USA, Academic Press.
- Manh A.G., G. Rabatel, L. Assemat and M.J. Aldon, 2001. In-field classification of weed leaves by machine vision using deformable templates. In: S. Blackmore, and G. Grenier (eds.). *Third European conference on precision agriculture, Montpellier, France*, pp.
- Mariotti M., L. Ercoli and A. Masoni, 1996. Spectral properties of iron-deficient corn and sunflower leaves. *Remote Sensing of Environment*, **58**, 282-288
- Marriott C.A., J.M. Fisher, K.J. Hood and M.A. Smith, 1997. Persistence and colonization of gaps in sown swards for grass and clover under different sward managements. *Grass and Forage Science*, **52**, 156-166
- Martin M.E. and J.D. Aber, 1997. High spectral resolution remote sensing of forest canopy lignin, nitrogen, and ecosystem processes. *Ecological Applications*, **7**, 431-443
- Masoni A., M. Mariotti and L. Ercoli, 1997. Effect of water stress and nitrogen nutrition on maize (*Zea mays* L.) leaf spectral properties. *Rivista di Agronomia*, **31**, 441-448

-
- Matlab, 2000. *Matlab 6.0, release 12*. Natick, Massachusetts, USA, The Mathworks Inc.
- Mccloy K.R., R. Schoneveld and D. Kemp, 1993. Measurement of pasture parameters from reflectance data. *International Journal of Remote Sensing*, **14**, 1107-1118
- Mckenzie F.R. and J.L. Jacobs, 2002. Effects of application of nitrogen fertilizer on concentrations of P, K, S, Ca, Mg, Na, Cl, Mn, Fe, Cu and Zn in perennial ryegrass/white clover pastures in south-western Victoria, Australia. *Grass and Forage Science*, **57**, 48-53
- Milton N.M., B.A. Eiswerth and C.M. Ager, 1991. Effect of Phosphorus Deficiency on Spectral Reflectance and Morphology of Soybean Plants. *Remote Sensing of Environment*, **36**, 121-127
- Mooij M. and T.V. Vellinga, 1993. *Verfijning stikstofbemestingsadvies voor grasland naar gebruikswijze*. Lelystad, The Netherlands, Proefstation voor de Rundveehouderij, Schapenhouderij en Paardenhouderij, 142
- Moshou D., H. Ramon and J. De Baerdemaeker, 1999. Neural network based classification of different weed species and crops. In: J.V. Stafford (ed.) *2nd European Conference on Precision Agriculture, Odense Congress Centre, Denmark, 11-15 July*, pp. 275-284
- Moshou D., E. Vrindts, B. De Ketelaere, J. De Baerdemaeker and H. Ramon, 2001. A neural network based plant classifier. *Computers and Electronics in Agriculture*, **31**, 5-16
- Murphy W.M., J.P. Silman and A.D. Mena Barreto, 1995. A comparison of quadrat, capacitance meter, HFRO sward stick, and rising plate for estimating herbage mass in a smooth-stalked, meadow grass-dominant white clover sward. *Grass and Forage Science*, **50**, 452-455
- Neuteboom J.H., E.A. Lantinga and E.N. Van Loo, 1992. The use of frequency estimates in studying sward structure. *Grass and Forage Science*, **47**, 358-365

- Park R.S., R.E. Agnew, F.J. Gordon and R.W.J. Steen, 1998. The use of near infrared reflectance spectroscopy (NIRS) on undried samples of grass silage to predict chemical composition and digestibility parameters. *Animal Feed Science and Technology*, **72**, 155-167
- Peeters A. and V. Van Bol, 1993. Relationships between aboveground dry weight and N, P, K concentrations in grassland species: A guide for the diagnosis of plant nutrient status. In: M.A.C. Fragoso, M.L. Van Beusichem, and A. Houwers (eds) *Optimization of plant nutrition*. pp. 144. Dordrecht [etc.], Kluwer Academic Publishers.
- Penuelas J., I. Filella, C. Biel, L. Serrano and R. Save, 1993. The reflectance at the 950-970 nm region as an indicator of plant water status. *International Journal of Remote Sensing*, **14**, 1887-1905
- Penuelas J., J.A. Gamon, A.L. Fredeen, J. Merino and C.B. Field, 1994. Reflectance indices associated with physiological changes in nitrogen- and water-limited sunflower leaves. *Remote Sensing of Environment*, **48**, 135-146
- Penuelas J. and Y. Inoue, 1999. Reflectance indices indicative of changes in water and pigment contents of peanut and wheat leaves. *Photosynthetica*, **36**, 355-360
- Petry W. and W. Kuhbauch, 1989. Automatic distinction of weed species using form parameters by means of digital image-processing. *Journal of Agronomy and Crop Science*, **163**, 345-351
- Pinar A. and P.J. Curran, 1996. Grass chlorophyll and the reflectance red edge. *International Journal of Remote Sensing*, **17**, 351-357
- PLS_Toolbox, 2000. *PLS_Toolbox version 2.1*. Manson, USA, Eigenvector Research Inc.
- Polder G. and G.W.A.M. Van Der Heijden, 2001. Calibration and characterization of spectral imaging systems. In: *Multispectral and hyperspectral image acquisition and processing, China*, SPIE 4548 pp.

-
- Polder G., G.W.A.M. Van Der Heijden and I.T. Young, 2002. Spectral image analysis for measuring ripeness of tomatoes. *Transactions of the ASAE*, **45**, 1155-1161
- Prummel J., 1973. *Factoren van invloed op het calcium - en fosforgehalte van gras [Factors of influence on calcium- and phosphorus content of grass]*. Haren, the Netherlands, Institute of Soil Fertility, report 3
- Railyan V.Y. and R.M. Korobov, 1993. Red edge structure of canopy reflectance spectra of Triticale. *Remote Sensing of Environment*, **46**, 173-182
- Richards I.R. and K.M. Wolton, 1975. A note on urine scorch caused by grazing animals. *Journal of the British Grassland Society*, **30**, 187-193
- Ripple W.J., 1985. Asymptotic reflectance characteristics of grass vegetation. *Photogrammetric Engineering and Remote Sensing*, **51**, 1915-1921
- Ripple W.J., 1986. Spectral reflectance relationships to leaf water stress. *Photogrammetric Engineering and Remote Sensing*, **52**, 1669-1675
- Rollin E.M. and E.J. Milton, 1998. Processing of high spectral resolution reflectance data for the retrieval of canopy water content information. *Remote Sensing of Environment*, **65**, 86-92
- Rosso O.A., S. Blanco, J. Yordanova, V. Kolev, A. Figliola, M. Schurmann and E. Basar, 2001. Wavelet entropy: a new tool for analysis of short duration brain electrical signals. *Journal Of Neuroscience Methods*, **105**, 65-75
- Rougoor C.W., T.V. Vellinga, R.B.M. Huirne and A. Kuipers, 1999. Influence of grassland and feeding management on technical and economic results of dairy farms. *Netherlands Journal of Agricultural Science*, **47**, 135-151
- Sanderson M.A., C.A. Rotz, S.W. Fultz and E.B. Rayburn, 2001. Estimating forage mass with a commercial capacitance meter, rising plate meter, and pasture ruler. *Agronomy Journal*, **93**, 1281-1286

- Sandmeier S., C. Muller, B. Hosgood and G. Andreoli, 1998. Physical mechanisms in hyperspectral BRDF data of grass and watercress. *Remote Sensing of Environment*, **66**, 222-233
- Schapendonk A.H.C.M., W. Stol, D.W.G. Van Kraalingen and B.A.M. Bouman, 1998. LINGRA, a sink/source model to simulate grassland productivity in Europe. *European Journal of Agronomy*, **9**, 87-100
- Schepers J.S., T.M. Blackmer, W.W. Wilhelm and M. Resende, 1996. Transmittance and reflectance measurements of corn leaves from plants with different nitrogen and water supply. *Journal of Plant Physiology*, **148**, 523-529
- Schils R.L.M., 1997. Effect of a spring application of nitrogen on the performance of perennial ryegrass-white clover swards at two sites in the Netherlands. *Netherlands Journal of Agricultural Science*, **45**, 263-275
- Schils R.L.M., T.J. Boxem, C.J. Jagtenberg and M.C. Verboon, 2000. The performance of a white clover based dairy system in comparison with a grass/fertiliser-N system. II. Animal production, economics and environment. *Netherlands Journal of Agricultural Science*, **48**, 305-318
- Schils R.L.M., T.V. Vellinga and T. Kraak, 1999. Dry-matter yield and herbage quality of a perennial ryegrass/white clover sward in a rotational grazing and cutting system. *Grass and Forage Science*, **54**, 19-29
- Schmidt K.S. and A.K. Skidmore, 2001. Exploring spectral discrimination of grass species in African rangelands. *International Journal of Remote Sensing*, **22**, 3421-3434
- Schulte R.P.O., 2001. *On the stability of mixed grasslands*. Thesis, Wageningen University, Wageningen.
- Seasholtz M.B. and B.R. Kowalski, 1990. Qualitative information from multivariate calibration models. *Applied Spectroscopy*, **44**, 1337-1348

-
- Shearer S.A. and R.G. Holmes, 1990. Plant identification using color co-occurrence matrices. *Transactions of the ASAE*, **33**, 2037-2044
- Silverman B.W., 1985. Some aspects of spline smoothing approach tot non-parametric regression curve fitting. *Journal of the Royal Statistical Society B*, **47**, 1-22
- Silvertown J., S.D. Prince and B.A. Smith, 1988. A field-portable instrument for mapping the micro-environment within grass canopies. *Functional Ecology*, **2**, 263-268
- Sinnaeve G., P. Dardenne, R. Agneessens and R. Biston, 1994. The use of near infrared spectroscopy for the analysis of fresh grass silage. *Journal of near Infrared Spectroscopy*, **2**, 79-84
- Skidmore A.K., G.W. Forbes and D.J. Carpenter, 1988. Non-Parametric Test of Overlap in Multispectral Classification. *International Journal of Remote Sensing*, **9**, 777-785
- Smit A.L., F.C.T. Guiking, L.J.M. Kater, A.A. Pronk, F.J.D. Ruijter, R. Schreuder, J.J. Schroder, A.G.T. Schut, M.H.A. De Haan, A.L. Smit, A.M. Van Dam, J.R. Van Der Schoot and H.V. Reuler, 2003. *Maatregelenpakketten om te voldoen aan MINAS2003 normen*. Wageningen, the netherlands, Plant Research International, in prep.
- Stein A., F. Van Der Meer and B. Gorte, 1999. *Spatial statistics for remote sensing*. Dordrecht, the Netherlands, Kluwer Academic Publishers.
- Stockdale C.R., 1984a. Evaluation of techniques for estimating the yield of irrigated pastures intensively grazed by dairy cows. 1. Visual assessment. *Australian Journal of Experimental Agriculture and Animal Husbandry*, **24**, 300-304
- Stockdale C.R., 1984b. Evaluation of techniques for estimating the yield of irrigated pastures intensively grazed by dairy cows. 2. The rising plate meter. *Australian Journal of Experimental Agriculture and Animal Husbandry*, **24**, 305-311

- Stockdale C.R. and K.B. Kelly, 1984. A comparison of a rising-plate meter and an electronic capacitance meter for estimating the yield of pastures grazed by dairy cows. *Grass and Forage Science*, **39**, 391-394
- Stoner E.R. and M.F. Baumgardner, 1981. Characteristic variations in reflectance of surface soils. *Soil Science Society of America Journal*, **45**, 1161-1165
- Ten Berge H.F.M., J.C.M. Withagen, F.J. De Ruijter, M.J.W. Jansen and H.G. Van Der Meer, 2000. *Nitrogen responses in grass and selected field crops*. Wageningen, Plant Research International, Report 24
- Thomas H., 1991. Accumulation and consumption of solutes in swards of *Lolium perenne* during drought and after rewatering. *New Phytologist*, **118**, 35-48
- Tomasel F.G., J.M. Paruelo, G. Abras, V. Ballarin and E. Moler, 2001. A chromaticity-based technique for estimation of above-ground plant biomass. *Applied Vegetation Science*, **4**, 207-212
- Van Delden A., 2001. *Yielding ability and weed suppression of potato and wheat under organic nitrogen management*. Thesis, Wageningen University, Wageningen.
- Van Den Berg J.C., 1999. *Wavelets in physics*. Cambridge, United Kingdom, Cambridge University Press.
- Van Der Meer H.G. and T. Baan Hofman, 2000. Effects of low-emission slurry application techniques and periods of application on the yield and nitrogen economy of a mixed sward of perennial ryegrass and white clover. In: H.G. Van der Meer (ed.) *Reducing inputs and losses of nitrogen and energy on dairy farms. Final Report Project AIR3 CT92-0332*. pp. Wageningen, The Netherlands, Plant Research International, Note 18.
- Van Dijk H., 1999. Goed graslandgebruik levert geld op. *Praktijkonderzoek*, 4-5

-
- Van Keulen H. and J. Wolf, 1986. *Modelling of agricultural production: weather, soils and crops*. Wageningen, the Netherlands, Centre for Agricultural Publishing and Documentation.
- Van Loo E.N., 1992a. Relationships between sward structure, plant density and dry matter yield of perennial ryegrass (*Lolium Perenne* L.). *Verlagen van de Nederlandse vereniging voor Weide- en Voederbouw*, **32**, 1-14
- Van Loo E.N., 1992b. Tillering, leaf expansion and growth of plants of two cultivars of perennial ryegrass grown using hydroponics at two water potentials. *Annals of Botany*, **70**, 511-518
- Van Loo E.N., 1993. *On the relation between tillering, leaf area dynamics and growth of perennial ryegrass (Lolium perenne L.)*. Thesis, Wageningen Agricultural University, Wageningen.
- Vellinga T.V., 1998. *Verfijning bemestingsadvies 1998*. Lelystad, the Netherlands, Proefstation voor de Rundveehouderij, Schapenhouderij en Paardenhouderij, 173
- Vellinga T.V. and E.N. Van Loo, 1994. *Perspectieven grassenveredeling voor bedrijfsinkomen en mineralenoverschotten*. Lelystad, the Netherlands, Proefstation voor de Rundveehouderij, Schapenhouderij en Paardenhouderij, 151
- Velthof G.L., J.J. Neeteson, H.G. Van Der Meer and O. Oenema, 2000. *Schatting van de netto stikstofmineralisatie en de biologische stikstofbinding in landbouwgronden*. Wageningen, Alterra, Research Institute for the Green World,, report 117
- Vickery P.J., I.L. Bennett and G.R. Nicol, 1980. An improved electronic capacitance meter for estimating herbage mass. *Grass and Forage Science*, **35**, 247-252
- Viitala J., E. Korpimäki, P. Polakangas and M. Koivula, 1995. Attraction of kestrels to vole scent marks visible in ultraviolet light. *Nature*, **373**, 425-427

- Virkajärvi P., 1999. Comparison of three indirect methods for prediction of herbage mass on timothy-meadow fescue pastures. *Acta Agriculturae Scandinavica Section B, Soil and Plant Science*, **49**, 75-81
- Vrindts E. and J. De Baerdemaeker, 1997. Optical discrimination of crop, weed and soil for on-line weed detection. In: J.V. Stafford (ed.) *The First European Conference on Precision Agriculture, Warwick University, 7-10 September 1997, United Kingdom*, pp. 537-544
- Vrindts E., J. De Baerdemaeker and H. Ramon, 1999. Weed detection using hyperspectral canopy reflectance. In: J.V. Stafford (ed.) *2nd European Conference on Precision Agriculture, Odense Congress Centre, Denmark, 11-15 July 1999*, pp. 257-264
- Wachendorf M., B. Ingwersen and F. Taube, 1999. Prediction of the clover content of red clover- and white clover-grass mixtures by near-infrared reflectance spectroscopy. *Grass and Forage Science*, **54**, 87-90
- Watanabe N., C. Fujii, M. Shirota and Y. Furuta, 1993. Changes in chlorophyll, thylakoid proteins and photosynthetic adaptation to sun and shade environments in diploid and tetraploid *Oryza punctata* Kotschy and diploid *Oryza eichingeri* Peter. *Plant Physiology and Biochemistry*, **31**, 469-474
- Watson C.A. and M.J. Goss, 1997. Estimation of N₂-fixation by grass-white clover mixtures in cut or grazed swards. *Soil Use and Management*, **13**, 165-167
- White M.A., G.P. Asner, R.R. Nemani, J.L. Privette and S.V. Running, 2000. Measuring fractional cover and leaf area index in arid ecosystems: digital camera, radiation transmittance, and laser altimetry methods. *Remote Sensing of Environment*, **74**, 45-57
- Woebbecke D.M., G.E. Meyer, K.V. Bargaen, D.A. Mortensen and K. Von Bargaen, 1995. Shape features for identifying young weeds using image analysis. *Transactions of the ASAE*, **38**, 271-281

-
- Wolton K.M., 1978. Dung and urine as agents of change: a review. In: A.H. Charles, and R.J. Haggard (eds) *Changes in sward composition and productivity* pp. 131-135. Hurley, United Kingdom, British Grassland Society.
- Wood C.W., D.W. Reeves, R.R. Duffield and K.L. Edmisten, 1992. Field Chlorophyll Measurements for Evaluation of Corn Nitrogen Status. *Journal of Plant Nutrition*, **15**, 487-500
- Yamasaki T., T. Kudoh, Y. Kamimura and S. Katoh, 1996. A vertical gradient of the chloroplast abundance among leaves of *Chenopodium album*. *Plant and Cell Physiology*, **37**, 43-48
- Zaag D.E.V.D. and D.E. Van Der Zaag, 1984. Reliability and significance of a simple method of estimating the potential yield of the potato crop. *Potato Research*, **27**, 51-73
- Zagolski F., V. Pinel, J. Romier, D. Alcayde, J. Fontanari, J.P. Gastellu-Etchegorry, G. Giordano, G. Marty, E. Mougín and R. Joffre, 1996. Forest canopy chemistry with high spectral resolution remote sensing. *International Journal of Remote Sensing*, **17**, 1107-1128
- Zarco Tejada P.J., J.R. Miller, G.H. Mohammed and T.L. Noland, 2000. Chlorophyll fluorescence effects on vegetation apparent reflectance: I. Leaf-level measurements and model simulation. *Remote Sensing of Environment*, **74**, 582-595
- Zhou Q. and M. Robson, 2001. Automated rangeland vegetation cover and density estimation using ground digital images and a spectral-contextual classifier. *International Journal of Remote Sensing*, **22**, 3457-3470
- Zwiggelaar R., 1998. A review of spectral properties of plants and their potential use for crop/weed discrimination in row-crops. *Crop Protection*, **17**, 189-206



Summary

Introduction

Dairy husbandry systems under temperate climatic conditions mostly use grass as a major feed source. Currently, grassland management on dairy farms largely depends on qualitative expert knowledge. Management practices may be improved with the help of objective and quantitative information on the actual status of grass swards. Such information may be obtained from digital sward images. Just before the project started, new imaging technology became available. With this new technology, hyperspectral images can be recorded instantaneously, providing means to combine spatial resolutions at sub-leaf level with reflection measurements in a large number of spectral bands. This means that leaf pixels in digital sward images can be differentiated from pixels containing dead material and soil, prior to spectral analysis. Sward images may then provide not only quantitative information on the presence of grass (leaves) but also on, for instance, nutritional status and nutritive value of the grass crop. The objectives in the study were (1) to develop and build an experimental imaging spectrometry system, capable of recording reflection of leaves within a standing grass sward in the visible and near infrared wavelength range; (2) to derive and select parameters from the images that characterise growth and heterogeneity and identify nutrient- and drought stress; and (3) to study and quantify the relations between image parameters and growth, dry matter (DM) yield, sward heterogeneity and growth capacity, clover coverage, degree of nitrogen (N) and drought stress, and nutritive value of grass swards.

Novel imaging spectroscopy

In Chapter 2, detailed information is provided on design, characteristics and test results of an experimental imaging spectroscopy system. From a height of 1.3 meter above the ground, the system detects reflections at high spatial ($0.28\text{-}1.45\text{ mm}^2$) and high spectral resolutions (5-13 nm) at wavelengths between 405 and 1659 nm.

Results show that reflection intensity of leaf pixels is related to leaf height position in the sward and leaf angle. With the described system, canopy structure can be characterised by ground cover, the distribution of reflection intensity over leaf pixels and image texture. Spectral characteristics can be obtained at leaf level, unconfounded by background influences.

Growth monitoring

The potential of this experimental imaging system for monitoring growth of grass swards is explored in Chapter 3. An experiment was conducted with 36 *Lolium perenne* L. mini swards, differing in the degree of sward damage. Classification procedures of images using maximum likelihood procedures yielded (several) estimates of image ground cover (GC) and an index of reflection intensity (IRI) indicating the proportion of highly reflecting grass pixels. Leaf pixels with similar reflection intensity were grouped in intensity classes (IC).

Results showed that image GC was highly correlated with visually scored GC ($R^2_{\text{adj}}=0.94$), Leaf Area Index (LAI) ($R^2_{\text{adj}}=0.88$), and light interception (LI) ($R^2_{\text{adj}}=0.94$, for dense swards under a cloudy sky). However, relations between GC and LI depended on sky cloudiness and sward quality. Under a cloudy sky, LI was linearly related to GC, whereas under a clear sky, this relation had a more logistic character. Open swards had on average a lower GC and a lower IRI when compared to dense swards at similar growth stages. Regression analysis of GC, IRI and dry matter (DM) yields showed correlations with R^2_{adj} ranging between 0.75-0.82. The mean error of DM yield estimates was 340 kg DM ha⁻¹. It was concluded that imaging spectrometry allows accurate, non-destructive monitoring of grass sward growth from increases in estimated GC and IRI.

Detection of nitrogen (N) stress

The potential of imaging spectroscopy for early detection of nitrogen stress is explored in Chapter 4. An experiment was conducted with 15 *Lolium perenne* L. mini swards and 5 N supply levels. Blue edge (BE), green edge (GE) and red edge (RE) positions were calculated for each IC.

It was found that both GC and IRI increased until harvest, with largest increases for liberal N supply. The width of the chlorophyll dominated absorption band around 680 nm (CAW, calculated as the difference between RE and GE position) increased up to a maximum of 133 nm for both liberal and limited N in the first two weeks after harvesting. The CAW decreased for limited N in the second half of the growth period in contrast to liberal N. At harvest, CAW explained 95% of the variation in relative DM yield between N treatments. Principal component analyses showed an intertwined response of

the principal components to both DM yield and N concentration. Edge positions changed strongly with IC.

Effects of leaf angle, leaf height and pigment content on reflectance

In Chapter 5, effects of leaf angle, leaf height and pigment content on reflectance spectra of grass swards are studied. An experiment was conducted with mini swards of *Lolium perenne* L. and 4 N supply levels. At harvest, swards were harvested in three strata (>16 cm, 9-16 cm, and 4-9 cm) and strata were analysed for chemical composition, including pigments. Effects of leaf angle and height were studied independently with the help of detached leaves. Contents of N and pigments, on average, increased with increasing N level and decreased downwards in the sward. BE, GE and RE showed strong, N treatment dependent, changes with IC. At harvest, CAW of intact swards increased with N level, with absolute values being similar to values measured at harvested material of the upper stratum. When upper strata were subsequently removed, CAW of the remaining sward decreased much less than expected from measurements at harvested material. Varying leaf angle from horizontal to nearly vertical shifted BE 2 nm, GE 6 nm and RE 2 nm, and increased CAW about 6 nm. Decreasing leaf height up to 20 cm, hardly affected BE, shifted GE 2.3 nm and RE 4.9 nm, and decreased CAW 2.6 nm. The ratio between red and blue reflectance was also strongly affected by leaf angle. Changes of edge positions with IC could only partly be explained by the summed effects of leaf height and leaf angle and may have been augmented by sensor characteristics. It is concluded that combinations of the red/blue ratio, shifts of GE with IC and CAW may be useful to separate effects of leaf angle on sward reflectance from effects of leaf pigment concentration *per se*.

Detection of drought stress

The potential of imaging spectroscopy for early detection of drought stress in grass swards is explored in Chapter 6. A climate chamber experiment was conducted with 9 *Lolium perenne* L. mini swards with drought stress treatments at two N levels. Wavelength position of inflection points of derivative spectra were estimated and analysed in relation to a progressively increasing degree of drought stress.

Drought stress increased leaf dry matter content and sugar concentration. Drought stress decelerated and ultimately reversed GC evolution, and kept IRI

at low values. In contrast to unstressed growth, all absorption features narrowed and became shallower under drought stress. The inflection points near 1390 and 1500 nm were most sensitive to drought stress. Differences between drought stressed and control swards were detected just before leaf water content dropped below 80%. The evolution of wavelength position of inflection points reversed under drought stress, except for the red edge of which the shift to longer wavelengths during growth accelerated. The relation between inflection points at 705 and 1390 nm differentiated unstressed swards in an early growth stage from drought stressed swards in a later growth stage.

Quantification of clover cover

In Chapter 7, the potential of imaging spectroscopy is explored for robust discrimination between grass, white clover and mixed mini swards at various growth stages. For this, spectra of grass and clover swards were compared and image line texture was analysed using spatial correlation, a special filter and wavelet entropy. In 2000, an experiment with mini swards was conducted including two white clover (*Trifolium repens* L.) swards, three perennial ryegrass (*Lolium perenne* L.) swards and four swards with a grass and white clover mixture.

Results showed that the mean spectral curves of pixels of grass and clover swards differed throughout the spectral range, but differences were small when compared to the variation in grass spectra. No specific discriminating spectral feature was found. Differences in edge positions between grass and clover swards were not consistent within growth periods. With image line texture, pure grass and clover swards could be separated with the filter, spatial correlation and wavelet entropy. Only wavelet entropy resulted in robust discrimination on all recording dates. With all three discriminating methods, results of mixed swards were intermediate between pure swards.

Assessment of total DM yield and sward quality

Relations between spatial heterogeneity of tiller density, LI, GC, and seasonal DM (SDM) yield are studied in Chapter 8. Sward heterogeneity was quantified with spatial standard deviation of GC (GC-SSD) and logistically transformed GC (TGC-SSD), and patterns in GC transects were quantified with wavelet entropy. An experiment was conducted with control swards (CS), naturally damaged swards (NDS) and artificially damaged swards (ADS).

Spatial variation of tiller density was larger for ADS and NDS than for CS. SDM was linearly related to a combination of seasonal means of GC and IRI ($R^2 = 0.93$). An increase of 1% unit in seasonal mean GC was shown to increase SDM with $0.31 \text{ t DM ha}^{-1}$. This is in agreement with predictions of a grass growth model. Values of GC-SSD and wavelet entropy were larger for ADS and NDS than for CS. GC-SSD of CS remained below 13% throughout the season, in contrast to values of NDS and ADS. Absolute differences in TGC-SSD between CS, ADS and NDS were largest within 8 days after harvest. Seasonal means of wavelet entropy ($R^2 = 0.70$) and GC-SSD ($R^2 = 0.63$) at harvest were linearly related to SDM. It was concluded that imaging spectroscopy provides accurate means for assessment of SDM and sward heterogeneity. Effects of sward management and botanical composition on heterogeneity require further study, before conclusions can be drawn with regard to the implications of sward heterogeneity for sward reseeding or renovation.

Imaging spectroscopy for pasture management

The accuracy of imaging spectroscopy as a tool to estimate dry matter (DM) yield, contents of N, crude fiber, ash, sugar and DM, and mineral concentration (P, K, S, Ca, Mg, Mn, Zn, and Fe) of grass swards is evaluated in Chapter 9. Two data sets were used from *Lolium perenne* L. experiments where the degree of sward damage or N application varied. Partial least square (PLS) regression models were built from the leaf reflectance data, and were calibrated and validated per data set. PLS models were evaluated per sensor and for a combination of 2 sensors. The 2-sensor PLS models were combined with GC and IRI. Furthermore, the potential reduction in model error was explored for 10, 25 and 50 observations per field for a large and small model bias contribution.

Results showed that the 2-sensor PLS model including GC and IRI performed best. The mean prediction errors for experiment 1 and 2 were 268 and $235 \text{ kg DM ha}^{-1}$, 0.24 and $0.34 \text{ N } (\%)$, 1.68 and $0.96 \text{ DM } (\%)$, 16.2 and $27.7 \text{ sugar } (\text{g kg}^{-1} \text{ DM})$, 6.5 and $5.8 \text{ ash } (\text{g kg}^{-1} \text{ DM})$ and 10.4 and $8.36 \text{ crude fiber } (\text{g kg}^{-1} \text{ DM})$. The predictions for P, K, S, and Mg allowed identification of deficiency levels, in contrast to Na. Predictions were poor for Zn, Mn and Ca. With 25 replicate measurements, the calculated prediction error of DM yield may be maximally reduced to $95\text{-}142 \text{ kg ha}^{-1}$ for fields with a within-field standard deviation of 300 kg ha^{-1} . It is concluded that imaging spectroscopy provides

robust and accurate means for assessment of DM yield and feeding quality of standing grass. The methodology, however, requires further evaluation under field conditions, including a range of grass species and management practices.

Effects of sampling strategy and effects of spatial resolution

In Appendix I calculations are given to assess effects of the used sampling strategy for image recording and spatial resolution (pixel width). Results showed that the mean errors made within a growth period with the used sampling strategy are small. This error was 2-5 times larger for heterogeneous swards than for homogeneous swards. Spatial resolution had a strong effect on reflectance characteristics. Increasing amounts of bare soil and dead material enlarged effects of spatial resolution.

Comparison of techniques for DM yield assessment

In Appendix II the accuracy of imaging spectroscopy for DM yield assessment is compared with that of a disk plate meter and Cropscan. Data from experiments varying in the degree of sward damage and N application were used. The disk plate meter resulted in R^2_{adj} values of 0.55-0.66 and Cropscan in R^2_{adj} values ranging between 0.59-0.87. Imaging spectroscopy calibrations resulted in R^2_{adj} values of 0.96-0.99, and prediction errors were between 235-268 kg DM ha⁻¹. It is concluded that imaging spectroscopy was more accurate for DM yield assessment than the disk plate meter and Cropscan.

General discussion

In Chapter 10, results of previous chapters and the appendices are evaluated, with consideration of the initial objectives. It was argued that, in the experiments reported here, imaging spectroscopy provided non-destructive and accurate means to monitor growth; to quantify N deficiency; to detect drought stress in an early stage; to assess DM yield at harvest and seasonal DM yield; to quantify the content of clover in mixtures of grass and clover; to quantify spatial heterogeneity and differentiate swards into groups with various degrees of sward damage; and to predict feeding value and nutrient content. The outcome of this study now needs to be tested under field conditions.

Application of imaging spectroscopy in fields on farms requires a mobile system that allows image recording while moving and with high spatial

coverage. Such a system should be able to record hyperspectral reflectance in the 400-1650 nm range, and should preferably be equipped with a camera capable of recording 2D images with high contrast between green material and background. The 2D image will allow both high spatial resolution and high spatial coverage. The system should be equipped with a global positioning system for visualisation of data and quantification of patterns on a spatial scale larger than one image (line). The system should exclude solar influence by working under dark or shadowed conditions. The vertically projected and slightly diverging light beam of the light sources used in the experimental system should be maintained. Finally, it is required that the dynamic range of the cameras is large enough to measure the full spectrum of leaves, even for vertically oriented leaves in low canopy positions.



Samenvatting

Introductie

Melkveehouderijsystemen in een gematigd klimaat gebruiken meestal gras als belangrijkste voedermiddel. Graslandmanagement is nog steeds voornamelijk gebaseerd op kwalitatieve expertise van de veehouder. Graslandmanagement kan mogelijk worden verbeterd met behulp van objectieve en kwantitatieve informatie over de actuele status van de graszode. Deze informatie kan mogelijk worden verkregen aan de hand van digitale beelden van de graszode. Net voor het project startte, kwam een nieuwe beeldvormende techniek beschikbaar. Met deze techniek kunnen instantaan hyperspectrale opnamen worden gemaakt. Hierdoor kunnen ruimtelijke resoluties op sub-bladniveau worden gecombineerd met reflectiemetingen in een groot aantal spectrale banden. Dit betekent dat bladpixels in digitale zodenbeelden kunnen worden onderscheiden van pixels met dood zodenmateriaal en grond voorafgaand aan spectrale analyse. Zodenbeelden kunnen dan niet alleen informatie verschaffen over de aanwezigheid van grasbladeren, maar mogelijk ook over bijvoorbeeld nutriëntvoorziening en voederwaarde van het gewas.

Deze studie had tot doel (1) om een experimenteel beeldvormend spectrometrisch systeem te ontwerpen en te bouwen waarmee reflectie kan worden gedetecteerd van bladeren in een te velde staand gewas in het zichtbare en nabij-infrarode golflengtegebied; (2) om beeldparameters te definiëren en selecteren waarmee groei, heterogeniteit, en nutriënt- en droogtestress kunnen worden gekarakteriseerd; (3) het bestuderen en kwantificeren van relaties tussen beeldparameters en groei, droge stof (DM) opbrengst, zodenheterogeniteit en groeicapaciteit, bedekking van klaver, de mate van stikstof (N) en droogtestress en de voederwaarde van een grasgewas.

Innovatief systeem voor beeldvormende spectroscopie

Hoofdstuk 2 geeft gedetailleerde informatie over ontwerp, eigenschappen en testresultaten van een experimenteel, beeldvormend spectroscopisch systeem. Het systeem detecteert reflectie met hoge ruimtelijke ($0,28-1,45 \text{ mm}^2$) en spectrale resolutie (5-13 nm) tussen 405 en 1659 nm op een hoogte van 1,3 m boven het grondoppervlak.

Uit de testresultaten blijkt dat reflectie-intensiteit van bladpixels is gerelateerd aan de hoogte van het blad in het gewas en de bladhoek. Met het systeem kan de structuur van het gewas worden beschreven door middel van grondbedekking, de verdeling van reflectie-intensiteit over bladpixels en

beeldtextuur. Op bladniveau kunnen spectrale karakteristieken worden verkregen, zonder versturende invloeden van de achtergrond.

Groeimonitoring

De mogelijkheden van dit experimentele beeldvormende systeem voor groeimonitoring van graszoden worden verkend in Hoofdstuk 3. Er is een experiment uitgevoerd met 36 *Lolium perenne* L. minizoden die verschilden in de mate van zodenschade. Classificatieprocedures voor beelden, gebruikmakend van ‘maximum likelihood’, resulteerden in (meerdere) schattingen voor grondbedekking en in een index voor reflectie intensiteit (IRI). Deze index is een maat voor het aandeel sterk reflecterende gewaspixels. Bladpixels met vergelijkbare reflectie-intensiteiten zijn gegroepeerd in intensiteitsklassen (IC).

De resultaten laten zien dat GC geschat uit beelden sterk was gecorreleerd met de visueel ingeschatte GC ($R^2_{\text{adj}}=0,94$), de leaf area index (LAI) ($R^2_{\text{adj}}=0,88$) en lichtonderschepping (LI) ($R^2_{\text{adj}}=0,94$ voor dichte zoden onder een bewolkte hemel). De relaties tussen GC en LI verschilden voor bewolkte en onbewolkte hemelcondities. Onder een bewolkte hemel was de LI lineair gerelateerd aan GC, terwijl deze relatie een meer logistisch karakter had bij een onbewolkte hemel. Open zoden hadden, vergeleken met dichte zoden bij vergelijkbare groeistadia, gemiddeld een lagere GC en een lagere IRI. Regressie analyse tussen GC, IRI en DM opbrengst resulteerde in correlaties met een R^2_{adj} van 0,75-0,82. De gemiddelde schattingsfout van DM opbrengst was 340 kg ha⁻¹. Geconcludeerd werd dat met beeldvormende spectroscopie, door middel van toename in geschatte GC en IRI, de groei accuraat en non-destructief kan worden gevolgd.

Detectie van stikstofstress

De mogelijkheden voor een vroege herkenning van stikstof (N) stress m.b.v. beeldvormende spectroscopie worden verkend in Hoofdstuk 4. Hiervoor is een experiment met 15 *Lolium perenne* L. minizoden en 5 N giften uitgevoerd. Blue edge (BE), green edge (GE) en red edge (RE) posities zijn berekend voor elke IC.

Zowel GC als IRI namen toe tot de oogst, met de grootste toename voor hoge N giften. De breedte van de chlorofyl-absorptieband (CAW, berekend als verschil tussen RE en GE positie) nam in de eerste 2 weken na oogst toe tot een

maximum van 133 nm, voor zowel hoge als beperkte N giften. Bij een lage N gift nam de CAW af in de tweede helft van de groeiperiode in tegenstelling tot de situatie bij een hoge N gift. Bij oogst verklaarde CAW 95% van de variatie in relatieve DM opbrengst tussen N giften. Principale componentenanalyse vertoonde een verstrengelde respons met betrekking tot DM opbrengst en N concentratie. De positie van de edges veranderde sterk met IC.

Effecten van bladhoek, -hoogte en pigment concentratie op reflectie

In Hoofdstuk 5 worden de effecten bestudeerd van bladhoek, bladhoogte en pigmentconcentratie op de reflectiespectra van graszoden. Er is een experiment uitgevoerd met *Lolium perenne* L. minizoden en 4 N giften. Bij oogst is het gewas geoogst in 3 strata (>16 cm, 9-16 cm en 4-9 cm) en strata zijn geanalyseerd op chemische samenstelling inclusief pigmenten. Effecten van bladhoek en -hoogte zijn onafhankelijk hiervan bestudeerd met behulp van geplukte bladeren.

Gehalten van N en pigmenten namen gemiddeld toe met de grootte van de N gift en namen gemiddeld af met toenemende diepte in het gewas. BE, GE en RE vertoonden een sterke verandering met IC, afhankelijk van N gift. Bij oogst nam de CAW van intacte zoden toe met de N gift, waarbij de absolute waarden overeenkwamen met waarden gemeten aan geoogst materiaal. Na oogst van het bovenste stratum nam de CAW van het overblijvende gewas minder af dan op basis van metingen aan geoogst materiaal verwacht kon worden. Het variëren van de bladhoek van horizontaal naar bijna verticaal verschoof BE 2 nm, GE 6 nm, en RE 2 nm en verhoogde de CAW met ongeveer 6 nm. Het verlagen van de bladhoogte met 20 cm had weinig effect op de BE, verschoof de GE met 2,3 nm en de RE met 4,9 nm en verlaagde de CAW met 2,6 nm. De ratio tussen reflectie bij rode en blauwe golflengten werd ook sterk beïnvloed door de bladhoek. Verschuivingen van hellingsposities met IC konden slechts gedeeltelijk worden verklaard door de gesommeerde effecten van bladhoek en bladhoogte en werden mogelijk versterkt door sensor eigenschappen. Geconcludeerd werd dat de combinaties van de verhouding tussen reflectie bij rode en blauwe golflengten, van verschuivingen van de GE met IC, en van CAW mogelijk gebruikt kunnen worden om de effecten van bladhoek en pigmentconcentratie op gewasreflectie te scheiden.

Detectie van droogtestress

De mogelijkheden voor een vroege herkenning van droogtestress m.b.v. beeldvormende spectroscopie worden verkend in Hoofdstuk 6. Hiervoor is een klimaatkamerexperiment met 9 *Lolium perenne* L. minizoden met droogtebehandelingen bij 2 N giften uitgevoerd. Golflengtepositie van buigpunten van afgeleide spectra werden geschat en geanalyseerd in relatie tot de progressief toenemende mate van droogtestress.

Door droogtestress nam het drogestofgehalte van bladeren en het suikergehalte toe. Droogtestress vertraagde en keerde de GC ontwikkeling uiteindelijk om en hield IR op lage waarden. In tegenstelling tot niet-gestresste groei werden alle absorptiebanden smaller en minder diep bij droogtestress. De buigpunten nabij 1390 en 1500 nm waren het meest gevoelig voor droogtestress. Verschillen tussen zoden met en zonder droogtestress werden gedetecteerd net voordat het watergehalte van bladeren onder 80% zakte. Het verloop van de golflengtepositie van buigpunten keerde om bij droogtestress, behalve voor de RE waarvan de verschuiving naar langere golflengten gedurende de groei werd versterkt. De relatie tussen buigpunten nabij 705 en 1390 nm onderscheidde niet-gestresste zoden in een vroeg groeistadium van gestresste zoden in een laat groeistadium.

Bepaling van de bedekkingsgraad van klaver

In Hoofdstuk 7 worden de mogelijkheden van beeldvormende spectroscopie verkend voor een robuust onderscheid tussen gras-, klaver- en gemengde zoden in verschillende groeistadia. Hiervoor zijn de spectra van deze zoden vergeleken en is de beeldlijntextuur geanalyseerd met behulp van ruimtelijke correlatie, een speciaal filter en wavelet entropie. In 2000 is een experiment met minizoden uitgevoerd met twee witte klaver (*Trifolium repens* L.) zoden, drie engels raaigras (*Lolium perenne* L.) zoden en vier gemengde zoden met gras en witte klaver.

Uit de resultaten bleek dat de gemiddelde spectrale curve van gras- en witte klaverpixels verschilden over het gehele gemeten golflengtebereik, maar dat de verschillen klein waren in vergelijking tot de variatie in spectra van graspixels. Er is geen specifiek onderscheidend spectraal kenmerk gevonden. Verschillen in hellingsposities tussen gras- en witte klaverzoden waren niet consistent binnen groeiperioden. Pure gras- en klaverzoden konden worden onderscheiden aan de hand van beeldlijntextuur, zowel met het filter, als de ruimtelijke

correlatie en wavelet entropie. Alleen wavelet entropie resulteerde in een robuust onderscheid op alle opnamedagen. De resultaten van gemengde zoden lagen tussen de resultaten van pure gras- en witte klaverzoden.

Schatting van jaaropbrengst en zodenkwaliteit

Relaties tussen ruimtelijke heterogeniteit van spruitdichtheid, LI, GC, en DM opbrengst in een seizoen (SDM) worden bestudeerd in Hoofdstuk 8. Zodeheterogeniteit is gekwantificeerd met de ruimtelijke standaard deviatie van GC (GC-SSD) en logistisch getransformeerde GC (TGC-SSD), patronen in GC transecten zijn gekwantificeerd met wavelet entropie. Een experiment is uitgevoerd met controle zoden (CS), zoden met een natuurlijke beschadiging (NDS) en kunstmatig beschadigde zoden (ADS).

Ruimtelijke variatie van spruitdichtheid was groter voor ADS en NDS dan voor CS. SDM was lineair gerelateerd aan een combinatie van GC en IRI ($R^2=0,93$). Het bleek dat een toename van 1% eenheid in het seizoensgemiddelde van GC de SDM deed toenemen met 0,31 t DM ha⁻¹. Dit komt overeen met voorspellingen van een grasgroeimodel. Waarden van GC-SSD en wavelet entropie waren groter voor ADS en NDS dan voor CS. GC-SSD van CS bleef beneden 13% gedurende het gehele seizoen, dit in tegenstelling tot de waarden voor NDS en ADS. Absolute verschillen in TGC-SSD tussen CS, ADS en NDS waren het grootst binnen 8 dagen na oogst. Seizoensgemiddelden van wavelet entropie ($R^2=0,70$) en GC-SSD ($R^2=0,63$) bij oogst waren lineair gerelateerd aan SDM. Geconcludeerd werd dat beeldvormende spectroscopie een accurate techniek is om SDM en zodeheterogeniteit in te schatten. Effecten van zodenmanagement en botanische samenstelling behoeven nadere studie voordat conclusies getrokken kunnen worden met betrekking tot de relatie tussen zodeheterogeniteit en de noodzaak van graslandverbetering.

Beeldvormende spectroscopie voor graslandmanagement

De nauwkeurigheid van beeldvormende spectroscopie als schatter van DM opbrengst, gehalten van N, ruwe celstof, ruwe as, suiker, droge stof, en concentratie van mineralen (P, K, S, Ca, Mg, Mn, Zn, Fe) van graszoden wordt geëvalueerd in Hoofdstuk 9. Twee datasets zijn gebruikt van *Lolium perenne* L. experimenten waarin de mate van zodenschade en N gift varieerde. Regressie modellen zijn samengesteld uit bladreflectie data door middel van de partiële kleinste kwadraten (PLS) methode en zijn gekalibreerd en gevalideerd per

dataset. PLS modellen zijn geëvalueerd per sensor en voor een combinatie van 2 sensoren. Het 2-sensor PLS model is gecombineerd met GC en IRI. Daarnaast is de potentiële reductie in modelfout verkend voor 10, 25 en 50 waarnemingen per veld met een grote en een kleine bijdrage van de modelafwijking.

De resultaten lieten zien dat het 2-sensor model in combinatie met GC en IRI het beste presteerde. De gemiddelde schattingsfouten voor experiment 1 en 2 waren 268 en 235 kg DM ha⁻¹, 0,24 en 0,34 N (%), 1,68 en 0,96 DM (%), 16,2 en 27,7 suiker (g kg⁻¹ DM), 6,5 en 5,8 ruwe as (g kg⁻¹ DM) en 10,4 en 8,36 ruwe celstof (g kg⁻¹ DM). De voorspellingen voor P, K, S en Mg lieten identificatie van tekorten toe, in tegenstelling tot Na. Voorspellingen voor Zn, Mn en Ca waren zwak. Voor velden met een variatie binnen het veld in DM opbrengst van 300 kg ha⁻¹ kan met 25 waarnemingen per veld de voorspellingsfout voor DM opbrengst met maximaal 95-142 kg DM ha⁻¹ worden gereduceerd. Geconcludeerd werd dat beeldvormende spectroscopie een robuust en accuraat middel is om DM opbrengst en voederwaarde van een grasgewas te schatten. De methodologie behoeft nog wel een evaluatie onder veldcondities, waaronder inbegrepen een breed spectrum aan grassoorten en verschillende vormen van graslandgebruik.

Effecten van bemonsteringsstrategie en ruimtelijke resolutie

In Appendix I worden berekeningen gemaakt om de effecten van de gebruikte bemonsteringsstrategie voor beeldopname en de ruimtelijke resolutie (pixel breedte) in te schatten. De resultaten toonden aan dat de gemiddelde fout in een groeiperiode die werd gemaakt met de gebruikte bemonsteringsstrategie klein was. Deze fout was 2-5 keer groter voor heterogene zoden dan voor homogene zoden. Ruimtelijke resolutie had een groot effect op reflectiekenmerken. Toenemende aandelen kale grond en dood materiaal versterkten het effect van ruimtelijke resolutie.

Vergelijking van technieken voor de schatting van grasopbrengst

In Appendix II wordt de nauwkeurigheid van de schatting van DM opbrengst van beeldvormende spectroscopie vergeleken met die van de gewashoogtemeter en de Cropscan. Er is gebruik gemaakt van data van experimenten waarin de mate van zodenschade en N gift varieerde. De gewashoogtemeter resulteerde in R^2_{adj} waarden van 0,55-0,66, voor de Cropscan lagen deze waarden op 0,59-0,87. Calibraties van beeldvormende spectroscopie resulteerde in R^2_{adj} waarden

van 0,96-0,99 en voorspellingsfouten lagen tussen 235 en 268 kg DM ha⁻¹. Geconcludeerd werd dat de DM opbrengstschattingen met beeldvormende spectroscopie nauwkeuriger waren dan met de gewashoogtemeter of met de Cropscan.

Algemene discussie

In Hoofdstuk 10 worden de resultaten van voorgaande hoofdstukken en de bijlagen geëvalueerd met betrekking tot de oorspronkelijk doelen. Beargumenteerd is dat, voor de besproken experimenten, beeldvormende spectroscopie een non-destructief en nauwkeurig middel is om groei te monitoren; om N gebrek te kwantificeren; om droogtestress in een vroeg stadium te detecteren; om DM opbrengst bij oogst en seizoensopbrengst van DM te schatten; om het aandeel van klaver in gemengde zoden met gras en witte klaver te schatten; om ruimtelijke zodeheterogeniteit te schatten en groepen te onderscheiden met een verschillende mate van zodenschade en om de voederwaarde en nutriëntgehalte te schatten. De resultaten van deze studie moeten nu getest worden onder veldomstandigheden.

Toepassing van beeldvormende spectroscopie op praktijkpercelen vereist een mobiel systeem waarmee al rijdend beelden kunnen worden opgenomen met een grote ruimtelijke dekkingsgraad. Een dergelijk systeem zou de mogelijkheid moeten hebben om hyperspectrale reflectie te detecteren van 400 tot 1650 nm en zou bij voorkeur uitgerust moeten zijn met een camera voor 2D beelden met een groot contrast tussen groen materiaal en achtergrond. De 2D beelden zorgen voor zowel een grote ruimtelijke resolutie als voor een grote ruimtelijke dekking. Het systeem zou uitgerust moeten zijn met een “global positioning system” voor de visualisatie van data en het kwantificeren van patronen op een ruimtelijke schaal die groter is dan een beeld(lijn). Het systeem moet de invloed van de zon uitsluiten door te werken onder donkere of beschaduwde condities. De vertikaal geprojecteerde en enigszins divergerende lichtbundel, zoals gebruikt in het experimentele systeem, zou opnieuw gebruikt moeten worden. Tenslotte moet het dynamisch bereik van de camera's groot genoeg zijn om het volledige spectrum van bladeren te bemeten, zelfs van verticaal georiënteerde bladeren onder in het bladerdek.

Appendix I

**Accuracy of imaging spectroscopy and
effects of spatial resolution**

A1.1 Introduction

The objective of this appendix is to identify and quantify error sources of the experimental imaging spectroscopy system, the sampling strategy and spatial resolution used in particular. Effects of six sampling strategies in mini swards with a low to intermediate heterogeneity and effects of replicate measurements on a single mini sward were evaluated. For this, 2-dimensional images, composed of 300 image lines were available from the drought experiment, as described in Chapter 6. Effects of spatial resolution on derivatives from mean leaf reflectance spectra from swards were also studied with data from the drought experiment. Other error sources, related to the instrument design and described by Jørgensen (2002), are summarised and discussed.

A1.2 Materials and methods

A1.2.1 Images available

The number of image lines recorded with the experimental imaging spectroscopy system was chosen at 42 per mini sward. To evaluate the effects of this choice, different recording strategies were compared.

In the drought experiment (Chapter 6) there were 2-dimensional (2D) hyperspectral images constructed from 300 adjacent image lines. These 300 image lines covered an area of 300 mm long and 133.1 mm wide. Images of three swards were used, from treatments control (mini sward 1), drought stressed with high N (mini sward 2) and drought stressed with low N (mini sward 3). The images recorded on 5, 9, 13, 17, 21 and 25 November were analysed, to include a range of growth stages.

Spatial variability is the determining factor in the number of recordings per mini sward required. In Chapter 6, it was concluded that drought stress did not significantly increase sward heterogeneity. Therefore, results of this study are only valid for swards with a comparable heterogeneity.

A1.2.2 Sampling strategies

The sampling strategies (SAST) included a number of distances between image lines in a regular grid (Table I.1). With regular distances between image

Table I.1 Sampling strategies (SAST) studied. In boldface, the default sampling strategy.

SAST	Distance between image lines (mm)	Image lines (#)	Replicates (#)
1	2	150	2
2	4	75	4
3	12	25	10
4	25	12	25
5	50	6	50
6	100	3	100

lines, this distance determined the number of image lines per SAST on the 300 mm surface. Shifting the starting position 1 mm resulted in a number of possible replicate recordings per sampling strategy. All possible starting positions for recording were considered and this resulted in a number of replicates per SAST.

The images were classified according to procedures described in Chapter 3. Only results of the V7 sensor were used. The means and standard deviations of GC, IRI and blue edge (BE) and green edge (GE) position were calculated from these replicates. These parameters were calculated per image line, in contrast to the procedure described in Chapter 3.

The errors made with sampling were compared with the mean value, calculated over the 300 image lines. The spatial standard deviation (SSD) was calculated as standard deviation over the 300 estimates.

The errors of sampling strategies were evaluated with the root mean square error, calculated for GC as:

$$RMSE_{s,t} = \sqrt{\frac{1}{6} \sum_{d=1}^6 \frac{1}{n} \sum_{r=1}^n \left(\frac{1}{300} \sum_{i=1}^{300} GC_{d,i} - \frac{1}{il} \sum_{i=1}^{il} GC_{d,r,i} \right)^2} \quad (1)$$

where s is the sampling strategy, t the mini sward, d is the recording date, r is replicate number, n is the total number of replicates, i is the number of image lines and il the number of image lines per sampling strategy.

A1.2.3 Replicate measurements in one mini sward

With the default sampling strategy, 42 image lines per mini sward, 8 replicate recordings were made on the same day in one mini sward. For this, the container with the mini sward was placed under the experimental system, and removed afterwards. This was repeated for each recording. The mini sward was unfertilised in 2002 and had a very heterogeneous colour pattern, with many dead leaves and dead leaf-tips. The coefficient of variance (CV, %) was calculated as the quotient between the mean and standard deviation, expressed as percentage.

A1.2.4 Effects of spatial resolution on GC, IRI and derivatives

The effects of spatial resolution were studied on the 2D-data from the drought experiment. Mean GC, IRI and reflection of green pixels were calculated from the 300 image lines. Positions of minimum or maximum derivatives at 518, 570, 1140, 1220 and 1390 nm were calculated according to procedures described in Chapter 6. Only data from the V7 and N17 sensor were used. For this, radiance data from several pixels on the image line were summed (before calculating reflectance, this is sometimes called 'binning'). This resulted in a lower number of pixels per image line. In total, five spatial resolutions were compared: 128, 32, 16, 8 and 4 pixels per image line for the N17, with pixel widths on the soil of 1.04, 4.16, 8.32, 16.64 and 33.28 mm respectively. For the V7 sensor, the compared spatial resolutions were 768, 192, 96, 48, 24, and 12 pixels per image line. This resulted in pixel widths on the soil of 0.20, 0.79, 1.59, 3.17, 6.35 and 12.71 mm respectively. The root mean square error was calculated as difference with the finest resolution, averaged over 6 dates.

A1.3 Results

A1.3.1 Spatial variability of GC in the mini swards

The GC-SSD of mini sward 1 was smaller than mini swards 2 and 3 from 9 November onwards (Table I.2). The SSD of BE and GE decreased strongly during growth for mini sward 1, whereas SSD of mini sward 2 and 3 increased.

Table I.2 Means \pm spatial standard deviation per mini sward.

Sward	5/11	9/11	13/11	17/11	21/11	25/11	Mean
-----GC (%)-----							
1	25.4 \pm 7.7	44.0 \pm 9.4	57.5 \pm 8.2	64.1 \pm 9.2	72.5 \pm 6.7	83.7 \pm 6.1	57.87
2	16.1 \pm 5.5	29.3 \pm 9.8	35.1 \pm 10.2	34.1 \pm 11.6	33.3 \pm 13.2	25.2 \pm 12.5	28.85
3	28.2 \pm 9.5	41.8 \pm 10.2	44.4 \pm 9.0	45.7 \pm 8.5	42.4 \pm 8.0	40.3 \pm 9.1	40.47
-----IRI (%)-----							
1	2.0 \pm 3.1	2.6 \pm 3.3	3.7 \pm 2.8	3.0 \pm 3.6	4.2 \pm 2.8	17.1 \pm 4.2	5.43
2	3.1 \pm 4.6	3.0 \pm 5.0	4.1 \pm 4.1	4.4 \pm 4.4	3.4 \pm 3.0	2.4 \pm 2.5	3.40
3	1.2 \pm 2.4	0.8 \pm 1.6	1.8 \pm 2.1	1.9 \pm 2.0	4.0 \pm 3.1	3.5 \pm 3.5	2.20
-----BE (nm)-----							
1	518.7 \pm 1.2	520.1 \pm 0.9	520.5 \pm 0.6	520.8 \pm 0.5	521.2 \pm 0.4	520.4 \pm 0.3	520.28
2	518.9 \pm 1.1	520.2 \pm 0.8	520.6 \pm 0.6	520.6 \pm 0.6	520.4 \pm 0.6	520.3 \pm 0.7	520.17
3	518.3 \pm 1.0	520.3 \pm 0.9	520.5 \pm 0.7	520.5 \pm 0.7	520.6 \pm 0.4	520.5 \pm 0.5	520.12
-----GE (nm)-----							
1	588.6 \pm 8.0	580.5 \pm 3.0	579.5 \pm 1.3	578.3 \pm 1.5	577.6 \pm 0.9	578.9 \pm 0.6	580.57
2	591.3 \pm 10.0	581.2 \pm 2.5	579.7 \pm 1.9	581.5 \pm 3.5	583.0 \pm 6.1	592.4 \pm 11.2	584.85
3	596.2 \pm 10.8	581.9 \pm 5.2	579.8 \pm 1.7	580.0 \pm 1.5	580.4 \pm 1.6	584.5 \pm 5.5	583.80

A1.3.2 Sampling strategies

As expected, the RMSE increased with lower sampling intensity (Table I.3). The mean RMSE of GC was larger for mini swards 2 (1.16%) and 3 (1.55%) than for mini sward 1 (0.72%). For homogeneous swards, the mean (absolute) error with the default sampling-strategy (SAST 5) was 0.95% GC and 0.59% IRI, 0.10 nm for the BE and 0.34 nm for the GE. These values increased for the more heterogeneous swards 2 and 3, as shown by the mean values. Reducing the RMSE with 50% requires an increase in sampling intensity of more than a factor two. There was a strong temporal effect in RMSE for the spectral characteristics. For mini sward 1, BE and GE RMSE decreased from 0.26 and 0.75 nm at the beginning of the growth period to 0.02 and 0.05 nm at the end of the growth period (Table I.4).

Table I.3 RMSE for sampling strategies (SAST) 1-6 in mini swards 1-3. Default sampling SAST is printed in boldface.

Sward	SAST 1	SAST 2	SAST 3	SAST 4	SAST 5	SAST 6	Mean
-----GC (%)-----							
1	0.12	0.37	1.00	0.65	0.95	1.21	<i>0.72</i>
2	0.06	0.27	0.85	0.99	1.7	3.07	<i>1.16</i>
3	0.22	0.52	1.06	1.94	3.34	2.22	<i>1.55</i>
Mean	<i>0.13</i>	<i>0.39</i>	<i>0.97</i>	<i>1.19</i>	2.00	<i>2.17</i>	
-----IRI (%)-----							
1	0.03	0.11	0.38	0.34	0.59	0.58	<i>0.34</i>
2	0.06	0.23	0.64	0.55	0.53	0.97	<i>0.50</i>
3	0.07	0.12	0.42	0.64	0.95	0.47	<i>0.45</i>
Mean	<i>0.05</i>	<i>0.15</i>	<i>0.48</i>	<i>0.51</i>	0.69	<i>0.67</i>	
-----BE (nm)-----							
1	0.01	0.02	0.07	0.05	0.10	0.19	<i>0.07</i>
2	0.02	0.05	0.11	0.06	0.13	0.16	<i>0.09</i>
3	0.01	0.04	0.11	0.16	0.26	0.12	<i>0.12</i>
Mean	<i>0.01</i>	<i>0.04</i>	<i>0.10</i>	<i>0.09</i>	0.16	<i>0.16</i>	
-----GE (nm)-----							
1	0.01	0.13	0.32	0.27	0.34	0.56	<i>0.27</i>
2	0.21	0.39	0.92	0.64	0.70	1.08	<i>0.66</i>
3	0.08	0.16	0.45	1.08	1.70	0.74	<i>0.70</i>
Mean	<i>0.10</i>	<i>0.23</i>	<i>0.56</i>	<i>0.66</i>	0.91	<i>0.79</i>	

The RMSE of GE of the drought stressed swards 2 and 3 first decreased, but then GE increased again. The RMSE value of BE remained at a higher level for mini swards 2 and 3 than mini sward 1, but did not show a consistent pattern.

A1.3.3 Replicate recordings on one sward

The replicate measurements were performed on a sward with an intermediate GCT-SSD (9.0%) and GCT-SSD (0.4) value, indicating a homogeneous sward, with 49.6% GC (Table I.5).

Table 1.4 Temporal aspects of sampling strategy 5 on blue edge (BE) and green edge (GE) RMSE in mini swards 1-3.

Sward	5 Nov	9 Nov	13 Nov	17 Nov	21 Nov	25 Nov
-----BE (nm)-----						
1	0.26	0.17	0.10	0.04	0.02	0.02
2	0.27	0.08	0.14	0.06	0.13	0.11
3	0.46	0.28	0.26	0.26	0.18	0.18
Mean	<i>0.33</i>	<i>0.18</i>	<i>0.17</i>	<i>0.12</i>	<i>0.11</i>	<i>0.10</i>
-----GE (nm)-----						
1	0.75	0.70	0.24	0.16	0.13	0.05
2	1.34	0.36	0.38	0.26	0.86	0.98
3	4.68	1.92	0.75	0.50	0.58	1.76
Mean	<i>2.26</i>	<i>0.99</i>	<i>0.46</i>	<i>0.31</i>	<i>0.52</i>	<i>0.93</i>

Table 1.5 Means, standard deviation of the mean (SDM) and coefficient of variance (CV, %) of 8 replicate measurements in a single mini sward for soil, dead material (DM), ground cover (GC), GC spatial standard deviation (SSD), logarithmically transformed GC (GCT) SSD, index of reflection intensity (IRI) and blue edge (BE) and green edge (GE) position.

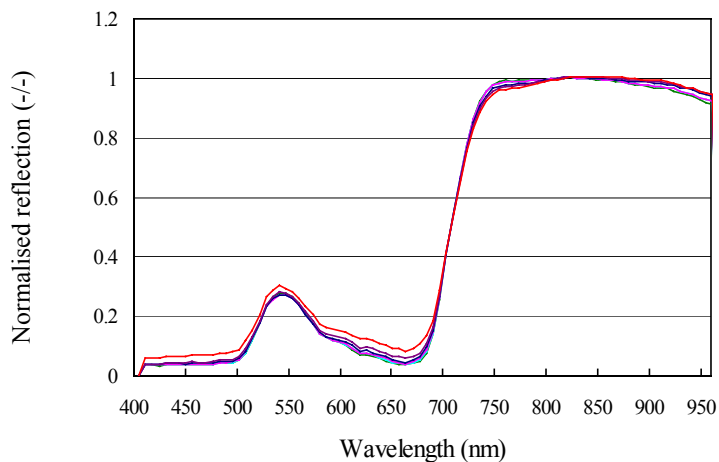
	Soil (%)	DM (%)	GC (%)	IRI (%)	GC-SSD (%)	GCT-SSD (%)	BE (nm)	GE (nm)
Mean	35.3	14.9	49.6	2.8	9.0	0.4	519.9	601.6
SDM	1.36	1.13	0.93	0.48	0.97	0.04	0.11	1.14
CV	3.8	7.6	1.9	17.2	10.7	10.8	0.02	0.19

The relative error of GC was small with a CV of 1.9%. The individual intensity classes had a CV of 7.5, 5.1, 4.8, 11.2, 17.6, 29.0 and 45.8 for GCG₀₋₆, where CV increased with a lower mean value.

A1.3.5 Effects of spatial resolution

Increasing the spatial resolution increases reflectance considerably (Figure I.1 and I.2). The largest changes can be found at wavelengths were reflection of

A



B

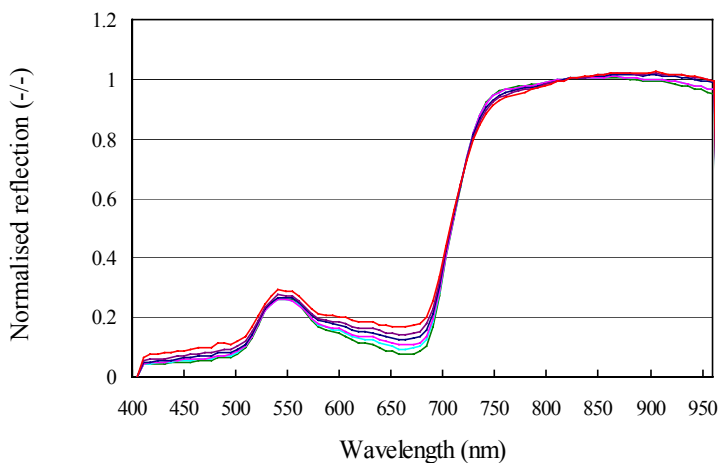
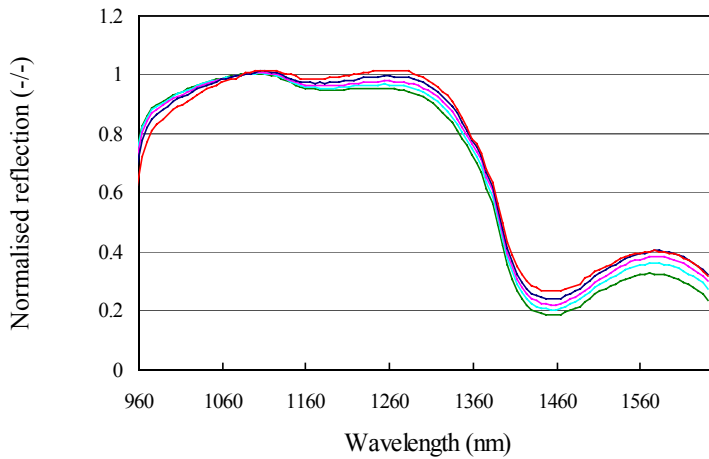


Figure I.1 Effects of pixel width on reflectance, measured on 17 November with the V7 sensor from mini sward 1 with adequate water supply (A) and mini sward 2 with drought stress (B). Pixel widths: 0.20 (—), 0.79 mm (—), 1.59 mm (—), 3.17 (—), 6.35 mm (—) and 12.71 mm (—).

green material is low. Spatial resolution had minor effect on reflectance at the transition from the red to the infrared *i.e.* all curves had similar normalised reflection at one wavelength on the edge.

A



B

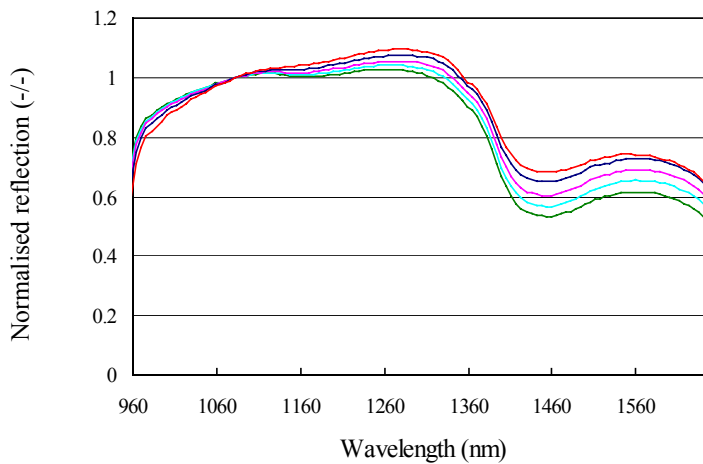
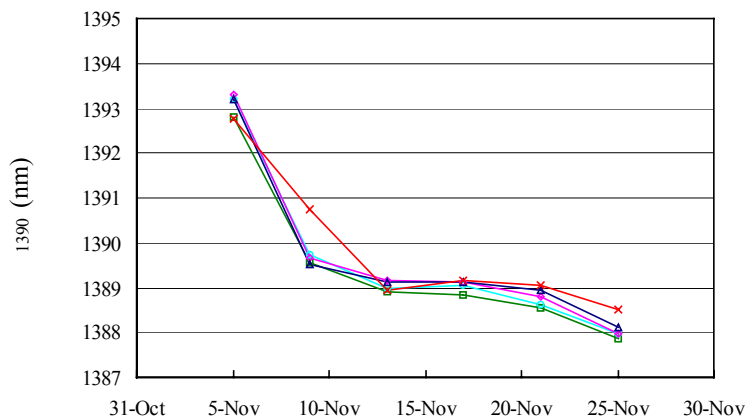


Figure I.2 Effects of pixel width on reflectance, measured on 17 November with the N17 sensor from mini sward 1 with adequate water supply (A) and mini sward 2 with drought stress (B). Pixel widths: 1.04 mm (—), 4.16mm (—), 8.32 mm (—), 16.64 mm (—) and 32.28mm (—).

The wavelength position of this crossing point was slightly higher for mini sward 2 than 1. The effects of spatial resolution were slightly larger for mini sward 2 than 1. This difference was probably due to the differences in GC, visible dead sward material and water content of the soil. On 17 November, GC was 64.1% for mini sward 1 and 34.1% for mini sward 2 (Table I.2).

A



B

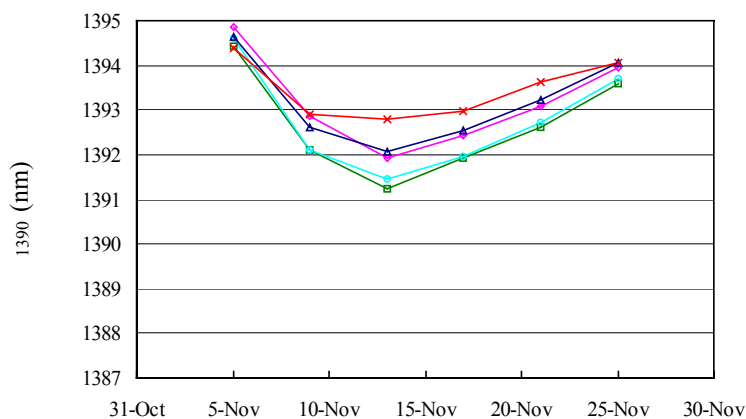


Figure I.3 Position of minimum derivative near 1390nm for mini sward 1 (A) and 2 (B). Pixel widths: 1.04 mm (—), 4.16mm (—), 8.32 mm (—), 16.64 mm (—) and 32.28mm (—).

Obviously, these changes in spectral curve also affected the position of minimum or maximum derivatives. As an example, the position of the minimum derivative near 1390 nm is shown (Figure I.3).

The effects of spatial resolution were stronger for mini sward 2 than 1 (Figure I.2). The trends were similar for various spatial resolutions. The water content of the soil under mini sward 2 was low, in contrast to the soil under mini sward 1. Therefore, the contrast in reflectance pattern between soil and green material was larger for mini sward 2 than 1. This effect was largest around 13 November, and thereafter the contrast decreased when leaves dried out, resulting in smaller differences between spatial resolutions (Figure I.3).

Increasing pixel widths affected the position of minimum and maximum derivatives stronger for mini sward 2 and 3 than 1 (Table I.6).

Based on these numbers, no critical pixel width could be identified. Positions of other minimum or maximum derivatives were in a similar fashion affected by spatial resolution. Although the spectra crossed at one point on the red edge, maximum derivatives showed shift in the position of the maximum derivative with spatial resolution for the drought-stressed mini sward 2, in contrast to mini sward 1.

Table I.6 Root mean squared error of position of minimum and maximum derivatives near 570 and 1390 nm, averaged over 6 dates, for various pixel widths.

Pixel Width (mm)	Mini sward 1	Mini sward 2	Mini sward 3	Mean
-----570 nm-----				
0.79	0.36	0.58	1.01	0.65
1.59	0.94	1.09	1.95	1.33
3.17	1.02	2.01	4.02	2.35
6.35	1.86	2.28	1.54	1.89
12.71	1.96	3.25	3.57	2.93
-----1390 nm-----				
4.16	0.51	0.33	1.00	0.61
8.32	0.72	1.36	1.95	1.34
16.64	0.71	1.41	1.93	1.35
32.28	1.49	2.31	2.22	2.01

A1.3.5 Error sources due to system design

Jørgensen (2002) described the error sources of lenses, dispersing spectrograph and camera extensively. The main sources of error are due to specifics of the imaging spectrograph and charge coupled device (CCD).

Consider the projection of an image line on the CCD, with spatial information on the horizontal axis and spectral information on the vertical axis. The location of specific wavelengths varies slightly with the position of the spatial axis. This means that if calibration is performed on the spectra in the centre of the spatial axis, there will be an error at the left and right end of the spatial axis. The manufacturer's test-report indicated that the bending across the spatial axis for the V7 sensor was 0.5 nm at 693 nm and 1.5 nm at 436 nm. Polder & Van der Heijden (2001) found a bending of 1.3 nm at 670 nm wavelength on a similar sensor. The bending ranged between 0.5-1.5 nm for the N10 sensor.

Lens distortions introduced also a bending on the vertical axis. The barrel distortion of the front lens is compensated by the pincushion distortion of the rear lens under the condition of symmetry. The diffraction in the PGP element causes asymmetry, and the barrel and pincushion distortions are no longer completely compensated.

Jørgensen (2002) found for the horizontal distortion ΔH on the CCD for their imaging spectrograph a relation of the form:

$$\Delta H = a \times d\lambda^2 \times dH$$

where ΔH indicates the error in mm, $d\lambda$ the displacement on the vertical axis when compared to the image centre and dH the displacement on the horizontal axis when compared to the image centre. This indicates that the error was largest on the outer-ends of the CCD-image.

The main error sources occurring in the CCD are due to dark current noise and pattern noise. Dark current noise is signal generated by the CCD itself, and strongly depends on temperature. Pattern noise arises from differences between pixels in *e.g.* size, material and thickness of coatings. Therefore, sensitivity to incident light varies between pixels. These error sources are important, and require pixel-based calibration.

A1.4 Discussion and conclusion

The errors made with the default sampling strategy were small for homogeneous swards. The mean RMSE (absolute error) of the default sampling strategy within a growth period was 0.95% GC, 0.59% IRI, 0.10 nm for the BE and 0.34 nm for the GE. It was shown that these values increased with a factor 2-5 for more heterogeneous mini swards. The RMSE of the spectral parameters BE and GE strongly decreased during the growth period for the homogeneous sward, from 0.36 nm (BE) and 0.75 nm (GE) at the beginning of the growth period to 0.02 nm (BE) and 0.05 nm (GE) at the end of the growth period.

The replicate measurements on a single sward showed a standard deviation (over replicate measurements) comparable to the default sampling strategy RMSE for GC and IRI, whereas the standard deviation was larger than RMSE for the spectral parameters BE and GE. This was probably due to the stronger spatial colour-heterogeneity of the sward on which the replicate measurements were performed. It should be noted that BE and GE were calculated per image line. Normally, the BE and GE were based on the average spectral curve of grass leaves in 42 image lines.

Spatial resolution had a strong effect on reflectance, and on the position of minimum and maximum derivatives. The amplitude of this effect depended on the width of the pixels on the image line, wavelength and background characteristics. Results of Horler *et al.* (1983) suggested that the derivative of the red edge position in field applications would be unaffected by ground cover, *i.e.* spatial resolution. Although different spatial resolutions had a common point where reflectance spectra crossed at the red edge, this point was not located at the point of maximum slope for mini swards 2 and 3. Therefore, the fraction of ground cover affected red edge position, probably because the background material may have had a clear reflectance slope from the red to the infrared.

The changes in reflection with spatial resolution were strongest in wavelength regions with low reflection. Increasing pixel widths up to 4 mm only slightly affected the mean reflection curve. This is equal to pixel sizes on the soil surface around 5.5 mm². The changes in reflection curve with increasing pixel widths were stronger for the drought stressed sward than for the control sward. These mini swards differed in GC and the amount of soil and dead material visible. This clearly illustrates that variation in spectral properties of the background must be accounted for, when measuring leaf reflectance with a system with pixel sizes equal or larger than leaf widths. Therefore, it is

concluded that background influence for field based systems, measuring under various background conditions, can be successfully reduced with pixel sizes smaller than leaf width.

Jørgensen (2002) identified and summarised a large number of potential error sources within imaging spectroscopy systems. The most important error sources were related to bending in horizontal and vertical direction on the image. The most important conclusion from this is that, when considering an image line, the spectral information of one location on the image line is influenced by its neighbours, where the amplitude depends on the position on the image line. The spectral information may also be somewhat shifted, *i.e.* the reflectance curve of a leaf in the centre of the image line deviates slightly from the reflectance curves from the same leaf measured at the left and right ends of the image line.

The influence of these two error sources on the measured reflectance is expected to be small for the V7 and N10 sensors, as spectral information was averaged over a large number of pixels on various image line positions. The spectral library contained spectra from various pixel positions on the image line. Therefore, the classes include variation due to position on the image line. From Chapter 3, it can be concluded that the spectral differences between classes were still large enough for successful classification.

These error sources become important when working with spectra of individual pixels, and appropriate calibrations should be performed (Jørgensen, 2002). Polder & Van der Heijden (2001) concluded that each position on the image line requires separate spectral calibration. From the work of Jørgensen, (2002) it can be concluded that pixel based calibrations are required in the spectral as well as the spatial direction.

The effects of dark current noise is limited by the short time lag between recording of 'standard' images (dark image and images of 50% reflecting surface) and by averaging over multiple reference images. The pattern noise was removed by pixel based calibration procedures. Dark current noise was probably the most important error source in the CCD, as the V7 and N10 sensors were not cooled.

Appendix II

**Comparison of imaging spectroscopy with disk plate
meter and Cropscan for dry matter yield
assessment**

A2.1 Introduction

Currently, there are a number of non-destructive grass dry matter (DM) yield assessment methods available, such as rulers, the disk-plate meter (DPM), capacitance meter or crop reflection meters. The disk or rising plate meter is a thoroughly studied method for non-destructive DM yield assessment in grass swards (Gabriels & Van den Berg, 1993; Harmony *et al.*, 1997; Murphy *et al.*, 1995; Sanderson *et al.*, 2001; Stockdale & Kelly, 1984; Virkajärvi, 1999). The crop reflection, measured with Cropscan (Cropscan Inc.), is currently used for fertilisation recommendation in a variety of crops (Booij *et al.*, 2001).

The accuracy of dry matter (DM) yield assessment with imaging spectroscopy was evaluated by means of comparison with DPM and Cropscan. For the sward damage and nitrogen experiment in 2000, crop height measurements were made at harvest with a disk plate meter. Crop reflection was measured with the Cropscan at three harvests. The Cropscan measurements were primarily intended for comparison of reflectance measurements with a low and high spatial resolution.

A2.2 Materials and methods

The crop height and crop reflection were measured in the sward damage experiment of 2000 (described in Chapter 3 and 8) and N experiment of 2000 (described in Chapter 4). The sward damage experiment will be referred to as experiment 1, the N experiment as experiment 2.

A2.2.1 Disk plate meter

Sward height was measured with a plate meter at all harvests. The plate meter consisted of a PVC rod surrounded by a circular polystyrene foam plate with a diameter of 0.6 m. The rod is placed on the soil and then the plate sinks on the grass and the height of the grass can then be read from the rod. The sward height measured with the DPM depends on the height and density of the sward. The PVC rod was placed in the centre of the mini swards and height of the foam plate was recorded. In experiment 2, some swards with high N supply were slightly lodged.

Gabriels and Van den Berg (1993) reported that logarithmic transformations of both DM yield and crop height resulted in approximately homogeneous residual

variances. Therefore, both DM yields and crop heights were logarithmically (ln) transformed. The coefficient of variance (CV) was calculated as:

$$CV(\%) = 100 \times \sqrt{e^{\sigma_r^2} - 1} \quad (1)$$

where σ_r^2 equalled the residual variance of ln transformed DM yield after regression.

A2.2.2 *Cropscan*

At three harvests, on 20 June, 29 August and 31 October, crop reflection was recorded with a Cropscan (Cropscan inc.). The Cropscan records reflection in 8 bands with centre wavelengths (and associated bandwidths) at 460 (27), 510 (32), 560 (25), 610 (27), 660 (26), 710 (33), 760 (28) and 810 (32) nm, under a viewing angle of 28°.

Crop reflection was recorded for all mini swards in experiment 2 and for mini swards with artificial and natural sward damage in experiment 1. The Cropscan was held 80 cm above soil surface, resulting in a field of view with 0.2 m radius. Means of two measurements, directed to opposite sides of the mini sward, were calculated. The Cropscan was used in the rain shelter, what might have influenced the results slightly.

In literature, a large number of vegetation indices are proposed for yield assessment from crop reflection measurements with remote sensing (*e.g.* Purevdorj et al., 1998). The weighted difference vegetation index (WDVI) and normalised difference vegetation index (NDVI) are widely used for dry matter yield assessment (Clevers, 1989; Clevers & Verhoef, 1993)

The NDVI was calculated as:

$$NDVI = \frac{R_{810} - R_{660}}{R_{810} + R_{660}} \quad (2)$$

where R_{810} and R_{660} is the crop reflection measured with the 810 and 660 nm band. The NDVI is sensitive to optical properties of the soil background (Baret & Guyot, 1991). The WDVI corrects for soil background and moisture content (Clevers, 1989). The WDVI was calculated as:

$$WDVI = R_{810} - S * R_{560} \quad (3)$$

where S is the soil correction factor and R_{560} is the crop reflection in the 560nm band. For S, a value of 2.1 was used. This assumes that for soil the reflection in the R_{810} band is 2.1 times higher than the R_{560} band.

A2.2.3 *Imaging spectroscopy*

The relation between GC, IRI and DM yield can be found in Chapter 3. In Chapter 9, results are presented on the predictive power of the combination of GC, IRI with spectral information for DM yield. For experiment 1, relations were taken from Chapter 3. In this appendix, these relations were estimated for experiment 2. Additionally, some regressions were made with data of the N experiment in 2001, as described in Chapter 5.

A2.2.4 *Statistics*

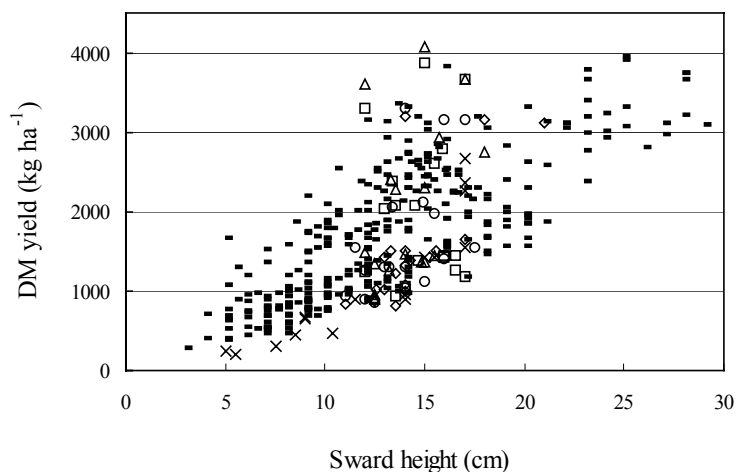
The experiments were studied separately. Where appropriate, an exponential or a linear relation was used for regression. When residuals deviated from the normal distribution, data were logarithmically converted. The equations were evaluated with the adjusted R^2 (R^2_{adj}) and with the standard error (SE) of observation. The SE of observation was calculated as the mean root square error of the residuals. For regressions on logarithmically converted data, the SE of observation was estimated with the relative error at the mean DM yield in the experiment.

A2.3 Results

A2.3.1 *Disk plate meter*

Preliminary regression between crop height and DM yield showed residual variances that were proportional to DM yield, *i.e.* the variation in DM yield increases with crop height (Figure II.1 A). Therefore, regressions were based on logarithmically transformed data. The sward height was linearly related to DM yield after logarithmic transformation in experiment 1 and 2 (Figure II.1 B). The CV was 32.1 and 40.6% for experiments 1 and 2 respectively. On log scale, the relative error was 32 and 39%, equivalent to an error of 555 and 645 kg DM ha⁻¹ at the mean yields (1733 and 1654 kg DM ha⁻¹) in experiment 1 and 2 (Table II.1).

A



B

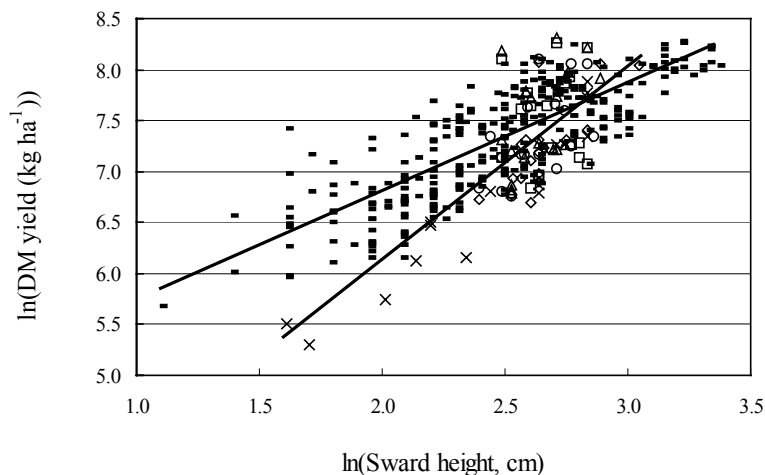


Figure II.1 Sward height measured with the disk plate meter vs. DM yield before (A) and after (B) logarithmic transformation for experiment 1 (-) and experiment 2 for 0N (x), 30N (◇), 60N(○), 90N(□) and 120N(△). See Table II.1 for regression equations.

The mean root squared error, calculated with the re-transformed regression equations was 419 and 541 kg DM ha⁻¹ in experiment 1 and 2. The mini swards with high N supply (90 and 120 kg N ha⁻¹ harvest⁻¹) in experiment 2 had a high DM yield but sward height remained below 20 cm. This was due to lodging of these swards.

A2.3.2 Cropscan

The NDVI was exponentially related to DM yield (Figure II.2). The discriminating ability of this relation is severely limited above 2000 kg DM ha⁻¹ or 0.8 NDVI.

The WDV_I was linearly related to DM yield (Figure II.3). The R²_{adj} was 0.47 for experiment 1 and 0.65 for experiment 2, with a standard error of observation of 298 and 638 kg DM ha⁻¹. The variation in DM yield increased with WDV_I value.

The red edge inflexion point was also significantly correlated to DM yield in experiment 2, with an R²_{adj} of 0.33. There was no significant correlation between red edge inflexion point and DM yield in experiment 1.

Regressing a combination of all significant bands against DM yield improved results (Figure II.4), with higher R²_{adj} and lower SE observation values (R²_{adj} = 0.72 and 215 kg DM ha⁻¹ SE obs. in experiment 1, and R²_{adj} 0.87 and 395 kg DM ha⁻¹ SE obs. in experiment 2). Unfortunately, bands selected in experiment 1 differed from bands selected in experiment 2 (Table II.1).

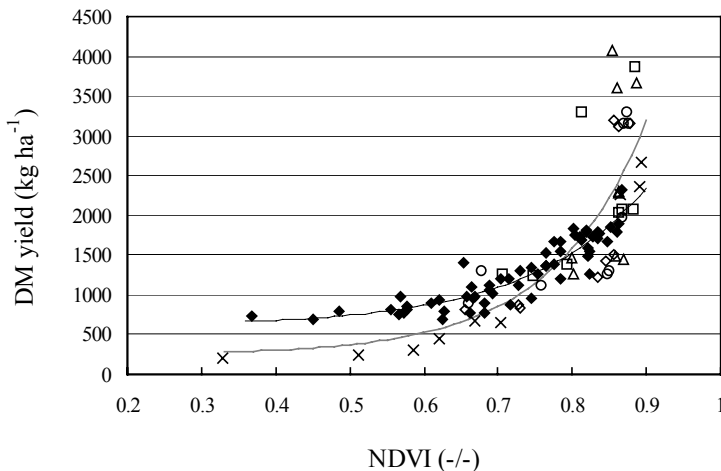


Figure II.2 Normalised difference vegetation index (NDVI) vs. DM yield for experiment 1 (◆) and experiment 2 for 0N (×), 30N (◇), 60N(○), 90N(□) and 120N(△). See Table II.1 for regression equations.

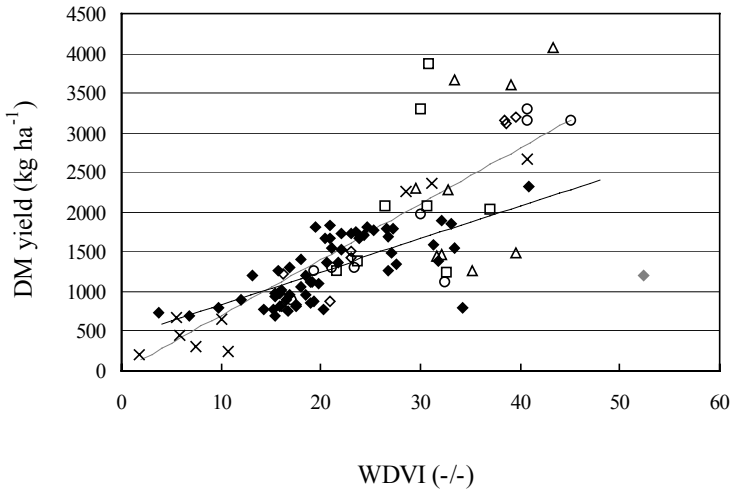


Figure II.3 Weighted difference vegetation index (WDVI) vs. DM yield for experiment 1 (◆) and experiment 2 for 0N (×), 30N (◇), 60N(○), 90N(□) and 120N(△). The observation with (◆) was not included in the analysis. See Table II.1 for regression equations.

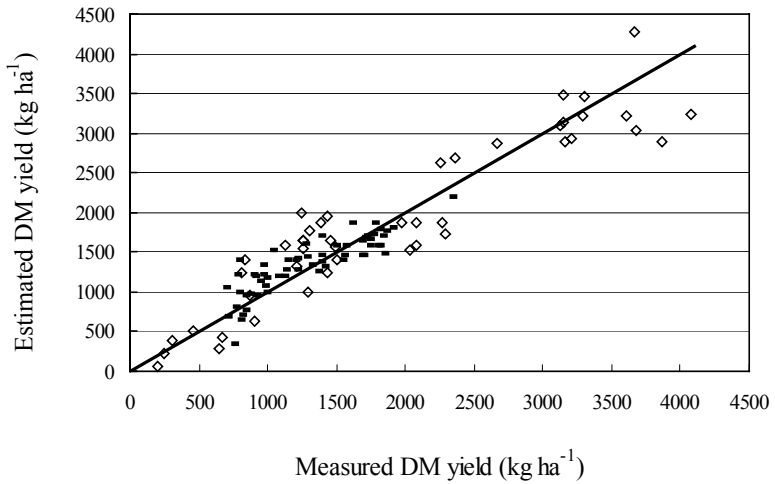


Figure II.4 Regression result of combinations of Cropscan bands vs. DM yield for experiment 1 (■) and experiment 2 (◇). See Table II.1 for regression equations.

A2.3.3 Relations between DM yield and GC and IRI

DM yield (in tons) was curvilinearly related to GC in experiment 1 with a R^2_{adj} of 0.82 ($GC = -7.9 + 91.5 \times (1 - e^{-1.44 \times \text{DM yield}})$) and in experiment 2 with a R^2_{adj} of 0.89 ($GC = 21.7 + 66.4 \times (1 - e^{-1.36 \times \text{DM yield}})$), as found in Chapter 3 earlier for experiment 1, $R^2_{\text{adj}} = 0.82$), see Figure II.5.

Although parameter values were slightly different between experiments 1 and 2, the maximum GC value was comparable, with 82.6 and 88.1 for experiments 1 and 2 respectively. The extinction coefficient values were also similar, with -1.44 in exp.1 and -1.36 in exp. 2, with a standard error of 0.1 in both experiments.

The combination of GC and IRI had a strong relation ($R^2_{\text{adj}}=0.82-0.89$) with DM yield (Table II.1). The relation between GC, IRI and DM yield did not require a logarithmic transformation in experiment 2, in contrast to experiment 1. Also the 2001 N experiment did not require a logarithmic transformation ($R^2_{\text{adj}}=0.92$, SE observation 289 kg DM ha⁻¹, data from Chapter 5).

The relation between GC-GCG₀-GCG₁, IRI and DM yield also had different parameter values for the three experiments in 2000 and 2001. These differences were partly explained by the relation between IRI and DM yield. In experiment 1 the relation between IRI and DM yield was: $IRI = -3.2 (\pm 0.7) + 8.1 (\pm 0.4) \times \text{DM yield (ton ha}^{-1})$, with $R^2_{\text{adj}}=0.56$ and SE observations of 4.94. In experiment 2

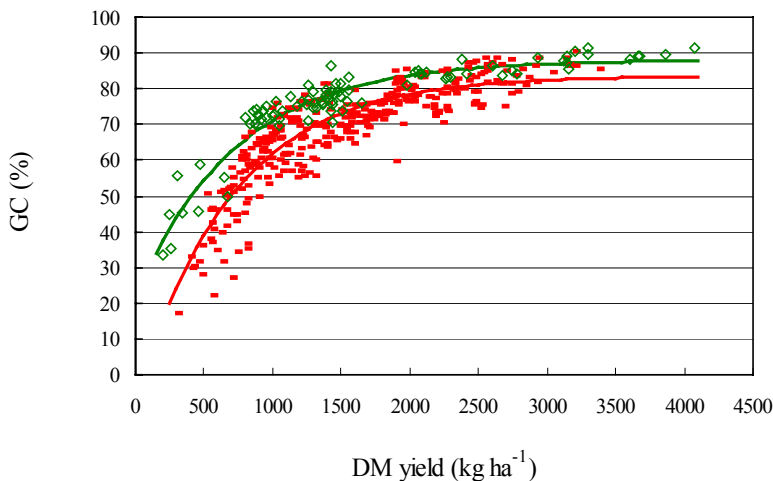
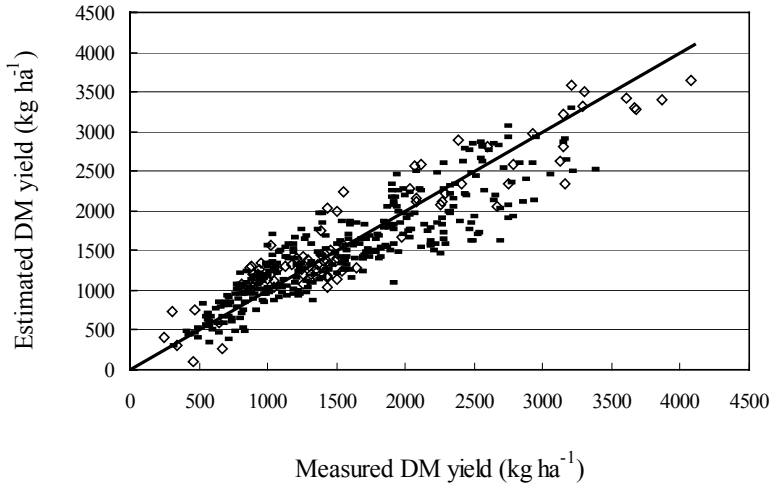


Figure II.5 DM yield vs. GC for experiment 1 (■) and experiment 2 (◇). See Table II.1 for regression equations.

A



B

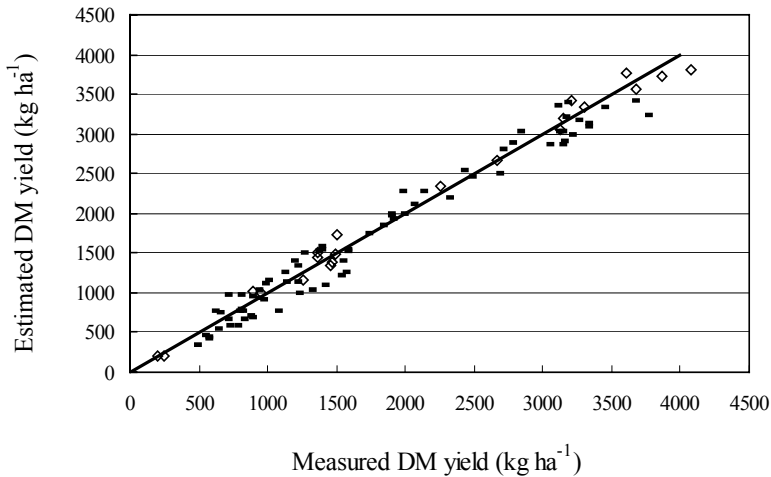


Figure II.6 Measured DM yield vs. estimates of DM yield calculated with GC and IRI (A) and PLS calibration models including GC and IRI (B) for experiment 1 (■) and experiment 2 (◇). See Table II.1 for regression equations.

this relation was $IRI = -2.3 (\pm 1.1) + 10.4 (\pm 0.5) \times DM \text{ yield (ton ha}^{-1}\text{)}$, $R^2_{adj} = 0.91$, $SE_{obs} = 3.72$. From the standard errors of the parameters, it can be concluded that the slope of these two relations was slightly, but significantly different.

The slightly stronger negative extinction coefficient in the DM yield and GC relation indicates that 1 ton DM yield difference affected GC stronger in experiment 1 than in experiment 2. Therefore, the differences between the experiments were also partly due to specific leaf area, as limited N supply in experiment 2 resulted in thicker leaves.

In Chapter 9 it was concluded that combining GC, IRI and spectral information of leaves resulted in an even stronger relation with DM yield, with a root mean square error of predictions of 268 and 235 kg DM ha⁻¹ for experiment 1 and 2. With only information of normalised spectra, root mean square errors of prediction were 286 and 343 kg DM ha⁻¹ for experiments 1 and 2. Obviously, these errors were smaller for the calibration sets with 188 and 322 kg DM ha⁻¹ for the normalised spectra and 183 and 109 kg DM ha⁻¹ for the normalised spectra in combination with GC and IRI for experiment 1 and 2 respectively (Table II.1).

A2.3.4 Comparing methods

The standard errors of the relations between DM yield and crop height measured with the disk plate meter were high, with 555 and 645 kg DM ha⁻¹ for experiment 1 and 2 (Table II.1). These errors were lower for Cropscan NDVI (163 kg DM ha⁻¹) and WDVI (298 kg DM ha⁻¹) in experiment 1, but higher in experiment 2 (689 and 638 kg DM ha⁻¹) than for crop height. The large differences between the experiments were due to the differences in DM yield range between the experiments, with maximum yields of 2293 kg DM ha⁻¹ in experiment 1 and 4075 kg DM ha⁻¹ in experiment 2 (Figure II.1 and II.2). DM yields of experiment 2 were clearly beyond the sensitivity range. Combining various Cropscan bands reduced SE of experiment 2 to 395 kg DM ha⁻¹, whereas SE in experiment 1 remained higher than with NDVI as regression variable.

The GC is strongly ($R^2_{\text{adj}}=0.79$ and 0.88) related to DM yield. This relation can only be used for DM yield estimation in the lower DM yield range (< 2000 kg DM ha⁻¹). Combining GC and IRI allowed a linear regression, especially when including only intensity classes with high reflection intensity (Chapter 3). With normalised spectra of 2 sensors as input for partial least square models (PLS), root mean square error of cross validation was still rather high (322 kg DM ha⁻¹) for experiment 2. This error was strongly reduced to 183 and 109 kg DM ha⁻¹ when including also GC and IRI in the model.

Table II.1 Regression equations for disk plate meter, Cropscan and the imaging spectroscopy system for DM yield.

Experiment	Observations #	Model	R ² _{adj}	SE	
-----Disk plate meter-----					
Crop height	1	306	$e^{4.69+1.06 \times \ln(\text{crop height})}$	0.66	555*
	2	98	$e^{2.35+1.90 \times \ln(\text{crop height})}$	0.55	645*
-----Cropscan-----					
NDVI	1	44	$608+5.68 \times 580^{\text{NDVI}}$	0.84	163
	2	59	$248+2.41 \times 2687^{\text{NDVI}}$	0.59	689
WDVI	1	44	$420 + 41.5 \times \text{WDVI}$	0.47	298
	2	59	$70.2 \times \text{WDVI}$	0.65	638
Band combinations	1	44	$1208-117.0 \times R_{460} + 98.5 \times R_{560} + 25.3 \times R_{610}-123.2 \times R_{660}$	0.72	215
	2	59	$1567 + 328.7 \times R_{460} -303 \times R_{510} - 199 \times R_{710} + 64.8 \times R_{760}$	0.87	395
-----Imaging spectroscopy-----					
GC	1	334	$236 + 59.2 \times 1.044^{\text{GC}}$	0.79	311
	2	100	$381 + 1.13 \times 1.092^{\text{GC}}$	0.88	308
GC+IRI	1	334	$e^{5.19 + 0.028 \times \text{GC} + 0.010 \times \text{IRI}}$	0.82	323*
	2	100	$13.94 \times \text{GC} -174.9 \times \text{IRI} + 2.601 \times \text{GC} \times \text{IRI}$	0.89	303
Two sensor model	1**	147	PLS	0.96	188
	2**	37	PLS	0.90	322
Two sensor model, with GC and IRI	1**	147	PLS	0.96	183
	2**	37	PLS	0.99	109

* Regression based on ln transformed data, SE approximated with the relative error at the average DM yield in the experiments.

** Calibration models, SE approximated with root mean squared error of cross validation.

A2.4 Discussion and conclusion

It is concluded that the accuracy of DM yield assessment with imaging spectroscopy (109-183 kg DM ha⁻¹) is better than with the disk plate meter (529-743 kg DM ha⁻¹) or Cropscan (215-395 kg DM ha⁻¹). The data used were not measured with the intention to compare methods. Therefore, data sets differed for Cropscan and disk plate meter and imaging spectroscopy, although measured in the same experiments. Cropscan data in experiment 1 did not include yields above 2500 kg DM ha⁻¹, and regressions results are, therefore, expected to be better than in a data set where higher DM yields are included.

The crop height, recorded with the disk plate meter was very sensitive for lodging of the swards, which occurred in the N experiment under high N supply. The spatial variability of damaged swards was large. This resulted in high values of CV (32.1 and 40.6) for the sward damage and N experiment. These values are comparable with data of grazed swards (Gabriels and Van den Berg, 1993).

The fitted equations yielded higher R² values for the Cropscan. The NDVI and WDV were severely limited in their applicability at higher DM yields, as sensitivity decreased strongly with DM yields above 2000 kg ha⁻¹. This is in accordance with findings of King *et al.* (1986). They concluded that the accuracy of sward reflection (red-far red ratio) was very similar to sward height measured with a 'sward stick' in the 700 to 1800 kg DM ha⁻¹ range and that reflection could not be used above LAI 3-4, or 2000 kg DM ha⁻¹. Lokhorst and Kasper (1998) compared Cropscan with DPM for dry matter yield assessment in the higher DM yield range and found that the performance of Cropscan was not better than DPM. Gabriels and Van den Berg (1993) concluded that refinements are necessary before the capacitance meter or DMP can be usefully integrated into a management system.

The reflection signals recorded with Cropscan and the experimental imaging spectroscopy system cannot be compared directly. Firstly, the characteristic of the light sources used differs. Secondly, the Cropscan records reflection from the combination of soil, crop and dead material, whereas soil and dead material influences are minimised in the used classification procedure of the experimental system. Thirdly, both systems will respond differently to changes in canopy geometry. Fourthly, the fixed and limited distance between light source and crop caused reflection intensity to respond strongly to crop height in

the imaging spectroscopy system, whereas this information is not available for systems based on solar radiation, such as the Cropscan.

The strong relations between imaging spectroscopy parameters and DM yield can be attributed to the accurate information of ground cover and index of reflection intensity. GC was exponentially related to DM yield and, therefore, only sensitive below 2000 kg DM ha⁻¹. Relations became more linear when including IRI, expanding the range of sensitivity considerably. In contrast to the disk plate meter, imaging spectroscopy was not very sensitive for lodging. Decreasing crop height decreases reflection intensity, but this effect is to a large extent compensated by a more horizontal leaf orientation. With normalised spectral information only, DM yield predictability was also good, with root mean square errors of prediction of 286 and 344 kg DM ha⁻¹ (Chapter 9). This can probably be attributed to the effects of canopy geometry (mean leaf height and angle) on the mean leaf spectra measured with the imaging spectroscopy system. Combining GC and IRI with leaf spectral information further reduced the prediction error, when compared to GC and IRI or spectral info alone, to 268 and 235 kg DM ha⁻¹.

Curriculum vitae

Anthוניus Gerardus Theodorus (Tom) Schut werd geboren op 5 december 1972 te Doetinchem. Vanaf 1991 studeerde hij aan de Christelijke Agrarische Hogeschool te Dronten. In 1995 rondde hij zijn studie af in de richting Rundveehouderij. In hetzelfde jaar is hij gestart met de studie Bodem Water Atmosfeer aan de Landbouw Universiteit te Wageningen. Als afstudeervak heeft hij bij het SC-DLO (nu Alterra) gewerkt aan een modelmatige verkenning van de nitraatuitspoeling van melkveehouderijbedrijven met verschillende grondsoorten en een “De Marke” bedrijfssysteem. In 1997 werd deze studie afgerond (cum laude). Vervolgens heeft hij 3 maanden bij het SC-DLO gewerkt aan het project “Beregenen op maat”. Vanaf oktober 1997 tot oktober 1998 heeft hij op het AB-DLO (nu onderdeel van Plant Research International) als wetenschappelijk onderzoeker gewerkt aan een modelmatige verkenning van potentiële en watergelimiteerde grasopbrengsten en aan het schrijven van een AIO voorstel. Van oktober 1998 tot oktober 2002 is hij werkzaam geweest als DLO-AIO bij de onderzoeksschool Productie Ecologie van de Landbouw Universiteit Wageningen. In deze periode was hij gedetacheerd bij het AB-DLO, later Plant Research International. In deze periode heeft hij bijdragen geleverd aan congressen in Peking (China), Montpellier en Toulouse (Frankrijk). In oktober 2002 is hij begonnen als wetenschappelijk onderzoeker bij Plant Research International.